

2013

Acoustic and sedimentological investigations of seabed conditions and related bio-geological parameters in a tidally energetic, fine-grained environment: York River Estuary, Virginia

Lindsey M. Kraatz

College of William and Mary - Virginia Institute of Marine Science

Follow this and additional works at: <https://scholarworks.wm.edu/etd>



Part of the [Geology Commons](#), and the [Oceanography Commons](#)

Recommended Citation

Kraatz, Lindsey M., "Acoustic and sedimentological investigations of seabed conditions and related bio-geological parameters in a tidally energetic, fine-grained environment: York River Estuary, Virginia" (2013). *Dissertations, Theses, and Masters Projects*. Paper 1539616722.
<https://dx.doi.org/doi:10.25773/v5-cq0w-8d39>

This Dissertation is brought to you for free and open access by the Theses, Dissertations, & Master Projects at W&M ScholarWorks. It has been accepted for inclusion in Dissertations, Theses, and Masters Projects by an authorized administrator of W&M ScholarWorks. For more information, please contact scholarworks@wm.edu.

Acoustic and sedimentological investigations of seabed conditions and related bio-physio-geological parameters in a tidally energetic, fine-grained environment: York River Estuary, Virginia.

A Dissertation

Presented to

The Faculty of the School of Marine Science

The College of William and Mary

In partial fulfillment

of the requirements for the degree of

Doctor of Philosophy

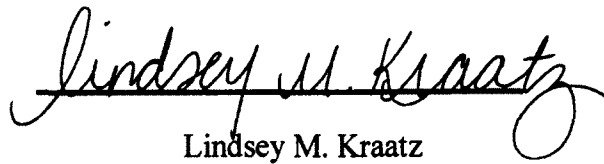
by

Lindsey M. Kraatz

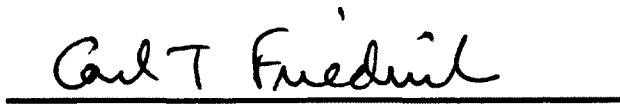
2013

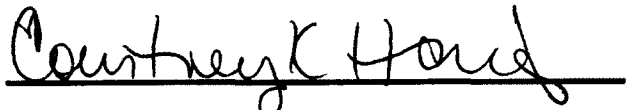
Approval Sheet

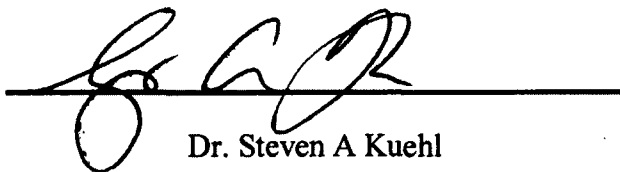
This dissertation is submitted in partial fulfillment of the
requirements for the degree of
Doctor of Philosophy
December 2013

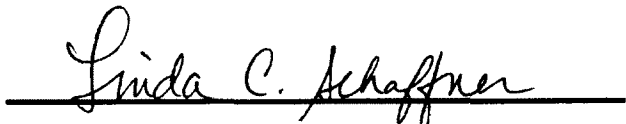

Lindsey M. Kraatz

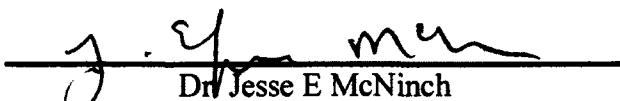
Academic Committee Members


Dr. Carl T. Friedrichs, Advisor


Dr. Courtney K Harris


Dr. Steven A Kuehl


Dr. Linda C. Schaffner


Dr. Jesse E McNinch
U.S. Army Corps of Engineers
Field Research Facility
Kitty Hawk, NC



Dr. Arthur C. Trembanis
University of Delaware
College of Earth, Ocean, and Environment
Newark, DE

Table of Contents

Acknowledgments	VI
List Of Tables	VII
List Of Figures	VIII
Abstract	XIII
Chapter 1: Introduction	1
1.1 BACKGROUND.....	2
1.2 SEDIMENT PROPERTIES ~ FLOCCULATION AND DEPOSITION.	4
1.3 SEDIMENT PROPERTIES ~ EROSION	5
1.4 BIOSTABILIZATION AND BIODESTABILIZATION.	6
1.5 TURBIDITY MAXIMA	8
1.6 ACOUSTIC MAPPING.....	9
1.7 ISOTOPE DATING.....	11
1.8 HIGH-RESOLUTION CORE CHARACTERIZATION METHODS.....	12
1.9. ESTUARINE SEDIMENT TRANSPORT MODELING.	14
1.10. STUDY AREA	15
1.11. OVERALL AIM AND ORGANIZATION	18
REFERENCES.....	20
Chapter 2: Approaches For Quantifying Seabed Morphology – Utilizing A Rotary Sonar System In A Cohesive Estuarine Environment	31
2.1 INTRODUCTION	32
2.2 DEVELOPMENT AND USE OF ROTARY SONAR.....	35
<i>Historic Applications Of Rotary Sonar</i>	36
2.3 STUDY AREA- COHESIVE SEDIMENT CASE STUDY ~ YORK RIVER ESTUARY	38
2.4 METHODS	40
2.5 RESULTS AND DISCUSSION.....	42
2.6 CONCLUSIONS.....	46
REFERENCES:	47
Chapter 3: Evolution Of The Seabed Of The York River Estuary, Virginia, Following Dissipation Of A Turbidity Maximum: Consolidation, Pelletization And Spring-Neap Disturbance	59

ABSTRACT.....	60
3.1. INTRODUCTION	61
3.2. STUDY AREA	66
3.3 METHODS	67
3.3.1. <i>Sediment Coring</i>	67
3.3.2. <i>Water Content, Organics, And Disaggregated Sediment Components</i>	68
3.3.3. <i>Pellets And Other Pellet-Sized Grains</i>	69
3.3.4. <i>Beryllium-7</i>	70
3.3.5. <i>Digital X-Radiography</i>	71
3.3.6. <i>Erodibility</i>	72
3.3.7. <i>Statistical Tests</i>	73
3.4 RESULTS	73
3.4.1. <i>Water Content, Organics, And Disaggregated Sediment Components</i>	74
3.4.2. <i>Pellets And Other Pellet-Sized Grains</i>	75
3.4.3. <i>Beryllium-7</i>	77
3.4.4. <i>Digital X-Radiography</i>	78
3.4.5. <i>Erodibility</i>	79
3.4.6 <i>Correlations Between Core Properties Within The Top Centimeter</i>	80
3.5. DISCUSSION	81
3.5.1. <i>Cruise Timing Relative To Seasonal Turbidity Transition And Spring-Neap Cycle</i>	81
3.5.2. <i>Bed Erodibility And Its Relation To Time And Tidal Disturbance</i>	83
3.5.3. <i>Observations Suggest Consolidation And Bed Together, Despite Limited Resolution</i>	84
3.5.4. <i>Controlling For The Possible Role Of Significant Net Erosion Or Deposition</i>	86
3.6. SUMMARY AND CONCLUSIONS.....	87
REFERENCES.....	90
Appendix 1: Fecal Pellet Analysis Methodology	115
Chapter 4: Seasonal Morphological Change In The York River Estuary, Chesapeake Bay Va	123
ABSTRACT.....	124

4.1 INTRODUCTION	124
4.2 STUDY AREA	126
4.3 METHODS	129
4.3.1. <i>General Surveying Approach And Associated Equipment</i>	130
4.3.2. <i>Correction For Water Level Variation</i>	131
4.3.3. <i>Speed Of Sound Calculations</i>	131
4.3.4. <i>Post-Processing In Grid And Fledermaus</i>	132
4.3.5. <i>Identification And Application Of Ground Control Points</i>	132
4.4 UNCERTAINTIES IN LOCATION AND ELEVATION ASSOCIATED WITH BATHYMETRIC SURVEYS.....	134
4.5 RESULTS	135
4.5.1. <i>Results For Uncertainties Based On Tide Gauge And Control Point Data</i>	135
4.5.2. <i>Overall Results By Subregion</i>	137
4.5.3. <i>Small Subsection Results</i>	138
4.6 DISCUSSION	139
4.6.1 <i>Relationship To Previous Studies Of Sediment Dynamics At Clay Bank</i>	139
4.6.2 <i>River Discharge And Corresponding Regionally-Averaged Patterns Of Deposition</i>	141
4.6.3 <i>Distinct Seabed Changes Within Sub-Environments</i>	142
4.6.4 <i>Possible Role Of Storms</i>	144
4.7 HISTORICAL BATHYMETRY	145
4.8 CONCLUSIONS.....	145
REFERENCES.....	148

Acknowledgments

To my major advisor, Dr. Carl T. Friedrichs for his support, guidance, and enthusiasm throughout the course of this project. To my committee members, Dr. Steven Kuehl, Dr. Courtney Harris, Dr. Linda Schaffner, Dr. Art Trembanis, and Dr. Jesse McNinch, for their insight and interest in my project. To the many individuals who assisted with or collaborated on field work, Dr. Grace Cartwright, Kelsey Fall, Carissa Wilkerson, Patrick Dickhudt, Dr. Samuel Lake, Justin Birchler, Julia Moriarty, Payal Dharia, and Cielomar Rodriguez. Also thank you to others for their support and guidance Wayne Reisner, Bob Gammisch, Timothy Gass, Dr. Paul Panetta, Dr. Tara Kniskern, Mark Mueller, Theresa Davenport, Dr. Fern Gibbons, Dr. Troy Hartley, Dr. Susan Park, Dr. Adam Skarke, Woody Hobbs, and Dr. John Milliman. Finally a big thank you to my family, who have given more to me than I will ever be able to return. Mom and Dad, I would not be here without you. Thank you for all your love and support. This work was part of the Multidisciplinary Benthic Exchange Dynamics (MUDBED) project supported by funding from the National Science Foundation (Grants #OCE-0536572, #OCE-1061564 and #DGE- 0840804).

List of Tables

Table		Page
2-1	Rotary sonar scan sequences variables determined to be the optimal initial settings in a cohesive, fine-grained, estuarine environment.	53
3-1	Cruise date, location, and station numbers.	98
3-2	Percent water content by weight of wet sediment, percent organic content by weight of dry sediment, and percent disaggregated sand-sized content by weight of dry sediment. Depth listed is center of 1-cm sample interval. Dashes indicate no data or bad data.	102
3-3	Phi class mud content by weight as percent of dry mud as determined by disaggregated grain pipette analysis. Depth listed is center of each 1-cm sample interval. Dashes indicate no data or bad data.	103
3-4	Weights of sediment for sieve intervals from 10.00 g of wet sediment. Dashes indicate no data or bad data.	105
3-5	Beryllium activity in dpm/gram dry sediment (including sand), \pm confidence interval, corrected for decay between time of core collection and analysis. Zero values indicate no ^7Be peak detected. Dashes indicate no data or bad data. ^7Be inventory in units of dpm/cm ² integrated over the top 10 cm of each core is displayed in the final row.	106
3-6	Eroded mass and critical erosion stress calculated from erodibility experiments.	109
3-7	Correlation r-values and p-values. Correlations with $p < 0.1$ or $0.1 \leq p < 0.2$ highlighted by dark or light shading, respectively	111
4-1	Cruise survey dates, day elapsed between sampling, and the tidal regime during the bathymetric surveys.	154
4-2	Estimated mean speed of sound velocities for each survey based on Coppen's (1981) equation as a function of temperature, salinity, and depth.	155
4-3	Seabed elevation for ground control points, along with calculated bathymetric change between surveys. The December survey was used as the baseline bed elevation for this study. The overall average bathymetric change value between cruises was used as the shift variable to align seabed elevations with the December survey.	157
4-4	Potential errors and uncertainties associated with bathymetric surveying (Modified from Umbach, 1976 and Byrnes et al., 2002).	160

List of Figures

Figure		Page
1-1	Map of York River Estuary. Location of Clay Bank study site indicated by black dot. Locations of US EPA long-term monitoring stations closest to Clay Bank indicated by red squares.	28
1-2	Map of Chesapeake Bay, highlighting the bathymetry and turbidity maximum zones throughout the region. The study area is delineated by a star, located in the Clay Bank region of the York River (modified from Newell et al., 2004).	29
1-3	The York River biological and physical gradient. X-rays: West Point ~ June 1981 (Schaffner et al., 2001), Clay Bank STM ~ February 2009, Clay Bank no STM ~ March 2009, Gloucester Point ~ February 2009, and Chesapeake ~ January 1995 (Schaffner et al., 2001).	30
2-1	Study location for the VIMS rotary tripod ~ Clay Bank within the York River Estuary. The tripod location is delineated by the red triangle.	51
2-2	A depiction of the real-time rotary sonar capabilities developed utilize IrisLink software and a communication cable, extending from the instrument to a radio modem, that deliver data back to the lab at the Virginia Institute of Marine Science. The two-way connection allowed for in-situ tuning of the sonar images, as well as real-time observations.	52
2-3	a) A Clay Bank 1 MHz rotary scan image, 1 meter above the bed (Range ~ 10m, 24dB gain). b) Diagram showing the 4 transects analyzed for acoustic backscatter comparison.	54
2-4	Wind speed, river discharge, and tidal data that correlated to the early rotary sonar studies in the York River.	55
2-5	Sidescan sonar surveys during rotary sonar deployment in order to correlate rotary sonar images to seafloor morphology changes. (a) The first survey showed well-developed longitudinal furrows extending up to 150m in length and 0.5 to 1 meter wide, occurring shortly after a large storm event with heavy winds. The left image highlights the location of the rotary tripod and the image on the right shows a furrow with an old piling or similar structure within the bedform. (b) The second survey was conducted at the end of the rotary sonar deployments and illustrates a smoother bottom and the same furrow with less definition.	56
2-6	Time series of backscatter amplitude at 5 meters from the rotary transducer along of the 4 transects (45°, 90°, 180°, and 225°).	57

2-7	Conceptual diagram of York River furrow morphologic change throughout the study. As winds increased during the rotary sonar deployment, sediment was deposited within the furrow and then was eroded after the stormy conditions subsided.	58
3-1	Map of York River Estuary. Location of Clay Bank study site indicated by the black dot. Locations of EPA long-term monitoring stations and NOAA tide gauge closest to Clay Bank indicated by red squares. The aerial photograph inset shows the Clay Bank MUDBED sites. The Yellow star depicts the secondary channel core location for this study. The VIMS Clay Bank Piling (green dot) and the MUDBED main channel core location (white dot) are shown for data comparisons between studies.	97
3-2	(a) Example of GOMEX core sampling in Virginia estuary Map of York River Estuary (photo courtesy of G. Cartwright). (b) Disaggregated particles (top) and gently sieved particles (bottom). The pellet weight in each size class (ϕ_{Pellet}) was given by $\phi_{Pellet} = \phi_{gentle_sieve} - \phi_{disaggregated}$.	99
3-3	(a) Dual core Gust microcosm as arranged during an erosion experiment. (b) Close-up of sediment suspension in a Gust microcosm with water circulation pattern highlighted by arrows.	100
3-4	Sediment mass profiles of (a) % water in wet sediment, (b) % organics in dry sediment, (c) % sand in dried sediment, (d) % water in wet mud matrix, (e) % organics in dry mud, and (f) % silt in dried mud. Size classes in figure reflect disaggregated sediment components.	101
3-5	Percent mass as a function of sieve size classes: (a) size distribution of pellets that withstood sieving but not disaggregation, (b) size distribution of “disaggregated” (i.e., coarse silt/fine sand and detritus that withstood disaggregation), (c) % organic of pellets, (d) % organic of “disaggregated”, (e) % pellets of all “collected” >45 microns, (f) % pellets relative to total disaggregated mud.	104
3-6	Beryllium-7 activity per mass of dry mud, corrected for time between coring and counting, for weekly sampling at the Clay Bank site between late April and late May, 2010.	107
3-7	(a)- (e) Example digital x-radiographs from cores collected on the five weekly sampling cruises. (f) Relative pixel intensity, averaged across the widths of the images in (a)-(e) width, for depths from 1 to 14 cm. The width-averaged pixel intensity was normalized on a scale of 0 to 1 such that the lowest width-averaged intensity for each core was set to 0, and the highest width-averaged intensity was set to 1.	107

3-8	Eroded mass as a function of critical erosion shear stress for weekly sampling at the Clay Bank site between late April and late May, 2010.	110
3-9	Conditions in the York River estuary in 2010: (a) USGS data for riverine discharge (3-day low-pass of Pamunkey plus Mattaponi gaging stations). EPA monitoring data for (b) salinity and (c) total suspended solids (spatial averages of observations collected at stations LE4.1 and LE4.2). (d) Tidal range (high water minus low water) calculated from Yorktown NOAA tide gauge with dashed lines indicating dates of coring cruises. (See Figure 1 for locations of LE4.1, LE4.2 and tide gauge.)	112
3-10	Comparison of eroded mass vs. stress for 2007 and 2010 cores collected at Clay Bank. (a) Mar-May 2007 monthly data compared to Apr-May 2010 weekly data; (b) Jun-Oct 2007 monthly data compared to Apr-May 2010 weekly data. 2007 data from Dickhudt et al. (2008).	113
3-11	(a) Mean eroded mass at 0.2 Pa for each of the five cruises along with a least-squares linear regression as a function of elapsed time in days. (b) Tide range at Yorktown averaged over the previous 11 tidal cycles. (c) Results of multiple regression of eroded mass versus both time and low-passed tidal range.	114
4-1	Map of the York River Estuary. Location of the Clay Bank high-resolution bathymetry and sub-bottom surveys are indicated by the yellow box. The dot represents the VIMS Clay Bank Observing station and the red lines represent the survey lines taken throughout the one-year survey between 2008 and 2009.	152
4-2	Location of the VECOS monitoring station in relation to the 2008-2009 bathymetric surveys. The VIMS Clay Bank Piling and the MUDBED core locations are shown for data comparisons between studies.	153
4-3	A bathymetry plot generated from the interferometric systems cover a $\sim 4\text{km}^2$ section of the York River Estuary. For this study, the survey area was divided into three blocks based on bathymetry and the availability for quality ground control points. The main channel block, delineated by the purple dashed line and the secondary channel/shoal region is highlighted by the light-blue dashed line. Between the main channel and secondary channel, no ground control points could be found and therefore the region in white is not further analyzed within this study.	156
4-4	Location map of ground control points (red circles) selected in Section 1 of the study area. This region is consists of the main channel, southeast flank, and shoal.	158
4-5	Location map of ground control points (red circles) selected in	159

	Section 3 of the study area. This region is consists of the secondary channel and shoal.	
4-6	Comparison analysis to assess the potential source of error between the VECOS water depth data and water height elevation captured in real-time during the surveys with Hypack. The mean absolute difference between the VECOS and despiked/low-passed filtered data for the 5 surveys was 2.2 centimeters. Values for each month are found within their respective sub-plots. Note that the analysis for the February comparison was for only the last 1.5 hours of the cruise.	161
4-7	Time-series of mean seabed elevation of the (a) main channel and (b) secondary channel.	162
4-8	Time-series of transect analysis of the Clay Bank main channel sub-section.	163-4
4-9	Time-series of transect analysis of the Clay Bank secondary channel sub-section.	165-6
4-10	Dickhudt et al.'s (2009) conceptual diagram depicting sediment transport processes in the York River estuary. Symbols courtesy of the Integration and Application Network (ian.umces.edu/symbols/), University of Maryland Center for Environmental Science.	167
4-11	April 2008 through March 2009, soft mud layer thickness contour maps for Clay Bank captured using a dual-channel echosounder (Rodriguez-Calderon and Kuehl, 2012). The shoreline and the boundaries of the channel sub-environments are indicated with black lines. Soft mud layer thickness scale is in meters (0-22 cm). Months and years are shown at the bottom left side of the maps. A reference figure is included at the bottom to indicate the location of each of the channel sub-environments: main channel NE flank (MCNE), main channel (MC), main channel SW flank (MCSW), inactive oyster reef (IOR), secondary channel (SC), secondary channel flank (SCF).	168
4-12	USGS riverine discharge data from the Mattaponi and Pamunkey Rivers between September 2008 and August 2009 (USGS, 2009: http://waterdata.usgs/nwis).	169
4-13	Bathymetric map of NOAA Digital Echo Sounder Data collected in 1947 (Survey H07181). Data was corrected for actual sound velocity and reprojected from NAD27 to NAD83, maintaining MLW as the vertical datum. Original sound positions are delineated by the circles. The bathymetric raster was interpolated using the kriging method. The slump mounds within the main channel, used for the postage stamp analysis, are highlighted by the red circle.	170
4-14	Bathymetric map of the Clay Bank region in December of 2008	171

used for comparison of the historic NOAA data. The slump mounds within the main channel, used for the postage stamp analysis, are highlighted by the red circle.

Abstract

The transport and fate of fine-grained sediments is a critical factor affecting the physical, chemical, and biological health of estuaries, coastal embayments, riverine, lacustrine, and continental shelf environments. A geophysical and sedimentological study of the York River as a part of the NSF Multi-disciplinary Benthic Exchange Dynamics (MUDBED) project was conducted to determine: 1) the primary drivers of sediment erodibility within a fine-grained system, 2) if these drivers can be accurately measured through sedimentological and acoustic information, and 3) the spatial and seasonal variability of erosion within the estuary. Previous studies indicate that increased erodibility within the York River Estuary is mainly due to recent ephemeral deposition, whereas lower erodibility is associated with eroded or biologically reworked conditions. By studying key physical and biological parameters in the York River estuary, we can more generally apply knowledge gained on relationships among sediment facies, seabed erodibility, and the recent history of deposition, erosion, consolidation, and biological reworking.

Three different experiments were conducted to look at erosion, deposition, consolidation, and biological reworking in the Clay Bank region of the York River Estuary, each highlighting varying scales of temporal change. The first experimental approach utilized an Imagenex 881A rotary sonar for one- to three-month deployments to examine surficial changes of the seabed, from hourly to monthly timescales, and allow scientists to track movement of sediment in and out of the system using sonar imagery. Optimized parameters were determined for cohesive sediment environments and a real-time observing rotary sonar was created to analyze the seabed on an hourly basis. In the second experiment, cores were collected on a weekly basis to investigate relationships between sediment properties and erodibility during the post-freshet dissipation of the mid-estuary turbidity maximum as well as over the spring-neap cycle. Grain size, water content, abundance of resilient pellets, the occurrence of ^7Be , and x-radiographs were analyzed and compared to the results of Gust microcosm erosion tests to further constrain the controls on erodibility. The third experimental approach utilized seven high-resolution bathymetric surveys conducted between September 2008 and August 2009 within a 3.75 km^2 region at Clay Bank. Seabed height was shown to vary both spatially and temporally in association with the spring freshet, likely related to the presence and migration of a local secondary turbidity maximum.

Chapter 1: Introduction

1.1. Background

Estuaries, coastal embayments, riverine shelves, and continental slope regions are often covered with muddy fine-grained sediment. Generally exhibiting a cohesive nature, muds have a defining “stickiness” that is difficult to predict and which fundamentally affects its mobility and the transport of sediment (Whitehouse, 2000). The sediment dynamics occurring within less cohesive sandy environments have been relatively well documented, with the finding that the dominant particle size of the bed sediment drives the behavior of the distribution and fate of the grains (van Rijn, 1984a; van Rijn, 1984b; van Rijn, 1984c; Nielsen, 1992; Soulsby, 1997; Komar, 1998). In contrast, less is known about the transport and dynamics of fine-grained sediment, despite the importance of particle dispersal within fine-grained environments.

Previous studies have shown that fine-grained sediment can have a detrimental impact on water quality and ecology, especially in estuarine systems. Often a considerable amount of sediment enters the system via runoff, riverine input, and the bay or ocean. However, the amount of sediment entering tidally energetic estuaries is often much less than that which is found within the water column. The surplus of sediment in suspension is thought to be due to the repeated resuspension of fine-grained sediment from the seabed (Kennedy, 1984; Dyer, 1986). Large quantities of suspended sediment can result in negative impacts within the estuary, including enhanced light attenuation, disruption and change of benthic community structure and distribution, modified transport of organic carbon, and changes in the location and duration of eutrophication and hypoxia (Whitehouse, 2000; Hardisty, 2007). In addition, contaminants are often concentrated in fine-grained systems. Due to physio-chemical attraction and large surface area, these fine cohesive particles are highly susceptible to contaminant adsorption (Olsen et al., 1993; Mitra et al., 1999; Whitehouse, 2000).

Previous studies have shown that the erodibility of sediment beds is a complex function of grain size, water content, mineralogical composition, deposition and erosion history, and biological activity. A number of techniques, including: laboratory flume tests, in-situ measurements using submersible flumes, and core analysis, have been developed to investigate controls on fine sediment erosion, but the general scientific consensus is that it is very difficult to predict (Parchure and Mehta, 1985; McNeil et al., 1996; Maa et al., 1993). More recent technology, incorporating Gust microcosms and Acoustic Doppler Velocimeters (ADVs), for example, has allowed for a deeper and a more field-oriented understanding of sediment erosion (Thorne and Hanes, 2002; Tolhurst et al., 2002; Betteridge et al., 2003; Porter et al., 2004; Dickhudt, 2008; Friedrichs et al., 2008). However, these techniques remain labor intensive and spatially limited in scope. If scientists were able to utilize remote sensing techniques to examine sediment erosion and deposition over various temporal and spatial scales, it would not only decrease the need for large-scale field operations but would allow for more continuous and widespread seabed measurements.

Over the past few decades, hundreds of studies have utilized geologic acoustic mapping in order to analyze the seabed. Many of the early studies came about during the era of World War II, using sonar to map the world's oceans (Jones, 1999). As acoustical theory and technology developed over the next few decades, improved measurements were collected and publications such as Heezen and Tharpe's (1957) "Physiographic Map of the North Atlantic" became available. Recent strides in technology have supplied researchers with equipment that can now provide measurement accuracies of mapping on centimeter scale. Geologic mapping of the seabed has been found to be of great importance for several applications including mapping and managing habitats, providing navigation information, as well as tracking environmental

conditions on multiple spatial and temporal scales (Caiti et al., 2006). As of late, estuaries have become a particular focus of mapping for habitat assessment, for improving navigational safety, and for national security protection (Hardisty, 2007).

1.2 Sediment Properties ~ Flocculation and Deposition

Depending on the degree of convergent sediment transport and the strength of waves and currents, fine-grained estuarine sediment particles can exist in four various states: mobile-suspended sediment (including various degrees of particle aggregation), high near bed sediment concentrations (e.g., fluid mud), unconsolidated sediment deposits, or consolidated sediment bed. If the fine-grained cohesive particles are in suspension, they are often susceptible to collision and cohesion with other sediment particles, resulting in particle flocculation and aggregation (Dyer, 1986). Factors affecting the aggregation of particles can be a result of physiochemical or biologic processes. Flocculation via particle collisions can be due to three mechanisms: Brownian motion for weak flocs, small-scale fluid shear which forms stronger flocculates, and differential rates of particle settling (Dyer, 1995). Conversely, biological processes may contribute to particle aggregation via biodeposition and organic binding. The size and abundance of flocculates and aggregates depends on sediment concentration, grain mineralogy, pH, organic content, and ionic strength, as well as biological packaging. It is important to consider this because flocculation and biological aggregation greatly enhance settling velocity. When comparing flocculated/aggregated grains to individual primary particles, the settling velocity can range several orders of magnitude greater (Dyer, 1995; Hill and McCave, 2001; Mikkelsen et al., 2007).

If the amount of deposition exceeds the rate of resuspension/erosion of the seabed, accretion will result. In physically dominated regions, multiple lamination layers may be present within the seabed due to discrete deposition events. Schaffner et al. (2001) defined the upper York River estuary as being predominately controlled by physical processes, where the primary sediment structures of the bed are laminations, and the majority of the physical sediment disturbance occurs on a scale of weeks to months. The authors found that the sediment record provided by these laminations supply a history of the estuary, illustrating erosional pockets between depositional periods ranging from centimeters to 10's of centimeters in sediment thickness. It was found in this area, storms provided a major source of erosion of the seabed, disturbing 10's –100's of centimeters of sediment. However, storms are infrequent, and therefore tides were identified as the primary mechanism for resuspending and eroding sediments during more quiescent periods (Schaffner et al., 2001).

1.3 Sediment Properties ~ Erosion

As stated previously, not all sediment is deposited and consolidated on the seabed. When the bottom shear stress, caused by the friction of water flowing over the bed surface, exceeds the seabed's resistance to erosion, sediment is resuspended (Whitehouse, 2000). Laboratory experiments have shown that the erosive potential of a mud matrix can be correlated to bed density (Thorn and Parsons, 1980), but grain size, degree of aggregation, sediment fabric, deposition/erosion history, and organic constituents also need to be considered. This concept differs from non-cohesive sandy systems where the erodibility of the seabed depends primarily on grain size. Density and consolidation of the cohesive grains is crucial in determining the magnitude of the critical shear stress needed for erosion and resuspension.

The greater the shear stress of water acting on the sediment surface, the higher the erosion potential. If the stress produced by the velocity of the wave orbitals and/or currents continues to increase, erosion and resuspension will continue until a maximum critical shear stress threshold is reached or the sediment matrix is consolidated enough to where the critical erosion shear stress of the bed is no longer exceeded by the externally imposed bed stress (Whitehouse, 2000). In estuarine systems, Dyer (1995) found that erodibility could be closely related to the nature of the bed layers existing very near the surface of the seabed. The author found that at slack water two bed layers were present, a thin fluid type mud and the underlying firm consolidated bed. The upper layer of fluid mud was found to be easily erodible and resuspended by incoming tides. Conversely, the lower unit was more difficult to erode, needing more intense conditions (i.e. storms, biological reworking, and extreme tides) with higher stresses to invoke sediment resuspension (Dyer, 1995).

1.4 Biostabilization and Biodestabilization.

Biostabilizers of the seabed have been documented for decades and are effective at reducing sediment erodibility by stabilizing the surface. Various studies over time have researched the impact of the mucilaginous secretions, known as extracellular polymeric substances (EPS), produced by diverse benthic creatures (Young and Southard, 1978; Dade et al., 1996; Taylor and Paterson, 1998; Noffke et al., 2001; Tolhurst et al., 2002). Organisms such as microalgae, worms, and crustaceans can pelletize sediment as they feed as well as excrete a protective adhesive matrix that allows for increased organism mobility, habitat protection, and desiccation prevention. The mucous layer can bind the sediment particles and strengthens the upper seabed matrix, thereby decreasing the rate of erosion acting upon the surface (Whitehouse, 2000). Dade et al. (1996) analyzed how *Alteromonas atlantica*, common marine benthic

bacteria, affected kaolinite clay in terms of yield stress. The authors found that as the bacteria began to secrete the exopolymer glue, the natural cohesive kaolinite particles became more resistant to shear stress resuspension. Fecal pellets and pseudofeces, often defined as biodeposition, can also have an impact on erodibility of the seabed, where it can either increase or decrease erosion (Whitehouse, 2000; Dickhudt, 2009). Dickhudt (2009) stated that pelletization of the seabed could be the cause of varying rates of erodibility within the York River. The author found that when erodibility of the seabed was low, the surficial sediment of the cores was dominated by fecal pellets; whereas at times of high sediment erosion, less strongly aggregated fine-grained sediment was prevalent with little to no fecal pellets present (Dickhudt, 2008).

Conversely, benthic organisms can have the opposite effect on the seabed by altering the bed roughness and erodibility potential of the surface sediment. As organisms create burrows, travel, or forage for food, the sediment may become weakened and susceptible to erosion (Eckman et al., 1981). The destabilization impact on the seabed can be a function of the population density of the benthic organisms, as well as seasonality (Schaffner et al., 2001; Anderson, 2005). In addition, as benthic activity intensifies and the degree of bioturbation increases, the friction of the seabed and the overlying water flow is altered and ultimately the amount of sediment resuspended may increase (Widdows et al., 2000; Patterson et al., 2000). A previous study of the Ems Dollard estuary in the Netherlands showed the impact of a benthic amphipod, *Corophium volutator*, on sediment transport (Kornman and deDeckere, 1998). The authors found that in 1996 the sediment erodibility within the estuary was significantly different between March and August due to biological activity. A March diatom bloom resulted in high levels of EPS concentrations within the sediment, which seemed correlated to the documented

decrease in suspended sediment concentrations within the study area. As the diatom adhesive EPS matrix degraded and amphipod bioturbation and grazing increased, the sediment concentration within the Ems Dollard estuary increased, linking the impacts of biological and physical forcings of fine-grained systems (Kornman and deDeckere, 1998).

1.5 Turbidity Maxima

Fine sediment resuspension is commonly noted within estuarine turbidity maxima (ETMs) (Geyer, 1993; Dyer, 1995). Residual water circulation and salinity fronts are thought to be the primary mechanisms for forming ETMs in partially-mixed estuaries, while tidal asymmetry is thought to be increasingly important as tidal energy increases (Dyer, 1986; Geyer, 1993). Classically, the ETM in partially-mixed estuaries is a region of high-suspended sediment concentrations that results from convergence near the salt limit (Postma, 1967; Burchard et al., 2004). In the York River, a primary ETM is often present near the head of salt in the region of the confluence of the Pamunkey and Mattaponi Rivers. Lin and Kuo (2001) found that the York's primary ETM is formed by both gravitational circulation and tidal asymmetry, with an additional factor being the inhibition of turbulence by estuarine stratification. The ETM often moves with the tides, with the location further upstream after the flood tide and downstream after ebb tide (Dyer, 1995). Tides provide the main source of energy for the ETM for short-term resuspension, with spatial evolution of the ETM occurring in response to changes in river discharge and the spring-neap cycle, and drastic changes of the ETM occurring during major storms and floods.

In addition to primary turbidity maxima, some estuaries can develop a secondary turbidity maximum (STM). Estuaries such as the Hudson River, Danshuei River, Paxtuxent

River, and the York River have all had STMs documented (Roberts and Pierce, 1976; Geyer et al., 2001; Lin and Kuo, 2003). Lin and Kuo (2003) found that the STM in the York River Estuary is formed as a result of four major mechanisms: resuspension of bottom sediments, bottom residual flow convergence, tidal asymmetries, and the suppression of turbulent diffusion due to stratification of the water column. The York River STM identified by Lin and Kuo (2001) is generally located about 40 kilometers up estuary, near the area known as Clay Bank. Because of channel shoaling in the region, this location is conducive to STM development as it is often a stratification transition zone from well-mixed to partially stratified (Lin and Kuo, 2003). Generally, STMs are ephemeral features whose appearance are largely controlled by the spring-neap tidal cycle and riverine discharge (and the effects of each on the estuarine salinity field). Both ETMs and STMs contain high amounts of mobile fine sediment that is constantly being deposited, reworked, and resuspended back into the water column. The sediment mass of the turbidity maximums are variable and dependent on hydrodynamic, seabed, and biological factors.

1.6 Acoustic Mapping

Over the past two centuries, hydrographic surveys have been conducted to map bathymetry of the world's oceans, coasts, and navigable waterways (Van Der Wal and Pye, 2003). Early mapping techniques utilized lead lines or sounding poles with triangular positioning in order to capture sounding depths (Cohen, 1970; Gustavson, 1975). With the advent of acoustic technology, new mapping tools became available to increase the accuracy of bathymetric maps using echo-sounders (Wright and Bartlett, 2000; Van Der Wal and Pye, 2003). Further advances in technology led to a shift to digital from paper data and allowed for a greater resolution via the development of swath bathymetry, airborne laser, sidescan sonar, etc. Currently, many regions

worldwide, especially estuaries due to their direct impact on human health, recreation, and industry, are being heavily surveyed. Regions such as San Francisco Bay, Narragansett Bay, Tay Estuary, and the Hudson River are prime examples of extensively mapped areas (Valente et al., 1992; Wewetzer and Duck, 1999; Foxgrover et al., 2004; Levinton and Waldman, 2006). Levinton and Waldman (ed., 2006) compiled various mapping studies to capture the dynamic interdisciplinary nature of the Hudson River Estuary, evaluating parameters ranging from sub-bottom seismics and surface bathymetry, to contaminant distribution and biological influences. By taking into account bathymetry, sub-bottom profiles, and sidescan imagery, scientists were able to infer and understand more about the Hudson system than if they only had one data set (Bell et al., 2006).

The timing of the mapping surveys is very important, and extreme events and extraneous conditions need to be taken into account while processing the data (Hardisty, 2007). Often these mapping efforts are time consuming and capture a snapshot in time; however, the spatial extent of the acoustic surveys greatly exceeds what is possible via a typical coring field study. By using swath bathymetry, chirp, and sidescan, one is able to get a detailed image of the seabed on a large spatial scale, but depending on the frequency of sampling, not always a good temporal trend. Within the last few years, scientists have begun deploying rotary sonars on the seabed in order to gain temporal information of particular areas of interest in various environments (Hay and Wilson, 1994; Irish et al., 1999; Mayer et al., 2007; Cheel and Hay, 2008). For example, Cheel and Hay (2008) used a rotating sonar to investigate how directional properties of incident waves affected cross-ripple bed formation. They captured 8-meter diameter images of the seabed at 30-minute intervals during quiescent times and every 10 minutes during storm events. By monitoring the seabed on a sub-hourly basis during 11 storms, Cheel and Hay (2008) were

able to relate changes of the seabed to unimodal incident wave directions. The combination of spatial and temporal studies is crucial for a detailed understanding of sediment transport and variable seabed changes, as well as providing valuable information to allow for better public policy and comprehension of the world's waterways.

1.7 Isotope Dating

In order to estimate the sediment mixing and accumulation rates occurring within a particular system, including biological effects, researchers have utilized particle-reactive radionuclides such as ^7Be and ^{137}Cs as chronological dating tools. ^7Be (53.3 day half-life) is useful in determining short-term rates of accumulation, seabed mixing and erosion (Dibb and Rice 1989a; Dibb and Rice, 1989b; Wallbrink and Murray, 1993; Cornett et al., 1994; Clifton et al., 1995; Papastafanou et al., 1995; Feng et al., 1999), while ^{137}Cs (30.13 year half-life) is better suited for detecting yearly and decadal changes within the seabed (Papastafanou et al., 1995; Kostaschuk et al., 2008). ^7Be is a naturally occurring radioisotope, formed by nuclear spallation as a consequence of secondary cosmic rays neutrons bombarding oxygen and nitrogen. ^7Be is usually produced in the stratosphere; however, a minimal portion of the isotope is created in the troposphere (Turekian et al. 1983). In order for the cosmogenic nuclides to be transported to earth, the isotopic particles circulate from the stratosphere to the troposphere where they attach to aerosols and are deposited on earth generally by precipitation (Kim et al., 2000). Most commonly, the stratosphere-troposphere mixing occurs during the spring and fall. At this time the layer between the two atmospheric layers, the tropopause, thins and allows for a greater amount of gas exchange to occur between the two layers (Turekian et al. 1983; Kim et al., 2000; Grew, 2002).

Unlike the naturally occurring radioisotope ^7Be , ^{137}Cs is a thermonuclear byproduct. When nuclear weapons were tested throughout the 1950's and 1960's, large quantities of ^{137}Cs were released into the atmosphere until atmospheric H-bomb testing ceased in 1972 (Sharma et al., 1987; Walling et al., 1999). The rates of atmospheric fallout varied over time but it was determined that the peak nuclear fallout occurred in 1963 ± 2 years (Sharma et al., 1987). The max ^{137}Cs atmospheric fallout generally corresponds with the highest Cs activities present in the sediment, allowing this radioisotope to be used as a dating horizon marker. The novel approach to the 1963 marker application is the ^{137}Cs has the monitoring ability to date upward mixing bioturbation (Bradshaw et al., 2006). Furthermore, ^{137}Cs has been found to be a valuable tool in bioturbation studies, especially in fine-grained environments because of the easy absorption of the nuclide to clay particles and organic matter (Robbins et al., 1979).

1.8 High-Resolution Core Characterization Methods

Within the last few decades, modern core logging systems have been developed to allow for continuous high-resolution data collection and incorporating multiple sensors capable of measuring a variety of parameters (Gunn and Best, 1998). The VIMS GEOTEK core logger is outfitted with gamma-ray attenuation, P-wave velocity, and color spectrophotometer sensors. The gamma-ray sensor allows for measurements of sediment bulk density, porosity, and water content (Weber et al., 1997; Best and Gunn, 1999). The P-wave velocity sensor helps determine variations in grain size, assess core quality, and, along with the gamma-ray sensor, helps provide information needed to construct synthetic seismograms of the sediment core (Weber et al., 1997; Best and Gunn, 1999). Lastly, the color spectrophotometer is able to detect small-scale changes in sediment color variability, and if applicable identify paleoclimatic cycles and events (Rothwell and Rack, 2006). In 2004, Carbotte et al. combined geophysical mapping data (chirp and

sidescan) with a collection of shallow gravity cores to look at environmental changes within the Hudson River estuary. Measurements of p-wave velocity, magnetic susceptibility, and gamma-ray attenuation were determined with a GEOTEK core logger. By combining the mapping and core logging data sets, the authors were able to map fossil oyster beds throughout the estuary and found that anthropogenic influences significantly impacted the paleo-oyster beds and the estuarine environment overall (Carbotte et al., 2004)

In muddy environments, visualization of the core sediment may not reveal as much information as a core collected within a sandy environment, due to the opacity of the sediment (Rothwell and Rack, 2006). Therefore, x-radiography has been utilized to envision bed structures and infer fine-scale density changes within fine-grained cores, which cannot be seen with the naked eye. Through the use of x-ray technology, processes such as sediment deposition, bioturbation, physical alteration, and erosion can be better recognized. Dickhudt (2008) collected x-rays concurrently with erosion cores, in order to compare properties of the seabed to the dominating physical and biological parameters of the study areas within the York River estuary. In the study, the author identified two end-member x-ray types, which were categorized by the dominating forces acting on the sediment bed. Laminated x-rays from Gloucester Point and Clay Bank were inferred to represent recent deposition and the samples were thought to be controlled by physical forcings. Laminated x-rays either had few to no bioturbators, or the physical parameters overwhelmed any biological activity at that site. Conversely, benthic biologically dominated systems produced mixed or mottled x-rays, indicating either high amounts of biotic influence or little to no recent sediment deposition (Dickhudt, 2008).

1.9. Estuarine Sediment Transport Modeling.

When sedimentological data is combined with mathematical modeling, scientists can develop a deeper understanding of how various factors are likely to influence the estuary and seabed. When modeling estuarine sediment transport, it is important to understand the hydrodynamics of the system, as well as the physics behind each transport mechanism. Sediment transport can be modeled various ways and in different dimensions, such as 3D, 2DH (horizontal), 2DV (vertical), 2D 2 layer, 1D, point models, and Lagrangian (particle) models (Whitehouse, 2000; Hardisty, 2007). Field data can be used to constrain sediment transport models, for example by helping to define sources of mud or providing measurements of suspended sediment concentrations for calibration. Field measurements can be used to adjust the model in order to provide a more realistic concept of the influencing parameters within an estuary, and the model can be utilized to predict the rate of sediment transport, along with locations of erosion and deposition. If field data is unavailable, mathematical models can still help determine dominant parameters within a system or set up various schematic tests to help in assessing hypotheses (Whitehouse, 2000).

In 2008, Rinehimer applied 1D and 3D models to the York River estuary focusing on sediment transport in this muddy fine-grained environment. The models were implemented specifically to look at feedback mechanisms between sediment flux and erodibility. The 1D model focused on the sensitivity of erodibility to forcing and bed parameters of the model and the influence of spatial and seasonal variations. Rinehimer et al. (2008) found that when the cohesive sediment bed model was implemented for the York River, it performed well when a constant erosion rate parameter was utilized in conjunction with a depth-varying critical erosion shear stress. Furthermore, it was documented that the spring-neap tidal cycle impacted erodibility and bed consolidation, which then fed back to influence turbidity (Rinehimer et al.,

2008). The 3D model calculated sediment concentrations and erodibility throughout the estuary and compared the results to observational data collected by Dickhudt (2008) (Rinehimer, 2008). By using an average grid spacing of 170 meters along-channel and 140 meters across-channel, the ROMS model was run for a 200-day period that coincided with field data collection. Rinehimer (2008) found that areas of persistently high concentration in the York River near Clay Bank were associated with transport convergence zones, recent deposition, and high bed erodibility.

1.10. Study Area

Over the years, many research projects have been conducted within the York River (Figure. 1-1) making it an increasingly well-documented study locale. Though the studies have ranged from biological fauna to watershed management, many have looked at the physical and geologic properties of the estuary. Most recently, these research initiatives have included various interdisciplinary components. Examples include research focusing on the biological and physical controls on seabed properties within the estuary (Dellapenna et al., 1998, 2003; Schaffner et al., 2001; Hinchey, 2002; Kniskern and Kuehl, 2003), tidal asymmetry, bed stress and stratification (Friedrichs et al., 2000; Kim et al., 2000; Scully and Friedrichs, 2003), turbidity maxima (Lin and Kuo, 2001; Lin and Kuo, 2003; Romine, 2004), and controls on bed erodibility and settling velocity (Friedrichs et al., 2008; Dickhudt et al., 2009, 2011; Cartwright et al., 2009, 2011).

The York River is a partially mixed sub-estuary of the Chesapeake Bay that extends 56 kilometers from the Bay to the confluence of the Pamunkey and Mattaponi Rivers. Although microtidal, the tidal currents within the river, particularly in the middle and upper portions of the

estuary, have been documented as being strong enough to regularly resuspended bottom sediments (Dellapenna et al., 1998). The main channel of the estuary averages about 10 meters in depth and is thought to be controlled by antecedent geology of an incised Paleo-river valley (Carron, 1976). The main channel bifurcates near Page's Rock Light and a shallower (~ 5 meter deep) secondary channel, which is considered partially abandoned, extends northward on the western flank of the main channel (Dellapenna et al., 2003). Two shoals flank the channels and have an average depth of ~ 2 meters.

Researchers have found that physical seabed processes dominate in the upper regions of the York River estuary, whereas biological processes are more dominant closer to the mouth (Kniskern and Kuehl, 2003) (Dellapenna et al., 1998). Schaffner and Dellapenna (Dellapenna et al., 1998; Dellapenna et al., 2001; and Dellapenna et al., 2003), along with other collaborators have done a tremendous amount of research within the York River. The work found that there are several distinct regions in the estuary. The broadest of the generalizations classify the estuary into three areas: upper, middle, and lower York. Due to the influences of river discharge and tidal energies, along with the location of the main estuarine turbidity maximum, little biological reworking takes place in the upper York, and the system there is physically dominated (Figure 1-2.) Conversely, the physical energy decreases further down estuary and biological conditions dominate in the lower York (Schaffner et al., 2001; Dellapenna et al., 2003).

Moving seaward through the middle portion of the York River estuary, the depth and cross-sectional area increase, and the middle York acts as a transition zone between the head and mouth of the estuary. Due to the deeper water and gradients in physical energy, this is often a region of changing stratification and convergent sediment transport (Lin and Kuo, 2001) (Lin and Kuo, 2003). There is also decreased physical reworking of the seabed within the middle part

of the system, and biological activity begins to become more prevalent. Another distinguishing characteristic of the middle part of the estuary is the secondary turbidity maximum (STM). The STM migrates throughout the middle section of the York and is present only at certain periods, typically following periods of increased river discharge. The ephemeral deposition and physical mixing associated with the STM is very intense at the seabed and seasonally creates conditions that are unfavorable to benthic activity (Lin and Kuo, 2003) (Figure 1-3).

Recently, several studies within the MUDBED project have been completed. Both Dickhudt (2008) and Rinehimer (2008) looked at the physical, geologic, and hydrodynamic forces acting upon Gloucester Point and Clay Bank to determine sediment characteristics and bed properties of each region. Dickhudt (2008) measured sediment erodibility of the three main MUDBED study sites over a 14-month time period. Cores were collected throughout the course of the study and spatial and temporal erodibility estimates were calculated using a Gust erosion microcosm. In addition to erodibility measurements, x-radiographs and the solids volume fraction were used to relate geologic facies to sediment transport; the results illustrated that erodibility was found to vary seasonally. High erodibility was associated with the secondary turbidity maxima at Clay Bank, and biological influences had a more systematic impact on the erodibility at Gloucester Point. Incorporating observations collected by Dickhudt, Rinehimer (2008) developed a three-dimensional numerical model to look at erodibility and movement of sediment within the York River estuary. The model showed a transient layer of sediment that moved in and out of the mid-estuary STM, and overall the model calculations appeared to be reproduce observed patterns. Rinehimer's results suggested that the ephemeral deposits of mud driving the STM tend to accumulate on the SW flank of the main channel, presumably as a result of lateral circulation patterns.

1.11. Overall Aim and Organization

This study focuses on a tidally energetic, fine-grained estuary, to assess and evaluate sediment erosion and deposition as a part the large cooperative and interdisciplinary investigation Multi-benthic Benthic Exchange Dynamics (MUDBED) project. The Clay Bank region of the York River was surveyed over several years to investigate a variety of time scales acting upon the surface of the seabed in a muddy, cohesive environment. The overall purpose is to assess patterns of deposition, erosion, and biological reworking on very short time scales (hourly/daily) (Chapter 2), as well as weekly (Chapter 3) and seasonal (Chapter 4) timescales. By investigating the spatial and temporal sediment deposition/erosion/biological reworking patterns, we aim to provide a greater understanding of sediment properties and their relationship with bed erodibility and hydrodynamic variability in cohesive estuarine environments.

By studying various physical and biological parameters in the York River estuary, we can ultimately use them to increase our knowledge of the relationships among sediment facies, seabed erodibility, and the recent history of deposition, erosion, and biological reworking on larger scales elsewhere. For example, current invasive techniques for measuring erodibility cannot easily be expanded to broader scales, but acoustic measurements ground-truthed with sedimentological data can potentially be used as a proxy for such key seabed properties over much more expansive spatial scales.

The results of this effort are presented in the following chapters. Chapter Two used a rotary sonar to document hourly and daily changes of the seabed by utilizing a furrow, or longitudinal sedimentary bedform, to identify period of erosion and deposition. Using a rotary sonar system both qualitatively and quantitatively can capture seabed changes at hourly and daily timescales, which are often missed when conducting cruise field surveys. Furthermore, a

methodology was created to analyze sediment bed erosion and deposition within a muddy environment, where rotary sonars are typically not employed, while incorporating a real-time component that allows fine tuning of the instrument in order to achieve optimal seafloor images.

Chapter Three evaluates changes in bed conditions and properties over the course of dissipation of a secondary turbidity maximum on a weekly time scales. The study aimed to look at identifying key differences in the bed and/or hydrodynamics for low versus high erodibility cores and determining if consolidation could be documented and measured as the spring freshet dissipates throughout the estuary, with samples being collected at the Clay Bank region. By investigating sediment properties, including grain size, organic and water content, ^{7}Be activity, along with sediment matrix and resilient pellet content, a weekly short-term analysis documents appropriate parameterization of time-dependent erodibility of muddy seabeds, thereby providing an improved understanding and accurate modeling of sediment dynamics.

Chapter Four presents a seasonal survey of bathymetric changes of the Clay Bank region of the York River Estuary aimed to better understand spatial sediment deposition patterns and associated sediment-trapping mechanisms in the central portion of a tidally energetic partially mixed estuary. Utilizing an interferometric swath system, high-resolution bathymetry was obtained for seven surveys over a one-year period. Overall, the cumulative Clay Bank bathymetric data set provides a comprehensive bathymetric change analysis, not often conducted in estuarine environments, contrasting monthly changes of seabed elevation as it related to the presence of the secondary turbidity maximum zones.

References

- Andersen, T.J., 2001. Seasonal Variation in Erodibility of Two Temperate, Microtidal Mudflats. *Estuarine Coastal and Shelf Science* 53, 1-12.
- Bell, R.E., Flood, R.D., Carbotte, S., Ryan, W.B.F., McHugh, C., Cormier, M., Versteeg, R., Bokuniewicz, H., Ferrini, V.L., Thissen, J., Ladd, J.W., Blair, E.A., 2006. Benthic Habitat Mapping in the Hudson River Estuary, in: Levinton, J.S., Waldman, J.R. (Eds.), *The Hudson River Estuary*. Cambridge, New York, pp. 51-64.
- Best, A.I., Gunn, D.E., 1999. Calibration of marine sediment core loggers for quantitative acoustic impedance studies. *Marine Geology* 160, 137-146.
- Betteridge, K.F.E., Williams, J.J., Thorne, P.D., Bell, P.S., 2003. Acoustic instrumentation for measuring near-bed sediment processes and hydrodynamics. *Journal of Experimental Marine Biology and Ecology* 285-286, 105-118.
- Bradshaw, C., Kumblad, L., Fagrell, A., 2006. The use of tracers to evaluate the importance of bioturbation in remobilizing contaminants in Baltic sediments. *Estuarine Coastal and Shelf Science* 66, 123-134.
- Burchard, H., Bolding, K., Villarreal, M.R., 2004. Three-dimensional modelling of estuarine turbidity maxima in a tidal estuary. *Ocean Dynamics* 54, 250-265.
- Caiti, A., 2006. *Acoustic Sensing Techniques for the Shallow Water Environment*. Springer, New York.
- Carbotte, S.M., Bell, R.E., Ryan, W.B.F., McHugh, C., Slagle, A., Nitsche, F., Rubenstone, J., 2004. Environmental change and oyster colonization within the Hudson River estuary linked to Holocene climate. *Geo-Marine Letters* 24, 212-224.
- Carron, M.J., 1976. *Geomorphic Processes of a Drowned River Valley: Lower York River Estuary, Virginia*. , 115. M.S. thesis, Virginia Institute of Marine Science/School of Marine Science, The College of William and Mary, Virginia.
- Cheel, R.A., Hay, A.E., 2008. Cross-ripple patterns and wave directional spectra. *Journal of Geophysical Research* 113.
- Clifton, R.J., Watson, P.G., Davey, J.T., Frickers, P.E., 1995. A study of processes affecting the uptake of contaminants by intertidal sediments, using the radioactive tracers: ^7Be , ^{137}Cs and unsupported ^{210}Pb . *Estuarine Coastal and Shelf Science* 41, 459-474.
- Cohen, P.M., 1970. *Bathymetric Navigation and Charting*. United States Naval Institute, Annapolis.

- Cornett, R.J., Chant, L.A., Risto, B.A., Bonvin, E., 1994. Identifying Resuspended Particles Using Isotope Ratios. *Hydrobiologia* 284, 69-77.
- Dade, W.B., Self, R.L., Pellerin, N.B., Moffet, A., Jumars, P.A., Nowell, A.R.M., 1996. The effects of bacteria on the flow behavior of clay-seawater suspensions. *Journal Of Sedimentary Research* 66, 39-42.
- Dellapenna, T.M., Kuehl, S.A., Schaffner, L.C., 1998. Sea-bed Mixing and Particle Residence Times in Biologically and Physically Dominated Estuarine Systems: a Comparison of Lower Chesapeake Bay and the York River Subestuary. *Estuarine Coastal and Shelf Science* 46, 777-795.
- Dellapenna, T., Kuehl, S., Pitts, L., 2001. Transient, longitudinal, sedimentary furrows in the York River Subestuary, Chesapeake Bay: Furrow evolution and effects on seabed mixing and sediment transport. *Estuaries and Coasts* 24, 215-227.
- Dellapenna, T.M., Kuehl, S.A., Schaffner, L.C., 2003. Ephemeral deposition, seabed mixing and fine-scale strata formation in the York River estuary, Chesapeake Bay. *Estuarine Coastal and Shelf Science* 58, 621-643.
- Dibb, J.E., Rice, D.L., 1989. The geochemistry of beryllium-7 in Chesapeake Bay. *Estuarine Coastal and Shelf Science* 28, 379-394.
- Dibb, J.E., Rice, D.L., 1989. Temporal and spatial distribution of beryllium-7 in the sediments of Chesapeake Bay. *Estuarine Coastal and Shelf Science* 28, 395-406.
- Dickhudt, P.J., 2008. Controls on erodibility in a partially mixed estuary: York River, Virginia. M.S. thesis, Virginia Institute of Marine Science/School of Marine Science, The College of William and Mary, Virginia
- Dyer, K.R., 1995. Sediment Transport Processes in Estuaries, in: Perillo, G.M.E. (Ed.), *Geomorphology and Sedimentology of Estuaries*. Elsevier Science, Amsterdam, pp. 423-446.
- Dyer, K.R., 1986. *Coastal and Estuarine Sediment Dynamics*. Wiley, Chichester; New York.
- Eckman, J.E., Nowell, A.R.M., Jumars, P.A., 1981. Sediment destabilization by animal tubes. *Journal of Marine Research* 39, 361-374.
- Evans, H.B. 1965. GRAPE — A device for continuous determination of density and porosity. *Proceedings of the 6th Annual SPWLA Logging Symposium*. 2, B1-B25. Society of Professional Well Log Analysts, Dallas, TX
- Foxgrover, A.C., Higgins, S.A., Ingraca, B.E., Jaffe, B.E., Smith, R.E., 2004. Deposition, erosion, and bathymetric change in south San Francisco Bay: 1858-1983. USGS Open-File Report 2004-1192.

- Friedrichs, C.T., Cartwright, G.M., Dickhudt, P.J., 2008. Quantifying benthic exchange of fine sediment via continuous, non-invasive measurements of settling velocity and bed erodibility. *Oceanography* 21, 168-172.
- Geotek., 2008. Multi-sensor Core Logger Manual Geotek, Northamptonshire, UK.
- Geyer, W., 1993. The importance of suppression of turbulence by stratification on the estuarine turbidity maximum. *Estuaries and Coasts* 16, 113-125.
- Gustavson, T.C., 1975. Bathymetry and sediment distribution in proglacial Malaspina Lake, Alaska. *Journal of Sedimentary Research* 45, 451-461.
- Hardisty, J., 2007. *Estuaries : Monitoring and Modeling the Physical System*. Blackwell Publ., Malden, Mass.
- Hawkesworth, C.J., 2003. Grew, E.S. (Ed.) *Beryllium Mineralogy, Petrology, and Geochemistry: Reviews in Mineralogy and Geochemistry*, 50, Washington, D.C. 824-825.
- Hay, A.E., Wilson, D.J., 1994. Rotary sidescan images of nearshore bedform evolution during a storm. *Marine Geology* 119, 57-65.
- Heezen, B.C., Tharp, M., 1957. Physiographic diagram, Atlantic Ocean (sheet 1).
- Hill, P. S. and I. N. McCave. 2001. Suspended particle transport in benthic boundary layers. In *The Benthic Boundary Layer: Transport Processes and Biogeochemistry*, edited by B. P. Boudreau and B. B. Jorgensen. Oxford University Press, pp. 78-103.
- Irish, J.D., Lynch, J.F., Traykovski, P.A., Newhall, A.E., Prada, K., Hay, A.E., 1999. A Self-Contained Sector-Scanning Sonar for Bottom Roughness Observations as Part of Sediment Transport Studies. *Journal of Atmospheric and Oceanic Technology* , 1830-1841.
- Jones, E.J.W., 1999. *Marine Geophysics*. Wiley, Chichester; New York.
- Kennedy, V.S., 1984. *The estuary as a filter*. Academic Press, New York, NY.
- Kim, G., Hussain, N., Scudlark, J.R., Church, T.M., 2000. Factors Influencing the Atmospheric Depositional Fluxes of Stable Pb, ²¹⁰Pb, and ⁷Be into Chesapeake Bay. *Journal of Atmospheric Chemistry* 36, 65-79.
- Kim, S., Friedrichs, C.T., Maa, J.P., Wright, L.D., 2000. Estimating Bottom Stress in Tidal Boundary Layer from Acoustic Doppler Velocimeter Data. *Journal of Hydraulic Engineering; Journal of Hydrologic Engineering*. 126, 399-406.

- Kniskern, T.A., Kuehl, S.A., 2003. Spatial and temporal variability of seabed disturbance in the York River subestuary. *Estuarine Coastal and Shelf Science* 58, 37-55.
- Komar, P.D., 1998. *Beach Processes and Sedimentation*. Prentice-Hall, Upper Saddle River, NJ.
- Kornman, B.A., de Deckere, E.M.G.T., 1998. Temporal Variation in Sediment Erodibility and Suspended Sediment Dynamics in the Dollard Estuary, in: Black, K.S., Paterson, D.M., Kramp, A. (Eds.), *Sedimentary Processes in the Intertidal Zone*, Special Publications 139 ed. Geological Society, London, pp. 231-241.
- Kostaschuk, R., Chen, Z., Saito, Y., Wang, Z., 2008. Sedimentation rates and heavy metals in a macrotidal salt marsh: Bay of Fundy, Canada. *Environmental Geology* 55, 1291-1298.
- Levinton, J.S., Waldman, J.R., 2006. *The Hudson River Estuary*. Cambridge University Press, Cambridge; New York.
- Lin, J., Kuo, A., 2003. A model study of turbidity maxima in the York River estuary, Virginia. *Estuaries and Coasts* 26, 1269-1280.
- Lin, J., Kuo, A., 2001. Secondary turbidity maximum in a partially mixed microtidal estuary. *Estuaries and Coasts* 24, 707-720.
- Maa, J.P.-., Wright, L.D., Lee, C.-., Shannon, T.W., 1993. VIMS Sea Carousel: a field instrument for studying sediment transport. *Marine Geology* 115, 271-287.
- Mayer, L.A., Raymond, R., Glang, G., Richardson, M.D., Traykovski, P., Trembanis, A.C., 2007. High-resolution mapping of mines and ripples at the Martha's Vineyard Coastal Observatory. *IEEE Journal of Ocean Engineering* 32, 133-149.
- McNeil, J., Taylor, C., Lick, W., 1996. Measurements of Erosion of Undisturbed Bottom Sediments with Depth. *Journal of Hydraulic Engineering* 122, 316.
- McNinch, J.E., 2004. Geologic control in the nearshore: shore-oblique sandbars and shoreline erosional hotspots, Mid-Atlantic Bight, USA. *Marine Geology* 211, 121-141.
- Mikkelsen, O. A., P. S. Hill, and T. G. Milligan, 2007. Seasonal and spatial variation of floc size, settling velocity, and density on the Apennine margin (Italy). *Continental Shelf Research*, 27: 417-430.
- Mitra, S., Dellapenna, T.M., Dickhut, R.M., 1999. Polycyclic Aromatic Hydrocarbon Distribution within Lower Hudson River Estuarine Sediments: Physical Mixing vs. Sediment Geochemistry. *Estuarine Coastal and Shelf Science* 49, 311-326.
- Nielsen, P., 1992. *Coastal Bottom Boundary Layers and Sediment Transport*. World Scientific, Singapore; River Edge, N.J.

- Newell, W. L., Clark, I., & Bricker, O. P., 2004. Distribution of Holocene Sediment in Chesapeake Bay as Interpreted from Submarine Geomorphology of the Submerged Landforms, Selected Core Holes, Bridge Borings and Seismic Profiles. US Department of the Interior, US Geological Survey.
- Noffke, N., Gerdes, G., Klenke, T., Krumbein, W.E., 2001. Microbially Induced Sedimentary Structures: A New Category within the Classification of Primary Sedimentary Structures. *Journal of Sedimentary Research* 71, 649-656.
- Olsen, C.R., Larsen, I.L., Lowry, P.D., Cutshall, N.H., Nichols, M.M., 1986. Geochemistry and Deposition of ^7Be in River-Estuarine and Coastal Waters. *Journal of Geophysical Research* 91.
- Olsen, C.R., Larsen, I.L., Mulholland, P.J., Karen L. von Damm, Grebmeier, J.M., Schaffner, L.C., Diaz, R.J., Nichols, M.M., 1993. The Concept of an Equilibrium Surface Applied to Particle Sources and Contaminant Distributions in Estuarine Sediments. *Estuaries* 16, 683-696.
- Papastefanou, C., Ioannidou, A., Stoulos, S., Manolopoulou, M., 1995. Atmospheric deposition of cosmogenic ^7Be and ^{137}Cs from fallout of the Chernobyl accident. *The Science of the Total Environment* 170, 151-156.
- Paterson, D.M., Tolhurst, T.J., Kelly, J.A., Honeywill, C., de Deckere, E.M.G.T., Huet, V., Shayler, S.A., Black, K.S., de Brouwer, J., Davidson, I., 2000. Variations in sediment properties, Skeffling mudflat, Humber Estuary, UK. *Continental Shelf Research* 20, 1373-1396.
- Pointecorvo, B. 1941. Neutron well-logging. *Oil and Gas Journal*, 40, 32-33.
- Porter, E.T., Sanford, L.P., Gust, G., Scott Porter, F., 2004. Combined water-column mixing and benthic boundary-layer flow in mesocosms: key for realistic benthic-pelagic coupling studies. *Marine Ecology Progress Series* 271, 43-60.
- Postma, H., 1967. *Sediment Transport and Sedimentation in the Estuarine Environment*. American Association for the Advancement of Science, Washington, D.C.
- Roberts, W.P., Pierce, J.W., 1976. Deposition in upper Patuxent River Estuary, Maryland, 1968-1969. *Estuarine and Coastal Marine Science* 4, 267-280.
- Rinehimer, J.P., 2008. Sediment transport and erodibility in the York River Estuary : a model study. M.S. thesis, Virginia Institute of Marine Science/School of Marine Science, The College of William and Mary, Virginia
- Rinehimer, J.P., C.K. Harris, C.R. Sherwood, and L.P. Sanford, 2008. Estimating cohesive sediment erosion and consolidation in a muddy, tidally-dominated environment: model

- behavior and sensitivity. *Estuarine and Coastal Modeling, Proceedings of the Tenth Conference, November 5-7, Newport RI. Spaulding, M.L., ed. 819-838.*
- Robbins, J.A., McCall, P.L., Fisher, J.B., Krezoski, J.R., 1979. Effect of deposit feeders on migration of Cesium-137 in lake sediments. *Earth and Planetary Science Letters* 42, 277-287.
- Romine, H.M., 2004. Documenting the suspended and bottom sediment dynamics of a two estuarine turbidity maximum system using ^{10}Be and ^{23}Th . M.S. thesis, Virginia Institute of Marine Science/School of Marine Science, The College of William and Mary, Virginia
- Rothwell, R.G., Rack, F.R., 2006. *New Techniques in Sediment Core Analysis: An Introduction*, in: Rothwell, R.G. (Ed.), *New techniques in sediment core analysis*. The Geological Society, London.
- Schaffner, L.C., Dellapenna, T.M., Hinchey, E., Friedrichs, C.T., Neubauer, M.T., Smith, M.E., Kuehl, S.A., 2001. Physical Energy Regimes, Seabed Dynamics, and organism–sediment Interactions Along an Estuarine Gradient, in: Aller, J.Y., Woodin, S.A., R.C. Aller, R.C. (Eds.), *Organism–Sediment Interactions*. University of South Carolina Press, Columbia, pp. 159-179.
- Scully, M.E., Friedrichs, C.T., 2003. The influence of asymmetries in overlying stratification on near-bed turbulence and sediment suspension in a partially mixed estuary. *Ocean Dynamics* 53, 208-219.
- Sharma, P., Gardner, L.R., Moore, W.S., Bollinger, M.S., 1987. Sedimentation and Bioturbation in a Salt Marsh as Revealed by ^{210}Pb , ^{137}Cs , and ^7Be Studies. *Limnology and Oceanography* 32, 313-326.
- Soulsby, R., 1997. *Dynamics of Marine Sands : A Manual for Practical Applications*. Telford, London.
- Taylor, I.S., Paterson, D.M., 1998. Microspatial Variation in Carbohydrate Concentrations with Depth in the Upper Millimetres of Intertidal Cohesive Sediments. *Estuarine Coastal and Shelf Science* 46, 359-370.
- Thorn, M.F.C., Parsons, J.G. Erosion of cohesive sediments in estuaries: an engineering guide. Proceeding of the 3rd International Symposium on Dredging Technology, British Hydraulics Research Association. Cranfield, UK. .349-358.
- Thorne, P.D., Hanes, D.M., 2002. A review of acoustic measurement of small-scale sediment processes. *Continental Shelf Research* 22, 603-632.
- Tolhurst, T.J., Gust, G., Paterson, D.M., 2002. The Influence of Extracellular Polymeric Substance (EPS) on Cohesive Sediment Stability, in: Winterwerp, J.C., Kranenburg, C.

- (Eds.), *Fine Sediment Dynamics in the Marine Environment*. Elsevier Science, Amsterdam, pp. 409-425.
- Turekian, K.K., Benninger, L.K., Dion, E.P. ^{7}Be and ^{210}Pb Total Deposition Fluxes at New Haven, Connecticut and at Bermuda. *Journal of Geophysical Research* 88.
- Valente, R., Rhoads, D., Germano, J., Cabelli, V., 1992. Mapping of benthic enrichment patterns in Narragansett Bay, Rhode Island. *Estuaries and Coasts* 15, 1-17.
- van Rijn, L., C., 1984a. Sediment Transport, Part II: Suspended Load Transport. *Journal of Hydraulic Engineering* 110, 1613-1641.
- van Rijn, L., C., 1984b. Sediment Transport, Part III: Bed Forms and Alluvial Roughness. *Journal of Hydraulic Engineering* 110, 1733-1754.
- van Rijn, L., C., 1984c. Sediment transport, part I: bed load transport . *Journal of Hydraulic Engineering* 110, 1431-1456.
- Vecchi, R., Valli, G., 1997. ^{7}Be in surface air: A natural atmospheric tracer. *Journal of Aerosol Science* 28, 895-900.
- Wallbrink, P.J., Murray, A.S., 1993. Use of fallout radionuclides as indicators of erosion processes. *Hydrologic Process.* 7, 297-304.
- Walling, D.E., He, Q., Blake, W., December 1999. Use of ^{7}Be and ^{137}Cs measurements to document short- and medium term rates of water-induced soil erosion on agricultural land. *Water Resources Research* 35, 3865-3874.
- Weber, M.E., Niessen, F., Kuhn, G., Wiedicke, M., 1997. Calibration and application of marine sedimentary physical properties using a multi-sensor core logger. *Marine Geology* 136, 151-172.
- Wewetzer, S.F.K., Duck, R.W., 1999. Bedforms of the Middle Reaches of the Tay Estuary, Scotland, in: Rogers, J., Smith, N.D. (Eds.), *Fluvial sedimentology VI* ; International Conference on Fluvial Sedimentology ed. Blackwell Science, Oxford, pp. 33-41.
- Whitehouse, R., 2000. *Dynamics of Estuarine Muds: A Manual for Practical Applications*. T. Telford, London.
- Widdows, J., Brown, S., Brinsley, M.D., Salkeld, P.N., Elliott, M., 2000. Temporal changes in intertidal sediment erodibility: influence of biological and climatic factors. *Continental Shelf Research* 20, 1275-1289.
- Wright, D.J., Bartlett, D.J., 2000. *Marine and Coastal Geographical Information Systems*. Taylor & Francis, London; Philadelphia.

Young, R., Southard, J.B., 1978. Erosion of fine-grained marine sediments: Sea-floor and laboratory experiments. *Geological Society of America Bulletin* 89, 663-672.

York River Estuary, Chesapeake Bay VA, USA

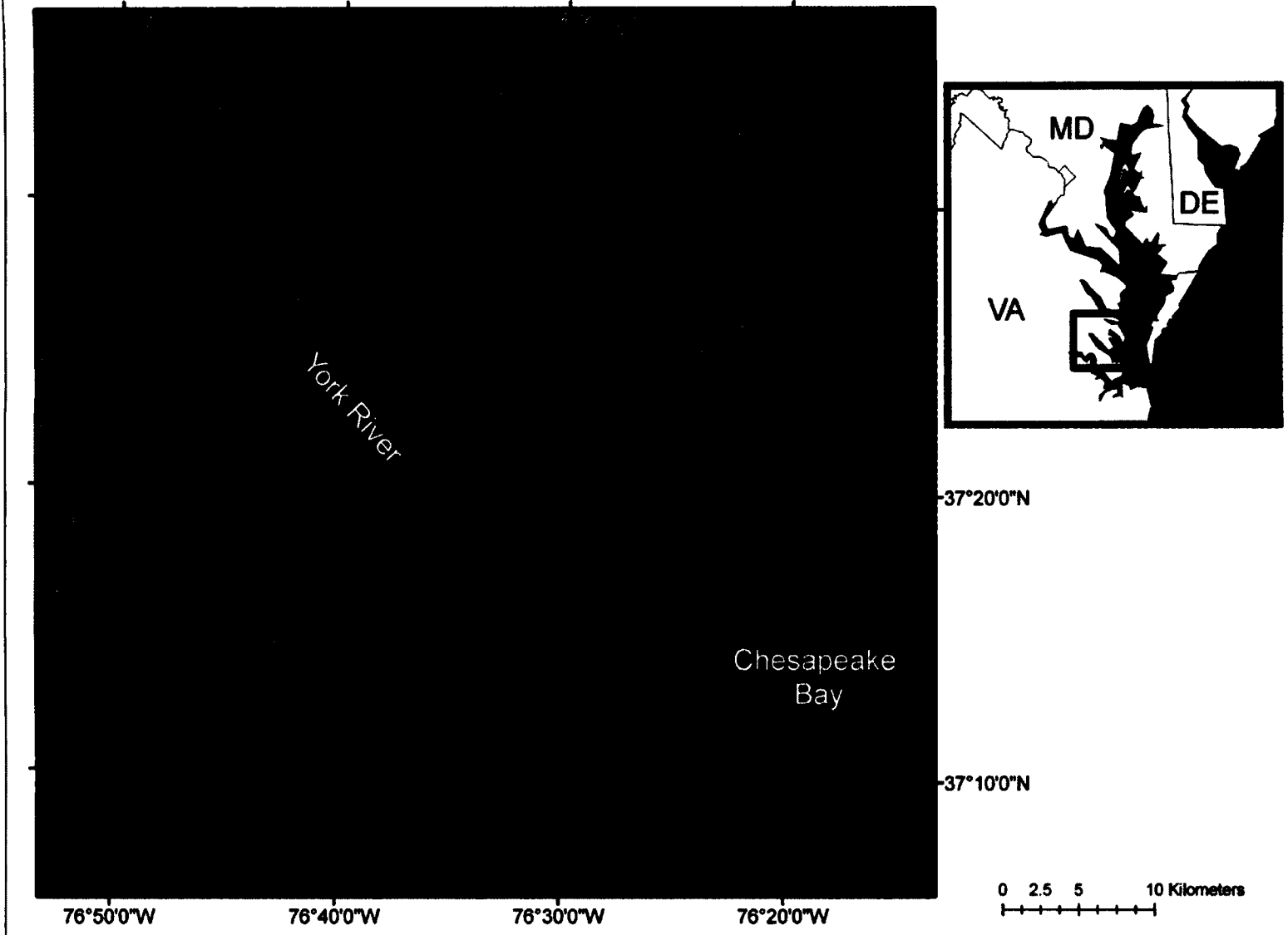


Figure 1-1. Map of York River Estuary. Location of Clay Bank study site indicated by black dot. Locations of US EPA long-term monitoring stations closest to Clay Bank indicated by red squares.

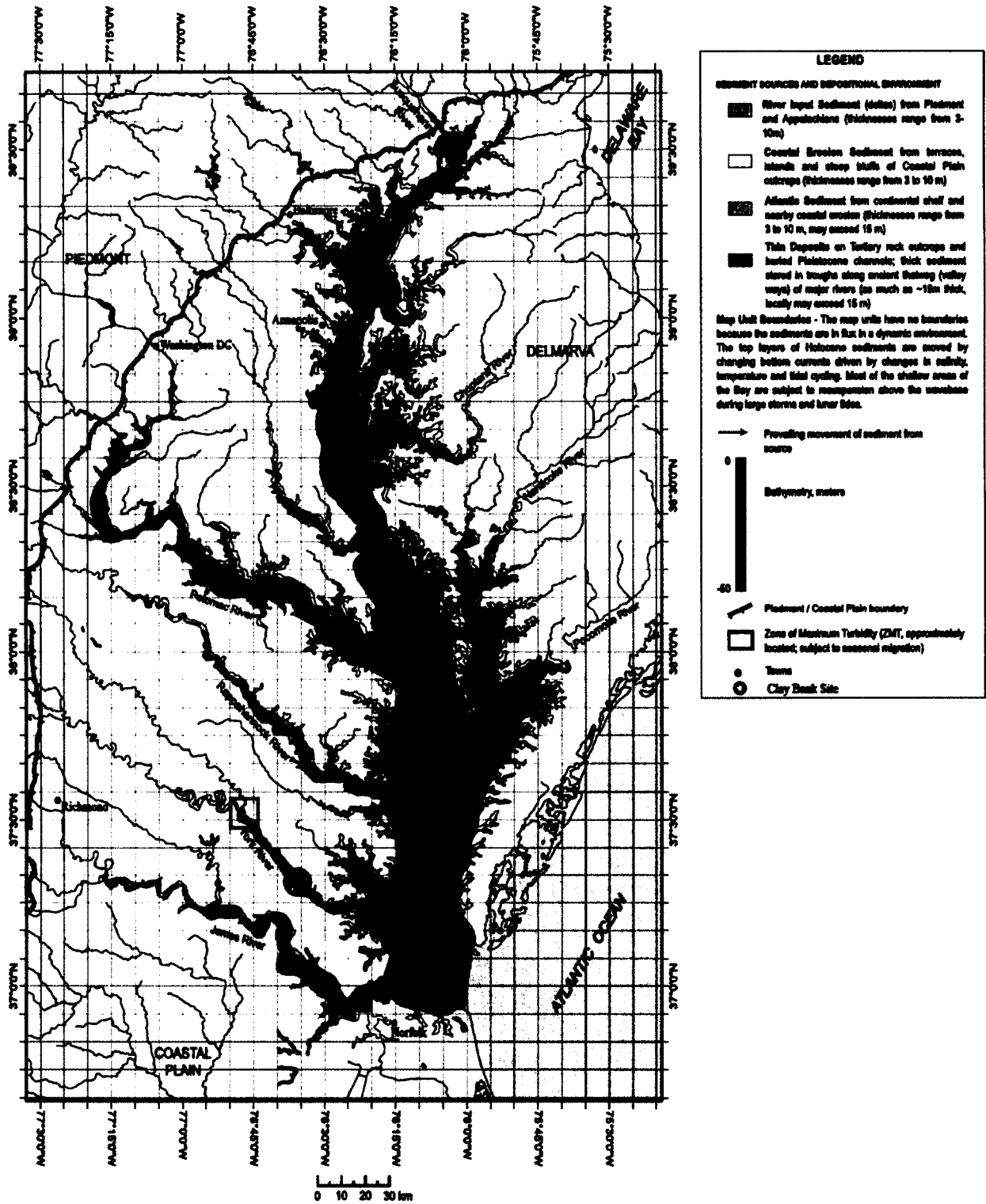


Figure 1-2. Map of Chesapeake Bay, highlighting the bathymetry and turbidity maximum zones throughout the region. The study area is delineated by a star, located in the Clay Bank region of the York River (modified from Newell et al., 2004).

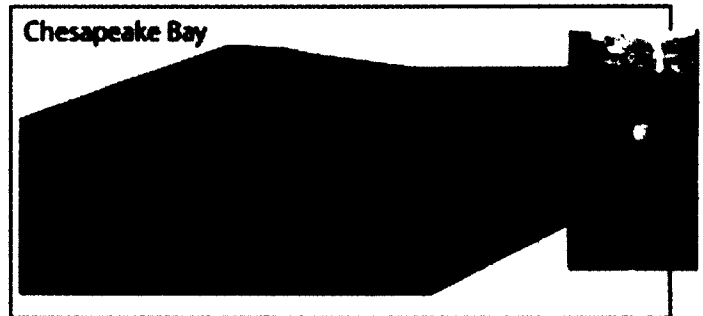
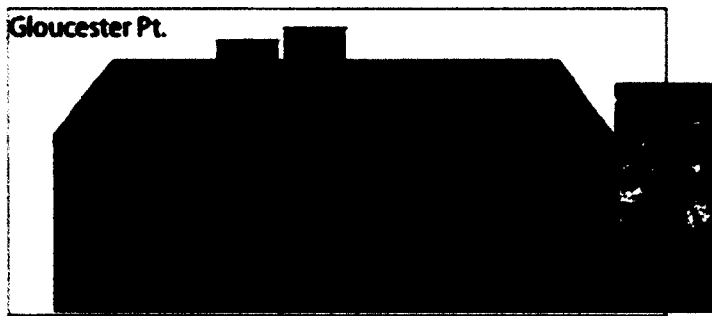
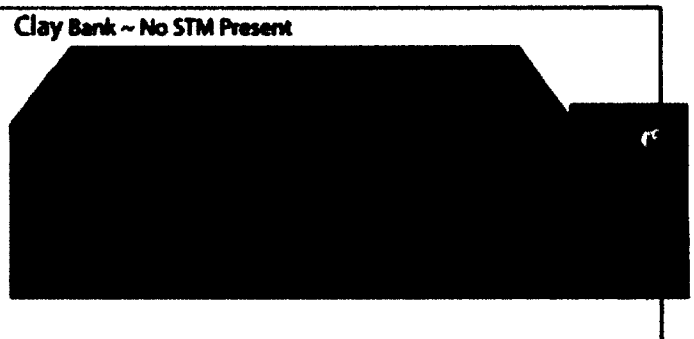
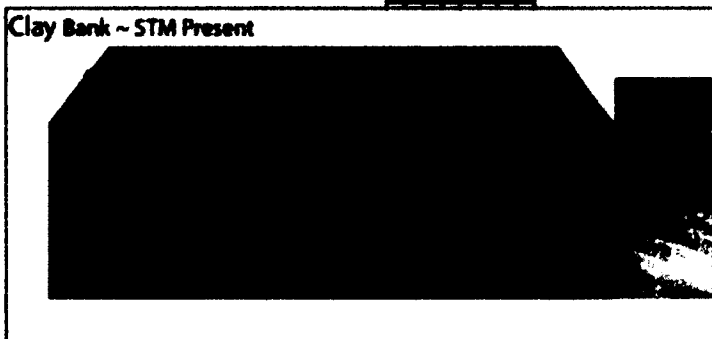
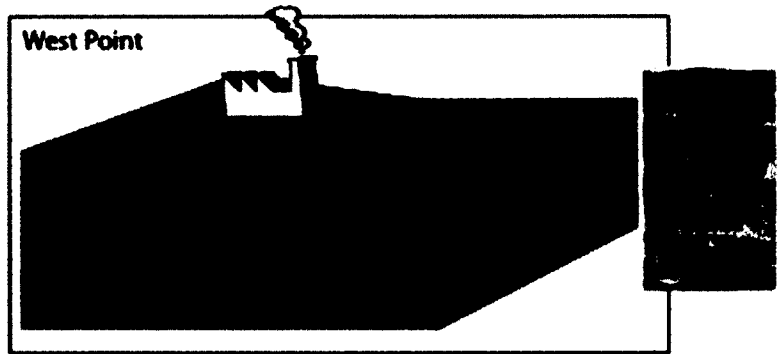
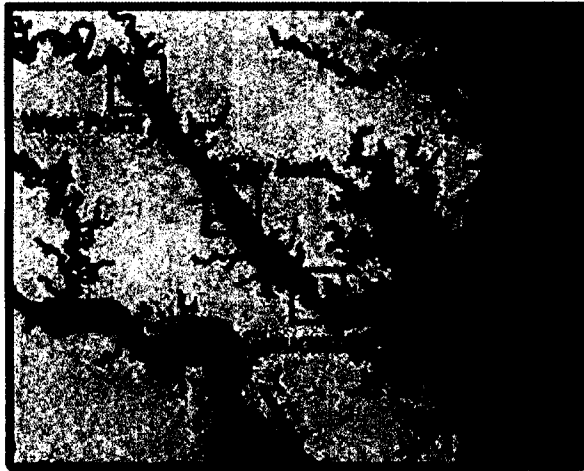


Figure 1-3. The York River biological and physical gradient.
X-rays: West Point ~ June 1981 (Schaffner et al., 2001), Clay Bank STM ~ February 2009, Clay Bank no STM ~ March 2009, Gloucester Point ~ February 2009, and Chesapeake Bay ~ January 1995 (Schaffner et al., 2001)

Chapter 2: Approaches for Quantifying Seabed Morphology – Utilizing a Rotary Sonar System in a Cohesive Estuarine Environment

Abstract:

Resuspension of fine-grained sediments is a critical factor affecting the physical, chemical, and biological health of estuarine and coastal environments. As a part of the MUDBED (Multi-disciplinary Benthic Exchange Dynamics) Project, a multi-frequency/multi-ranging rotary sonar was used to help assess the relationship between seabed properties and resulting bed erodibility in the York River sub-estuary, Chesapeake Bay, VA. A tripod-mounted Imagenex 881A rotary sonar was deployed to obtain 360° surface images on an hourly basis, capturing a nearly continuous time series of side-scan backscatter. Rotary sonar instrumentation is a versatile tool for the observation of seafloor morphology with a wide variety of potential applications. This chapter presents a review of rotary sonar development and implementation, followed by analysis of seafloor morphological evolution based on rotary sonar observations low-energy cohesive environment, the York River Estuary. Optimized parameters were determined for cohesive sediment environments and a real-time observing rotary sonar was created to analyze the seabed on an hourly basis. A methodological approach for rotary sonar deployment, utilization, and data analysis is provided which can also be utilized in other cohesive estuarine environments. Though it can be difficult to utilize rotary sonars in fine grained environments, this study found key tunable parameter sequences for cohesive estuarine environments, including using frequencies of 675 and 1000kHz, 0.5 m above the bed.

2.1 Introduction

Precise observations of the dynamic processes interacting at the sediment-water interface are crucial to understanding seafloor morphology and associated chemical and biological processes. The magnitude and frequency of hydrodynamic forcing often dictates the resulting

morphologic response. Large-scale events, including extratropical storms and nor'easters, can be a catalyst for abrupt changes that may dissipate quickly; conversely, daily processes acting on the seafloor (i.e. tides, waves, and currents) may not provide an instantaneous response, but rather yield gradual changes and environmental modifications over longer timescales. Rotary sonar technology has allowed for precise observations of seabed morphologic evolution.

The transport and fate of seafloor sediments are critical factors affecting the physical conditions, chemical composition, and the biological health of ecosystems, especially in estuaries, along shorelines, and on continental shelf environments (Whitehouse, 2000). The erodibility potential of sediment beds is a complex function of grain size, bed roughness, water content, mineralogical composition, deposition and erosion history, physical water column conditions, and local biological activity (Soulsby, 1997; Whitehouse, 2000). General models of sediment transport relate sediment mobility to hydrodynamic shear stress exerted on the bed by wave orbital and current velocities, the degree to which flow is turbulent, seafloor roughness, and sediment grain size (Soulsby, 1997).

Transport of sands, or non-cohesive sediment ($\leq 10\%$ of grains smaller than $63\mu\text{m}$), is important to understand, as it is vital to harbor development (initial and maintenance dredging), navigational channel administration (safety of commercial shipping and recreational boating), shoreline maintenance (beach nourishment), coastal protection (shoreline structures), engineered structures (platforms and pipelines), benthic habitat assessment, and commercial fisheries management. The sediment dynamics occurring within non-cohesive sandy environments has been relatively well documented (van Rijn, 1984a; van Rijn, 1984b; van Rijn, 1984c; Nielsen, 1992; Soulsby, 1997; Komar, 1998). General models of sediment transport relate sediment mobility to hydrodynamic shear stress exerted on the bed by wave orbital and current velocities,

the degree to which flow is turbulent, seafloor roughness, and sediment grain size (Soulsby, 1997). It is generally understood that the dominant particle size of the bed sediment drives the behavior and distribution of the grains within the system (van Rijn, 1984a; van Rijn, 1984b; van Rijn, 1984c; Nielsen, 1992; Soulsby, 1997; Komar, 1998). Grains larger than 2mm are classified as gravel and their transport behavior is primarily dependent upon bed permeability rather than grain size. In beds composed of mixed sand and mud, the effects of electrochemical and biological cohesion become important to transport processes if the relative mud composition exceeds 10%. Mixed sediments such as these are more resistant to erosion than either pure sands or pure mud (Soulsby, 1997).

In contrast, muds (cohesive sediment) have a “stickiness” that is difficult to define or predict, which fundamentally affects its mobility and transport (Whitehouse, 2000). Less is known about the transport and dynamics of fine-grained sediment, despite the importance of the particle dispersal within these environments. Often a considerable amount of sediment enters the system via surface runoff, riverine input, and oceanic influx. However, the amount of sediment entering tidally energetic estuaries is often much less than that which is found within the water column. Even when sediment input is small, energetic tidal currents and waves can retain or resuspend sediment into the water column. The surplus of sediment in suspension is thought to be due to the repeated resuspension of fine-grained sediment from the seabed (Kennedy, 1984; Dyer, 1986). Large quantities of suspended sediment have negative impacts within an estuary, including enhanced light attenuation, disruption and change of benthic community structure and distribution, modified transport of organic carbon, and changes in the location and duration of eutrophication and hypoxia (Whitehouse, 2000; Hardisty, 2007). In addition, contaminants are often concentrated in fine-grained systems. Due to physio-chemical attraction and large surface

area, these fine cohesive particles are highly susceptible to contaminant adsorption (Olsen et al., 1993; Mitra et al., 1999; Whitehouse, 2000). One method in which sediment transport can be estimated is by observation of the seabed over a variety of timescales. The objective of this paper is to address the use of rotary sonar technology to assess changes in bedform morphology and determine sediment patterns of erosion and deposition within cohesive fine-grained environments.

2.2 Development and Use of Rotary Sonar

In the past, in water SCUBA divers or optical instruments measurements were the only way to determine morphologic seabed changes. Initial field-based attempts to monitor the morphological state and evolution of the seafloor relied on SCUBA divers marking the bed profile on a semi-buried Plexiglas board with a grease pencil (Inman, 1957). This technique was not useful during time of high-suspended sediment concentrations, which obscured diver visibility and resulted in spatially and temporally limited observations due to the relatively short period of time divers could be on the bottom. Data collection was also necessarily limited to fair-weather conditions when diving was safe and bed evolution was least dynamic. Subsequent investigations utilized optical based systems, such as in-situ photography, which allowed for persistent observation of a field site. However, these were also often insufficient to provide consistently clear images of the seabed suitable for morphological interpretation due to the varying conditions of sediment suspension. Acoustic instrumentation overcame these early observational challenges, and over the past fifty years, sonar has become increasingly common in oceanographic research (Blondel, 2009; Irish et al., 1999; Traykovski et al., 1999).

Sonar technology first appeared in the early 1900's as a way to detect icebergs. Interest of the sound navigation and ranging technology increased in the 1910's during the eve of World War I to help military interests detect submarines by means of echolocation (Spindel, 1985). Since that time, towed side-scan sonar units have provided images of the seafloor around the world, with a resolution on the order of centimeters to meters. However towed side scan sonar is not designed for continuous monitoring of a singular site and cannot easily make consistent time-lapse imagery of bed evolution.

Historic Applications of Rotary Sonar

Since the 1970's, rotary sonar technology has been widely used by the offshore community for structural inspection and remotely operated vehicle navigation. Typically supplying a 360° image of the seabed rather than a swath pattern, rotary sonars have provided observations of the seabed morphology, allowing for insight into the acting hydrodynamic regimes affecting the surficial sediment of the seabed (Rubin et al., 1977). Within the scientific community, rotary sonars have primarily provided observations of seafloor morphology supporting investigations of interactions between seafloor sediments and hydrodynamic processes (Rubin et al., 1983). Notable sediment dynamics studies that have incorporated rotary sonar data include the Sandy Duck 97 experiment (Maier and Hay, 2009; Cheel and Hay, 2008; Hay and Mudge, 2005), the Sediment Acoustics Experiments in Florida (SAX99 and SAX04) (Tang et al., 2009; Hay, 2008;) mine burial off Martha's Vineyard (Traykovski et al., 2007), shelf processes at the LEO-15 site in New Jersey (Traykovski, 2007; Irish et al., 1999; Traykovski et al., 1999) continental shelf analysis offshore of California (Irish et al., 1999), lacustrine research (Hay and Wilson, 1994), marine archaeology in the Black Sea (Trembanis et al., 2011), and lab experiments (Lacy et al., 2007).

Of these studies, one of the first was Rubin et al. (1983) who used a rotating side sonar to analyze bedform migration on varying time scales from a fixed point above the bed surface (2 meters) in the San Francisco Bay. Radial scans of the seafloor were taken at several locations for various lengths of time ranging from a few hours up to 8 months. These unique studies characterized both large storm events and longer-term seasonal cycles. Images captured by the instrument revealed ripples (wavelengths $\geq 30\text{cm}$) visible in high-resolution imagery of the seabed on short timescales, while long-term migration of sand waves were documented over an 8 month deployment (Rubin et al., 1983).

A decade later, Hay and Wilson (1994) used a 2.25 MHz rotary sonar offshore of Lake Huron. Images from the instrument showed the movement and transformation of ripples, cross ripples, and megaripples over 1-2 hour time scales within a 10-meter diameter. Also during this time, Irish et al. (1999) utilized rotary sonars to investigate sediment transport and changes in bottom roughness for the STRESS III experiment (Sediment Transport on Shelves and Slopes), off the coast of northern California, the LEO-15 project, located within the mid-Atlantic bight, and lastly as a part of the Strataform project, focused on sediment transport off the coast of the Eel River. They found that even with contrasting environments on the east and west coasts, sector scanning rotary sonars could provide a unique and novel approach to capturing changes of bedform roughness. In contrast, Lacy et al. (2007) used a rotary sonar to look at morphology and evolution of bed forms in a closed, controlled system, specifically a four-meter wide sediment flume subjected to waves and currents. They were able to look at dominant orientation of each bed form and then compare results to previously predicted patterns thought to occur due to various hydrographic regimes and variables.

More recently, long-term or permanent cabled installations of rotary sonars at coastal observatories have become more common. Investigators have used long-term records collected at the Martha's Vineyard Coastal Observatory (Traykovski et al., 1999), the Mid-Atlantic Coastal Ocean Observatory (Traykovski, 2007; Styles and Glenn, 2005), and the Southeast Coastal Ocean Observing System (Voulgaris and Morin, 2008), to investigate existing equilibrium ripple models and develop new non-equilibrium models.

Until recently rotary sonar technology has been underutilized but new studies along with those previously mentioned are demonstrating the potential of this technology to provide transformative insight into the dynamic processes of seabed morphological evolution. For this paper, we present analysis of seafloor morphological evolution based on rotary sonar observations made in the York River Estuary, a low-energy cohesive muddy environment. Additionally, we present a methodological approach for deployment of rotary sonar instrumentation, and analysis of resulting data.

2.3 Study Area- Cohesive Sediment Case Study ~ York River Estuary

The York River Estuary is a tidally-dominated system that forms at the confluence of the Mattaponi and Pamunkey Rivers in southeastern Virginia (Figure 2-1). This tidally-dominated estuary is microtidal (tidal range $\approx 0.7\text{m}$) but the tidal currents within the system have been documented as strong enough to resuspend bottom sediments (Dellapenna et al., 1998, Maa and Kim, 2002). Tidal currents within the river are on average greater than 60 cm s^{-1} but velocities tend to decrease near the river mouth to 40 cm s^{-1} . The York River Estuary is defined as a cohesive sediment environment, with a predominate grain size of less than $63\mu\text{m}$, with muds occasionally exceeding 80% of the total sediment. In terms of sediment resuspension, tides are

generally the dominate processes acting upon the sediment, with waves increasing the erodibility in depths shallower than one meter (Friedrichs, 2009).

The main channel of the York averages 10 meters deep throughout the estuary and is thought to be controlled by antecedent geology of an incised Paleo-river valley (Carron, 1976). A secondary channel also exists in the estuary and begins where the main channel bifurcates near Page's Rock Light. A much shallower channel, which is considered partially abandoned, extends northward on the western flank of the main channel (Dellapenna et al., 2003). Additionally, the secondary channel is significantly shallower than the main channel, reaching an average depth of only 5 meters., Overall the region ranges from 2.5 - 6 meters in depth, is generally free from boat traffic during the winter months, and suitable for instrument deployment and surveying.

Furrows within the York River Estuary have been documented in both the main channel and secondary channel (Dellapenna et al., 2001) near the Clay Bank and Capahosic/Ferry Point regions. Furrows are rectilinear bedforms that are oriented parallel to water flow direction (Dyer, 1982). These sedimentary features were initially documented during a laboratory experiment when Allen (1969) observed them in a non-recirculating flume. The experiment was designed to analyze the effects of bedforms, Reynolds Number, and a mean current velocity. Often observed in depositional areas with occasional strong flow conditions, historically, furrows range from 10s of meters to kilometers long. Additionally, these rectilinear bedforms have dimensions with spacing of 10-100 meters, widths approximately 1/10 of the furrow spacing, and heights reaching 1-2 meters. The sedimentary features are found in various systems around the world, including the deep sea [Titanic (Cochonat et al., 1989), Saharan Rise (Lonsdal, 1978), Bahama Outer Ridge (Flood and Hollister, 1980), and Gulf of Mexico (Bryant et al., 2004)], deep lakes [Lake Superior (Flood, 1989; Viekman et al., 1992)], deltas [Mississippi delta front

(Coleman et al., 1981)], Mediterranean Sea (Puig et al., 2008), and rivers and estuaries [Hudson (Flood and Bokuniewicz, 1986), Southampton (Flood, 1981), York River (Dellapenna et al., 2001)]. In this study, we focused our survey efforts in the Clay Bank region within the secondary channel, where furrows have been found to be present at various times throughout the year.

First identified as a ridge and furrow bedform system, Dellapenna et al (2001) mapped these features in the York River Estuary in January of 1995. The authors found that these features were present during conditions of low river flow and had a spacing ranging from 0.7 to 7 meters. Over three years these rectilinear bedforms were mapped and were suspected to be transient in nature. Overall, Dellapenna et al. (2001) used the presence of furrows to classify three main morphologies present within the York River, near the Clay Bank region: 1. well-developed furrows (found at times of lowest mean currents), 2. meandering furrows (found at times of intermediate mean current), and 3. no furrows (found at times of high current conditions).

For this study, furrows were used as an evaluation marker, or stationary feature used for observation, in order to track sediment transition and movement processes within the middle of the York River estuary. Previous studies have shown that furrows act an area of deposition and erosion, but the dynamics of how the two processes interact is not well understood (Viekman et al., 1992 and Dellapenna et al., 2001).

2.4 Methods

A tripod-mounted Imagenex 881A rotary sonar, in conjunction with an ASL IRIS data logger, was used to assess the relationship between erosion and deposition on short-term scales

(e.g. hourly and daily) in the York River Estuary (Figure 2-2). The 881A instrument is a tunable multi-frequency/ranging digital profiling imaging sonar, equipped with frequencies from 280 kHz to 1.1 MHz and radius range scales from varying increments of 1 to 200 meters. Other variables, such as pulse length and absorption, can also be adjusted on the rotary sonar to obtain the best quality sonar images. For this study, a real-time data transfer was utilized in the data collection process, where a communication cable extended from the rotary sonar to a radio modem on the surface, which sent data back to the lab every hour. This two-way connection allows for in situ tuning of the sonar settings and real-time observations, enabling strategic timing of rapid response cruises to collect samples of the seabed following changes in bed conditions. In addition to the real-time connection, the rotary sonar was connected to an ASL Iris Data Logger for internal logging purposes and sonar run commands, which allowed for four independent programmable sequences to be run. The proprietary data logger software, IrisLink, providing the capabilities that allow for real-time data downloads, checking instrument status, and modifying instrument parameters for the optimization of the images based on the current conditions (Figure 2-2).

A variety of frequencies and instrument heights above the bed were tested to determine the best parameters for a cohesive sediment environment. Frequencies of 280, 500, 675, 900, 1000, and 1175 kHz were tested. In addition, the instrument was placed 10, 25, 50, 80, 100, 110, and 135 centimeters above the bed to determine optimal visualization of bedform features. Furthermore, a separate study was conducted at Clay Bank to determine the optimal parameter settings for gain and absorption to establish sequences that could be used during monthly deployments at the study area. In conjunction with this study, a YSI 6600 CTD Sonde was deployed simultaneously to see how the sonar responded to increasing and decreasing turbidity

over tidal cycles, and to establish parameter sequences that could be used during monthly deployments at the study area.

Once initial settings were chosen, the tripod was deployed for one month (between August 27, 2009 to September 30, 2009) to obtain 360° surface images on an hourly basis, capturing a nearly continuous time series of the seabed (Table 2-1). Four sequences were programmed to be run every hour through the data logger. The first of these sequences was run four times consecutively every hour, and the images were temporally averaged in Matlab® to reduce the effect of background noise and improve the overall image quality. All rotary sonar images were processed in Matlab® using modified scripts to convert sonar files into viewable imagery and accessible acoustic backscatter measurements (Figure 2-3a).

Due to the prevalence of fine-grained sediments, at of Clay Bank, it was thought rotary sonars may not be as useful as they have been in coarser grained environments, as the presence of rapidly evolving bedforms are not as prevalent within York River Estuary benthic environment. However, on occasion furrow formations have been observed on the sediment surface. During the September 2009 rotary deployment, two features were present within the sonar field of view, helping to categorize the changes occurring on the seafloor: an elongated furrow (upper right quadrant) and intermittent exposure of oyster clutch (lower left quadrant). Hourly changes of acoustic backscatter were calculated along four transects, at azimuths of 45°, 90°, 180°, and 225°, and analyzed to investigate exact points at 5m and 7m along of each transect to look at specific locations within the sonar's field of view (Figure 2-3b).

2.5 Results and Discussion

Within the York River Estuary, optimal parameter settings for fine-grained environments were determined using the 881A rotary sonar. During the testing phase, it was concluded that 675, 1000, and 1175 kHz provided the best images of the seabed for fine-grained sedimentary environments. In addition, the optimal transducer position above the surface was at least 1 meter above the bed, where 1.0, 1.1, and 1.35 meters yielded the best results. Furthermore, when the rotary sonar was deployed in the real-time setting over the course of a tidal cycle, there appeared to be no adverse effect to the images due to an increase in suspended sediment concentrations during maximum flow conditions.

In order to correlate rotary sonar images to seafloor morphology changes, regional mapping surveys were conducted prior to the main analysis in February of 2008. The objective was to establish a suitable rotary sonar tripod location and image the seafloor, utilizing a 900 kHz Marine Sonic sidescan sonar towfish. During the study, sedimentary furrows were identified and located within the study area. The rotary sonar tripod was deployed twice to finalize optimal cohesive sediment-estuarine environmental parameters of the sensor, while capturing the sedimentary furrow bedforms within the study area.

During the first deployment, well-developed furrows were observed using sidescan sonar. It is important to note, that less than a week before the deployment a large storm event swept through the region, bringing high winds and large amounts of rainfall (Figure 2-4). An abundance of longitudinal furrows were mapped using the sidescan sonar and general trends and observations were recorded at the start of the first deployment. The sidescan sonar analysis identified 15+ furrows greater than 150 meters in length in the study region, most of which had a width of between 0.5 and 1 meter. Observations showed that the most well-developed bedforms usually occurred in the presence of an old piling or similar structure within the furrow channel

(Figure 2-5). These pilings are wide spread since one of the historic fishing practices in this study area utilized staked gill nets. Furthermore, smaller seafloor ripples were observed on top of the large furrows at several locations.

The rotary tripod was retrieved after several days in the field to analyze the quality of the sonar images. The initial deployment of the rotary sonar used frequencies of 675 and 1175 kHz at a height on 1 meter about the seabed. Once retrieved, the images were analyzed and it was determined that the first deployment returned dark images, often too difficult to visualize furrows and other bedform morphologies. Therefore, it was concluded that gain and absorption values of the rotary sonar system needed to be adjusted in order to optimize image quality.

The second rotary sonar deployment occurred about a week later with adjusted sensor settings. During that time, current speeds and wind conditions were considerably lower than the previous survey. At the end of the rotary deployment, the seabed was mapped again with the sidescan sonar towfish, to locate bedforms to use as a comparison of seafloor morphology between deployments and with the rotary sonar images. Furrows were found to be less abundant and were not as well-defined as previously observed (Figure 2-5b). Even though the sedimentary bedforms were not as prominent as during the second rotary deployment, images from the sensor were of high quality. These images were able to capture bedform changes during the deployment and were found to be suitable for longer term deployment and analysis.

The main rotary sonar survey occurred in 2009 and results for the Clay Bank experiment showed that upon examination of each transect, there was little change in the characteristic backscatter at 90 and 225 degree transects over time (Figure 2-6). Hourly acoustic backscatter counts are plotted (color) with a smoothing filter (black) to help eliminate noise and enhancing daily change patterns that occur upon the seabed. Conversely, an increase in the acoustic

backscatter at the 5 meter point along the 180° transect was observed on the beginning of September 18, 2009. These large backscatter values continued to persist for several days and then returned to average conditions. This change of higher backscatter values appears to coincide with both an increase in wind speed and an increasing maximum wind gust in the area as well as a period when winds shifted direction from across the estuary to along river. With the high wind energy oriented along the estuary, it appears that a layer of fine-grained sediment was resuspended off the seabed, exposing the underlying relict oyster reef found in the secondary channel of the York River Estuary. Oyster shell has a characteristically high backscatter count due to the strong return of the acoustic signal on the hard surface of the shell (Blondel, 2009). As the time elapsed, backscatter attenuation counts decreased as the wind energy dissipated, providing conditions favorable to sediment deposition. When the reef became buried by a layer of fine-grained sediment, the muds dampened the acoustic signal, providing weaker backscatter intensity compared to the hard, solid surface of the exposed oyster shell.

The 45° transect showed the most abrupt change in backscatter intensity in comparison to the other three transects (Figure 2-6). The main difference in this transect is that the elongated furrow intersects the survey line between 4 and 7 meters away from the sonar transducer. Throughout the deployment, the backscatter values remained relatively constant, but a large increase in the attenuation was observed around September 20, 2009. The meteorological conditions showed an abrupt change in the wind direction, showing a brief shift of a day from blowing along the estuary to across the estuary and the furrow. The increase in the backscatter amplitude shows a decrease in the slope of flanks of the furrow, which may correspond to the acoustic shadow created by the higher elevation of the furrow flank in comparison to the seabed elevation (Figure 2-7). As the backscatter values increased during this time, the furrow began to

narrow, providing a smaller acoustic shadow. In addition, the opposite slope of the furrow became more exposed, appearing acoustically brighter, thereby giving larger backscatter values. After this event, the wind shifted again back to the southeast, and the furrow appeared to return its previous state, when compared to the rest of the deployment.

Using rotating side-scan sonars in cohesive systems is still in its early stages, yet there are many applications for which this technology would be useful. These studies should include a more robust comparison of data to hydrologic conditions, other localized scientific equipment (i.e. LISST, CTD, ADV, etc.), and a ground-truthing sediment analysis. Examples of possible future studies could include mapping movements of turbidity maxima to the more broad application of monitoring channel morphology for shipping navigation.

2.6 Conclusions

Understanding seafloor morphology and its evolution is critical to scientific investigations of boundary layer processes. The papers reviewed and field studies presented in this document illustrate the versatility and applicability of the rotary sonar instrument for morphological monitoring. Despite the fact that it is uniquely suited to a variety of seafloor investigation, rotary sonar instrumentation remains largely underutilized by the scientific community. The wider application of this tool for seafloor monitoring will yield greater scientific insights and improved engineering and management decisions.

References:

- Allen, J.R.L., 1969, Erosional current marks of weakly cohesive mud beds: *Journal of Sedimentary Petrology*, v. 39, p. 607-623.
- Blondel, P. (2009). "*The Handbook of Sidescan Sonar.*" Praxis Publishing Limited, New York.
- Bryant, W. R. & Slowey, N. C. 2004. Deep-sea furrows: physical characteristics, mechanisms of formation and associated environmental processes, a joint industry project. Texas A&M University, Department of Oceanography and Offshore Technology Research Center, internal report.
- Carron, M.J., (1976). *Geomorphic Processes of a Drowned River Valley: Lower York River Estuary, Virginia.* , 115. M.S. thesis, Virginia Institute of Marine Science/School of Marine Science, The College of William and Mary, Virginia.
- Cheel, R.A. and Hay, A.E. (2008) Cross-ripple patterns and wave directional spectra. *Journal of Geophysical Research*, 113, C10009.
- Clifton, H.E. and Dingler, J.R. (1984), Wave formed structures and paleoenvironmental reconstruction. *Marine Geology*, 60, 165-198.
- Cochonat, P., Ollier, G., and J.L. Michel. (1989). Evidence for slope instability and current induced sediment transport, the RMS Titanic wreck search area, Newfoundland Rise. *Geomarine Letters*, 9: 145-152.
- Coleman, J.M., Prior, D.B., and C.E. Adams (1981). Erosional furrows on continental shelf edge, Mississippi Delta region. *GeoMarineLetters*, 9:11-15.
- Dellapenna, T.M., Kuehl, S.A. and Schaffner, L.C., (1998). Seabed mixing and particle residence times in biologically and physically dominated estuarine systems: a Comparison of Lower Chesapeake Bay and York River Subestuary. *Estuarine, Coastal and Shelf Science*, 46: 777-795.
- Dellapenna, T.M., Kuehl, S.A. and Pitts, L., (2001). Transient, longitudinal, sedimentary furrows in the York River Sub estuary, Chesapeake Bay: Furrow evolution and effects on seabed mixing and sediment transport. *Estuaries*, 24(2): 215-227.
- Dellapenna, T.M., Kuehl, S.A., Schaffner, L.C. (2003). Ephemeral deposition, seabed mixing and fine-scale strata formation in the York River estuary, Chesapeake Bay. *Estuary, Coastal, and Shelf Science*. 58, 621-643.
- Dyer, K. R. (1982), The initiation of sedimentary furrows by standing internal waves. *Sedimentology*, 29: 885-889.
- Flood, R.D, (1981). Distribution, morphology, and origin of sedimentary furrows in cohesive sediments, Southampton Water. *Sedimentology*, 28:511-529.

- Flood, R.D., (1989). Submersible studies of current modified bottom topography in Lake Superior. *Journal of Great Lakes Research*, 15: 3-14.
- Flood, R.D., and H.J. Bokuniewicz, (1986). Bottom morphology in the Hudson River and New York Harbor. *Northeastern Geology*, 8: 130-140.
- Flood, R.D. and C.D. Hollister. (1980). Submersible studies of deep-sea furrows and transverse ripples in cohesive sediments, 36 (102): Pages M1-M9.
- Friedrichs, C.T. (2009) York River physical oceanography and sediment transport. *Journal of Coastal Research*, SI 57: 17-22.
- Hardisty, J., 2007. Estuaries: Monitoring and Modeling the Physical System. Blackwell Publ., Malden, Mass.
- Hay, A.E. and Wilson, D.J. (1994) Rotary sidescan images of nearshore bedform evolution during a storm. *Marine Geology*, 119, 57-65.
- Hay, A.E. and Mudge, T. (2005) Primary bed states during SandyDuck97: Occurrence, spectral anisotropy, and the bed state storm cycle. *Journal of Geophysical Research*, 110, C03013.
- Hay, A.E. (2008) Near-bed turbulence and relict wave formed sand ripples: Observations from the inner shelf. *Journal of Geophysical Research*, 113, C04040.
- Inman, D.L. (1957) Wave-generated ripples in nearshore sands. *US Army Corps of Engineers, Beach Erosion Board, Technical Memorandum*, 100, 67pp
- Irish, J.D., Lynch, J.E., Traykovski, P.A., Newhall, A.E., Prada, K., and Hay, A.E. (1999) A self-contained sector-scanning sonar for bottom roughness observations as part of sediment transport studies. *Journal of Atmospheric and Oceanic Technology*, 16, 1830-1841.
- Kennedy, V.S., (1984). The estuary as a filter. Academic Press, New York, NY.
- Komar, P.D., (1998). Beach Processes and Sedimentation. Prentice-Hall, Upper Saddle River, NJ.
- Lacy, J.R., Rubin, D.R., Ikeda, H., Mokudai, K., Hanes, D. (2007) Bed forms created by simulated waves and currents in a large flume. *Journal of Geophysical Research*, 112, C10018.
- Lonsdale, P.F., (1978). Bed Forms and the Benthic Boundary Layer in the North Atlantic: A Cruise Report of Indomed, Leg 11: Scripps Institution of Oceanography, Reference 78-30, Scripps Institute of Technology, La Jolla, California.

- Maa, J.P.Y. and Kim, S.C., (2002). A Constant erosion model for fine sediment in the York River, Virginia. *Environmental Fluid Mechanics*, 1: 345-360.
- Maier, I. and Hay, A.E. (2009) Occurrence and orientation of anorbital ripples in nearshore sands. . *Journal of Geophysical Research*, 114, F04022.
- Mitra, S., Dellapenna, T.M., Dickhut, R.M., (1999). Polycyclic Aromatic Hydrocarbon Distribution within Lower Hudson River Estuarine Sediments: Physical Mixing vs. Sediment Geochemistry. *Estuarine Coastal and Shelf Science* 49, 311-326.
- Nielsen, P., (1992). *Coastal Bottom Boundary Layers and Sediment Transport*. World Scientific, Singapore; River Edge, N.J.
- Olsen, C.R., Larsen, I.L., Mulholland, P.J., Karen L. von Damm, Grebmeier, J.M., Schaffner, L.C., Diaz, R.J., Nichols, M.M., (1993). The Concept of an Equilibrium Surface Applied to Particle Sources and Contaminant Distributions in Estuarine Sediments. *Estuaries* 16, 683-696.
- Puig, P., Palanques, A., Orange, D.L., Lastras, G., Canals, M. (2008). Dense shelf water cascades and sedimentary furrow formation in the Cap de Creus Canyon, northwestern Mediterranean Sea, *Continental Shelf Research*, 2017-2030.
- Rubin, D., McCulloch, D.S., and Hill, H.R (1977) Bedform observations with a bottom-mounted rotating side-scan sonar in San Francisco Bay, California. *Transactions of the American Geophysical Union*, 58, 1162.
- Rubin, D., McCulloch, D.S., and Hill, H.R. (1983) Sea-floor-mounted rotating side scan sonar for making time-lapse sonographs. *Continental Shelf Research*, 1, 295-301.
- Skarke, A. and A.C. Trembanis (2011). Parameterization of bedform morphology and defect density with fingerprint analysis techniques, *Continental Shelf Research*, 31(16): 1688-1700.
- Soulsby, R. (1997). *"Dynamics of Marine Sands: A Manual for Practical Applications"*. Thomas Telford Publications, New York, NY.
- Spindel, R.C. (1985). Sound Transmission in the Ocean. *Annual Review of Fluid Mechanics*, 17, 217-37.
- Styles, R. and S.M. Glenn (2002). Modeling bottom roughness in the presence of wave-generated ripples, *Journal of Geophysical Research*, 107, C8, 24/1-24/15.
- Swart, D.H. (1974) *"Offshore sediment transport and equilibrium beach profiles"*. Delft Hydraulics Laboratory, Delft, Netherlands. 302 pp.

- Tang, D., Williams, K.L., and Thorsos, E.I. (2009) Utilizing high-frequency acoustic backscatter to estimate bottom sand ripple parameters. *IEEE Journal of Oceanic Engineering*, 34 (4), 431-443.
- Traykovski, P., Hay, A.E., Irish, J.D., and Lynch, J.F. (1999) Geometry, migration, and evolution of wave orbital ripples at LEO-15. *Journal of Geophysical Research*, 104, 1505-1524.
- Traykovski, P. (2007) Observations of wave orbital scale ripples and a non-equilibrium time-dependant model. *Journal of Geophysical Research*, 112, C06026.
- Traykovski, P., Richardson, M.D., Mayer, L.A., and Irish, J.D. (2007) Mine burial experiments at the Martha's Vineyard Coastal Observatory. *IEEE Journal of Oceanic Engineering*, 32 (1), 150-166.
- Trembanis, A., Nebel, S., Skarke, A., Coleman, D.F., Ballard, R.A., Yankovsky, A., Buynevich, I.V., and Voronov, S. (2011). Bedforms, coastal-trapped waves, and scour process observations from the continental shelf of the northern Black Sea, in *Geology and Geoarchaeology of the Black Sea Region: Beyond the Flood Hypothesis*. I. Buynevich, V. Yanko-Hombach, A. Gilbert, R. E. and Martin, Eds. Geological Society of America Special Paper 473.
- van Rijn, L., C., (1984a). Sediment Transport, Part II: Suspended Load Transport. *Journal of Hydraulic Engineering* 110, 1613-1641.
- van Rijn, L., C., (1984b). Sediment Transport, Part III: Bed Forms and Alluvial Roughness. *Journal of Hydraulic Engineering* 110, 1733-1754.
- van Rijn, L., C., (1984c). Sediment transport, part I: bed load transport. *Journal of Hydraulic Engineering* 110, 1431-1456.
- Viekman BE, Flood RD, Wimbush M, Faghri M, Asaka Y, Van Leer JC (1992) Sedimentary furrows and organized flow structure: A study of Lake Superior. *Limnology and Oceanography*. 37:797-812
- Voulgaris, G, and Morin, J.P. (2008). A long-term real time sea bed morphology evolution system in the south Atlantic Bight. *Proceedings of the IEEE/OES/CMTC Ninth Working Conference on Current Measurement Technology*, March 17-19, 2008, Charleston, SC.
- Whitehouse, R., (2000). "Dynamics of Estuarine Muds : A Manual for Practical Applications". Thomas Telford Publications, London.

York River Estuary, Chesapeake Bay VA, USA

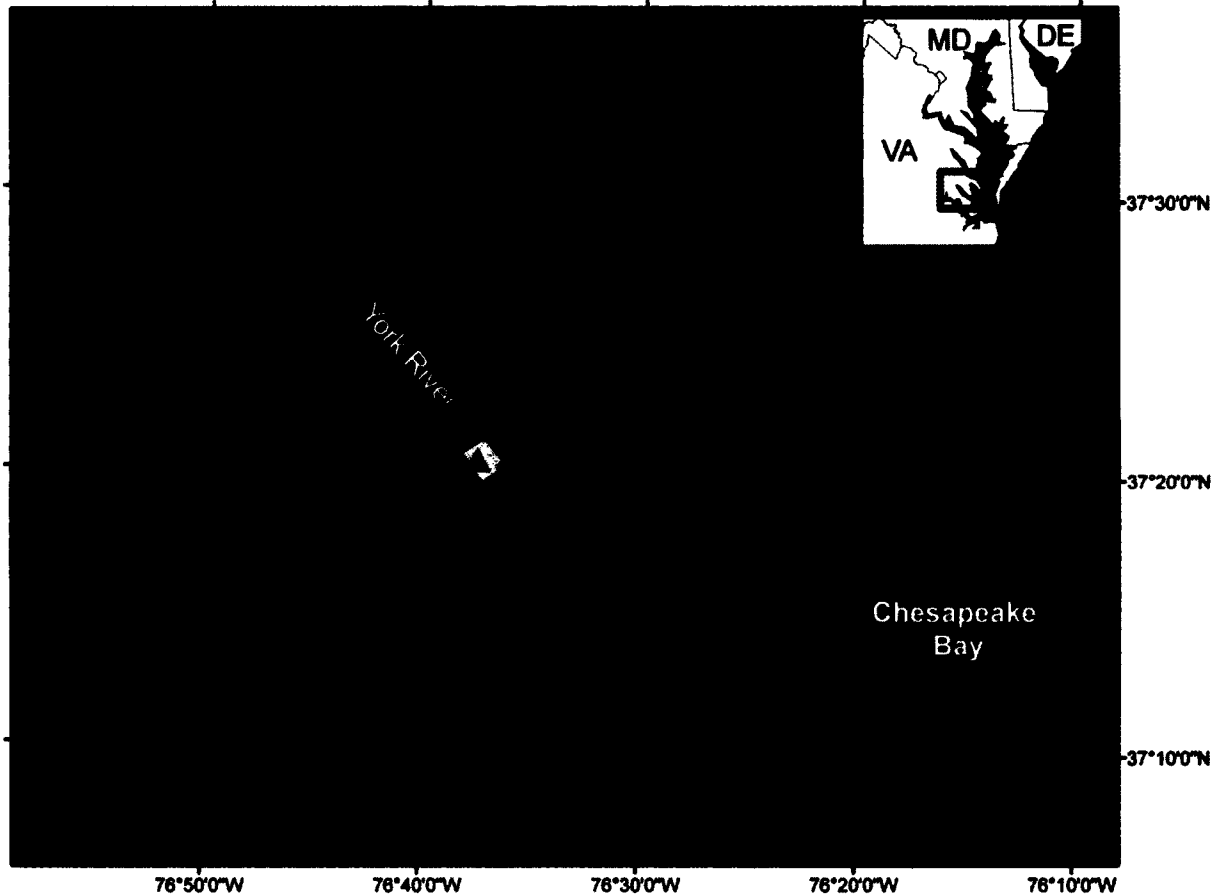


Figure 2-1. Study location for the VIMS rotary tripod ~ Clay Bank within the York River Estuary. The tripod location is delineated by the red triangle.

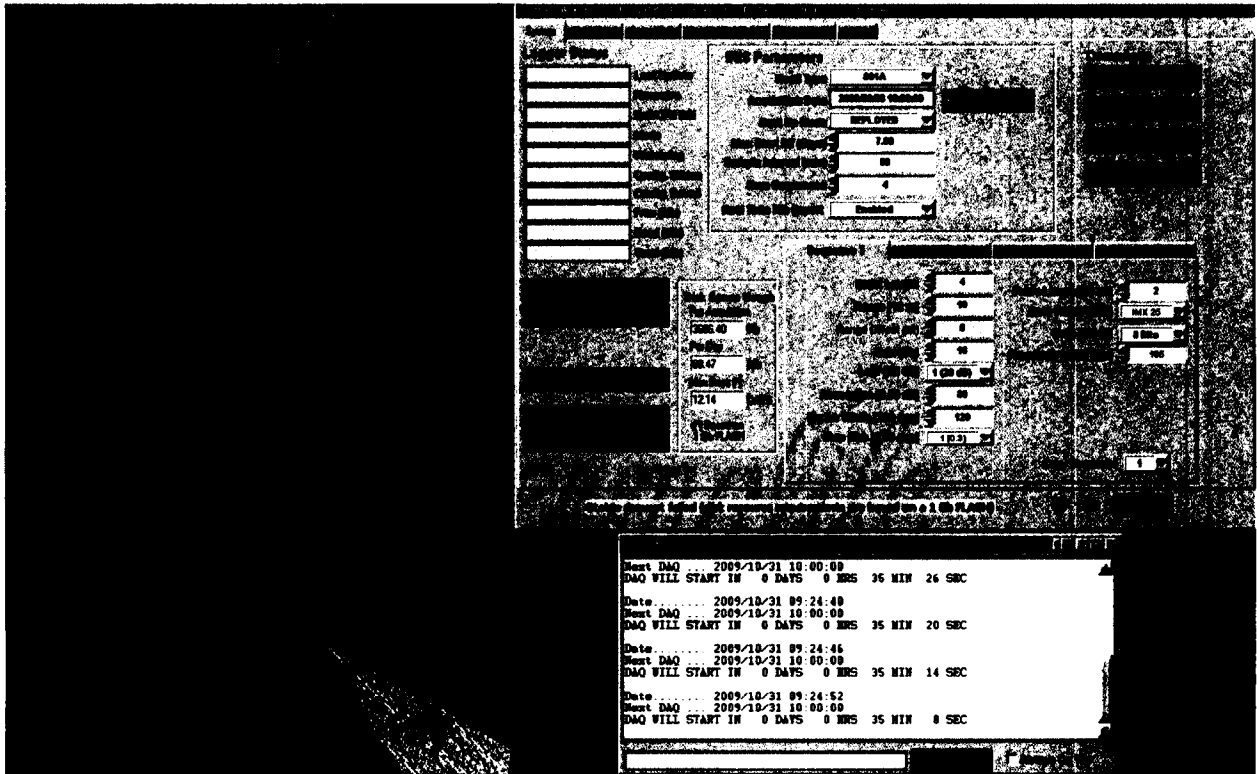


Figure 2-2. A depiction of the real-time rotary sonar capabilities developed utilize IrisLink software and a communication cable, extending from the instrument to a radio modem, that deliver data back to the lab at the Virginia Institute of Marine Science. The two-way connection allowed for in-situ tuning of the sonar images, as well as real-time observations.

Table 2-1. Rotary sonar scan sequences variables determined to be the optimal initial settings in a cohesive, fine-grained, estuarine environment.

Sequence	1	2	3	4
Range radius (m)	10	10	10	20
Frequency (kHz)	1000	1000	675	675
Gain (db)	18	24	18	18
Absorption (dB)	0.60	0.60	0.20	0.20
# of rotations per hour	4	1	1	2

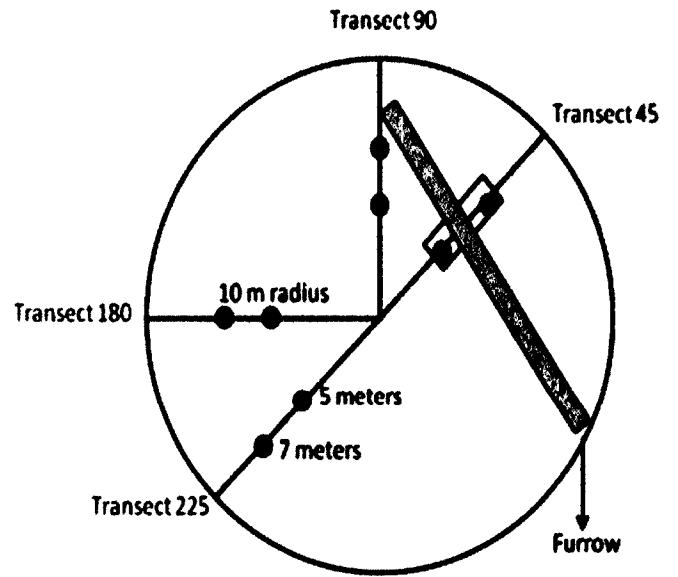
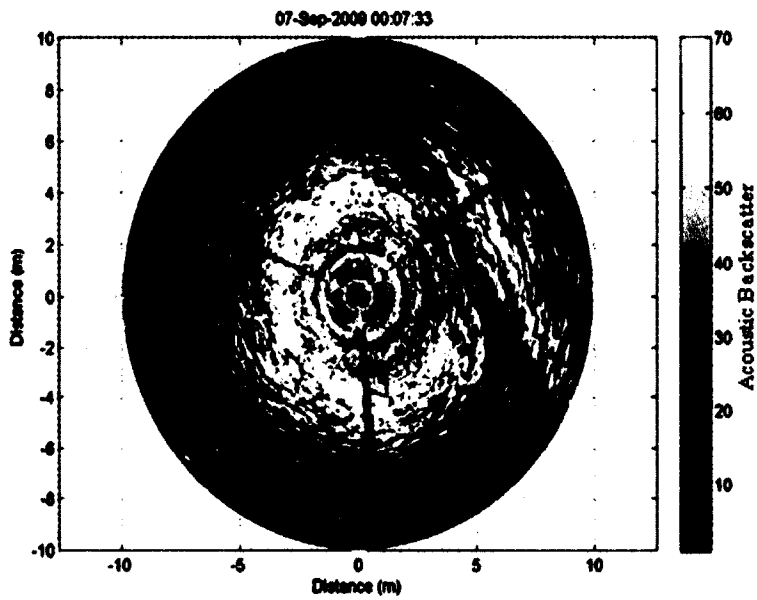


Figure 2-3. a) A Clay Bank 1 MHz rotary scan image, 1 meter above the bed (Range ~ 10m, 24dB gain). b) Diagram showing the 4 transects analyzed for acoustic backscatter comparison.

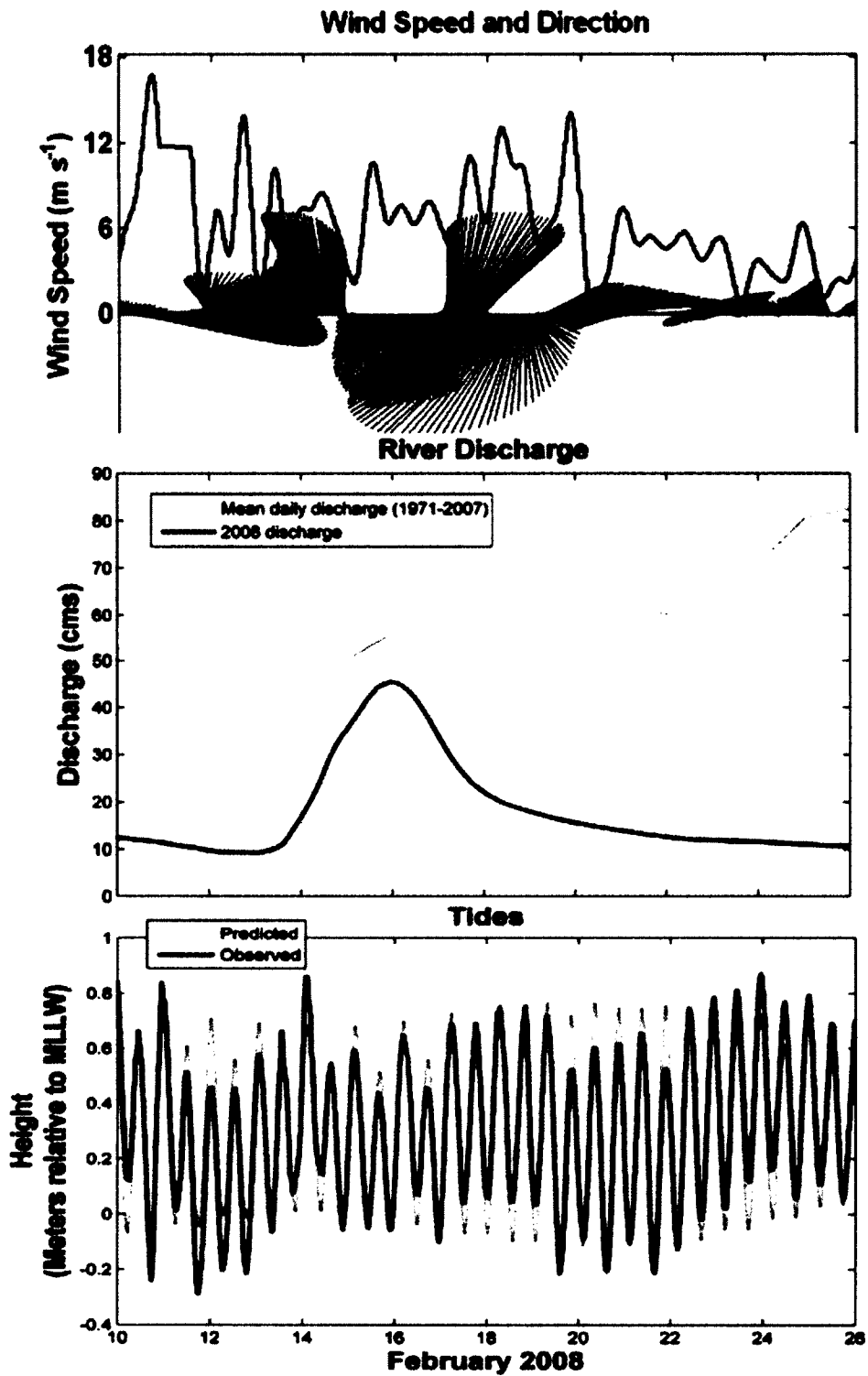


Figure 2-4. Wind speed, river discharge, and tidal data that correlated to the early rotary sonar studies in the York River.

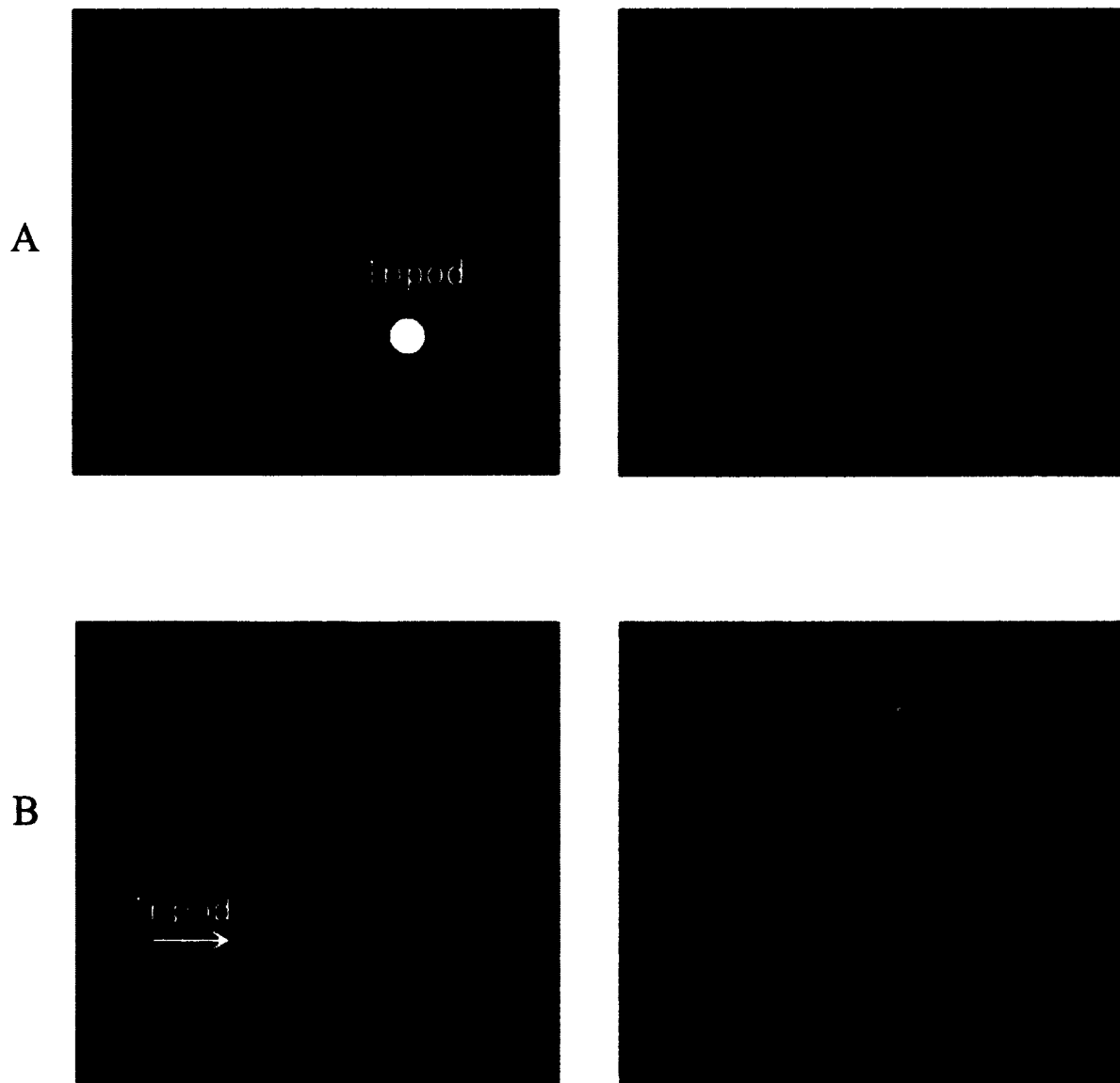


Figure 2-5. Sidescan sonar surveys during rotary sonar deployment in order to correlate rotary sonar images to seafloor morphology changes. a) The first survey showed well-developed longitudinal furrows extending up to 150m in length and 0.5 to 1 meter wide, occurring shortly after a large storm event with heavy winds. The left image highlights the location of the rotary tripod and the image on the right shows a furrow with an old piling or similar structure within the bedform. b) The second survey was conducted at the end of the rotary sonar deployments and illustrates a smoother bottom and the same furrow with less definition.

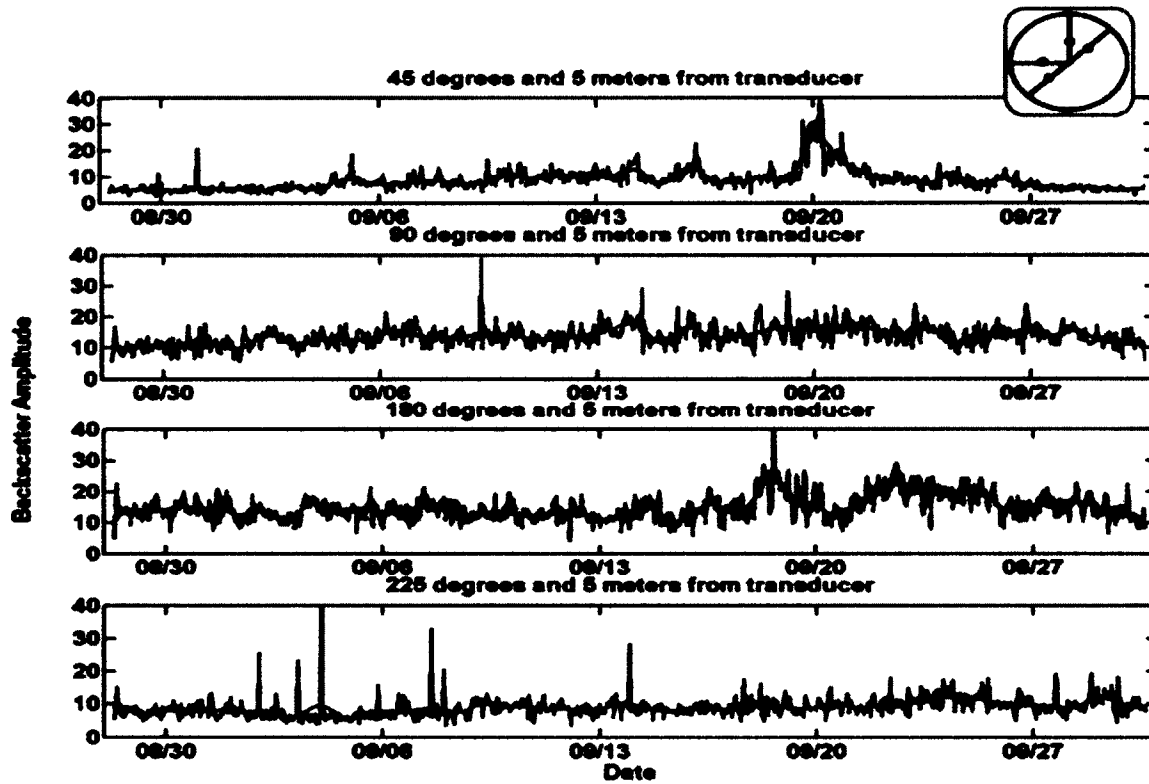


Figure 2-6. Time series of backscatter amplitude at 5 meters from the rotary transducer along of the 4 transects (45°, 90°, 180°, and 225°).

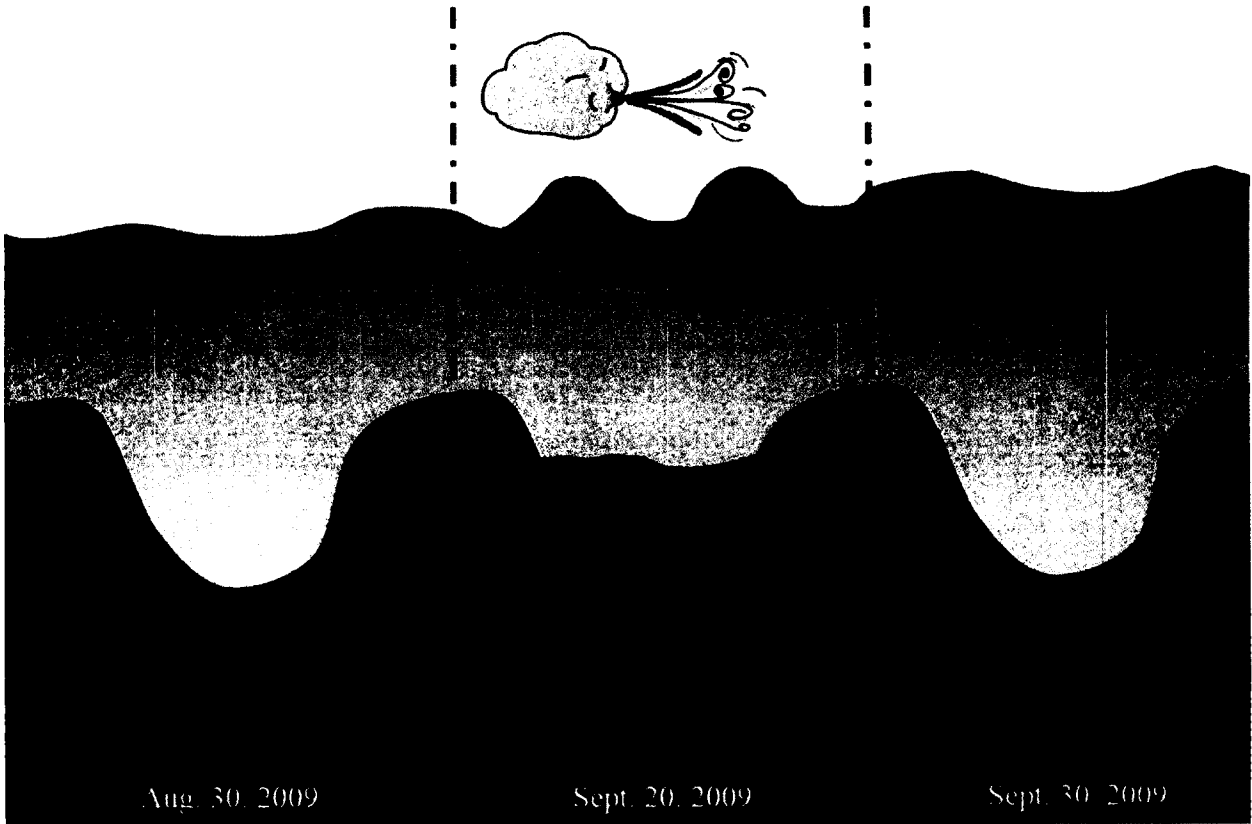


Figure 2-7. Conceptual diagram of York River furrow morphologic change throughout the study. As winds increased during the rotary sonar deployment, sediment was deposited within the furrow and then was eroded after the stormy conditions subsided.

Chapter 3: Evolution of the seabed of the York River Estuary, Virginia, following dissipation of a turbidity maximum: consolidation, pelletization and spring-neap disturbance

Abstract:

Further investigation of the muddy seabed properties that determine time-dependent erodibility is essential to improved understanding and modeling of sediment dynamics. During April and May of 2010, weekly cores were collected following dissipation of the York River Estuary's secondary turbidity maximum, while also resolving the estuary's spring-neap cycle. Erodibility of the surface of the cores was determined via a Gust microcosm and cores were analyzed for sand/silt/clay, organic and water content, ^7Be activity, response to x-radiography sediment structure, and based on gentle sieving, resilient pellet content. In general, common patterns in vertical structure and properties below 1-cm depth suggested that neither significant net erosion nor net deposition was responsible for observed variations in erodibility. Trends observed in the uppermost cm were consistent with simultaneous consolidation and bed armoring. As time passed, sand content, median sand size, percent pellets, and median pellet size were all observed to increase at the surface, while the percent water, organics, silt, ^7Be activity and erodibility decreased. Along with a tendency for erodibility to decrease with time, this study identified a superimposed temporal oscillation in erodibility correlated to a 6-day low-pass of tidal range, presumably because strong tidal currents acting over several preceding days disturb the bed, partly counteracting the temporal effects of consolidation. Simultaneous consolidation and bed armoring, consolidation time-scales on the order of several days to a week, and "resetting" of consolidation by resuspension are all qualitatively consistent with recently developed theoretical models for time-dependent mixed seabed erodibility.

3.1. Introduction

Estuaries receive a mix of non-cohesive and cohesive sediment from locations ranging from the continental shelf to upland riverine sources 7. Fine sand and muddy particles are deposited, eroded, and transported throughout many tidal estuaries in a repeating, quasi-cyclical pattern based on the ebb and flow of the daily and spring-neap tidal fluctuations interacting with seasonal and event-scale variations in freshwater input, waves, and wind forcing. This repetition is occasionally altered, as estuaries act as effective trapping mechanisms, characterizing the environment as sediment sinks (Meade, 1982; Wong and Moy, 1984; Dyer, 1988; Hobbs et al., 1992; Shen and Haas, 2004).

Fine-grained sediment strongly impacts estuarine ecosystems. As mud particles are suspended into the water column, light attenuation can significantly increase. Along with impacting light availability, intense fine sediment transport can diminish macrobenthic diversity and abundance, leading to a degraded habitat (Summerhayes et al., 1985; Angradi, 1999; Schaffner et al., 2001; Lowe and Bolger, 2002; Weigelhofer and Waringer, 2003; Salant and Renshaw, 2007). These adverse effects are further compounded as pollutants are introduced in the estuary. The greater percentage of fines on the seabed and within the water column, the greater chance for pollutants to remain within the estuary as contaminants are attracted and absorbed onto muddy particles (Olsen et al., 1982). As estuarine watersheds become progressively more populated, chances for erosion and input of contaminants (either point or non-point sources) increase dramatically.

Regions in estuaries where cycles of fine sediment trapping and resuspension are clearly evident on event to seasonal time scales include estuarine turbidity maximums (ETMs), which are often associated with along-estuary changes in stratification associated with fronts,

transitions in mixing and/or the landward limit of the salt intrusion (ETM) (Roberts and Pierce, 1976; Dyer, 1988; Geyer, 1993; Wolanski et al., 1995; Li and Zhang, 1998; Lin, 2001; Geyer et al., 2001; Sanford. et al., 2001). As well as the primary ETM near the transition to freshwater, a secondary ETM may form within estuaries due to a variety of mechanisms, including: bottom residual flow convergence, tidal asymmetries, the suppression of turbulence diffusion due to stratification of the water column, and/or enhanced resuspension in a region of high erodibility (Nichols et al., 1991; Lin and Kuo, 2001; Dellapenna et al., 1998; Dellapenna et al., 2003; Dickhudt et al., 2009).

Sediment erodibility has been studied extensively for decades in numerous coastal, estuarine and laboratory settings (Gorsline, 1984; Mehta, 1988; Amos et al., 1992; Friedrichs et al., 2000; Geyer et al., 2001; Harris and Wiberg, 2001; Uncles, 2002; Harris et al., 2003; Schaaff et al., 2006; Sanford, 2008; Dickhudt et al., 2009; Friedrichs, 2009; Ralston and Geyer, 2009). Non-cohesive sediments, by definition, are controlled by gravitational and frictional resistance to motion, and the erosion potential mainly depends on grain size. Conversely, cohesive sediments are more difficult and complex to predict and model due to the dependence of erodibility on a greater number of factors, with physical/geological effects including: particle size distribution, porosity, bulk density, and surrounding fluid properties, which include salinity and water temperature (Dyer, 1986; Aberle et al., 2004; Andersen, 2001; Winterwerp, 2004; Debnath et al., 2007). These variables factor into the inter-particle bonds resulting into cohesive forces between grains, which further depend upon the mineral composition. Classically, though, the dominant control on erodibility in cohesive sediment is thought to be its degree of consolidation, i.e., the strengthening of the bed due to dewatering and the rearrangement of particles which together increase overall cohesion (e.g., Mehta and McAnally, 2008).

Although physical sediment properties are important to erodibility, additional variables and processes associated with the benthic community can either enhance or reduce erodibility. Biological effects include mechanical bioturbation, formation of pellets by physical compaction, production of shells and other detritus, construction of sediment structures such as mounds, secretions which enhance cohesion such as extracellular polymeric substances (EPS), and direct biological suspension of sediment into the water column (Edelvang and Austen, 1997; Austen et al., 1999; Andersen, 2001; Andersen and Pejrup, 2002; Widdows et al., 2000; Perkins et al., 2003; Perkins et al., 2004; Underwood and Paterson, 2003). Pellets formed by benthic organisms that repackage sediment can be transported intact even during strongly turbulent conditions. Pelletized sediment typically has a lighter density than that of a comparable sand sized particle, allowing it to remain in suspension longer (Cartwright et al., 2011). Organisms including annelids (i.e. *Heteromastus filiformis*, *Mediomastus ambiseta*, *Streblospio benedicti*), mollusks (i.e. *Hydrobia*, *Macoma baltica*), etc. are responsible for creating these biogenic pellets which can make up more than 50% of the surficial sediment depending on the location and the current tidal condition (Kraeuter and Haven, 1970; Schaffner et al., 2001; Drake et al., 2002; Gillett and Schaffner, 2009).

Numerous physical and biological properties of the seabed have been qualitatively associated with changes in bed erodibility, yet few field studies to date have been able to demonstrate in situ the temporal changes in mud properties which lead to significant changes in erodibility over key consolidation time scales of several days to a few weeks. Some success has been seen in this regard in intertidal flat environments, where changes in erodibility have been conclusively related to colonization by benthic algae (e.g., Andersen et al., 2010). However directly observed quantitative associations between bed properties and erodibility in subtidal

(i.e., light-limited) cohesive environments have been especially elusive. Furthermore, the studies that have attempted to relate erodibility to seabed properties in subtidal environments have tended to focus on spatial and/or seasonal time-scales (e.g., Dickhudt et al., 2009, 2011; Stevens et al., 2007; Wiberg et al., 2013) rather than the key, local consolidation time-scale of days to weeks. Constraining relationships between bed properties and erodibility based on in situ data is extremely important to the sediment transport community given that bed erodibility is one of the most important, but least constrained parameters controlling the amount of fine sediment in suspension in coastal and estuarine numerical models (Rinehimer et al., 2008; Sanford, 2008).

Recent studies in subtidal cohesive environments have been inconclusive regarding even seasonal controls on erodibility in subtidal muddy environments. Stevens et al. (2007) compared erodibility at nine muddy bottom sites along the western margin of the Adriatic Sea to water content, organic and inorganic carbon, colloidal carbohydrate and sand-to-mud ratio in late winter versus early summer. No consistent seasonal changes in bed constituents could be related to temporal changes in erodibility, and the spatial trends that were observed were contrary to expectations, in that erodibility decreased with greater porosity. For a muddy tidal channel-flat complex in Willapa Bay, Wiberg et al. (2013) found that spatial variations in porosity just below the sediment surface in winter was a significant predictor of spatial variations in bed erodibility, but porosity was not related to erodibility in spring or summer. Dickhudt et al. (2009, 2011) related erodibility of fine sediment to the surface content of cores collected every one to two months over an 18-month period from the York River estuary, including percent water, total organics, colloidal carbohydrate, extracellular polymeric substances, and sand-silt-clay, but no relationships were found to be significant at 95% confidence. The only relationship significant at even 90% was increased erodibility with a lower clay: silt ratio. Based on upper seabed fabric

revealed by x-radiographs, Dickhudt et al. (2009, 2011) concluded that seabed disturbance, in the form of periodic deposition and erosion associated with ETM migration, was the dominant control on subsequent bed erodibility.

The main goal of this study was to investigate the influence of sedimentological properties versus seabed disturbance on the erodibility of a cohesive seabed within a subtidal, muddy estuarine environment over several weeks during a time period when bed consolidation was likely occurring. As far as we are aware, this represents the first in-situ study to successfully and quantitatively relate classic bed properties (i.e., water content and grain size) to evolving erodibility over this key consolidation time-scale in a subtidal cohesive estuarine environment. Logistics and recent findings of others (e.g., Friedrichs et al., 2008; Dickhudt et al., 2009, 2011; Rodriguez, 2010; Rodriguez and Kuehl, 2012) favored the Clay Bank region of the York River estuary for this examination. Previous work at this same site (Dickhudt et al., 2009, 2011) had documented a dramatic decrease in bed erodibility before and after dissipation of an STM, but these studies had been unable to quantitatively relate fine-scale properties of the bed, such as water content and grain size, to changing bed erodibility. In addition, this study aimed to assess the role of spring-neap variations in tidal currents on the seabed erodibility. Previous coring efforts (e.g., Dellapenna et al., 2001; Dickhudt et al., 2009; Rodriguez and Kuehl, 2012) had been too coarse in time to capture spring-neap bed evolution, and undocumented spring-neap variation may have confounded previous attempts to relate erodibility to time-varying bed conditions. In the process, this study also proposed to resolve possible relationships between bed pelletization, consolidation and erodibility. Previous work (Dickhudt et al., 2009; Rodriguez, 2010) hypothesized that non-pelletized mud was associated with times of high erodibility,

whereas pellet-rich muddy beds were associated with times of low erodibility. But observations at monthly or longer intervals likewise limited past quantitative investigations of pelletization.

3.2. Study Area

The York River estuary (Figure 3-1) is located in southeastern Virginia on the Mid-Atlantic Coast of the United States and was created by the drowning of a river valley approximately 12,000 years ago due to the melting of glaciers during the beginning of the Holocene (Hobbs, 2009; Reay and Moore, 2009). Today, the estuary is formed at the confluence of the Mattaponi and Pamunkey Rivers and empties into the Chesapeake Bay at its mouth. As the Chesapeake's fifth largest tributary, the York River watershed encompasses an area approximated 6900 km², slightly larger than the state of Delaware. The estuary has a mean depth of 4.9 meters, with the deepest area located near the Gloucester Point region with a maximum depth of over 20 meters. The estuary's main channel, which averages about 10 meters deep, bifurcates near Page's Rock Light, and a shallower (~ 6 meter deep) secondary channel extends northward on the western flank of the main channel. Two shoals flank the channels and have an average depth of ~ 2 meters. Salinity in the lower estuary is usually partially stratified, while the shallower upper estuary is weakly stratified (Friedrichs, 2009). Although microtidal, surface tidal currents within the middle and upper portions of the estuary reach ~ 1 m/s at spring tide, and bed stress is strong enough to regularly resuspend bottom sediments (Schaffner et al., 2001).

The surficial sediments of the main and secondary channels of the York River Estuary are muddy, with the percent clay plus silt generally exceeding 70% (Nichols et al., 1991). In the muddy reaches of the secondary channel, near the site of the present investigation, near-bed tidal suspensions can seasonally exceed 1 gram/liter (Friedrichs et al., 2000). There are seasonally

persistent along-estuary peaks in turbidity along the York River estuary associated with two major ETMs. The main ETM is typically located near the head of the salt intrusion, while a secondary ETM is often found in the middle estuary, about 20 to 40 km from the mouth of the York after the winter/spring freshet, when there tends to be a decrease in stratification at that location (Lin and Kuo, 2001).

Radioisotope geochronology studies in the York River Estuary have shown that physical reworking, possibly associated with migration of furrowed bedforms or transport events in response to major storms, may result in annual to decadal physical disturbance and reworking to depths as much as 1 m (Dellapenna et al., 1998; Kniskern and Kuehl, 2003). Over seasonal or shorter time-scales associated with local ETMs, x-radiography and dual-frequency echo sounder surveys have identified ephemeral, migrating mud deposits on the order of 10 cm that suppress macrobenthic activity and produce characteristic parallel laminations in x-rays (Schaffner et al., 2001; Dickhudt et al., 2009; Rodriguez and Kuehl, 2012). In the absence of these ephemeral deposits, biological reworking eventually leads to a mottled pattern in x-radiographs characteristic of at least moderate bioturbation (Schaffner et al., 2001; Dickhudt et al., 2009). Dickhudt et al. (2009) and Rodriguez and Kuehl (2012) found that the seasonal deposition associated with the middle-estuary ETM led to low erodibility in the Clay Bank region of the middle estuary, but that after the ETM and associated deposits dissipated, erodibility increased once more.

3.3 Methods

3.3.1. Sediment Coring

Seabed coring was conducted from a small vessel (~ 8-m length) once a week for five weeks in the spring of 2010 (Table 3-1). The sampling occurred at the Clay Bank Secondary

Channel study location in water depths averaging ~ 6 m. During each research cruise, the vessel was anchored and allowed to drift slightly around the anchoring site. At a local scale, this allowed random sampling of the seabed. Sediment samples were collected using an Ocean Instruments Gomex box corer (surface area 625 cm²) (Figure 3-2a), in order to preserve the sediment-water interface. The collections occurred at slack tide to best ensure even and level core penetration, and the box core was generally able to penetrate 15 to 30 cm into the seabed. Intact GOMEX box cores were immediately subsampled for a variety of laboratory analyses. Acrylic subcores were then pushed by hand into the top of the retrieved box core and removed for further analysis. Unfortunately, on occasion box-cores were discarded because of “blow-outs”, where large shells or other objects impeded the closure of the box core, thereby allowing sediment and water to escape.

The subcores were sampled for grain size, water content, organic content, ⁷Be activity, presence of resilient pellets/aggregates, and erodibility, and were also imaged with digital x-radiography. Samples for the first three analyses were extruded, sliced, and separated on board at 1-cm intervals down to the bottom of each subcore. For the ⁷Be samples, 2-cm intervals were obtained after the first ten 1-cm intervals, to reduce costs and data analysis time. Analysis for resilient pellets/aggregates was limited to the top two intervals (i.e., 0-1 cm and 1-2 cm). Sliced samples were immediately put in airtight containers and placed on ice in order to preserve the integrity of the sample and prevent moisture loss. Whole cores were obtained concurrently for Gust microcosm erosion experiments and for x-radiography slabs. Together, these samples were collected in hopes of gaining a deeper understanding of how erodibility may be related to the composition and structure of the upper-most seabed.

3.3.2. Water Content, Organics, and Disaggregated Sediment Components

Water content samples were processed immediately after returning from the field to help ensure accurate sediment moisture measurements. The standard wet weight vs. dry weight method was utilized to determine percent moisture vs. solids of each 1-cm interval sample. Each wet sediment sub-sample was homogenized, and ~ 200 to 300 mg was placed in a foil dish and weighed to provide the wet sample weight. The dish was then placed in an oven at 103°C until the sample visually appeared completely dry. Each dry sample was then weighed, returned to the oven for an additional hour, and reweighed until consecutive weight differences were less than 0.5 mg. This approach includes salt (typically ~1% of the total weight) within the sediment portion of the measurements. The total solids vs. water volume was calculated using the dry sediment weight and the assumed density of the sediment grains (2.65 g/cm³) and water (1.0 g/cm). Total organics content was determined for previously dried samples by determining the loss on ignition (LOI) after at least one hour in a muffle oven, set to 550°C. The remaining ash weight was assumed to be sediment particles that were entirely inorganic.

Grain size for the mud component was determined by using the wet pipetting method for grains less than 63µm. The sediment was initially disaggregated using 10 mL of dispersant, sonicated for an hour, and passed through a 63µm mesh sieve to isolate the mud component. Using standard pipetting practices, each 1-cm sample was analyzed at 1 phi intervals between 4 and 10 phi, based on settling velocities established using Stokes Law. Percent sand was determined by the fraction of total sediment dry weight caught on the 63µm mesh sieve.

3.3.3. Pellets and Other Pellet-Sized Grains

The presence of resilient fecal pellets and/or biologically compacted mud aggregates (from now on referred to simply as pellets) were determined for the depth intervals of 0-1 cm and 1-2 cm using a combination and modification of the Black et al. (2002) and Rodríguez-

Calderon (2010) pellet calculation methods. For each depth interval in each core, two 10.00-gram (± 10 -mg) wet sediment samples were sieved through four mesh sieves (150 micron, 90 micron, 63 micron, and 45 micron). The first set of sediment was sieved using traditional sieving methods, where the sediment was initially disaggregated using dispersants and sonification in distilled water. The aim of disaggregation was to capture the original population ($\varphi_{disaggregated}$) of relatively large particles (e.g., fine sand and coarse silt, small shell fragments, plant debris) in the absence of pelletization (Figure 3-2b). The sediment caught on each sieve was dried at 103°C and weighed to determine mass percentages of each size class and then muffled at 550°C to determine the LOI of the non-pellet sediment sample.

Conversely, the second sample set was not disaggregated, and careful attention was paid as to minimize physical disturbance of the sample. Using the same amount of sediment (10.00 grams ± 10 mg), the second sample was gently sieved through the same four sieve sizes, using water with similar salinity to the field site (~ 15 ppt) rather than distilled. Each sample was gently shaken within a porcelain bowl and no direct contact or pressured water spray was placed on the grains. This continued until all the sediment particles were sieved and the water ran clear. Sediment from each sieve was then dried to obtain the weight of the intact pellet-sized sediment in the form it was collected from the box core φ_{gentle_sieve} (Figure 3-2b). The intact wet sieved sample was also muffled to determine its LOI. The pellet weight in each size class (φ_{Pellet}) was then given by

$$\varphi_{Pellet} = \varphi_{gentle_sieve} - \varphi_{disaggregated}$$

3.3.4. Beryllium-7

Sediment samples for measurement of ^7Be activity were sliced onboard the research vessel at 1-cm intervals for the first 10 cm and 2-cm intervals for the rest of the core. Back in the lab,

sediment collected from each depth horizon was individually homogenized, and if excess water was present, the sample was centrifuged, and the extraneous water was decanted. Each sample was measured using a semi-planar intrinsic germanium detector to analyze the gamma decay of the ^7Be isotope, in conjunction with a multi-channel analyzer. Three detectors at VIMS were used in the analyses (a Low Energy Germanium detector (LeGe), a Broad Energy Germanium detector (BeGe), and, occasionally, a Well-shaped Intrinsic Germanium detector (WeGe), to assess net count activity rates of each sample at 477 KeV. Samples counted in the BeGe and LeGe detectors were run for 25 hours or on the WeGe for 50 hours in order to sufficiently determine the disintegrations per minute (dpm). Each sample was then corrected for decay that occurred due to time elapsed between sediment collection and counting. Activity rates (dpm/g) for each sample were calculated and then normalized based on both sediment weight and grain size, as ^7Be intrinsically attaches more easily to mud particles, rather than sand particles. In addition, the ^7Be inventories (I) were calculated for the upper 3cm of each core applying the equation:

$$I=(A_i \rho_s(1- \phi))$$

Where A_i = the specific activity based on the efficiency factors at 477KeV, ρ_s = average particle density of 2.65 gcm^{-3} and ϕ = the porosity (Dibb and Rice, 1989; Kniskern and Kuehl, 2003; Romine, 2004; Rodriquez and Kuehl, 2013).

3.3.5. Digital X-radiography

Sediment slabs (12 cm x 2.5 cm x (up to) 30 cm) were collected from the Gomex box-cores each week and imaged back at VIMS using a Varian Paxscan digital x-radiographic panel. Following Schaffner et al. (2001) and Dickhudt et al. (2011), the sediment fabric apparent in the

grayscale images from each x-ray allowed a visual assessment of the degree of physical layering versus biological reworking of bed. In addition, changes in the darkness of each image from top to bottom provided a proxy for vertical variations in density. Here we present x-rays as negatives such that lighter shades of gray indicate higher density, and darker shades indicate lower density.

3.3.6. Erodibility

On each cruise, two subcores were obtained from separate box-cores and brought back to the lab (< 1 hour by boat) for immediate erodibility analysis using a Gust erosion microcosm (Figure 3-3). Subcores (10-cm inside diameter) were carefully selected, making sure both cores appeared level, uniform, and with an undisturbed sediment-water interface. The erodibility measurements utilized two concurrent microcosm experiments with a rotating disc placed at the top of each core (Gust and Muller, 1997; Dickhudt et al., 2011). The setup required that the sediment surface was located 10 cm from the revolving disc and that local water filled the upper 10 cm. When the disc rotated, it produced a circulation pattern that applied a uniform shear stress over the sediment-water interface. Over the course of 2.5 hours, seven shear stresses were applied to the seabed within the core (nominally set to 0.01, 0.05, 0.1, 0.2, 0.3, 0.45, and 0.6 Pa). The first setting of 0.01 Pa was considered to act as a flushing mechanism to remove any “washload” initially present in the core tube, and it is operationally defined that zero true bed erosion occurs at this very low stress. After 30 min at 0.01 Pa setting, the Gust microcosm increased rotation to each larger shear stress for 20 min. Actual disc rotation rates, which were recorded by the Gust system during each experiment, were used to after the experiment to more precisely calculate the true shear stresses applied. It was discovered after the final Gust experiment that the nominal 0.6 Pa setting did not function correctly.

As the rotating disc began applying stress, a constant stream of water was suctioned from the core and the effluent was passed through a flow-cell of a Hach 2100-N turbidimeter, which provided NTU readings of the suspended sediment withdrawn from the core. Concurrently, estuarine water collected at the field site was pumped into the microcosm the same rate. The effluent from each shear stress step was then filtered onto a 0.7 μ m glass-fiber filter to calibrate the turbidimeter and determine the total mass of sediment eroded from the core. The measurements of eroded mass (m) from the bed as a function of time (t) were analyzed using Sanford and Maa's (2001) erosion rate formulation as implemented by Dickhudt et al. (2011):

$$E(m,t) = M(m)[\tau_b(t) - \tau_c(m)]$$

where E is the erosion rate, M is the depth-varying erosion rate "constant", τ_b is shear stress, and τ_c is the critical shear stress for erosion. The key output of fitting observed data to the above relation is the profile of τ_c into the bed as a function of eroded mass, m. For each core, a least-squares regression was applied to τ_c vs. m for stress levels 2 through 5 in order to quantify changes in erodibility from week to week.

3.3.7. Statistical Tests

P-values were used to determine statistical significance, with a significance cut-off of $p < 0.1$ (i.e., less than a 10% chance that randomly selected observations would not produce a similarly significant result if none in fact existed). A one-way ANOVA was used to distinguish whether population means were different. P-values associated with linear regressions were used to test the one-sided null hypothesis in correlations. The p-values themselves were calculated by routines provided by the software package MATLAB (MathWorks, 2013).

3.4 Results

3.4.1. Water Content, Organics, and Disaggregated Sediment Components

A consistent pattern seen in all the cores was a decrease in water content and organics with depth down-core, accompanied by an increase in content of disaggregated sand-sized particles (Figure 3-4a-c, Table 3-2) ($p < 0.01$ for all cores except $p > 0.1$ for % sand on 5 May). Percent water was determined relative to the initial weight of the wet sediment, while percent organics and sand were relative to the sediment's dry weight. Dickhudt et al. (2011) found that for similar York River Estuary cores collected in 2007, sediment samples that were muddier tended to contain more water and organics than samples that were sandier. To further examine patterns in water and organic content while normalizing for the sand content, the water and organic percentages were replotted relative to the mud matrix alone, i.e., by effectively removing the sand-sized (presumably inorganic) particles while leaving the water, mud and organics behind in the calculation (Figure 3-4d-e).

Once the sand had been removed from the calculation, the water content and organic content did indeed vary less in the upper part of the cores. The standard deviation (SD) was used to quantify the degree of variability within the upper part a given core (depth shallower than 8 cm) for water content and organic content. The standard deviation (SD) for percent water for depths shallower than 8 cm depth dropped from 5.6 to 3.8 percentage points when considering the mud matrix alone, and the SD of organic content dropped from 1.20 to 0.93 percentage points, changes that were both found to be significant at $p < 0.1$. Lower in the cores (deeper than 8 cm), normalizing for sand content actually increased the inter-core variability in water and organic content. Sources of increased heterogeneity below 8 cm may include inherent spatial variability (the week-to-week cores were collected at least 10s of meters apart – see Table 3-1). The extreme excursion in normalized values at ~10 cm for April 29th may be due to the presence

of relatively large pieces organic detritus -- it is important to recognize that organics may occasionally be present as sand-sized component particles (i.e., even after disaggregation).

The mass of the disaggregated silt-size fraction relative to the mud matrix (Figure 3-4f; calculated from data in Table 3-3) was generally similar from core to core. Except for the May 5th case, the silt fraction of mud was about 40% from the surface down to ~11 cm. All five cores then exhibited an increase in silt of about 10 percentage points between 11 cm and the bottom of the core. Omitting a few anomalous measurements on May 5th (those below 30%), the silt content of the mud matrix shallower than 11 cm averaged 39.6%, while the silt content deeper than 12 cm averaged 47.4 %. This increase in silt content deeper than 12 cm on all dates was significant at $p < 0.0001$.

3.4.2. Pellets and Other Pellet-Sized Grains

Overall, the size distributions for the pellets and the pellet-sized disaggregated particles (i.e., “disaggregated” coarse silt and fine sand) were roughly similar (Figure 3-5a,b; calculated from data in Table 3-4), with the most abundant size by mass always found on either the 63 or the 90-micron sieve. Also, in all cases, the third most mass was caught on the 45-micron sieve, and the least was caught on the 150-micron sieve. Thus the range of sieves chosen successfully spanned the peak of the size distribution in every case. The 50th percentile size (d_{50}) for pellet size distributions in Figure 5a averaged 81.0 microns, while the d_{50} for the “disaggregated” silt/sand size distributions in Figure 3-5b was virtually identical and statistically indistinguishable ($p > 0.7$) from the pellet samples with an average value of 80.3 microns. However, the pellets exhibited more variability in their size distribution between samples, as quantified by the standard deviation of the pellet size distribution around the mean of 5.7%. In contrast, the SD for the “disaggregated” silt/sand size distribution around the mean was

significantly less ($p < 0.001$) at only 2.4 percentage points. Also, the mean fraction of pellets larger than 150 microns (8.4 %) was significantly larger ($p < 0.001$) than the mean fraction of “disaggregated” particles (3.3 %), while the mean fraction of pellets in the 90 to 150 microns class was significantly less than “disaggregated” particle fraction (28.4 % vs. 34.4 %, $p < 0.02$). Differences in the mean fractions of pellets versus “disaggregated” particles for the other two size classes were insignificant ($p > 0.6$).

The pellets contained significantly more organic matter than the “disaggregated” silt and sand grains on average for every size class ($p < 0.001$) (Figure 3-5c-d). When summed over all four size classes according to the classes’ relative abundance, the average organic content was 9.4 % for the pellets and only 1.5 % for the “disaggregated” particles (difference significant at $p < 0.0001$). For both pellets and “disaggregated” material, percent organic matter was significantly higher for the largest size class ($p < 0.002$), averaging 15.2 and 6.1 percent, respectively. This is likely due to the occasional presence of larger pieces of organic detritus in both the pelletized and “disaggregated” particle populations. Since the abundance of the largest size class was small in each case, the occasional pieces of large organic detritus did not strongly affect the organic content averaged across size classes for either the pellets or the coarse silt/fine sand.

When weighted for relative abundance of size classes, pellets made up an average of 36.2 % of the mass contained in the total “gentle_sieve” (i.e., pellet plus “disaggregated”) particles caught on 45 micron or larger sized sieves (Figure 3-5e). The percentage of pellets relative to total particle mass was largest for the > 150 micron size class, at 59.2 % ($p < 0.001$). Examining percent water and organics relative to the mud matrix reduced variance in the upper section of cores (see Section 3.4.1). Thus the percentage mass of pellets relative the total mud matrix was

also examined. To estimate the total mud content in the core slices used for pellet analysis, the values for disaggregated sand-sized content caught on sieves ≥ 63 microns during the “disaggregated” particle analysis (contained in Table 3-4) were scaled in percentage terms to match the percent sand content for the corresponding dates and depths in Table 3-2. Consistent scaling factors were then used to determine the percent of pellets relative to total dry sediment. The resulting values for mass percent of mud contained in pellets relative to the total dry mass of the mud matrix are displayed in Figure 3-3f. Unlike the percent water or percent organics (or percent silt) in Figure 3-4c-e, however, percent mass contained in pellets was highly variable as a percent of total mud from core to core (Figure 3-5f). Summed across all four size classes within individual cores, pellet content ranged from a low of 5.1 % of all mud to a high of 29.0 % of all mud.

3.4.3. Beryllium-7

All of the cores exhibited ^7Be activity that was clearly detectable above background and which dropped off at relatively similar rates with depth into the bed. Beryllium-7 activity per gram of dry sediment as a function of depth into the bed (corrected for decay time since field collection) is contained in Table 3-5 and plotted in Figure 3-6 for the five sampling cruises. The profiles in Figure 3-6 have additionally been normalized using information from Table 3-2 to “remove” the sand so that the ^7Be activity is plotted as activity per gram of mud. This was done because ^7Be in the York River Estuary is known to adsorb much more efficiently to the greater surface area per mass of mud versus sand (Romine, 2004). All of the cores exhibited relatively strong activities of at least 0.8 dpm per gram of dry mud at least as deep as the 1-2 cm depth interval. Moving downward from the surface, eight of the ten cores last exhibited an activity greater than 0.2 dpm/g of mud within 1-cm thick horizons centered at 4.5 to 6.5 cm. There was

also notable variability from core to core. Activities at the surface ranged from 3.0 to 1.0 dpm/g of mud, and the SD for activity among the 0-1 and 0-2 cm slices across all ten cores was 0.89 dpm/g. However, when the top two slices for the two cores from each sampling date were grouped, there was found to be no significant difference ($p > 0.1$) in mean activity between any two dates, likely due in part to the small number of samples.

3.4.4. Digital X-radiography

X-radiography revealed mottled patterns of light and dark banding within ~ 1 cm of the surface on every coring date (Figure 3-7a-e), characteristic of moderate bioturbation (e.g., Dickhudt et al. 2009). There were no obvious sequences of several cm-thick parallel laminations at the surface of the cores, such as those Dickhudt et al. (2009) associated with periods of rapid seasonal deposition at Clay Bank. In every x-radiograph, there was an overall increase in gray-scale brightness from the top of the core toward the bottom, consistent with an overall decrease in water content with depth. There was also evidence on every cruise date of a step-like increase in brightness between about 7 and 10 cm below the sediment-water interface. In an effort to examine this transition in brightness semi-quantitatively, pixel intensity across each x-radiograph in Figure 7a-e was averaged and then plotted as a function of depth between 1 and 14 cm. The 0-1 cm interval was not included because of ambiguities in brightness associated with averaging across the slightly uneven core surface. The width-averaged pixel intensity was then normalized on a scale of zero to one such that the lowest width-averaged intensity between 1 and 14 cm for each core was set to zero, and the highest width-averaged intensity was set to one (Figure 3-7f). In every core, this analysis highlighted a zone of gradually increasing pixel brightness from 1 to ~ 7 cm, a rapidly increasing intensity layer located in the vicinity of 7 to 10 cm, and a layer of nearly uniform pixel intensity between ~ 10 cm to 14 cm.

3.4.5. Erodibility

All ten of the erodibility experiments associated with the five coring cruises (Table 3-6; Figure 3-8) clearly exhibited Type 1 depth-limited erosion, as was also the case for the York River Estuary cores eroded in Gust chambers by Dickhudt et al. (2009, 2011). Each time stress was increased in the Gust microcosm for the experiments displayed Figure 3-8, erosion occurred rapidly at first and then dramatically slowed as the eroded depth in the core approached the depth where the critical erosion stress, τ_c , equaled the external stress applied by the microcosm. When a seabed in a tidal estuary is characterized by strongly depth-limited erosion, as was the case here, the erodibility of a given core can be fully characterized by the relationship between eroded mass and τ_c , as plotted in Figure 3-8. This is because the time-scale over which erosion reaches the depth where τ_c nearly equals the externally applied bed stress (~ 10 minutes for most York cores) is much shorter than the characteristic time scale over which tidal stress changes (~ 2 hours). As a result, the depth-varying erosion rate “constant” (which is poorly constrained in any case), is not important to determining how much sediment is eroded.

To compare erodibility between dates, eroded mass values from Figure 3-8 were interpolated to 0.2 Pa, and then paired cores for each date were grouped. A stress of 0.2 Pa was used because field observations of bed stress at Clay Bank have indicated 0.2 Pa to be a typical amplitude for bed stress at maximum tidal velocity (Friedrichs et al., 2008). In comparing erodibility among dates, mean erodibility was lowest (0.083 kg/m^2 at 0.2 Pa) on 11 May (significantly so against all but 20 May, $p < 0.1$), and mean erodibility was highest (0.228 kg/m^2 at 0.2 Pa) on 29 April, although it was not significantly greater on 29 April than on 5 May or 27 May ($p > 0.1$). As was the case for ^7Be , the low number of significant differences may be due in

part to the small sample size. Pooling all 10 cores together, the mean eroded mass at 0.2 Pa was 0.147 kg/m² with a SD of 0.068 kg/m².

3.4.6 Correlations Between Core Properties Within the Top Centimeter

In order to statistically identify likely influences on and signatures of sediment erodibility and consolidation, correlation analysis was performed on the various sediment properties measured within the uppermost centimeter of the seabed (Dickhudt et al., 2009, 2011; Stevens et al., 2007; Wiberg et al., 2013). If more than one observation of a given property was obtained from the 0-1 cm interval on a given cruise date, the multiple values for that date were averaged before the correlations across cruise dates were applied. The application of correlation analysis was limited to the uppermost centimeter because only a few millimeters or less of sediment was eroded at 0.2 Pa during each Gust microcosm experiment. In Figure 3-8, 0.2 Pa corresponds to < ~ 0.2 kg/m², i.e., only ~ 0.02 grams/cm². Even at 90% porosity, this would have corresponded to just 2 mm of sediment of erosion.

Table 3-7 contains a listing of correlation r-values and p-values among parameter values of interest that were measured within the 0-1 cm interval. Significant correlations based on a one-sided p-value less than 0.1 are highlighted in Table 3-7 by dark shading. Correlations with $0.1 \leq p < 0.2$ are highlighted with light shading as trends that may be worth noting, although they did not actually satisfy our definition of significance. Other than sand content and particle grain size, the properties examined were normalized relative to mud content, given that properties of the “mud matrix” are thought to be more important to erodibility of muddy beds than are properties involving sand content (Dickhudt et al., 2011). In addition to core properties, elapsed time (in days since the first cruise) was also considered.

The results in Table 3-7 indicate that over the course of time from late April to late May 2010, the median size of sand and pellets present became significantly coarser, and the organic content of the mud decreased. In addition, the sand content tended to increase, the water and silt content of the mud tended to decrease, and the erodibility of the bed tended to decrease. Among these tendencies, the decrease in erodibility was significantly correlated to the decrease in silt content. The concentration of pellets in the mud matrix was significantly correlated to the percentage of disaggregated sand in the bed as a whole and was negatively correlated to ^7Be activity. There also was a tendency for pellet concentration to decrease as water content increased. In addition, ^7Be activity per gram of dry mud was negatively correlated with percent sand, tended increase with mud water content, and tended to decrease as pellet size increased.

3.5. Discussion

3.5.1. Cruise Timing Relative to Seasonal Turbidity Transition and Spring-Neap Cycle

The York River Estuary coring cruises described above began a few weeks after the end of the 2010 winter-to-spring freshet (Figure 3-9a), providing an opportunity to study in detail the evolution of the seabed following the annual dissipation of the secondary turbidity maximum. The general hydrodynamic setting before, during and after the coring cruises can be inferred from daily river gauging data provided by the U.S. Geological Survey (USGS, 2013) and from monthly water quality samples collected by the Environmental Protection Agency (EPA, 2013). In 2010, the seasonal pattern of discharge, salinity and suspended sediment in the York River Estuary (Figure 3-9a-c) followed the typical trend previously observed by others, i.e., a progression from a wetter winter/spring to a drier summer/fall, with the transition in conditions centered around the late spring to early summer (Lin and Kuo, 2001; Friedrichs et al., 2008; Dickhudt et al., 2009; Fall, 2012).

Although the EPA monitoring data in the York are sparse in time and space, the EPA data suggest that the coring cruises in this study were well-timed relative to the annually recurring, seasonal dissipation of the mid-estuary turbidity maximum as outlined by Dickhudt et al. (2009). Together with USGS discharge time-series, EPA data suggest that in spring 2010 a seasonal transition from high to low discharge (Figure 3-9a) led to a temporal shift in the middle-estuary from salinity stratification to more vertically mixed conditions (Figure 3-9b). The reduction in salinity stratification presumably eliminated the physical trapping mechanism that favored sediment accumulation in the middle estuary. So suspended sediment concentrations in the middle estuary then declined (Figure 3-9c). The data in Figure 3-9 capture the progressive temporal lag from decreasing discharge to decreasing stratification to decreasing TSS. These patterns are supported by an averaging of EPA data collected upstream and downstream of the Clay Bank coring site, suggesting this is a spatially wide-spread phenomena (for EPA station locations see Figure 3-1). The 2010 coring cruises, which extended from late April to late May, encompassed the temporal change in stratification in the middle estuary and the resulting temporal change in near-bed suspended sediment concentration.

The approximate once-a-week spacing of the coring cruises in the York River Estuary also encompassed the spring-neap variability in tidal forcing typical of the York River and many other tidal estuaries (Figure 3-9d). Continual monitoring of tidal elevation in the York River estuary was provided by a National Ocean and Atmospheric Administration tide gauge (NOAA, 2013), mounted on the Yorktown Coast Guard Pier. Figure 9d displays the twice-daily range (high water minus low water) observed over the period of the coring cruises, with the timing of each cruise indicated by a vertical line. Because of diurnal inequality between the two daily tidal

cycles, the tide range did not simply oscillate from spring to neap each week. Nonetheless, the coring cruises still sampled the seabed in conjunction with a diverse set of tidal conditions.

3.5.2. Bed Erodibility and Its Relation to Time and Tidal Disturbance

In comparison to the erodibility of cores sampled at the same location in 2007 by Dickhudt et al. (2009), the erodibility of the April-May 2010 cores examined here was intermediate, consistent with a transition period of gradually increasing consolidation following the departure of the secondary turbidity maximum. Figure 3-10 displays the April through May 2010 erosion data in comparison to the erosion data collected at Clay Bank between March and October 2007. For critical shear stresses between 0.1 and 0.3 Pa, cores from spring of 2007 exhibited significantly more eroded mass ($p < 0.0001$) than those from 2010 (Figure 3-10a), whereas cores from summer and fall of 2007 exhibited significantly less eroded mass ($p < 0.02$) than those from 2010 (Figure 3-10b). The 2007 cores, which were collected at monthly or longer intervals, were bimodal in character, in that erodibility was consistently high when the secondary turbidity maximum was present and much lower after the turbidity maximum had been dispersed (Dickhudt et al. 2009). It is likely that monthly sampling was too coarse in time for Dickhudt et al. (2009) to capture relatively rapid consolidation. In contrast, the more frequently collected data reported here from April through May 2010 allow an examination of evolving erodibility over time-scales more consistent with the several days to a week or two expected for substantial changes in muddy bed consolidation (e.g., Mehta and McAnally, 2008).

An examination of the spring 2010 cores as a time-series revealed a tendency for erodibility to decrease with time along with a superimposed temporal oscillation correlated to low-passed tidal range (Figure 3-11). To evaluate erodibility as a time-series, eroded mass values from Figure 3-8 were interpolated to 0.2 Pa, and the paired cores were then averaged to produce

a single value for each date (Figure 3-11a). By testing a range of low-pass time-scales and lag-times, it was found that the correlation between eroded mass and low-passed tidal range peaked when tidal range was averaged over the 11 tidal cycles (5.7 days) immediately preceding core collection. Tested on its own, the tendency for erodibility to decrease in time was a trend rather than being statistically significant (see Table 3-7), but the correlation with low-passed tidal range was significant on its own ($r = 0.76$, $p < 0.07$; Figure 3-11b). Interestingly, a multiple linear regression of eroded mass versus both time and low-passed tidal range notably improved the overall correlation, increasing the r-value for the combination to $r = 0.94$ and decreasing the p-values associated with the proportionality coefficients to more significant values of $p < 0.08$ and $p < 0.05$ for time and tidal range, respectively. Together these correlations suggest that consolidation with time reduces erodibility, but disturbance by tidal resuspension tends to increase erodibility. The peak correlation with tidal range averaged over the previous 11 tidal cycles suggests a characteristic bed consolidation time scale of about 5 to 6 days. Consolidation over several day time-scales, “reset” by intermittent resuspension events, is qualitatively consistent with recently developed models for time-dependent cohesive seabed erodibility (Rinehimer et al., 2008; Sanford, 2008).

3.5.3. Observations Suggest Consolidation and Bed Together, Despite Limited Resolution

Correlations of seabed properties with time and each other (see Table 3-7) suggest the seabed of the York River Estuary was simultaneously subject to both consolidation and bed armoring following dispersal of the turbidity maximum. Overall, the trends observed in this study are consistent with both dewatering and a progressive winnowing of the most easily suspended material from the sediment surface, including coarse silt, small pellets, and organic-rich flocs, leaving behind and concentrating sand and larger pellets. As time passed, the sand

content, median sand size, percent pellets, and median pellet size were all observed to increase at the surface (Table 3-7), while the percent water, organics, silt, ^{7}Be activity and erodibility decreased. Although some of these correlations with time were weak, these parameters were often additionally correlated with each other in a sense that supports this overall interpretation.

Classically, a decrease in the percent water of the mud matrix, i.e., dewatering, is synonymous with cohesive consolidation (e.g., Dickhudt et al., 2011), whereas an increase in size and concentration of sand-sized particles, i.e., coarsening of the bed, is synonymous with bed armoring (e.g., Wiberg et al., 1994). Consolidation and bed armoring each lead to lower erodibility. Typically, however, consolidation and bed armoring are each associated with cohesive and non-cohesive sediment, respectively and exclusively. The results of this study suggest that cohesive-like consolidation and non-cohesive-like bed armoring may occur simultaneously in mixtures of pelletized mud and sand, even when the overall concentration of disaggregated clay and silt would classically define the bed to behave more like pure mud (Law et al., 2008). The possible simultaneous occurrence of consolidation and bed armoring in mixed muddy beds is also consistent with recent advances in cohesive bed modeling (Sanford, 2008).

In this study, it is likely that limited eroded mass, associated sampling complexities, a small overall number of cores, and confounding tidal variability all conspired to make a clearer resolution of the relationship between core properties and erodibility difficult. As described in Section 3.4.6, only about 2 mm of sediment was likely to have been eroded in the Gust chamber at 0.2 Pa. Based on experience, the smallest surface core thickness interval that could reliably be sampled in the field while retaining representative water content was about 1 cm. If the top 1 cm did not optimally represent the key properties of the top 2 mm, then a strong correlation of parameters within the top 1 cm to erodibility might be difficult to obtain. Statistically speaking,

the overall number of cores processed was also relatively small; however, collection and processing of any more cores any more frequently over a five-week period was not logistically possible. Finally, tidal disturbance likely affected erodibility significantly; but tidal range was not found to be notably correlated to any of the parameters in Table 3-6 other than erodibility, even at $p < 0.2$ (details of correlations with tidal range not shown). Thus the imprint of tidal disturbance on erodibility in particular may have added additional “noise” to erodibility’s potential correlation to other factors.

3.5.4. Controlling for the Possible Role of Significant Net Erosion or Deposition

Evidence from ~15 cm profiles of sediment properties from multiple cores collected during this study argues against a dominant role for major deposition or erosion in modulating erodibility. Across the five weeks of coring examined here, a layer of relatively less variable percent water of mud, less variable percent organic content of mud, and less variable x-radiography pixel intensity was consistently documented from the surface down to ~ 7 cm depth, below which notably greater variability was seen. This also roughly corresponded to the maximum depth across the multiple cores at which ^7Be activity was last seen above background levels. If notable net erosion or deposition had occurred during the five-week sampling period, one would have expected this transition to migrate upward or downward in time. The nature of layering above ~ 7 cm from x-radiographs was also observed to be mottled on every cruise date, which additionally argued against significant deposition.

Clearly properties found any further than ~ 1 cm below the top of the cores examined here cannot directly control surface erodibility, because mass erosion during a given tidal cycle can penetrate only several millimeters into the bed at most. Nonetheless, the relatively uniform properties found in each core between 1 and 7 cm below the surface is still an important finding

in this study, because it simplifies a potentially confounding role for depositional history. At this same site, Dickhudt et al. (2009) found that periodic rapid deposition associated with seasonal formation of the turbidity maximum was responsible for the dramatic seasonal increases in erodibility that they documented. Thanks to the relative seabed stability documented during the present study, this set of observations set may provide an especially useful data set for constraining relatively simple but time-dependent models for time-dependent consolidation and/or bed armoring of mixed grain muddy deposits in the absence of major erosion or deposition.

3.6. Summary and Conclusions

Appropriate parameterization of time-dependent erodibility of muddy seabeds is a significant barrier to improved understanding and accurate modeling of sediment dynamics in estuaries and coastal seas. This sedimentological study in the middle reaches of the York River estuary investigated controls on cohesive bed erodibility by assessing changes in seabed properties over weekly timescales. As far as we are aware, this represents the first in-situ study to successfully and quantitatively relate classic bed properties (i.e., water content and grain size) to evolving erodibility over this key consolidation time-scale in a subtidal cohesive estuarine environment.

During April and May of 2010, multiple GOMEX box cores were collected over a five-week period chosen to correspond with the annual post-freshet dissipation of the York River Estuary's secondary turbidity maximum, while also resolving the estuary's spring-neap cycle. Once a week for five weeks, box cores were subsampled to a depth of ~ 15 cm for profiles of disaggregated sand/silt/clay, organic and water content, and ⁷Be activity. Based on gentle sieving, resilient pellet concentration and pellet size distribution was determined for the

uppermost 2 cm. In addition, images of internal fabric were collected via digital x-radiography, and erodibility of the surface of the cores was determined via a Gust microcosm.

All the cores across all five weeks were characterized by a decrease in water content and organics with depth, accompanied by an increase in content of disaggregated sand-sized particles. When normalized by mud content, however, water and organic content in the upper part of the cores (> 1-cm and < ~ 7-cm depth) varied only slightly. From ~ 1 to 7 cm, x-radiographs suggested persistent, moderate bioturbation, and ^7Be was often present. Below ~ 7 cm, variability in water and organic content of mud significantly increased, the pixel brightness of X-radiographs markedly increased, and ^7Be was always absent. In general, these common patterns in vertical structure present during all five weeks suggested that neither significant net erosion nor net deposition was responsible for observed variations in erodibility.

In contrast to relatively stable properties below 1-cm depth in the cores, surficial properties evolved in response to the recent dissipation of the middle-estuary turbidity maximum. Overall, the trends observed in this study were consistent with both a dewatering and a progressive winnowing of the most easily suspended material from the uppermost cm. As time passed, the sand content, median sand size, percent pellets, and median pellet size were all observed to increase at the surface, while the percent water, organics, silt, ^7Be activity and erodibility decreased. Consistent with recent advances in cohesive bed modeling, the results of this study suggest that cohesive-like consolidation and non-cohesive-like bed armoring may occur simultaneously in mixtures of pelletized mud and sand.

Motivated by previous studies which associated muddy seabed pelletization with decreased erodibility, this study developed a methodology to consistently sample for resilient

muddy pellets and described their occurrence and size distribution in detail. The 50th percentile (d_{50}) for pellet size distributions averaged 81.0 microns and significantly increased over the course of the study. The organic content of the pellets averaged 9.4% compared to only 1.5% for the sand and coarse-silt-sized particles that survived classical laboratory disaggregation. Before disaggregation, mud pellets which survived gentle sieving made up, by dry weight, 36% of all particles > 45 microns and 59% of all particles > 150 microns.

Along with a tendency for erodibility to decrease with time, this study identified a superimposed temporal oscillation in erodibility correlated to low-passed tidal range, presumably because stronger tidal currents disturbed the bed, partly counteracting the temporal effects of consolidation. It was found that the correlation between eroded mass and low-passed tidal range peaked when tidal range was averaged over the 11 tidal cycles immediately preceding core collection, suggesting a characteristic bed consolidation time scale of about 5 to 6 days. Consolidation over a several day time-scales, “reset” by intermittent resuspension events, is also qualitatively consistent with recently developed models for time-dependent cohesive seabed erodibility.

References

- Aberle, J., Nikora, V., & Walters, R., 2004. Effects of bed material properties on cohesive sediment erosion. *Marine Geology*, 207(1), 83-93.
- Amos, C.L., Feeney, T., Sutherland, T.F., and Luternauer, J.L., 1997. The stability of fine-grained sediments from the Fraser River delta. *Estuarine, Coastal, and Shelf Science* 45, 507-524.
- Andersen, T.J., 2001. Seasonal Variation in Erodibility of Two Temperate, Microtidal Mudflats. *Estuarine Coastal and Shelf Science* 53, 1-12.
- Andersen, T. J., Lanuru, M., van Bernem, C., Pejrup, M., & Riethmueller, R., 2010. Erodibility of a mixed mudflat dominated by microphytobenthos and *Cerastoderma edule*, East Frisian Wadden Sea, Germany. *Estuarine, Coastal and Shelf Science*, 87(2), 197-206.
- Andersen, T. J., & Pejrup, M., 2002. Biological mediation of the settling velocity of bed material eroded from an intertidal mudflat, the Danish Wadden Sea. *Estuarine, Coastal and Shelf Science*, 54(4), 737-745.
- Angradi, T. R., 1999. Fine sediment and macroinvertebrate assemblages in Appalachian streams: a field experiment with biomonitoring applications. *Journal of the North American Benthological Society*, 49-66.
- Austen, I., Andersen, T. J., & Edolvang, K., 1999. The influence of benthic diatoms and invertebrates on the erodibility of an intertidal mudflat, the Danish Wadden Sea. *Estuarine, Coastal and Shelf Science*, 49(1), 99-111.
- Cartwright, G.M., C.T. Friedrichs, and L.P. Sanford, 2011. In situ characterization of estuarine suspended sediment in the presence of muddy flocs and pellets. In: P. Wang, J.D. Rosati, and T.M. Roberts (eds.), *Coastal Sediments 2011*, World Scientific, pp. 642-655.
- Cooper, S. R., & Brush, G. S., 1993. A 2,500-year history of anoxia and eutrophication in Chesapeake Bay. *Estuaries*, 16(3), 617-626.
- Debnath, K., Nikora, V., Aberle, J., Westrich, B., & Muste, M., 2007. Erosion of cohesive sediments: Resuspension, bed load, and erosion patterns from field experiments. *Journal of hydraulic engineering*, 133(5), 508-520.
- Dellapenna, T.M., Kuehl, S.A., Schaffner, L.C., 1998. Sea-bed Mixing and Particle Residence Times in Biologically and Physically Dominated Estuarine Systems: a Comparison of Lower Chesapeake Bay and the York River Subestuary. *Estuarine Coastal and Shelf Science* 46, 777-795.

- Dellapenna, T.M., Kuehl, S.A., Schaffner, L.C., 2003. Ephemeral deposition, seabed mixing and fine-scale strata formation in the York River estuary, Chesapeake Bay. *Estuarine Coastal and Shelf Science* 58, 621-643.
- Dibb, J. E. and D. L. Rice, 1989. The geochemistry of Beryllium-7 in Chesapeake Bay. *Estuarine, Coastal, and Shelf Science*. 28, 379-394.
- Dickhudt, P.J., 2008. Controls on erodibility in a partially mixed estuary: York River, Virginia. M.S. thesis, Virginia Institute of Marine Science/School of Marine Science, The College of William and Mary, Virginia.
- Dickhudt, P. J., Friedrichs, C. T., Schaffner, L. C., & Sanford, L. P., 2009. Spatial and temporal variation in cohesive sediment erodibility in the York River estuary, eastern USA: A biologically influenced equilibrium modified by seasonal deposition. *Marine Geology*, 267(3), 128-140.
- Dickhudt, P. J., Friedrichs, C. T., & Sanford, L. P., 2011. Mud matrix solids fraction and bed erodibility in the York River estuary, USA, and other muddy environments. *Continental Shelf Research*, 31(10), S3-S13.
- Drake, Pilar, Alberto M. Arias, Francisco Baldó, José A. Cuesta, Antonio Rodríguez, Alfonso Silva-Garcia, Ignacio Sobrino, Diego García-González, and Carlos Fernández-Delgado., 2002. "Spatial and temporal variation of the nekton and hyperbenthos from a temperate European estuary with regulated freshwater inflow." *Estuaries* 25 (3) 451-468.
- Dyer, K.R., 1995. Sediment Transport Processes in Estuaries, in: Perillo, G.M.E. (Ed.), *Geomorphology and Sedimentology of Estuaries*. Elsevier Science, Amsterdam, pp. 423-446.
- Dyer, K.R., 1986. *Coastal and Estuarine Sediment Dynamics*. Wiley, Chichester; New York.
- Edelvang, K., & Austen, I., 1997. The temporal variation of flocs and fecal pellets in a tidal channel. *Estuarine, Coastal and Shelf Science*, 44(3), 361-367.
- EPA, 2013. Chesapeake Bay Program Data Hub. <http://www.chesapeakebay.net/data> (as of July, 2013).
- Fall, K.A., 2012. Relationships among fine sediment settling and suspension, bed erodibility, and particle type in the York River estuary Virginia. M.S. Thesis, M.S. thesis, Virginia Institute of Marine Science/School of Marine Science, The College of William and Mary, Virginia
- Friedrichs, C.T. 2009. York River physical oceanography and sediment transport. *Journal of Coastal Research*, SI 57: 17-22.

- Friedrichs, C.T., Cartwright, G.M., Dickhudt, P.J., 2008. Quantifying benthic exchange of fine sediment via continuous, non-invasive measurements of settling velocity and bed erodibility. *Oceanography* 21, 168-172.
- Friedrichs, C.T., Wright, L.D., Hepworth, D.A., and Kim, S.C., 2000. Bottom-boundary-layer processes associated with fine sediment accumulation in coastal seas and bays. *Continental Shelf Research* 20, 807-841.
- Galler, J. J., & Allison, M. A., 2008. Estuarine controls on fine-grained sediment storage in the Lower Mississippi and Atchafalaya Rivers. *Geological Society of America Bulletin*, 120(3-4), 386-398.
- Geyer, W., 1993. The importance of suppression of turbulence by stratification on the estuarine turbidity maximum. *Estuaries and Coasts* 16, 113-125.
- Geyer, W. R., Woodruff, J. D., & Traykovski, P., 2001. Sediment transport and trapping in the Hudson River estuary. *Estuaries*, 24(5), 670-679.
- Gillett, D. J., & Schaffner, L. C., 2009. Benthos of the York River. *Journal of Coastal Research*, 80-98.
- Gorsline, D. S., Kolpack, R. L., Karl, H. A., Drake, D. E., Thornton, S. E., Schwalbach, J. R., and Fleischer, P., 1984. Studies of fine-grained sediment transport processes and products in the California Continental Borderland. *Geological Society, London, Special Publications*, 15(1), 395-415.
- Gust, G., and Muller, V., 1997. Interfacial hydrodynamics and entrainment functions of currently used erosion devices. In: *Cohesive sediments*, Burt, Parker, and Watts (Eds), Wallingford, U.K., 149-174.
- Harris, C. K., & Wiberg, P. L., 2001. A two-dimensional, time-dependent model of suspended sediment transport and bed reworking for continental shelves. *Computers & Geosciences*, 27(6), 675-690.
- Harris, C. K., Butman, B., & Traykovski, P., 2003. Winter-time circulation and sediment transport in the Hudson Shelf Valley. *Continental Shelf Research*, 23(8), 801-820.
- Hobbs III, C. H., Halka, J. P., Kerhin, R. T., & Carron, M. J., 1992. Chesapeake Bay sediment budget. *Journal of Coastal Research*, 292-300.
- Hobbs, C., 2009. York River Geology. *Journal of Coastal Research*, 10-16.
- Kniskern, T.A., Kuehl, S.A., 2003. Spatial and temporal variability of seabed disturbance in the York River subestuary. *Estuarine Coastal and Shelf Science* 58, 37-55.

- Kraeuter, J., & Haven, D. S., 1970. Fecal pellets of common invertebrates of lower York River and lower Chesapeake Bay, Virginia. *Chesapeake Science*, 11(3), 159-173.
- Law, B. A., Hill, P. S., Milligan, T. G., Curran, K. J., Wiberg, P. L., & Wheatcroft, R. A., 2008. Size sorting of fine-grained sediments during erosion: results from the western Gulf of Lions. *Continental Shelf Research*, 28(15), 1935-1946.
- Li, J., & Zhang, C., 1998. Sediment resuspension and implications for turbidity maximum in the Changjiang Estuary. *Marine Geology*, 148(3), 117-124.
- Lin, J., Kuo, A., 2003. A model study of turbidity maxima in the York River estuary, Virginia. *Estuaries and Coasts* 26, 1269-1280.
- Lin, J., Kuo, A., 2001. Secondary turbidity maximum in a partially mixed microtidal estuary. *Estuaries and Coasts* 24, 707-720.
- Lowe, W. H., & Bolger, D. T., 2002. Local and Landscape-Scale Predictors of Salamander Abundance in New Hampshire Headwater Streams. *Conservation Biology*, 16(1), 183-193.
- MathWorks, 2013. MathWorks Documentation Center. <http://www.mathworks.com/help/index.html> (as of July 2013).
- Meade, R. H., 1969. Landward transport of bottom sediments in estuaries of the Atlantic coastal plain. *Journal of Sedimentary Research*, 39(1), 222-234.
- Meade, R. H., 1982. Sources, sinks, and storage of river sediment in the Atlantic drainage of the United States. *The Journal of Geology*, 235-252.
- Mehta, A. J., 1989. On estuarine cohesive sediment suspension behavior. *Journal of Geophysical Research: Oceans (1978–2012)*, 94(C10), 14303-14314
- Mehta, A. J., & McAnally, W. H., 2008. Fine-grained sediment transport. In: M. Garcia (ed.), *Sedimentation Engineering, ASCE Manual No. 110*, pp. 253-306
- Nichols, M.M., S.C. Kim, and C.M. Brouwer, 1991. Sediment characterization of the Chesapeake Bay and its tributaries, Virginian Province. National estuarine inventory: supplement. NOAA.
- NOAA, 2013. NOAA Tides & Currents. <http://tidesandcurrents.noaa.gov> (as of July 2013).
- Olsen, C. F., Cutshall, N. H., & Larsen, I. L., 1982. Pollutant—particle associations and dynamics in coastal marine environments: a review. *Marine Chemistry*, 11(6), 501-533.
- Perkins, R. G., Honeywill, C., Consalvey, M., Austin, H. A., Tolhurst, T. J., & Paterson, D. M., 2003. Changes in microphytobenthic chlorophyll and EPS resulting from sediment

- compaction due to de-watering: opposing patterns in concentration and content. *Continental Shelf Research*, 23(6), 575-586.
- Perkins, R. G., Paterson, D. M., Sun, H., Watson, J., & Player, M. A., 2004. Extracellular polymeric substances: quantification and use in erosion experiments. *Continental Shelf Research*, 24(15), 1623-1635.
- Ralston, D. K., Geyer, W. R., & Lerczak, J. A., 2008. Subtidal salinity and velocity in the Hudson River estuary: Observations and modeling. *Journal of Physical Oceanography*, 38(4), 753-770. Strategic Assessment Branch. 88 p.
- Reay, W. G., & Moore, K. A., 2009. Introduction to the Chesapeake Bay National Estuarine Research Reserve in Virginia. *Journal of Coastal Research*, 1-9.
- Rinehimer, J.P., C.K. Harris, C.R. Sherwood, and L.P. Sanford, 2008. Estimating cohesive sediment erosion and consolidation in a muddy, tidally-dominated environment: model behavior and sensitivity. In: M.L. Spaulding (ed.), *Estuarine and Coastal Modeling, Proceedings of the Tenth Conference*, ASCE, pp. 819-838.
- Roberts, W.P., Pierce, J.W., 1976. Deposition in upper Patuxent River Estuary, Maryland, 1968-1969. *Estuarine and Coastal Marine Science* 4, 267-280.
- Rodríguez-Calderón, C., 2010. Spatial and Temporal Patterns in Erosional and Depositional Processes: Physical and Biological Controls in the York River, Chesapeake Bay, Virginia. M.S. thesis, Virginia Institute of Marine Science/School of Marine Science, The College of William and Mary, Virginia.
- Rodríguez-Calderón, C., & Kuehl, S. A., 2012. Spatial and temporal patterns in erosion and deposition in the York River, Chesapeake Bay, VA. *Estuarine, Coastal and Shelf Science*.
- Romine, H.M., 2004. Documenting the suspended and bottom sediment dynamics of a two estuarine turbidity maximum system using ^7Be and ^{234}Th . M.S. thesis, Virginia Institute of Marine Science/School of Marine Science, The College of William and Mary, Virginia.
- Salant, N. L., Renshaw, C. E., & Magilligan, F. J., 2006. Short and long-term changes to bed mobility and bed composition under altered sediment regimes. *Geomorphology*, 76(1), 43-53.
- Sanford, L.P., and Maa, J.P.-Y., 2001. A unified erosion formulation for fine sediments. *Marine Geology* 179, 9-23.
- Sanford, L. P., 2008. Modeling a dynamically varying mixed sediment bed with erosion, deposition, bioturbation, consolidation, and armoring. *Computers & Geosciences*, 34(10), 1263-1283

- Schaaff, E., Grenz, C., Pinazo, C., & Lansard, B., 2006. Field and laboratory measurements of sediment erodibility: A comparison. *Journal of Sea Research*, 55(1), 30-42.
- Schaffner, L.C., Dellapenna, T.M., Hinchey, E., Friedrichs, C.T., Neubauer, M.T., Smith, M.E., Kuehl, S.A., 2001. Physical Energy Regimes, Seabed Dynamics, and organism–sediment Interactions Along an Estuarine Gradient, in: Aller, J.Y., Woodin, S.A., R.C. Aller, R.C. (Eds.), *Organism–Sediment Interactions*. University of South Carolina Press, Columbia, pp. 159-179.
- Shen, J., & Haas, L., 2004. Calculating age and residence time in the tidal York River using three-dimensional model experiments. *Estuarine, Coastal and Shelf Science*, 61(3), 449-461.
- Stevens, A. W., Wheatcroft, R. A., & Wiberg, P. L., 2007. Seabed properties and sediment erodibility along the western Adriatic margin, Italy. *Continental Shelf Research*, 27(3), 400-416.
- Summerhayes, C. P., Ellis, J. P., & Stoffers, P., 1985. *Estuaries as sinks for sediment and industrial waste-a case history from Massachusetts Coast.-Contributions to Sedimentology 14*. Stuttgart, Schweizerbartsche Verlagsbuchhandlung, pp. 45-47.
- Uncles, R. J., 2002. Estuarine physical processes research: some recent studies and progress. *Estuarine, Coastal and Shelf Science*, 55(6), 829-856.
- Underwood, G. J., & Paterson, D. M., 2003. The importance of extracellular carbohydrate production by marine epipelagic diatoms. *Advances in botanical research*, 40, 183-240.
- USGS, 2013. USGS Water Data for the Nation. <http://waterdata.usgs.gov/nwis> (as of July 2013).
- Van Ledden, M., Van Kesteren, W. G. M., & Winterwerp, J. C., 2004. A conceptual framework for the erosion behavior of sand–mud mixtures. *Continental Shelf Research*, 24(1), 1-11.
- Weigelhofer, G., & Waringer, J., 2003. Vertical distribution of benthic macroinvertebrates in riffles versus deep runs with differing contents of fine sediments (Weidlingbach, Austria). *International Review of Hydrobiology*, 88(3-4), 304-313.
- Wiberg, P. L., Drake, D. E., & Cacchione, D. A., 1994. Sediment resuspension and bed armoring during high bottom stress events on the northern California inner continental shelf: measurements and predictions. *Continental Shelf Research*, 14(10), 1191-1219.
- Wiberg, P. L., Law, B. A., Wheatcroft, R. A., Milligan, T. G., & Hill, P. S., 2013. Seasonal variations in erodibility and sediment transport potential in a mesotidal channel-flat complex, Willapa Bay, WA. *Continental Shelf Research*. 60S, S185-S197.

- Widdows, J., Brown, S., Brinsley, M.D., Salkeld, P.N., Elliott, M., 2000. Temporal changes in intertidal sediment erodibility: influence of biological and climatic factors. *Continental Shelf Research* 20, 1275-1289.
- Winterwerp, J. C., & Van Kesteren, W. G., 2004. *Introduction to the physics of cohesive sediment dynamics in the marine environment*.
- Wolanski, E., & Gibbs, R. J., 1995. Flocculation of suspended sediment in the Fly River estuary, Papua New Guinea. *Journal of Coastal Research*, 754-762.
- Wong, G. T., & Moy, C. S., 1984. Cesium-137, metals and organic carbon in the sediments of the James River Estuary, Virginia. *Estuarine, Coastal and Shelf Science*, 18(1), 37-49.

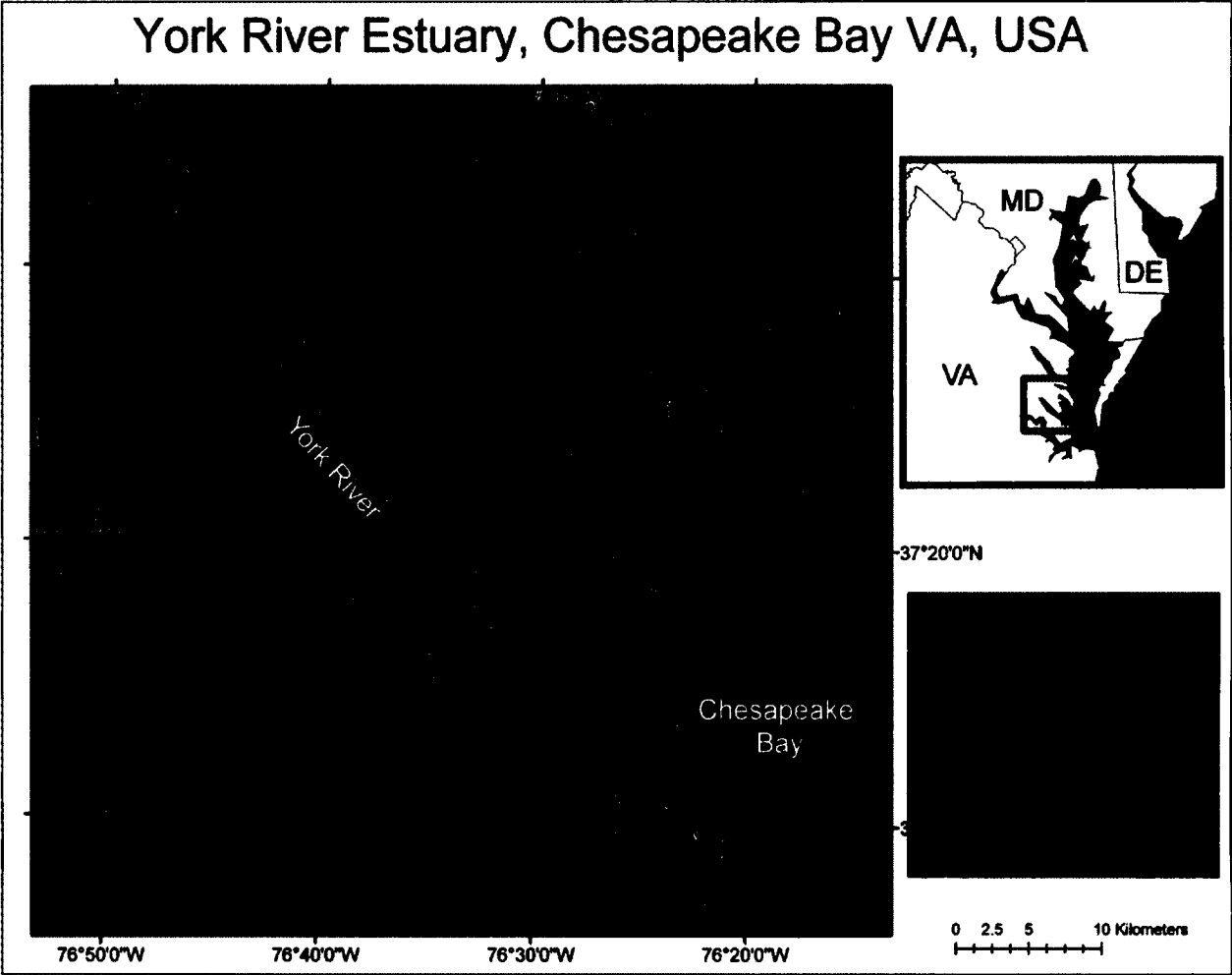


Figure 3-1. Map of York River Estuary. Location of Clay Bank study site indicated by the black dot. Locations of EPA long-term monitoring stations and NOAA tide gauge closest to Clay Bank indicated by red squares. The aerial photograph inset shows the Clay Bank MUDBED sites. The Yellow star depicts the secondary channel core location for this study. The VIMS Clay Bank Piling (green dot) and the MUDBED main channel core location (white dot) are shown for data comparisons between studies.

Table 3-1. Cruise date, location, and station numbers.

Cruise date	Latitude (minutes north of 37 degrees)	Longitude (minutes west of 76 degrees)	Log-book core numbers
29 April 2010	20.49	37.48	4872-4878
5 May 2010	20.46	37.44	4879-4885
11 May 2010	20.47	37.49	4886-4893
20 May 2010	20.45	37.47	4894-4901
27 May 2010	20.48	37.50	4902-4909

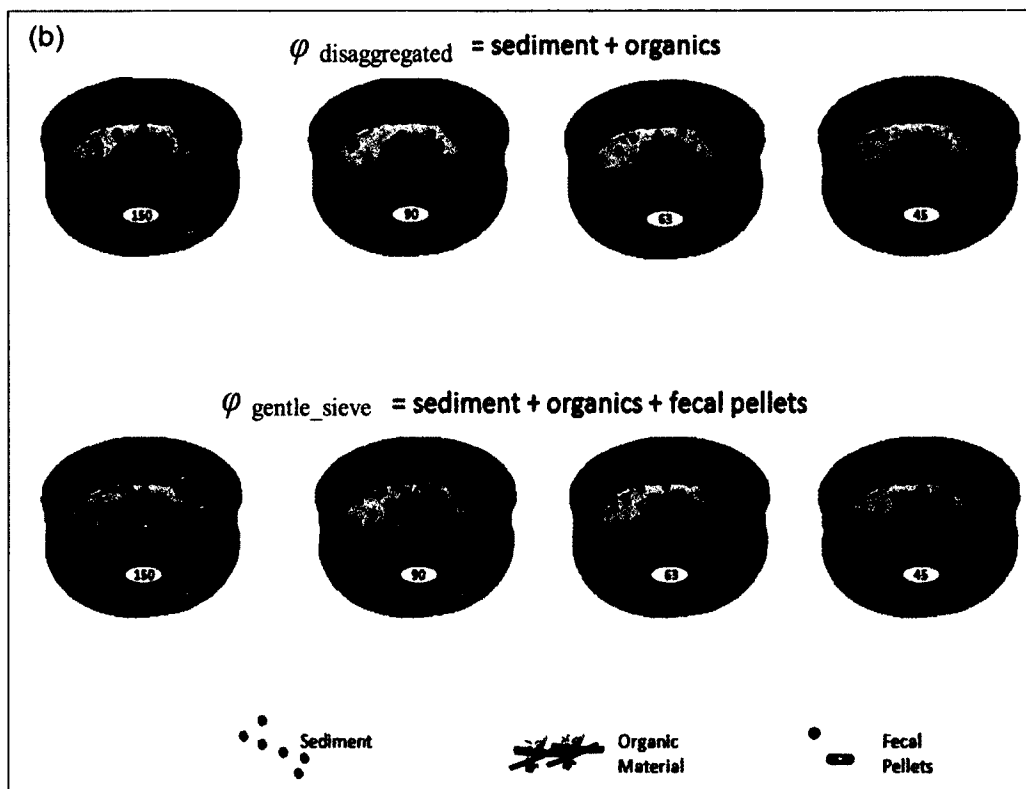


Figure 3-2. (a) Example of GOMEX core sampling in Virginia estuary Map of York River Estuary (photo courtesy of G. Cartwright). (b) Disaggregated particles (top) and gently sieved particles (bottom). The pellet weight in each size class (φ_{Pellet}) was given by $\varphi_{\text{Pellet}} = \varphi_{\text{gentle_sieve}} - \varphi_{\text{disaggregated}}$

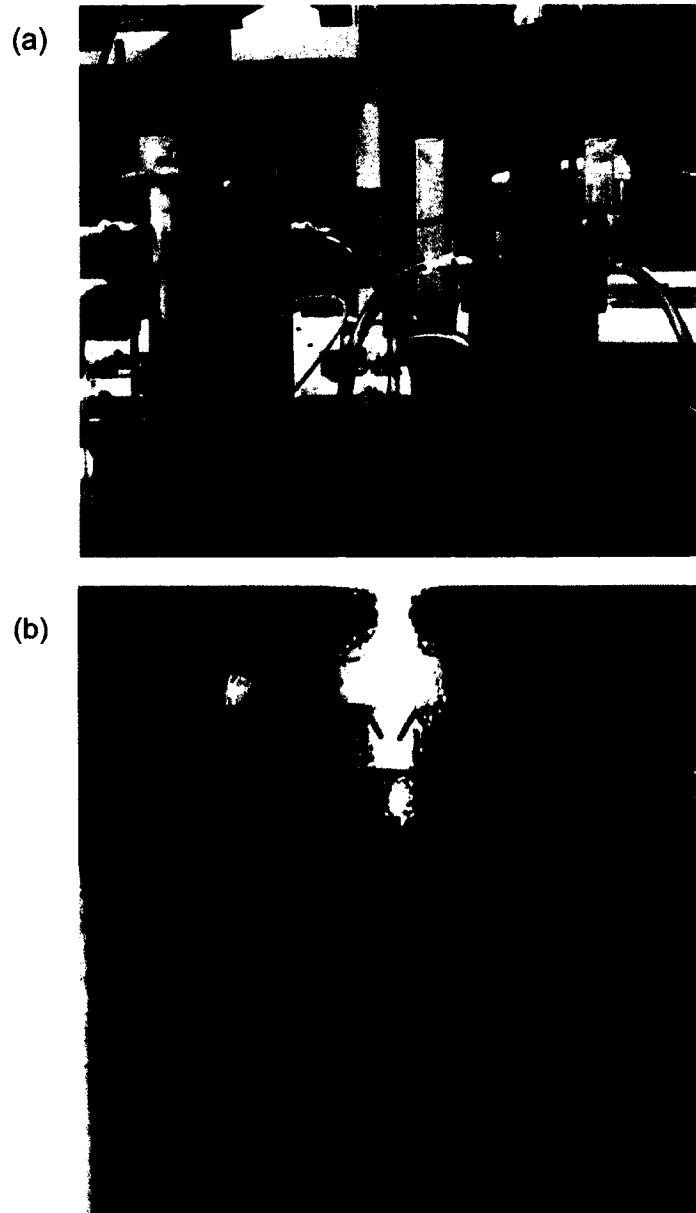


Figure 3-3. (a) Dual core Gust microcosm as arranged during an erosion experiment. (b) Close-up of sediment suspension in a Gust microcosm with water circulation pattern highlighted by arrows.

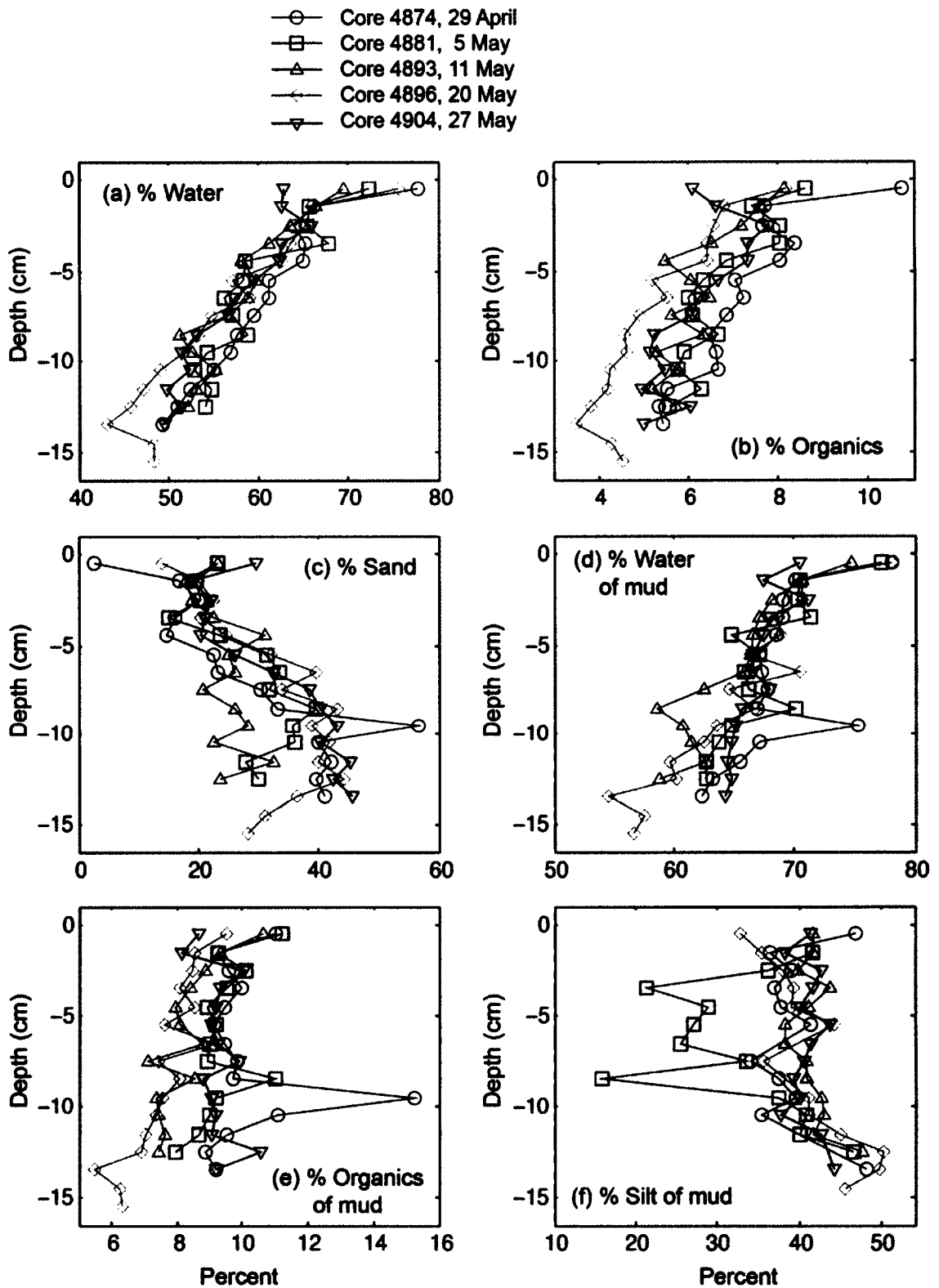


Figure 3-4. Sediment mass profiles of (a) % water in wet sediment, (b) % organics in dry sediment, (c) % sand in dried sediment, (d) % water in wet mud matrix, (e) % organics in dry mud, and (f) % silt in dried mud. Size classes in figure reflect disaggregated sediment components.

Table 3-2. Percent water content by weight of wet sediment, percent organic content by weight of dry sediment, and percent disaggregated sand-sized content by weight of dry sediment. Depth listed is center of 1-cm sample interval. Dashes indicate no data or bad data.

Depth (cm)	29 April, Core 4874			5 May, Core 4881			11 May, Core 4893		
	H ₂ O	Organ	Sand	H ₂ O	Organ	Sand	H ₂ O	Organ	Sand
0.5	77.75	10.73	2.71	72.36	8.61	23.14	69.40	8.14	23.21
1.5	66.25	7.71	16.75	65.74	7.44	19.85	66.46	7.62	18.09
2.5	64.05	7.65	19.99	65.40	8.02	20.55	63.54	7.18	18.89
3.5	65.16	8.35	16.23	67.89	8.06	15.17	61.22	6.52	22.72
4.5	65.03	8.06	14.88	58.52	6.84	23.61	58.02	5.49	30.89
5.5	61.27	7.07	22.47	58.26	6.33	31.44	59.71	6.05	24.95
6.5	61.11	7.24	23.36	56.22	5.99	33.59	58.78	6.49	26.11
7.5	59.53	6.87	30.38	57.26	6.08	31.74	56.78	5.63	20.93
8.5	57.53	6.50	33.35	58.71	6.66	39.68	51.14	6.34	26.06
9.5	57.00	6.61	56.58	54.30	5.92	35.72	52.69	5.28	28.18
10.5	55.12	6.66	39.81	52.96	5.77	36.04	55.37	5.79	22.39
11.5	52.37	5.51	42.09	54.86	6.28	27.77	53.22	5.18	32.33
12.5	50.96	5.36	39.67	54.00	5.57	30.08	52.14	5.70	23.56
13.5	49.40	5.44	40.83	-	-	-	-	-	-

Depth (cm)	20 May, Core 4896			27 May, Core 4904		
	H ₂ O	Organ	Sand	H ₂ O	Organ	Sand
0.5	75.54	8.20	14.02	62.81	6.11	29.47
1.5	65.80	6.80	20.17	62.68	6.62	18.87
2.5	65.16	6.58	22.71	65.81	7.82	22.10
3.5	63.61	6.45	20.46	62.58	7.33	21.26
4.5	62.57	6.41	24.77	62.33	7.34	20.44
5.5	57.27	5.19	31.99	59.48	6.68	26.13
6.5	59.02	5.53	39.51	57.36	6.24	32.44
7.5	54.79	4.92	33.92	56.67	6.08	38.59
8.5	53.34	4.57	43.27	53.24	5.25	40.37
9.5	51.64	4.64	38.91	51.55	5.16	43.25
10.5	49.15	4.27	41.88	52.34	5.49	40.19
11.5	47.11	4.22	39.88	49.83	4.96	45.37
12.5	45.74	3.85	44.15	51.50	6.06	42.50
13.5	43.29	3.51	36.27	49.60	5.02	45.46
14.5	48.35	4.32	30.95	-	-	-
15.5	48.46	4.55	28.27	-	-	-

Table 3-3. Phi class mud content by weight as percent of dry mud as determined by disaggregated grain pipette analysis. Depth listed is center of each 1-cm sample interval. Dashes indicate no data or bad data.

Phi	Depth (cm)															
	0.5	1.5	2.5	3.5	4.5	5.5	6.5	7.5	8.5	9.5	10.5	11.5	12.5	13.5	14.5	
29 April, Core 4874																
4-5	14.1	11.7	15.4	11.7	11.3	12.3	-	8.6	11.6	11.1	5.4	-	-	12.9	-	
5-6	13.2	10.6	9.0	9.9	10.1	12.3	-	8.4	11.4	11.8	12.6	-	-	14.5	-	
6-7	10.9	8.7	8.2	8.9	9.3	6.7	-	8.8	8.0	9.1	8.5	-	-	11.8	-	
7-8	8.7	5.3	6.4	6.5	6.9	10.1	-	8.2	6.5	7.6	8.8	-	-	8.9	-	
8-9	5.0	6.7	4.1	5.1	4.3	6.0	-	6.0	7.4	4.9	5.7	-	-	9.6	-	
9-10	6.1	4.2	9.8	5.9	7.7	8.3	-	7.7	7.5	8.6	8.4	-	-	5.0	-	
>10	42.0	52.8	47.1	52.0	50.4	44.3	-	52.3	47.6	46.9	50.6	-	-	37.3	-	
5 May, Core 4881																
4-5	-	11.1	8.7	6.8	7.2	9.9	8.3	6.6	3.4	8.8	12.0	12.5	11.6	-	-	
5-6	-	13.9	9.8	4.6	7.3	6.8	6.7	9.4	3.5	9.0	12.5	12.1	13.3	-	-	
6-7	-	10.2	10.4	4.9	7.4	5.6	5.6	8.9	3.8	12.3	8.8	8.4	12.0	-	-	
7-8	-	6.4	7.2	5.0	6.9	4.8	4.8	8.7	5.2	7.4	7.5	7.1	9.8	-	-	
8-9	-	7.7	5.2	3.6	4.4	4.6	3.8	8.5	7.2	7.1	6.9	6.3	9.3	-	-	
9-10	-	6.9	17.7	14.4	7.6	7.1	6.7	9.3	11.1	7.3	8.9	7.2	8.6	-	-	
>10	-	43.8	41.0	60.7	59.2	61.2	64.1	48.6	65.8	48.1	43.4	46.4	35.4	-	-	
11 May, Core 4893																
4-5	12.3	10.4	11.6	13.9	11.8	10.5	9.3	10.8	11.6	11.6	10.5	12.1	13.8	-	-	
5-6	13.1	14.1	12.5	13.1	12.7	11.6	11.6	12.4	16.8	13.4	14.0	11.8	15.0	-	-	
6-7	8.8	9.6	9.4	9.1	13.1	9.5	9.4	9.7	4.8	9.0	9.8	10.1	10.2	-	-	
7-8	7.4	7.5	6.3	7.6	3.4	6.6	7.9	8.0	7.7	8.8	8.6	7.7	8.5	-	-	
8-9	6.8	7.0	7.7	6.9	6.6	7.2	7.4	7.4	6.2	6.8	6.3	5.6	8.9	-	-	
9-10	9.3	8.5	5.6	8.3	8.3	8.2	8.3	8.5	8.2	8.2	8.8	7.2	6.1	-	-	
>10	42.3	42.9	46.9	41.1	44.1	46.4	46.1	43.2	44.7	42.2	42.0	45.5	37.5	-	-	
20 May, Core 4896																
4-5	10.5	14.3	10.7	12.2	10.2	12.1	-	11.4	-	12.8	13.6	16.1	13.9	14.9	12.4	
5-6	11.2	11.8	11.7	12.2	11.7	13.0	-	11.0	-	13.8	11.4	11.6	16.1	16.7	13.7	
6-7	5.8	4.8	7.2	7.6	8.6	10.4	-	8.1	-	8.2	9.7	8.9	11.0	8.7	10.4	
7-8	5.4	4.5	8.3	7.2	8.6	8.7	-	5.2	-	6.3	6.4	8.3	9.1	9.4	9.1	
8-9	4.5	4.3	5.2	2.4	5.7	8.6	-	5.5	-	7.3	6.4	6.4	10.7	8.5	10.7	
9-10	7.4	5.6	6.0	9.0	8.2	9.3	-	5.1	-	6.0	7.2	7.0	3.5	10.2	10.8	
>10	55.2	54.7	50.9	49.4	47.0	37.9	-	53.7	-	45.6	45.3	41.7	35.7	31.6	32.9	
27 May, Core 4904																
4-5	15.3	10.7	12.7	10.7	12.6	13.0	11.5	10.5	10.7	10.9	8.8	12.8	-	11.0	-	
5-6	12.1	10.6	12.3	13.3	11.0	13.9	13.5	11.1	11.5	13.6	10.9	11.3	-	13.2	-	
6-7	8.1	8.8	9.5	8.8	9.7	10.1	8.0	11.9	9.0	7.6	11.1	10.0	-	10.7	-	
7-8	6.0	8.1	8.1	8.9	6.7	6.7	8.4	7.2	8.0	8.1	7.0	8.6	-	9.3	-	
8-9	5.8	4.7	6.4	6.8	6.7	8.3	8.8	6.3	7.0	5.3	5.3	7.5	-	12.2	-	
9-10	7.7	7.7	8.0	8.2	7.1	9.2	8.3	9.8	9.4	10.1	10.1	9.8	-	1.3	-	
>10	45.0	49.4	43.0	43.3	46.2	38.8	41.5	43.2	44.4	44.4	46.8	40.0	-	42.3	-	

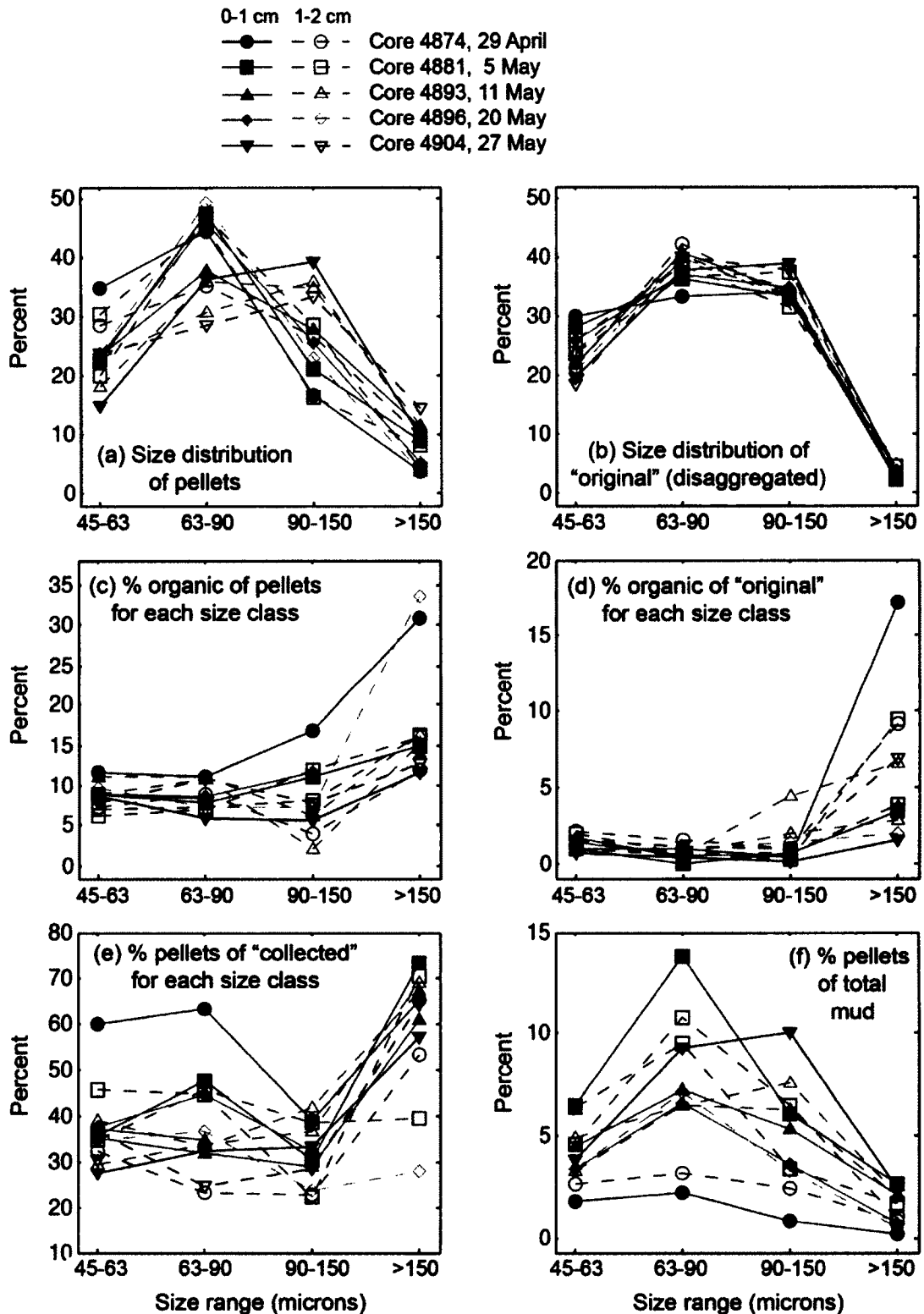


Figure 3-5. Percent mass as a function of sieve size classes: (a) size distribution of pellets that withstood sieving but not disaggregation, (b) size distribution of "disaggregated" (i.e., coarse silt/fine sand and detritus that withstood disaggregation), (c) % organic of pellets, (d) % organic of "disaggregated", (e) % pellets of all "collected" >45 microns, (f) % pellets relative to total disaggregated mud.

Table 3-4. Weights of sediment for sieve intervals from 10.00 g of wet sediment. Dashes indicate no data or bad data.

Size (μ m) D=dupl.	"Collected" (Gently sieved)				"Original" (Disaggregated)			
	Dried (mg)		Muffled (mg)		Dried (mg)		Muffled (mg)	
	0-1 cm	1-2 cm	0-1 cm	1-2 cm	0-1 cm	1-2 cm	0-1 cm	1-2 cm
29 April, Core 4874								
45-63	103.6	239.7	95.9	230.5	41.5	162.8	41.1	159.3
63-90	125.6	411.8	116.3	398.3	46.4	317.4	45.9	312.3
90-150	77.4	321.1	72.2	315.4	47.5	248.9	47.3	246.2
>150	10.0	49.1	7.4	43.9	3.5	23.0	2.9	20.9
5 May, Core 4881								
45-63	222.2	252.2	213.7	242.6	143.2	164.7	141.7	161.3
63-90	349.5	451.5	336.3	434.9	183.2	246.0	183.1	244.3
90-150	242.3	325.0	232.9	314.3	168.8	200.0	167.6	199.5
>150	43.2	45.6	38.1	40.1	11.6	27.6	11.2	25.0
45-63 D	-	301.8	-	291.4	-	164.6	-	162.8
63-90 D	-	456.2	-	439.8	-	253.4	-	251.4
90-150 D	-	330.6	-	320.2	-	257.5	-	255.7
>150 D	-	52.1	-	45.7	-	15.5	-	14.9
11 May, Core 4893								
45-63	253.4	264.0	242.3	253.2	159.7	161.3	157.0	159.7
63-90	428.5	413.5	414.8	397.0	280.4	276.8	279.2	275.1
90-150	296.3	381.6	289.7	368.4	-	222.1	-	212.3
>150	71.1	68.6	63.7	60.2	24.2	22.8	23.3	21.3
45-63 D	260.5	251.1	251.0	240.3	169.7	177.9	167.5	175.3
63-90 D	465.7	433.4	450.1	415.1	317.6	287.8	317.1	285.8
90-150 D	376.1	389.6	369.0	376.0	267.3	248.4	266.3	243.5
>150 D	71.5	67.8	65.1	59.6	28.1	21.2	27.4	20.6
20 May, Core 4896								
45-63	146.9	261.9	140.8	251.4	92.3	171.4	91.0	169.8
63-90	237.6	515.0	227.7	497.7	131.3	327.2	130.6	323.6
90-150	183.4	373.4	175.7	362.7	124.2	285.2	123.4	281.0
>150	20.7	53.8	18.5	48.0	8.6	38.9	-	38.1
27 May, Core 4904								
45-63	321.0*	228.9	311.4*	220.0	233.0*	145.7	231.1*	143.4
63-90	661.2*	413.3	646.4*	398.5	448.9*	312.7	446.9*	308.9
90-150	690.8*	412.6	676.6*	400.4	461.3*	294.8	460.2*	291.8
>150	100.1*	80.6	92.8*	72.0	43.2*	28.9	42.5*	26.9
45-63 D	-	237.0	-	228.6	-	164.8	-	162.4
63-90 D	-	417.1	-	402.9	-	-	-	-
90-150 D	-	423.9	-	412.1	-	263.8	-	262.3
>150 D	-	77.6	-	69.8	-	-	-	-

*9.50 grams of wet sediment used instead of 10.00

Table 3-5. Beryllium activity in dpm/gram dry sediment (including sand) \pm confidence interval, corrected for decay between time of core collection and analysis. Zero values indicate no ^7Be peak detected. Dashes indicate no data or bad data. ^7Be inventory in units of dpm/cm² integrated over the top 10 cm of each core is displayed in the final row.

Depth (cm)	29 April		5 May		11 May		20 May		27 May	
	Core 4872	Core 4873	Core 4879	Core 4880	Core 4886	Core 4887	Core 4894	Core 4895	Core 4902	Core 4903
0-1	2.89 \pm .21	.95 \pm .10	.94 \pm .12	.69 \pm .08	1.23 \pm .13	.88 \pm .11	1.84 \pm .16	-	.69 \pm .07	.79 \pm .10
1-2	.97 \pm .09	.74 \pm .09	.80 \pm .10	.65 \pm .08	1.05 \pm .11	.40 \pm .07	.74 \pm .10	3.29 \pm .24	.71 \pm .10	.83 \pm .11
2-3	.46 \pm .09	1.21 \pm .10	1.13 \pm .12	.30 \pm .06	.72 \pm .09	.80 \pm .12	.00	.78 \pm .09	.47 \pm .06	.00
3-4	.38 \pm .08	.95 \pm .10	.67 \pm .10	.01 \pm .04	.92 \pm .09	.43 \pm .07	.62 \pm .07	.70 \pm .09	.32 \pm .08	.02 \pm .07
4-5	.08 \pm .03	.05 \pm .04	.43 \pm .06	.04 \pm .05	.08 \pm .05	.60 \pm .09	.49 \pm .08	.58 \pm .07	.21 \pm .09	.02 \pm .01
5-6	.26 \pm .06	.00	.23 \pm .07	.00	.39 \pm .07	.00	.07 \pm .03	.01 \pm .05	.13 \pm .06	.05 \pm .02
6-7	.00	.23 \pm .04	.34 \pm .08	.08 \pm .09	.00	.00	.01 \pm .03	.10 \pm .04	.00	.00
7-8	.00	.00	.14 \pm .04	.07 \pm .03	.00	.00	.00	.02 \pm .02	.00	.02 \pm .01
8-9	.01 \pm .02	.04 \pm .02	.02 \pm .03	.00	.01 \pm .04	.02 \pm .03	.00	.00	.00	.00
9-10	.00	.00	.02 \pm .02	.00	.00	.00	.00	.00	.00	.00
10-12	.03 \pm .02	.06 \pm .02	.00	.11 \pm .10	.10 \pm .01	.00	.02 \pm .01	.00	.00	.00
12-14	.00	.00	.00	.04 \pm .02	.00	.00	.02 \pm .01	.02 \pm .04	.00	.01 \pm .01
14-16	.00	.00	.00	.05 \pm .04	.05 \pm .01	-	.01 \pm .02	.02 \pm .02	.00	.06 \pm .04
0-10	1.82 \pm .21	3.29 \pm .32	3.85 \pm .30	1.46 \pm .18	3.50 \pm .34	2.49 \pm .27	1.71 \pm .22	1.61 \pm .21	2.11 \pm .24	1.46 \pm .27

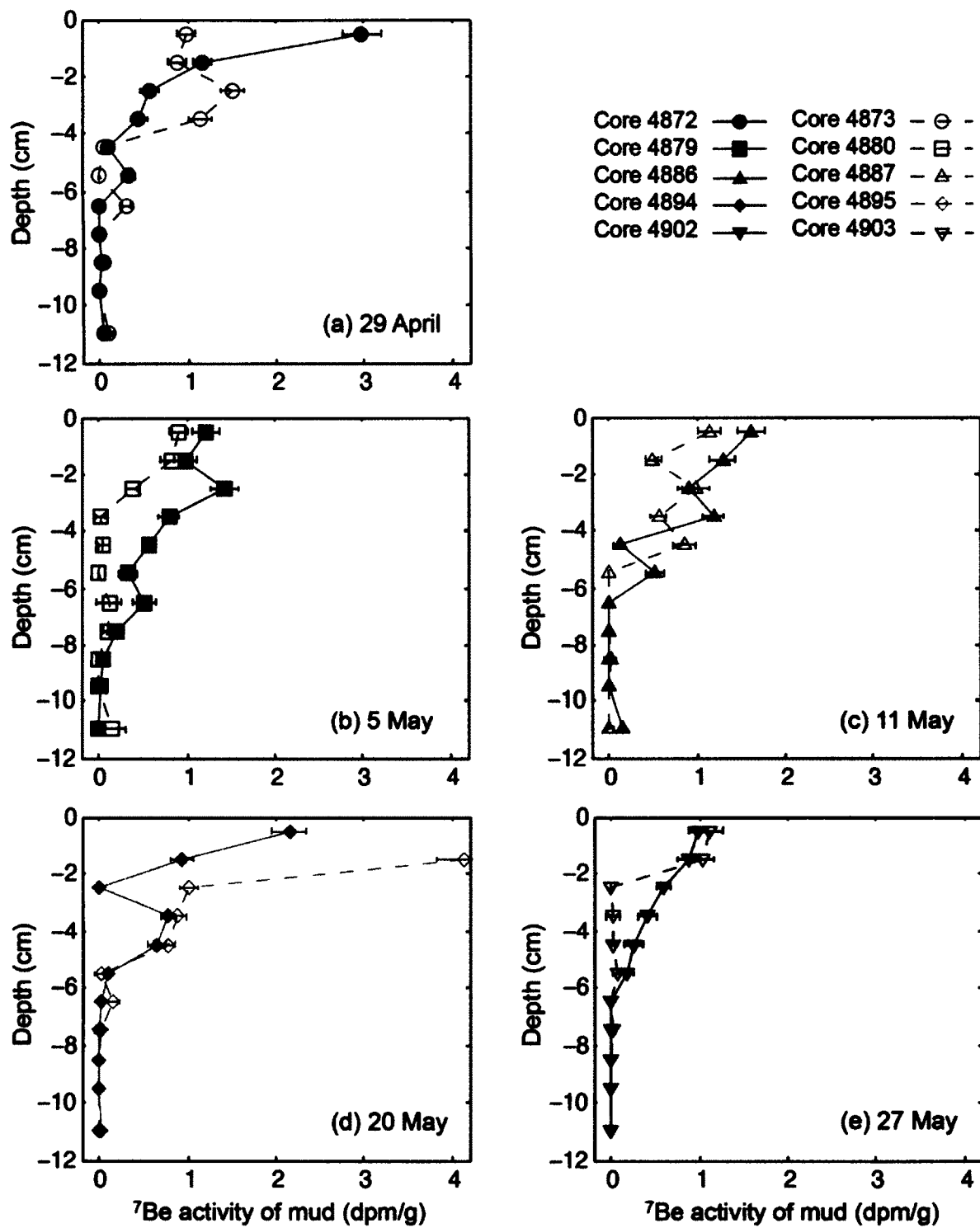


Figure 3-6. Beryllium-7 activity per mass of dry mud, corrected for time between coring and counting, for weekly sampling at the Clay Bank site between late April and late May, 2010.

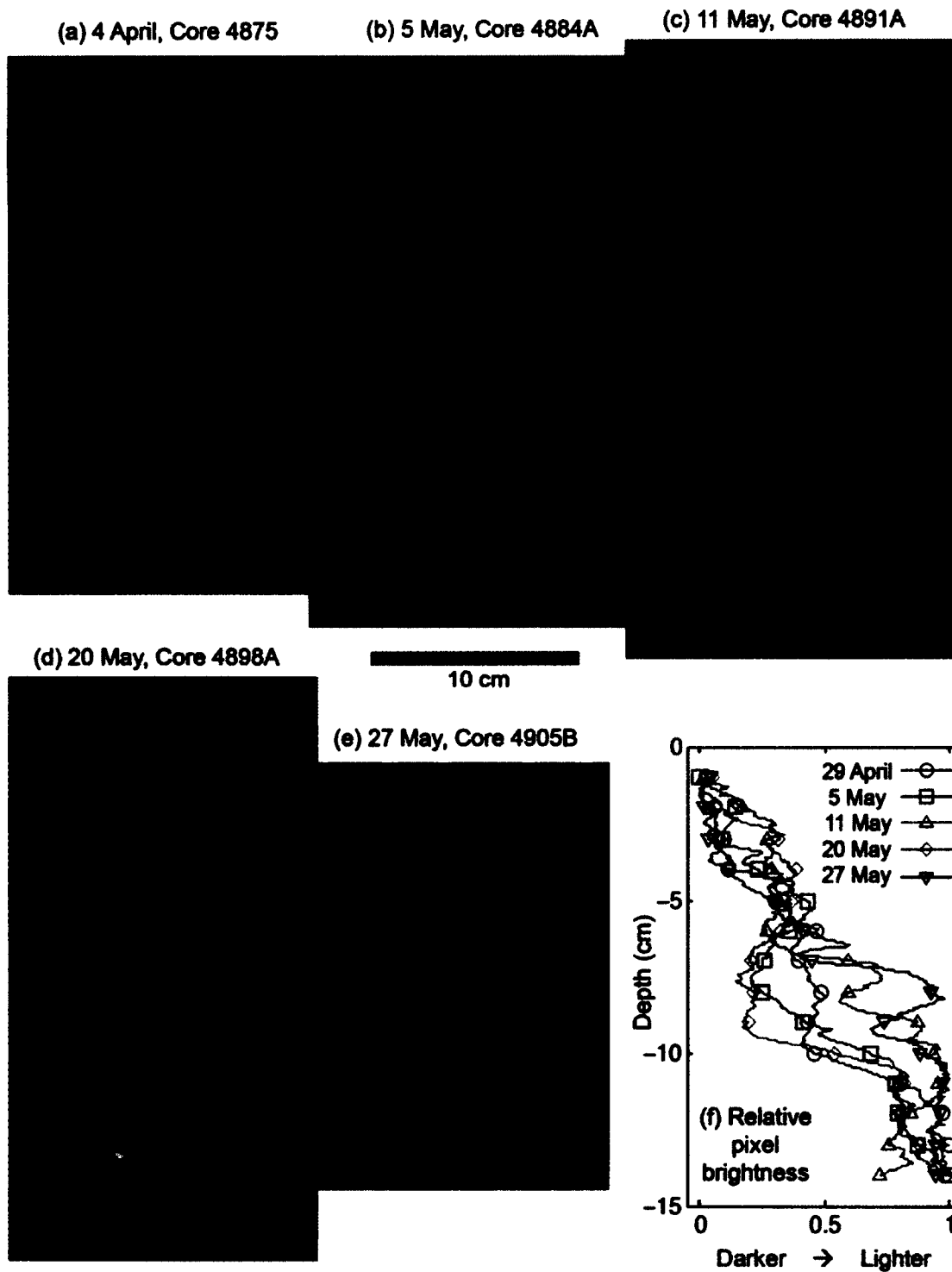


Figure 3-7. (a)-(e) Example digital x-radiographs from cores collected on the five weekly sampling cruises. (f) Relative pixel intensity, averaged across the widths of the images in (a)-(e) width, for depths from 1 to 14 cm. The width-averaged pixel intensity was normalized on a scale of 0 to 1 such that the lowest width-averaged intensity for each core was set to 0, and the highest width-averaged intensity was set to 1.

Table 3-6. Eroded mass and critical erosion stress calculated from erodibility experiments.

		Critical erosion stress (Pa)	Eroded mass (kg/m ²)		Critical erosion stress (Pa)	Eroded mass (kg/m ²)
29 April	Core 4875			Core 4877		
		0.0478	0.0276		0.0377	0.0370
		0.0702	0.0765		0.0643	0.0939
		0.1201	0.1505		0.1123	0.1788
		0.2129	0.2003		0.2481	0.3097
		0.4007	0.3166		0.3716	0.4680
5 May	Core 4882			Core 4883		
		0.0388	0.0229		0.0381	0.0276
		0.0748	0.0585		0.0709	0.0550
		0.1648	0.1106		0.1594	0.1129
		0.2160	0.1849		0.2105	0.1946
		0.3567	0.3118		0.3513	0.3237
11 May	Core 4889			Core 4890		
		0.0419	0.0091		0.0433	0.0093
		0.0854	0.0278		0.0934	0.0290
		0.1663	0.0669		0.1838	0.0706
		0.2647	0.1227		0.2621	0.1188
		0.3660	0.2228		0.3810	0.1935
20 May	Core 4899			Core 4900		
		0.0453	0.0151		0.0348	0.0141
		0.0771	0.0358		0.0621	0.0427
		0.1445	0.0617		0.1534	0.0958
		0.2405	0.1010		0.2408	0.1490
		0.3700	0.1491		0.4003	0.2336
May 27	Core 4907			Core 4908		
		0.0383	0.0193		0.0399	0.0194
		0.0609	0.0467		0.0664	0.0374
		0.1205	0.0972		0.1217	0.0775
		0.2076	0.1725		0.2165	0.1432
		0.3005	0.3379		0.3494	0.2667

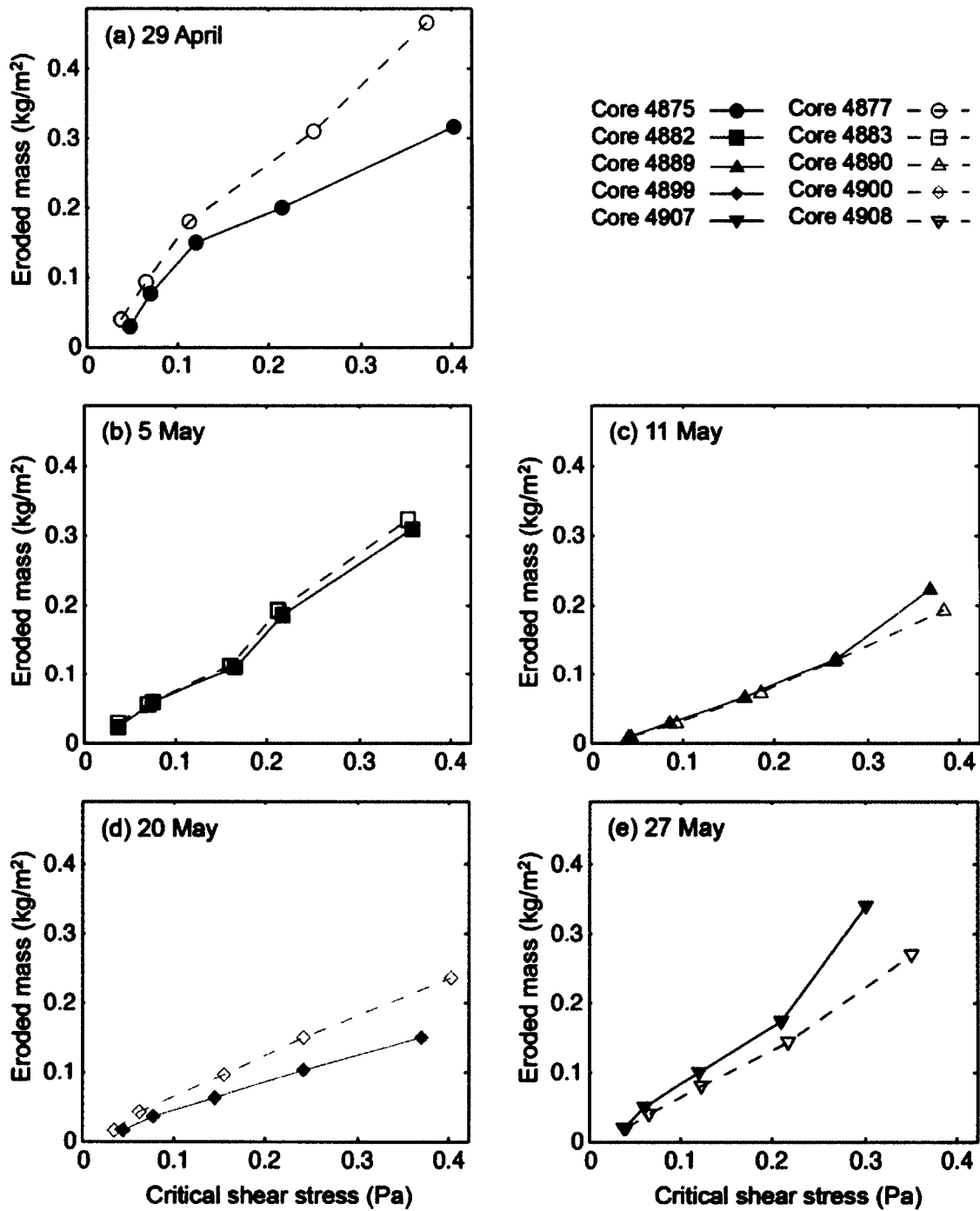


Figure 3-8. Eroded mass as a function of critical erosion shear stress for weekly sampling at the Clay Bank site between late April and late May, 2010.

Table 7. Correlation r-values and p-values. Correlations with $p < 0.1$ or $0.1 \leq p < 0.2$ highlighted by dark or light shading, respectively.

r-values	% Sand	*Sand d_{50}	% Water of mud	% Organics of mud	% Silt of mud	Pellet d_{50}	% Pellets of mud	^7Be activity of mud	Erosion at 0.2 Pa	Days since 1 st cruise
% Sand				-0.457	-0.218				-0.534	0.633
*Sand d_{50}					-0.131		0.390	-0.446	-0.408	
% Water of mud				0.678	-0.117		-0.528	0.680	0.251	-0.681
% Organics of mud	-0.457		0.678		0.475		-0.212	0.077	0.366	
% Silt of mud	-0.218	-0.131	-0.117	0.475		-0.219	-0.183	-0.289		-0.611
Pellet d_{50}					-0.219		0.684	-0.660	-0.488	
% Pellets of mud		0.390	-0.528	-0.212	-0.183	0.684			-0.329	0.408
^7Be activity of mud		-0.446	0.680	0.077	-0.289	-0.660			0.072	-0.199
Erosion at 0.2 Pa	-0.534	-0.408	0.251	0.366		-0.488	-0.329	0.072		-0.571
Days since 1 st cruise	0.633		-0.681		-0.611		0.408	-0.199	-0.571	

One-sided p-values	% Sand	*Sand d_{50}	% Water of mud	% Organics of mud	% Silt of mud	Pellet d_{50}	% Pellets of mud	^7Be activity of mud	Erosion at 0.2 Pa	Days since 1 st cruise
% Sand				0.220	0.362				0.177	0.126
*Sand d_{50}					0.417		0.258	0.226	0.248	
% Water of mud				0.104	0.426		0.180	0.104	0.342	0.103
% Organics of mud	0.220		0.104		0.209		0.366	0.451	0.272	
% Silt of mud	0.362	0.417	0.426	0.209		0.362	0.384	0.319		0.137
Pellet d_{50}					0.362		0.102	0.113	0.202	
% Pellets of mud		0.258	0.180	0.366	0.384	0.102			0.294	0.248
^7Be activity of mud		0.226	0.104	0.451	0.319	0.113			0.454	0.374
Erosion at 0.2 Pa	0.177	0.248	0.342	0.272		0.202	0.294	0.454		0.157
Days since 1 st cruise	0.126		0.103		0.137		0.248	0.374	0.157	

* d_{50} of sand plus coarse silt trapped by sieves after disaggregation as in Figure 5b.

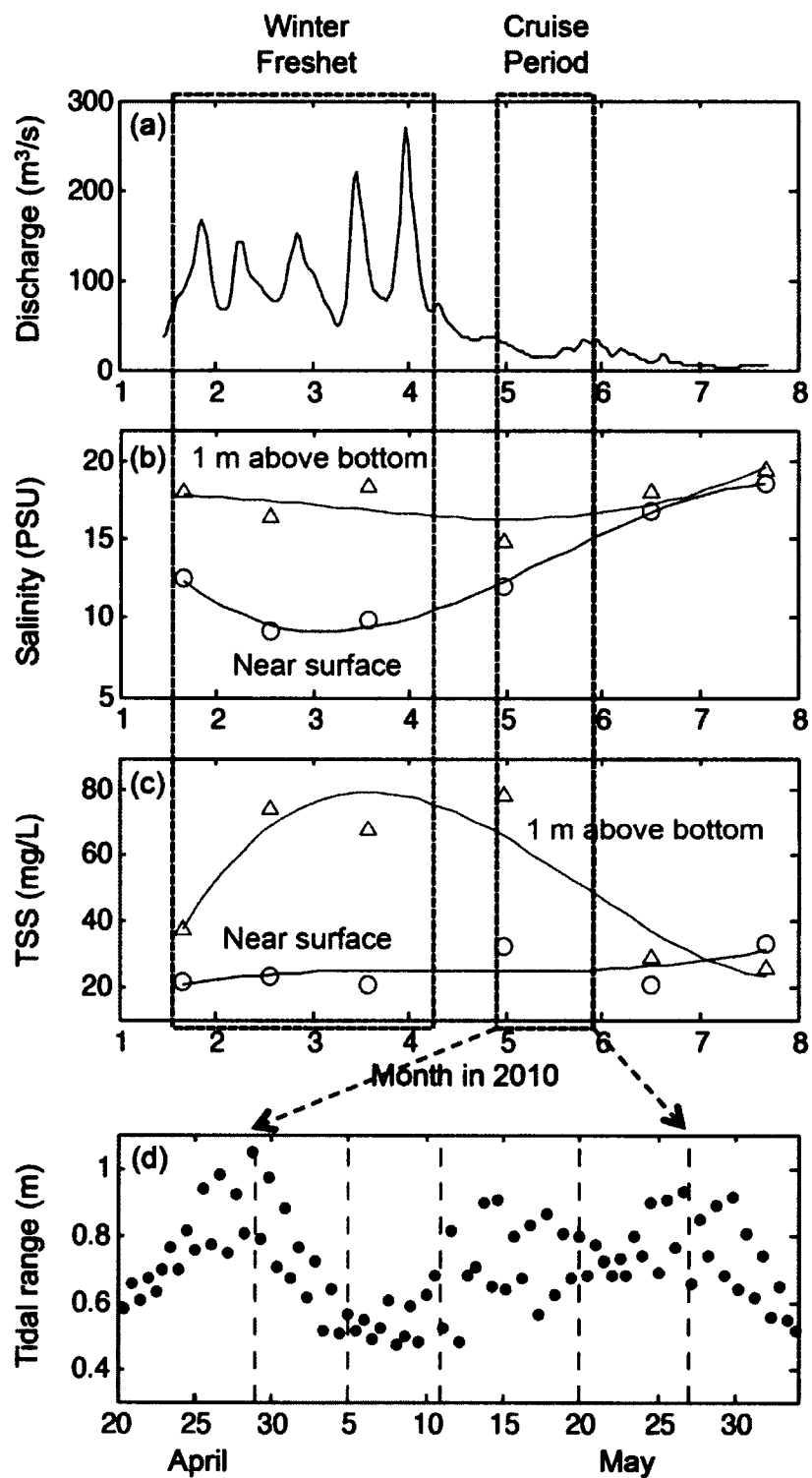


Figure 3-9. Conditions in the York River estuary in 2010: (a) USGS data for riverine discharge (3-day low-pass of Pamunkey plus Mattaponi gaging stations). EPA monitoring data for (b) salinity and (c) total suspended solids (spatial averages of observations collected at stations LE4.1 and LE4.2). (d) Tidal range (high water minus low water) calculated from Yorktown NOAA tide gauge with dashed lines indicating dates of coring cruises. (See Figure 1 for locations of LE4.1, LE4.2 and tide gauge.)

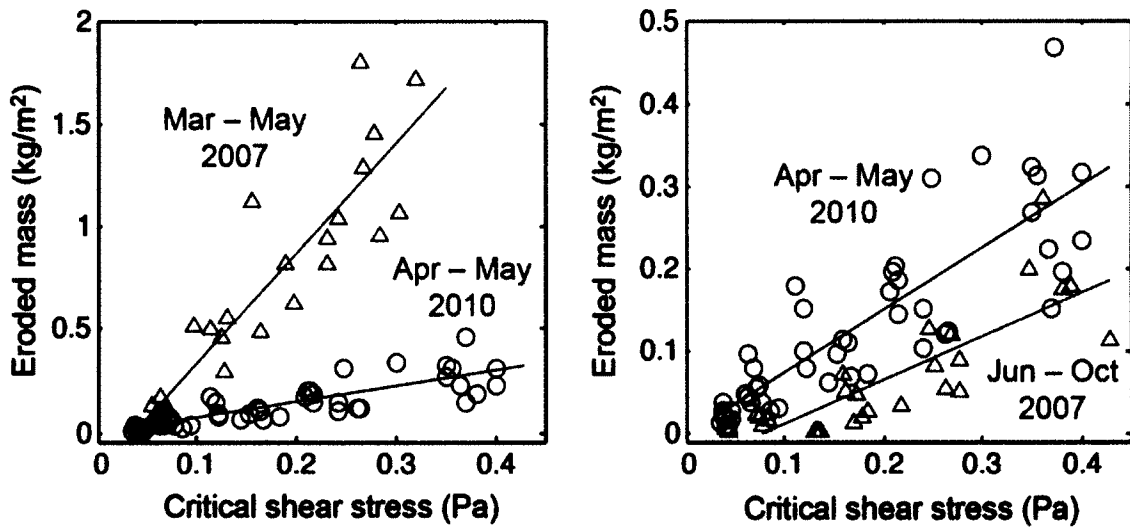


Figure 3-10. Comparison of eroded mass vs. stress for 2007 and 2010 cores collected at Clay Bank. (a) Mar-May 2007 monthly data compared to Apr-May 2010 weekly data; (b) Jun-Oct 2007 monthly data compared to Apr-May 2010 weekly data. 2007 data from Dickhudt et al. (2008).

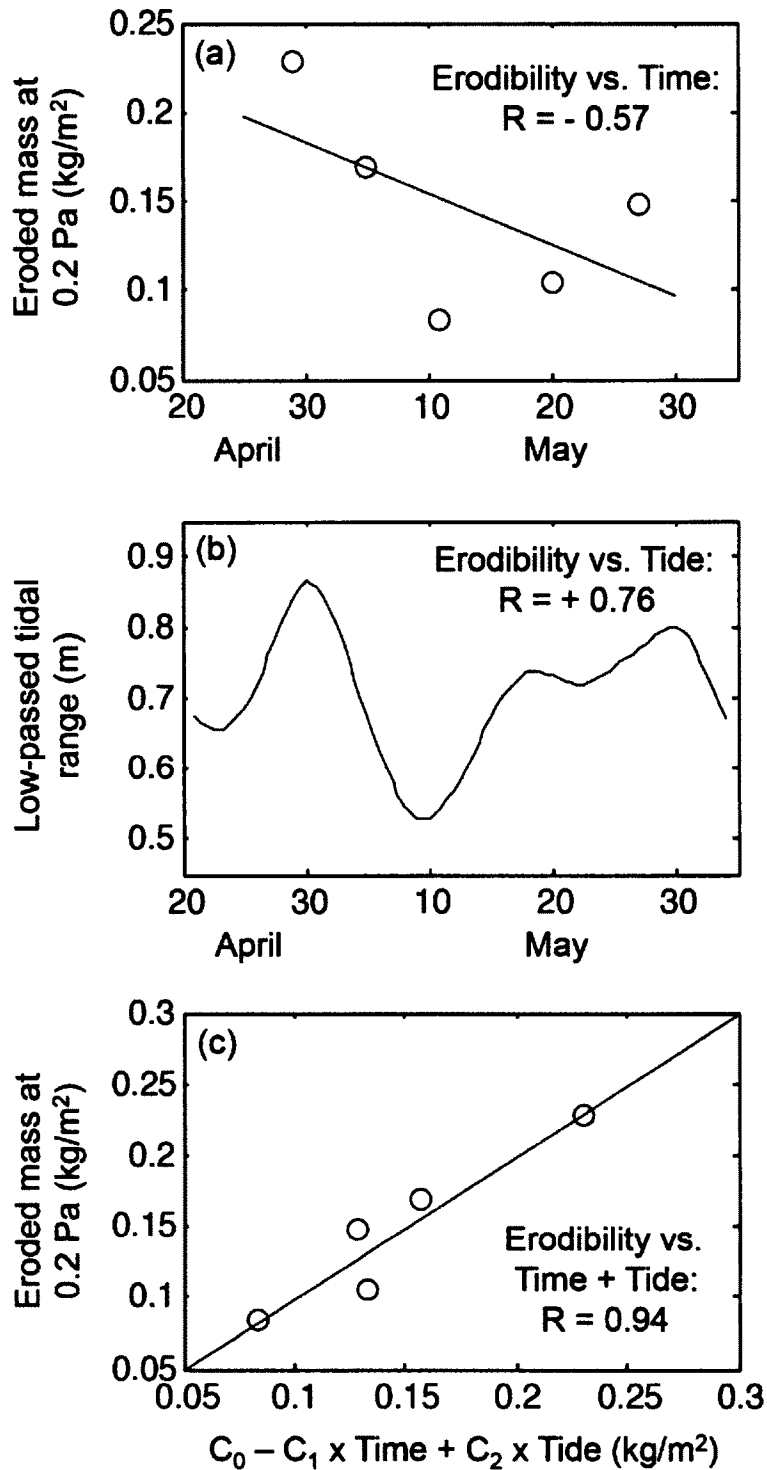


Figure 3-11. (a) Mean eroded mass at 0.2 Pa for each of the five cruises along with a least-squares linear regression as a function of elapsed time in days. (b) Tide range at Yorktown averaged over the previous 11 tidal cycles. (c) Results of multiple regression of eroded mass versus both time and low-passed tidal range.

Appendix 1: Fecal Pellet Analysis Methodology

**Pellet Analysis:
Standard Operating Procedure
By L. Kraatz**

Setup:

<i>Tupperware to collect sediment samples</i>	<i>DI water bottles</i>
<i>2L graduated cylinders</i>	<i>Small and Large porcelain bowls</i>
<i>Graduated cylinder mixing rod</i>	<i>Sonicator</i>
<i>Eppendorf Pipette</i>	<i>Scoopula</i>
<i>20 mL pipette rod</i>	<i>Glass rods for stirring</i>
<i>10% Calgon Solution</i>	<i>Stir plate and stir bars</i>
<i>Balance with accuracy to 0.0001 grams</i>	<i>150 micron sieve</i>
<i>150 mL beakers (2 for each sample)</i>	<i>90 micron sieve</i>
<i>50 mL beakers (8 per each sample)</i>	<i>63 micron sieve</i>
<i>Aluminum trays (2 per each sample)</i>	<i>45 micron sieve</i>

Prior to Experiment:

1. Muffle all beakers needed for experiment for one hour. Place in oven at 550°C.
2. Label graduated cylinders and 150 mL beaker to match each sample name.

*****Note.** *There will be two analyses done for every sediment sample. One sample will have Calgon added to the sediment and sonicated to disaggregate any pellets and flocculants. This sample will be referred to as the ORIGINAL GRAINS sample. The second sample will have only water added and will be referred to as the FECAL PELLETT sample.*
3. Label and pre-weigh 50 mL beakers (you will need eight for every sample. 4 for each sieve and 1 set for each type of sample)
 - a. Label beakers, place in oven (103-105°C) for at least an hour and weigh twice (weights should be within 0.0005 g of each other)
 - b. Record weights in excel sheet.

*****Note:** *you need to wear gloves anytime you handle the beakers that contain or will contain sediment!*
4. Check Calgon solution to make sure you have enough for the experiment. If you are low this is how you make the CHSD Lab Calgon Solution:

To make 10% Calgon solution: In a small beaker, weigh out:
51g of Sodium Metaphosphate and
0.3g of Sodium Bicarbonate
Place this mixture in a 1liter flask and stir vigorously until all of the powder is dissolved (you can use a stir plate/magnets to help this process along).

Prepping Samples:

1. Stir each sample to homogenize.

*****Note.** *Be gentle with the sediment as to not break up the fecal pellets.*
2. Weigh labeled 150 mL beaker, tare to zero
3. Weigh out 10.0 grams of each sample into beakers. **Make sure to record these weights. You want the weight of the sediment to be the same for the ORIGINAL SEDIMENT sample and the FECAL PELLETT sample.**

For the ORIGINAL SEDIMENT samples ONLY

4. Add 10 mL of 10% Calgon solution to the samples.
5. Add DI water to 60 mL using the DI squirt bottles (also squirt down any sediment on the sides)
6. Place samples in the sonicator for one hour.

For the FECAL PELLETS samples ONLY

4. Add 60 mL of DI water to the beakers. Carefully squirt down any sediment on the sides and only add water from the side of the beakers. Do not exert any extra force or pressure onto the FECAL PELLETS samples.
5. Cover the beakers with parafilm.
6. Let samples sit in the refrigerator overnight. Do not let the samples sit out at room temperature. You do not want any of the organic material to begin breaking down.

Sieving:

For the ORIGINAL SEDIMENT samples ONLY

1. Grab 150 micron, 90 micron, 63 micron, and 45 micron sieves, and 2-3 porcelain bowls
2. Once samples have been sonicated stir up the sample in the beaker with a glass rod. Try to rid the sample of any clumps before commencing the sieve process.
3. **Place 150 micron sieve over bowl and pour sample onto sieve.** Rinse beaker with DI water bottle onto the sieve to make sure all sediment is removed from the container and captured for analysis.
4. Using the DI squirt bottle (and as little water as possible), squirt all the mud and sand through the sieve into the bowl. Shells and other large particles should be caught on this sieve.

****Note. Sieving the sediment through the 150 micron sieve will be the most tedious of the sieves and will use the most water. Sieve the sample as diligently and use as little water as possible. When the sieved water is clear, you can stop sieving and continue to the next step. If the material is still running through the sieve after 700 mL of water has been used, continuing sieving for another 5 minutes and stop. At times sediment will continue to go through the sieve so in order to conserve water for the rest of the experiment, a cap is needed to continue the experiment.*

5. Use DI water hose from a sink and work all the shells to the bottom of the sieve, then use the DI water squirt bottle to squirt sample from the sieve into its labeled beaker.

****Note. If sediment was still coming through the sieve after the allotted time, make a note on the spreadsheet and make sure to clean the remaining sediment on the sieve. We want to ensure that the sediment left on the sieve and moved to the beaker is indicative of sediment greater than 150 microns.*

6. Place the labeled beaker in the oven (103-105°C) until water has evaporated.
7. Thoroughly rinse out the 150 micron sieve

****Note. To clean the sieve, make sure to turn sieve upside down and rinse from the bottom.*

8. **Next, place the small 90 micron sieve over second porcelain bowl**

9. Pour previously sieved sample (left in bowl) over the 90 micron sieve and use DI squirt bottle to get all of the sediment out of the bowl. Use the DI squirt bottle and work the sediment from one end of the sieve to the other, using as little water as possible
****Note. As you do this, empty the porcelain bowl into a neighboring porcelain bowl periodically to see keep track of your progress (the ultimate goal is for the water in the porcelain bowl to be clear without using more than 2000mL). You will need to continue to repeat the sieving of sediment until this goal is met!*
10. Once the water runs clear, use DI water hose from a sink and work all the sediment to the bottom of the sieve, then use the DI water squirt bottle to squirt sample from the sieve into its labeled beaker.
11. Place the labeled beaker in the oven (103-105°C) until water has evaporated.
12. Thoroughly rinse out the 90 micron sieve
13. **Next, place the small 63 micron sieve over a new porcelain bowl**
14. Pour previously sieved sample (left in bowl) over the 63 micron sieve and use DI squirt bottle to get all of the sediment out of the bowl. Use the DI squirt bottle and work the sediment from one end of the sieve to the other, using as little water as possible
**** Note. Watch how much water you have used. Again, you can only use 2L.*
15. Once the water runs clear, use DI water hose from a sink and work all the sediment to the bottom of the sieve, then use the DI water squirt bottle to squirt sample from the sieve into its labeled beaker.
16. Place the labeled beaker in the oven (103-105°C) until water has evaporated.
17. Thoroughly rinse out the 63 micron sieve
18. **LAST SIEVE: Next, place the small 45 micron sieve over the porcelain bowl**
19. Pour previously sieved sample (left in bowl) over the 45 micron sieve and use DI squirt bottle to get all of the sediment out of the bowl. Use the DI squirt bottle and work the sediment from one end of the sieve to the other, using as little water as possible
7. Once the water runs clear, pour the remaining sieved water into the graduate cylinder and cover it with parafilm to ensure that no dust settles in them before the experiment is performed.
8. Place graduated cylinders to the side for pipette analysis and place beakers in the (103-105°C) oven for at least 24 hours then begin weighing procedure.
****Note. Place the cylinders in a region that is not easily disturbed once you start pipetting the area cannot be hit, bumped, etc., as it will disrupt the sediment fall velocity and mess up your results.*

For the FECAL PELLETS samples ONLY

1. Grab 150 micron, 90 micron, 63 micron, and 45 micron sieves, and 2-3 porcelain bowls.
2. First, place the 90 micron sieve in the bottom of the bowl.
3. Fill the porcelain bowl with DI water, just to the top of the sieve surface.
4. Gently stir your FECAL PELLET sample beaker to break up as much of the clumps as possible.
****Note. DO NOT vigorously stir the sample. You want the pellets to remain intact. This process is just to get some of the sediment in suspension and not all in one clump.*

5. Pour the FECAL PELLET sample onto the 90 micron sieve and carefully rinse the beaker with DI water onto the sieve to make sure all sediment is removed from the container and captured for analysis.
****Note. Try not put water on the sediment directly but rather on the beaker sides and let the water push down the sediment.*
6. Slowly move the bowl in circular motions to begin moving the sediment across the sieve surface.
7. Occasionally (once a minute), pick up the sieve to allow sediment to readjust and move the sediment.
8. Continue steps 6 and 7 for 5 minutes.
9. Place porcelain bowl on stir plate and put a medium size stir bar under the sieve. Place stir plate on medium-high stir speed and let sit for 5 minutes.
10. Remove bowl from stir plate along with the stir bar. Rinse stir bar into bottom of bowl so no sediment is lost.
11. Transfer sieved water from one bowl to new one and begin again to track the progress of how much sediment remaining is passing through the sieves.
12. Repeat steps 4-11 until water runs clear.
****Note. As you do this, empty the porcelain bowl into a neighboring porcelain bowl periodically to see keep track of your progress (the ultimate goal is for the water in the porcelain bowl to be clear without using more than 2000mL). You will need to continue to repeat the sieving of sediment until this goal is met!*
13. Once the water runs clear, use DI water hose from a sink to CAREFULLY work all the sediment to the bottom of the sieve, then use the DI water squirt bottle to squirt sample from the sieve into its labeled beaker (ex. Sample#_0-1cm_90um_FP).
14. Keep this sediment beaker out. You will be sieving this sample again later.
15. Thoroughly rinse out the 90 micron sieve.
16. Pour previously sieved sample (left in bowl) over the 63 micron sieve and carefully rinse the beaker with DI water onto the sieve to make sure all sediment is removed from the container and captured for analysis.
****Note. Try not put water on the sediment directly but rather on the beaker sides and let the water push down the sediment.*
17. Follow the same procedure as before (steps 4-12). Once the water runs clear, use DI water hose from a sink to CAREFULLY work all the sediment to the bottom of the sieve, then use the DI water squirt bottle to squirt sample from the sieve into its labeled beaker (ex. Sample#_0-1cm_63um_FP)..
18. Place the labeled beaker in the oven (103-105°C) until water has evaporated.
19. Thoroughly rinse out the 63 micron sieve.
20. Next, pour previously sieved sample (left in bowl) over the 45 micron sieve and carefully rinse the beaker with DI water onto the sieve to make sure all sediment is removed from the container and captured for analysis.
21. Follow the same procedure as before (steps 4-12). Once the water runs clear, pour the remaining sieved water into the graduate cylinder and cover it with parafilm to ensure that no dust settles in them before the experiment is performed.
22. Place graduated cylinders to the side for pipette analysis and place beakers in the (103-105°C) oven for at least 24 hours then begin weighing procedure.

**Note. Place the cylinders in a region that is not easily disturbed once you start pipetting the area cannot be hit, bumped, etc., as it will disrupt the sediment fall velocity and mess up your results.*

23. Thoroughly rinse out the 45 micron sieve.
24. Grab the 150 micron sieve and place the sieve in a large porcelain bowl.
25. Fill the porcelain bowl with DI water, just to the top of the sieve surface.
26. Next, take the 90 micron sediment sample that was collected at the beginning of the sieving procedure pour the FECAL PELLET sample onto the 150 micron sieve. Carefully rinse the beaker with DI water onto the sieve to make sure all sediment is removed from the container and captured for analysis.
27. Slowly move the bowl in circular motions to begin moving the sediment across the sieve surface.
28. Occasionally (once a minute), pick up the sieve to allow sediment to readjust and move the sediment.
29. Continue steps 27 and 28 for 5 minutes.
30. Place porcelain bowl on stir plate and put a medium size stir bar under the sieve. Place stir plate on medium-high stir speed and let sit for 5 minutes.
31. Remove bowl from stir plate along with the stir bar. Rinse stir bar into bottom of bowl so no sediment is lost.
32. Transfer sieved water from one bowl to new one and begin again to track the progress of how much sediment remaining is passing through the sieves.
33. Repeat steps 27-32 until water runs clear.
34. Once the water runs clear, use DI water hose from a sink to CAREFULLY work all the sediment to the bottom of the sieve, then use the DI water squirt bottle to squirt sample from the sieve into its labeled beaker (ex. Sample#_0-1cm_150um_FP).
35. Place the labeled beaker in the oven (103-105°C) until water has evaporated.
36. Thoroughly rinse out the 150 micron sieve.
37. Finally, pour previously sieved sample (left in bowl) over the 90 micron sieve and carefully rinse the beaker with DI water onto the sieve to make sure all sediment is removed from the container and captured for analysis.
38. Follow the same procedure as before (steps 27-32). The water that comes through the sieve should be clear and only sediment between 150 and 90 microns should remain.
39. Once the water runs clear, use DI water hose from a sink to CAREFULLY work all the sediment to the bottom of the sieve, then use the DI water squirt bottle to squirt sample from the sieve into its labeled beaker (ex. Sample#_0-1cm_90um_FP).
40. Place the labeled beaker in the oven (103-105°C) until water has evaporated.
41. Thoroughly rinse out the 90 micron sieve.

Pipette Analysis

Need Specifically: 2L graduated cylinders (2 for each sample)
 Mixing rod
 20 mL pipette with bulb
 Aluminum trays (4 per each sample)

- 9.
10. Label and Pre-weigh aluminum dishes. There will be two dishes for each sample (two for ORIGINAL SEDIMENT sample and two for FECAL PELLET sample)

- a. Label trays, place in oven (103-105°C) for at least an hour and weigh twice (weights should be within 0.0005 g's of each other).
 - * *Reminder: do not handle aluminum trays with bare hands. Use gloves or tweezers!*
 - b. Record weights in excel sheet.
11. Check the room temperature (right at the location of the graduated cylinders). This temperature determines the length of time between the first withdrawal and 8 phi withdrawal times. For the first withdrawal, we are capturing sediment that is less than 45 microns. 45 microns falls between 4 and 5 phi, which is considered silt.

Sediment Withdrawal

12. Withdrawal for mud is 20 mL (use pipette) at a depth of 20 cm. (mark your pipette with sharpie to make easier).
13. Rigorously stir sample for 20 seconds
14. Withdrawal 20 mL from the cylinder at 20 cm and place in correct aluminum tray.
15. Rinse the stirring rod in the first cylinder and clean again in the second to remove any extra sediment. Next rinse the pipette with the DI water from the beaker between sediment withdrawing from each sample.
16. Watch the clock and use time sheet to know when to do each sample. There will be a long break between 4phi and 8phi. During this break recover the cylinders with parafilm and be sure not to bump the graduated cylinders and cover your 4 phi sample trays OR put them in the oven.
17. **For 8 phi: DO NOT STIR BEFORE WITHDRAWL!!!** When it is time for 8phi simply withdrawal 20 mL from the cylinder, but this time at 10 cm instead of 20cm and place in correct aluminum tray.
18. When experiment is complete place trays in oven (103-105°C) for at least 24 hours then begin weighing procedure.

Weighing Procedure

1. Place in oven (103-105°C) for at least 24 hours
 - After samples have been dried**
2. Pull out of oven (103-105°C), let cool in desiccator (~20 minutes) and weigh; recording the weight in spreadsheet
3. Place back in oven for at least an hour (103-105°C) then reweigh
4. Repeat until weights are within 0.0005 grams of each other

Determine organic content

5. To determine organic content place in muffle (550°C) for at least an hour
6. Pull out of muffle and transfer samples to a regular oven tray to cool for 15 minutes so that the samples don't melt the desiccator shelves.

**Note: if you leave the samples out for more than 5 minutes then place them in the 103-105°C in order to remove any moisture that may have been absorbed.*

7. Place samples in desiccator to cool (~20 minutes) and weigh; recording the weight in spreadsheet.
8. Place back in oven for at least an hour (103-105°C) then reweigh
9. Repeat until weights are within 0.0005 grams of each other.

Timing for experiments

Temp	Phi	Time from start of stirring (HH:MM:SEC)
22	First withdrawal	00:00:20
	8	01:56:32
23	First withdrawal	00:00:20
	8	01:53:49
24	First withdrawal	00:00:20
	8	01:51:12

Chapter 4: Seasonal morphological change in the York River Estuary, Chesapeake Bay VA

Abstract

Seasonal changes in seabed height within the Clay Bank region of the York River Estuary were assessed using, seven high-resolution bathymetric surveys conducted between September 2008 and August, 2009. Classified as a dynamic fine-grained cohesive sediment environment, the Clay Bank region was surveyed using interferometric swath bathymetry to calculate seabed elevation within a 3.75 km² region. Seabed height was shown to vary both spatially and temporally in association with the spring freshet, likely related to the presence and migration of a local secondary turbidity maximum. Based on shifts in control points from cruise-to-cruise, confidence intervals on individual point measurements of bathymetric change in the main and secondary channel regions were estimated to be ± 0.46 m and ± 0.24 m, respectively. Averaging across many bathymetric soundings was then used to reduce uncertainties in estimates of regional values of mean depth. Overall, bathymetric data suggested that significant seasonal net deposition, averaging 0.19 ± 0.07 m, occurred over the secondary channel sub-region in spring of 2009, as calculated by the use of ground control points and tidal data comparisons. Across-channel transects in both the main channel and secondary channel sub-regions showed that surface elevations in depressions between bathymetric promontories tended to increase during spring, while the elevations of the promontories themselves remained relatively constant.. Though a more detailed understanding is needed to fully constrain the dynamic changes occurring in cohesive, estuarine seabeds such as that of the York River, this study nonetheless demonstrated the types of spatial and morphologic changes that can be identified using high-resolution interferometric bathymetry.

4.1 Introduction

Estuaries are ubiquitous ecosystems that account for some of the most productive and

diverse environments in the world. Estuaries are generally defined as semi-enclosed bodies of water, having a free connection with the open sea, where salinity throughout the system is measurably diluted by freshwater from land and riverine drainage (Pritchard, 1967). While estuaries are prominent along most coastlines, they are relatively short-lived geologic features that act as dynamic transitional environments between freshwater and oceanic ecosystems. Moreover, a variety of factors including local geology, physical dynamics, biological and chemical processes, as well as anthropogenic effects influence these systems (Nichols and Biggs, 1985). Many of these processes make estuaries effective traps for sediment that can enter from either upstream rivers or the mouth of the system where oceanic sediment influx can occur (Dalyrmples et al., 1992).

Within estuaries, areas of high sediment resuspension occur in the estuarine turbidity maximum (ETM) zones (Eisma, 1993; Woodruff et al., 2001). Residual water circulation and salinity fronts are thought to be the primary mechanisms for forming ETMs in partially-mixed estuaries, while tidal asymmetry is thought to be increasingly important as tidal energy increases (Dyer, 1986; Geyer, 1993). Classically, the ETM in partially-mixed estuaries is a region of high-suspended sediment concentrations that results from convergence near the salt limit (Postma, 1967; Burchard et al., 2004). In addition to primary turbidity maxima, some estuaries develop a secondary turbidity maximum (STM). Generally, STMs are ephemeral features whose appearances are largely controlled by the spring-neap tidal cycle and riverine discharge, and the effects of each on the estuarine salinity field. Both ETMs and STMs contain high amounts of mobile fine sediment that is constantly being deposited, reworked, and resuspended back into the water column. The sediment mass of the turbidity maximums is variable and dependent on hydrodynamic, seabed, and biological factors (Roberts and Pierce, 1976; Geyer et al., 2001; Lin

and Kuo, 2003). In regions of the ETM and STM, resuspended particulate matter collides, favoring aggregation and flocculation of the fine-grained cohesive material (Whitehouse et al., 2000; Winterwerp, 2002). The increased amounts of aggregation and flocculation enhances the settling rate of the material and thereby deposition, favoring the formation of ephemeral deposits that migrate along with the ETMs (Eisma, 1991; Whitehouse et al., 2000; Guan et al., 2005).

The geologic reconnaissance survey described in this chapter was conducted as part of the NSF Multi-Disciplinary Benthic Exchange Dynamics “MUDBED” project with the aim of better understanding the relationship between physical, geologic, and biologic processes with the surficial and subsurface geology. The consideration of these interdisciplinary processes affords a broad picture of the ecosystem that allows for a more complete understanding of the intricacies of this dynamic environment. This study aims to clarify processes that govern erodibility, and enhance the knowledge of transport and dynamics of fine-grained sediments using data collected during the MUDBED project. This study incorporated interferometric swath bathymetric surveys to create a time-varying three-dimensional representation of the Clay Bank region in the York River sub-estuary.

4.2 Study Area

The York River estuary is located in southeastern Virginia on the Mid-Atlantic Coast of the United States (Figure 4-1), and was created by the drowning of a river valley approximately 12,000 years ago when glaciers melted during the beginning of the Holocene (Hobbs et al., 2009). Today, the estuary is formed at the confluence of the Mattaponi and Pamunkey Rivers and empties into the Chesapeake Bay at its mouth. As the Chesapeake’s fifth largest tributary, the York River watershed encompasses approximately 6900 square kilometers and is characterized as a humid sub-tropical climate, receiving an annual precipitation of 112-120

centimeters/year. Presently, the York's watershed is relatively less developed compared to many other Chesapeake Bay tributaries and is predominately bounded by rural landmasses with forest cover as a majority of the land classification, totaling 61%. The other 39% of the watershed is classified as agriculture (21%), wetlands (7%), and barren land (1%). The remaining area is covered by water (Nichols et al., 1991; Reay and Moore, 2009).

The estuary has a mean depth of 4.9 meters, with the deepest area is located near Gloucester Point where the depth exceeds 20 meters. The main channel of the estuary averages about 10 meters in depth and is thought to be controlled by antecedent geology of the incised paleo-river valley (Carron, 1976). The main channel bifurcates near Page's Rock Light and a shallower (~ 5 meter deep) secondary channel, which is considered partially abandoned, extends northward on the western flank of the main channel (Dellapenna et al., 2003). Two shoals flank the channels and have an average depth of ~ 2 meters. Although microtidal, the tidal currents within the river, particularly in the middle and upper portions of the estuary, have been documented as being strong enough to regularly resuspended bottom sediments (Dellapenna et al., 1998).

Over the years, many research projects have been conducted within the York River, ranging from studies of biological fauna to watershed management practices, with many focusing on both physical and geologic properties of the estuary. Most recently, these research initiatives have included interdisciplinary components, which have shed light on complex process interactions. Examples include research focusing on the biological and physical controls on seabed properties within the estuary (Dellapenna et al., 1998; Dellapenna et al., 2001; Schaffner et al., 2001; Hinchey, 2002; Dellapenna et al., 2003; Kniskern and Kuehl, 2003; Dickhudt et al., 2009; Rodriquez-Calderon and Kuehl, 2012), tidal asymmetry, bed stress and

stratification (Friedrichs et al., 2000; Kim et al., 2000; Scully and Friedrichs, 2003), turbidity maxima (Lin and Kuo, 2001; Lin and Kuo, 2003; Romine, 2004), modeling (Rinehimer, 2008, Fall, 2012), and controls on bed erodibility and settling velocity (Friedrichs et al., 2008; Cartwright et al., 2009; Dickhudt et al., 2009; Cartwright et al., 2011; Dickhudt et al., 2011).

Researchers have found that physical seabed processes dominate in the upper regions of the York River sub-estuary whereas biological processes are more dominant closer to the mouth of the river (Dellapenna et al., 1998; Dellapenna et al., 2001; Schaffner et al., 2001; Dellapenna et al., 2003; Kniskern and Kuehl, 2003; and Gillett and Schaffner, 2009). These previous studies distinguished several regions of the river based on the relative influence of physical versus biological processes along the estuarine gradient. The broadest of the generalizations classify the river into three areas: the upper, middle, and lower York River. Due to the influences of the river discharge, tidal energies, along with the location of the main estuarine turbidity maximum, little biological reworking takes place in the upper York, and the system there is physically dominated. Conversely, the physical energy decreases down river and biological conditions dominate in the lower York (Schaffner et al., 2001).

The specific study site for this investigation was located in the Clay Bank region of the estuary (Figure 4-2). Located approximately 30 kilometers from the mouth of the river and 6 meters in depth, the Clay Bank region is influenced by both physical and biological factors. Based on various environmental parameters, the study site is often impacted by pelletization and flocculation. In addition, the region is also the location of an ephemeral deposit associated with the secondary turbidity maximum. Lin and Kuo (2003) attributed the presence of the STM in the York River Estuary to four major mechanisms: resuspension of bottom sediments, bottom residual flow convergence, tidal asymmetries, and the suppression of turbulent diffusion due to

stratification of the water column. The York River STM identified by Lin and Kuo (2001) is generally located about 40 kilometers up estuary, near the area known as Clay Bank. Because of channel shoaling in the region, this location is conducive to STM development as it is often a stratification transition zone from well-mixed to partially stratified (Lin and Kuo, 2003). Rinehimer (2008) developed a three-dimensional numerical model to examine the erodibility and movement of sediment associated with the STM. The model showed a transient layer of sediment that moved in and out of the STM region.

Dickhudt et al. (2009) and Rodriguez and Kuehl (2012) also focused on the ephemeral deposit associated with the seasonal presence of the STM near Clay Bank. Dickhudt et al. (2009) identified depositional events from physical layering in x-radiographs and they determined the occurrence of recent deposition versus erosion to be by far the most important control on subsequent bed erodibility. In association with inferred deposition events, Dickhudt found physical layering to span the entire depth of ~ 20-centimeter x-ray cores. Along with x-radiography, Rodriguez et al. (2012) used dual frequency sonar to seasonally map the spatial distribution of the ephemeral mud deposit. Based on separation of the dual sonar reflections, Rodriguez et al. (2012) estimated seasonal deposition in the vicinity of the STM to be on the order of 20 centimeters.

Both Dickhudt et al. (2009) and Rodriguez and Kuehl (2012) inferred the presence of the ephemeral deposit indirectly via sediment properties associated with near-surface sediment. In an effort to observe seasonal deposition and erosion directly via changes in bed elevation, this study utilized an interferometric swath mapping system.

4.3 Methods

4.3.1. General Surveying Approach and Associated Equipment

All surveys conducted for this study relied on equipment and research vessel availability, as well as suitable weather conditions for surveying. Originally, the study aimed to collect high-resolution bathymetry data for the Clay Bank region every month, but sampling during some months was prevented by various limitations. In total, seven months were surveyed between September, 2008 and August, 2009 for bathymetric analysis (Table 4-1), incorporating over 350 kilometers of high-resolution bathymetry data, repeatedly encompassing an area of ~3.75 square kilometers. Survey lines were established and used in each survey of the study site to provide near complete bathymetric swath coverage of the seafloor. Each data collection field sampling survey incorporated the same survey track lines as closely as possible, so the area mapped remained nearly constant throughout the study with slight variability due to the presence of crab pots, gill nets, and various obstructions.

An interferometric swath system (Submetrix Series; 234 kHz) was used to map shallow water bathymetry (~1 – 15 meters) aboard the RV Elis Olsson. For each of the seven surveys, position was spatially referenced in real-time using a Trimble 4700/5100 Real-time Kinematic (RTK)-GPS unit and related to the UTM18N/WGS84 and Geoid 03 NAVD88 datum geoids. An RTK base station was located within close proximity of the study area, ideally allowing for horizontal and vertical control of ± 5 centimeters (McNinch, 2004). Bathymetry data were recorded in Submetrix's proprietary software, Swath, which georeferenced each sounding with navigational information from the RTK-GPS. An IXSEA Octans Motion Sensor mounted on the survey vessel and equipped with a fiber optic gyroscope, corrected the data from variations of pitch, roll, heave, surge, and sway of the boat during each survey in real-time. Five calibration survey lines were conducted at the beginning and end of each survey to provide correction

parameters for both the port and starboard transducers during data processing. The calibration corrections were calculated to 0.005 meters in order to insure the greatest accuracy possible and remove any inconsistencies in pitch and roll of the vessel throughout the duration of each cruise.

4.3.2. Correction for Water Level Variation

Two tidal and water level variation sources were utilized for this study. By using Hypack, a hydrographic survey software package, the vertical change in water level due to the tidal variation was calculated in real-time utilizing RTK-GPS, ideally for direct incorporation into the bathymetric processing. A secondary water level source was collected using the VECOS Clay Bank continuous monitoring station (Figure 4-2). As part of VECOS, water depth measurements were collected every fifteen minutes using YSI 6600 data sondes with the Clean Sweep Extended Deployment System and were corrected for barometric pressure in post-processing. Due to Hypack failures associated with two surveys (September and August) along with significant Hypack data gaps during two other surveys (January and February), the VECOS data exclusively were used for water level correction during bathymetric processing. But periods with good Hypack data were still utilized to assess potential sources of error by calculating the absolute differences between the VECOS and vertically shifted Hypack data, which is discussed later in the chapter.

4.3.3. Speed of Sound Calculations

Speed of sound velocity measurements were calculated for each survey based on Coppen's (1981) equation estimating speed of sound in sea-water as a function of temperature and salinity for shallow water depth:

$$c(S,t) = 1449.05 + 45.7t - 5.21t^2 + 0.23t^3 + (1.333 - 0.126t + 0.009t^2)(S - 35) \text{ (eq.1)}$$

where $t = T/10$, with T = temperature (Celsius), and S = salinity (ppt). The variables for each survey cruise were obtained from the VECOS Clay Bank continuous monitoring station at the study site, and the mean was used as an approximation of the speed of sound during data processing. Values ranged from 1,438 meters/second (February) to 1,523 meters/second (August) (Table 4-2). Each of these variables, i.e., roll, speed of sound, and tidal variability were applied to the bathymetric soundings during processing to increase the accuracy of the morphologic data.

4.3.4. Post-Processing in GRID and Fledermaus

With the input of roll calibration corrections, speed of sound estimates, and tidal and water level variations, bathymetric soundings were processed at 1-meter horizontal resolution and were then despiked, filtered, and smoothed in GRID, the Submetrix proprietary processing software. The data from each survey line were individually processed, filtered, and visually inspected within Fledermaus to remove any outliers, water column hits (i.e. boat wakes and fish), and bad data points. A single user conducted this estimation, in order to reduce additional subjective differences in data analysis that could be increased by multiple individuals contributing to the data processing. Although the Swath Interferometric system is capable of collecting data from a swath of over 10 to 15 times water depth, the total swath width utilized in this survey was limited to no more than 6 times water depth in order to retain cleaner data (Gostnell et al., 2006).

4.3.5. Identification and Application of Ground Control Points

To help compensate for possible user inaccuracies and uncertainties associated with the set-up and usage of the RTK-GPS system, ground control points were identified throughout as much of the study area as possible. Over a majority of the study region, the seabed is relatively smooth, with the exception of a few key locations along the edges of the main and secondary channel (Figure 4-3). For this reason, the optimal control points ended up being concentrated along rough areas within the main channel and the secondary channel regions of the study area, respectively, and not within the smoother region between these two areas. The concentration of control points in these two separate regions favored the focusing of further analysis on these two regions specifically, with less justification for further analysis of the section in between, which contained no control points.

The main channel block is delineated by the purple dashed line toward the right side of Figure 4-3, whereas the secondary channel block is delineated by the light-blue dashed line toward the left side of Figure 4-3. Due to the lack of control points within the central region (surrounded by white dashes in Figure 4-3) it was not analyzed further for monthly changes in bathymetry. A total of twelve prominent points located on apparent mounds and/or promontories, which persisted and were assumed to remain relatively stable, were analyzed for depth comparison (Table 4-3). Five control points were located in the deep channel block (Figure 4-4), and seven control points were located in the secondary channel block (Figure 4-5).

For this study, the results of the December survey were selected to be the baseline bathymetry. After correcting for water level using the VECOS tide data, the bathymetric change since December was averaged across the twelve control points for each cruise in turn (Table 4-3). The average change in bathymetry across the control points for each cruise since December was then used to uniformly shift all of the bathymetry each month so that there was no longer

any change in mean control point depth between cruises.

4.4 Uncertainties in Location and Elevation Associated with Bathymetric Surveys

In order to calculate reliable estimations of seabed elevation of a region, quantification of error and uncertainties is essential for bathymetric surveys. A rigorous understanding is critical to provide the most robust insights possible into the sediment transport pathways within a system, the magnitude of the transport, and a validation of any sediment budget calculated in subsequent analyses. Two fundamental measurements are the cornerstone of any bathymetric survey: the horizontal position (X-Y location) and vertical depth (underwater elevation of measured object) (Byrnes et al., 2002). Each measurement is associated with a variety of errors and uncertainties based on the methodology of the study (Table 4-4) (Umbach, 1976).

As mentioned previously, the RTK-GPS System and base station control setup ideally allowed for horizontal control of ± 5 centimeters (McNinch, 2004). With that level of accuracy, any horizontal misalignment captured between bathymetric surveys could be identified if a particular feature can be recognized in multiple surveys. However, any shift in the X-Y direction requires careful interpretation, and for this study, any visual shifts in the horizontal position of prominent features are attributed to observation error and uncertainty, rather than real change. Over steep topography, such as along the flanks of the deep channel, errors in horizontal control may be especially problematic because a slight horizontal offset from cruise-to-cruise may translate to apparently large but erroneous cruise-to-cruise changes in water depth.

Under ideal circumstances, collective uncertainties incorporating average density/spacing of soundings, vessel movement, GPS positioning, speed of sound, and acoustic attenuation are expected to lead to a local vertical bathymetric resolution of approximately ± 15 -20 centimeters

(McNinch, 2004). In our case, it was determined that human error in cruise-to-cruise control of the RTK-GPS vertical datum favored the use of control points for establishing the absolute cruise-to-cruise vertical datum instead. In addition, failures in the Hypack recording of time-varying vessel elevation meant that the local VECOS tide gauge was the best available choice for water level correction. Together, these substitutions suggest that the local uncertainty in bathymetry values for individual points in our case may be significantly more than ± 15 -20 centimeters.

However, averaging of soundings in space has the potential of significantly reducing uncertainty in mean elevations for whole regions relative to individual soundings by averaging across local uncertainties that are randomly distributed and/or may tend to cancel each other out. Uncertainties that contribute to local elevation errors but tend to be reduced by spatial averaging include boat rocking and small uncertainties in horizontal position over gentle topography. Spatial averaging may also reduce effects of mean boat tilt if one assumes the resulting biases to each side of the vessel are of opposite sign. After spatial averaging, for example, McNinch (2004), found that ground truth comparisons between interferometric system measurements and more conventional physical soundings off Duck, NC differed by less than 1 cm.

4.5 Results

4.5.1. Results for Uncertainties Based on Tide Gauge and Control Point Data

The likely magnitude of two sources of uncertainty can be estimated directly from data collected during the surveys: (i) the remaining water level uncertainty during a single survey after the VECOS water level correction and (ii) the remaining vertical datum uncertainty between cruises after application of mean control point shifts. In order to assess the potential

source of error in the difference between VECOS data and actual water height at the boat, as calculated by the RTK-GPS, the VECOS vs. Hypack data consistency were tested for the dates that had partially usable Hypack data (Figure 4-6). The average absolute differences between the VECOS and vertically shifted Hypack data were examined for each available cruise and ranged from 1.2 to 3.2 centimeters. According to the VECOS operators, the absolute uncertainty in VECOS water levels at the site of the gauge is on the order of ± 1 cm or less (D. Parrish, pers. comm.).

In order to assess the vertical accuracy of the bathymetric datasets, the standard deviations of the vertical shift in elevation required at the twelve control points for each month were examined in order to estimate the remaining month-to-month uncertainty in the vertical datum between cruises. The standard deviations for monthly bathymetric changes for all twelve control points (Table 4-3) ranged from 0.10 m to 0.26 m, averaging 0.17 m. With a population of twelve samples (assuming a normal distribution), an average standard deviation of 0.17 m translates to a 95% confidence bound on the mean of ± 0.10 m. In other words, the observed consistency among the month-to-month shifts across all twelve control points suggests the remaining uncertainty in vertical datum from cruise to cruise is about ± 0.10 m. This means that mean bed elevations averaged across the entire survey region have the potential of uncertainties as low as ± 0.10 m.

However, it is important to note that these statistics suggest that the mean uncertainty in vertical datum for the entire survey area, if considered as a whole, is on the order ± 0.10 m. When analyzed separately, the standard deviations on the control point shifts were consistently larger in the main channel (averaging 0.23 m) than in the secondary channel (averaging 0.12 m). With a population of five control points in the main channel subregion and seven control points

in the secondary channel subregion, the 95% uncertainty values for vertical control in the main channel and secondary channel subregions become approximately ± 0.22 m and ± 0.09 m, respectively.

Although the uncertainty in the mean datum from month to month is relatively low, the uncertainty in the elevation of individual bathymetric soundings relative to that datum is somewhat higher. Assuming that the elevation of the control points did not change from cruise to cruise, then the remaining variability observed among the best-fit shifts for these twelve points for a given cruise can be used as an estimate of individual point uncertainty. An average standard deviation in vertical shift of 0.17 m for the twelve individual control points that presumably shifted uniformly translates to a 95% confidence on these individual measurements of about twice that, or $\sim \pm 0.34$ m for individual points over the entire survey area. Furthermore, if we were to focus on the main channel, the 95% confidence on individual measurements there becomes about ± 0.46 m (including the main channel uncertainty of 0.22m), and thereby the 95% confidence on individual measurements within the secondary channel becomes about ± 0.24 m (including the secondary channel uncertainty of 0.09m).

4.5.2. Overall Results by Subregion

Monthly bathymetric maps for the main channel and secondary channel blocks, corrected for estimated datum shifts (a total of fourteen maps), are presented in the appendix to this chapter. Given that the local uncertainties for observed changes between months for individual points were estimated to be relatively large (± 0.46 m in the main channel and ± 0.24 m in the secondary channel), it was helpful to reduce the uncertainties somewhat by averaging bathymetric changes across each of the two regions. Figure 4-7 presents time-series for mean depth, averaged entirely over each region, including their uncertainty ranges. Overall results

from the main channel did not provide a signal for net change that exceeded or surpassed the uncertainty bounds (Figure 4-7a).

However, results from the secondary channel do show a significant change (Figure 4-7b), in that the mean depths in May, June and August of 2009 were each significantly less than the mean depths in September of 2008 and January of 2009. In other words, mean depth analysis for the secondary channel suggests significant net deposition was present in the secondary channel after May 2009 relative to conditions in the previous September and January. The statistics can also be examined for averages before and after May 1. For the secondary channel region, the average of the three cruises after May 1 minus the average of the four cruises before May 1 gives an average seasonal net change of 0.19 m. In this calculation, the monthly uncertainties in mean bed elevation ($\Delta h \approx \pm 0.09$ m) propagate following an average of root means squares, i.e., the uncertainty in the average seasonal change of 0.19 m becomes approximately $((1/3) + (1/4))^{1/2}$ $\Delta h = \pm 0.07$ m. Finally, the net seasonal change in the secondary channel region bed elevation is then estimated to be $+ 0.19 \pm 0.07$ m.

4.5.3. Small Subsection Results

Particular regions of interest within the study area were further investigated with detailed, small sub-section analyses. Two locations were chosen that included ground control points and other features that were present in all surveys. The first sub-section location was selected in the northern portion of the study site, within the main channel. This area had prominent, stable mound features in each monthly survey. Along-channel and across-channel transects were analyzed to qualitatively assess bathymetric changes within the main channel (Figure 4-8). Based on visual analysis, the along channel transects displayed very little change of the course of the study, maintaining similar profiles for all seven months mapped. In contrast, the across-

channel transects recorded variations in bed elevation between the mounds and the northeast flank of the main channel. During the September, December, and January surveys the depth of the seabed between the mounds was ~ 9.5 meters. As time progressed, the bathymetric transects show the surface elevation between the mounds shifting to ~9.0 meters in May, June, and August.

Similarly, a sub-section analysis of the secondary channel was completed. For this inquiry only an across-channel profile was evaluated. The area was chosen once again because of prominent morphologic features that were easily identifiable in all surveys and were in the vicinity of ground control points. Over time, the transect analysis showed changes in seabed elevation between the mound features (Figure 4-9). The transects for the surveys between September and February depict a ridge and runnel type feature with a deeper seabed between two ridges. As spring approached, the elevation difference between the ridge and trough dissipated, showing a more flattened topography and shallower seabed elevation in May and June than were previously mapped. Eventually, the August profile showed the seabed returning to a more pronounced ridge and runnel feature, similar to those mapped in the fall and winter cruises.

4.6 Discussion

4.6.1 Relationship to Previous Studies of Sediment Dynamics at Clay Bank

The Clay Bank region within the York River Estuary provides an excellent natural laboratory for studying a wide range of estuarine processes associated with cohesive sediment dynamics and benthic community structure, and it has been well studied over the last few decades. (Nichols et al., 1991; Wright et al., 1995; Dellapenna et al., 1998; Dellapenna et al., 2001; Schaffner et al., 2001; Dellapenna et al., 2003; Kniskern et al. 2003; Rinehimer, 2008; Dickhudt et al., 2009; Gillett and Schaffner, 2009; Cartwright et al., 2011; Dickhudt et al., 2011;

Fall, 2012; Rodriguez-Calderon and Kuehl, 2012; Cartwright, 2013). Most recently, the MUDBED program has conducted a variety of experiments which aimed to provide a greater understanding of sediment properties and their relationship with bed erodibility and hydrodynamic variability.

Dickhudt et al. (2009) illustrated seasonal patterns of erodibility within the York River Estuary with a conceptual model, highlighting various physical parameters impacting the seabed at Clay Bank. The conceptual model was based on monthly surveys of sediment properties in 2006 and 2007, including Gust microcosm erodibility measurements, grain size, and water content (Figure 4-10). These instantaneous monthly snapshots of data from the Clay Bank region, in the main and secondary channel, provided the input data for a three-dimensional computational model, developed by Rinehimer (2008), to further investigate mechanisms driving seabed evolution. Overall, both studies concluded that deposition in association with the spring freshet resulted in higher erodibility of the seabed during spring months at the study site, whereas a decrease in erodibility was documented in the late summer and fall following lower discharge conditions (Rinehimer, 2008; Dickhudt et al., 2009).

The overall trend of seabed erodibility at Clay Bank can be complicated by a variety of conditions, including: stratification, sediment flux, and the presence and migration of the local secondary turbidity max (STM). Previous studies detailing the STM have associated it with an easily resuspended pool of sediment that migrates between the middle and upper York River (20-45km from the mouth of the river) depending on the riverine discharge and gravitational circulation of the estuary (Lin and Kuo, 2001; Romine, 2004). With low river discharge, the STM moves further upstream. Conversely, with high discharge from the Mattaponi and Pamunkey rivers, the STM migrates further downstream potentially into the Clay Bank region

(Romine, 2004).

In addition to these previous studies, several acoustic sub-bottom surveys were conducted between April 2008 and March 2009 (Rodriguez-Calderon and Kuehl, 2012), three of which were collected simultaneously with the high-resolution bathymetric mapping reported here. Following the same survey lines as those tracked in this study, Rodriguez-Calderon and Kuehl (2012) utilized the differences in bottom depth obtained by two channels in a dual-frequency echosounder as a proxy of the thickness of the layer of soft mud present at the surface (Figure 4-11). The dual-channel echosounder utilized a higher frequency (200 kHz) to capture the upper surface of the soft mud layer and lower frequencies (10-100 kHz) to capture seabed reflectors possibly associated with the bottom of the soft mud layer. Rodriguez-Calderon and Kuehl (2012) found that between April 2008 and March 2009, the thickest soft layers occurred during spring and the thinnest occurred during fall, providing more evidence of the seasonal cycle has that been discussed by others (e.g., Lin and Kuo, 2001; Rinehimer, 2008; Dickhudt et al., 2009).

4.6.2 River Discharge and Corresponding Regionally-Averaged Patterns of Deposition

As the presence of the STM at Clay Bank is generally associated with an increase in freshwater discharge from the Mattaponi and Pamunkey Rivers, USGS discharge data were examined to characterize river flow during 2008-2009 study period (Figure 4-12). The May and June cruises each occurred a few weeks after the highest pair of discharge events of the year. Often a lag time of a few weeks is apparent between discharge and the presence of an STM (Dickhudt et al., 2009), and these bathymetric collection surveys fell within the allotted timeframe of highly suitable conditions for the STM. Therefore, after each of the large discharge events, a new pool of material may have moved into the region and been deposited. The data also correlate with trends in Rodriguez-Calderon and Kuehl's (2012) analysis of variations in soft

mud layer thickness in the Clay Bank region, where mud layer thickness also increased in association with discharge events. The average depth analysis presented here for the secondary channel revealed a statistically significant increase in bed elevation consistent with deposition in the May to June STM time-frame (see Figure 4-7b). This trend is once again consistent with the conceptual model of the Clay Bank region, where sediment is deposited following the wettest periods of the year versus little to no deposition or erosion during drier conditions.

Unfortunately the uncertainty bounds were larger for elevation change in the main channel, and the effect of the STM could not be statistically established for the main channel region as a whole.

4.6.3 Distinct Seabed Changes within Sub-environments

Sediment exchange between sub-environments can affect the seabed height, as movement of bed material between the shoal and the channels, especially during storm events and increased wave and current conditions can be significant (Dellapenna et al., 2003). In the Clay Bank region, Kniskern and Kuehl (2003) assessed four sub-environments (shoal, flank, secondary channel, and main channel) and examined the changes in these sub-environments over time based on spring-neap cycles and seasonal events. Rodriguez-Calderon and Kuehl (2012) further examined across channel gradients and determined differences in the soft mud layer thickness between the main and secondary channels. For April 2008 to March 2009, they found that overall mud layer thicknesses were generally greater in the secondary channel, except in March 2009 when the soft mud layer thickness was more prominent in the main channel. In the following paragraphs, seabed elevation changes are discussed focusing specifically on the Clay Bank region's sub-environments.

For the main channel sub-environment, the STM has been found to play a strong role in

both deposition and reworking of the sediment in this region of the study area, with seabed mixing depths ranging from 30-100cm historically (Dellapenna et al., 2003) and sometimes up to 150cm (Kniskern and Kuehl, 2003). Generally dominated by physical processes and typically comprised of laminations, the sediment composition is mostly mud and long-term accretion rates are low. Interesting bathymetric changes within the main channel sub-environment are visible in the maps of the main channel contained in the Appendix. However, given the uncertainties calculated for point measurements, the sub-region specific findings discussed here must be considered only as possible qualitative trends. Between September and February, the bathymetric maps of the main channel displayed little obvious elevation change; however, apparent deposition on the seabed could be seen locally on the northwestern flank of the main channel between May and June, possibly in response to the presence of the annual spring STM. These changes generally correspond in time with the infilling between mounds seen in Figure 4-8. After the May and June surveys, the main channel appeared to return to an equilibrium state. These localized bathymetric changes seem to reinforce the pattern documented by previous studies.

Another key sub-environment examined during this study was the secondary channel. Dellapenna et al. (2003) found that this region was typically dominated by deep physical mixing, with short-term deposition rates up to 20-50 cm in a given year. During 2008 and 2009, Rodriguez-Calderon and Kuehl (2012) specifically identified the northern portion of the secondary channel as physically dominated, usually comprised of thick sedimentary laminations due to the presence and migration of the STM. However, further south, laminations were only apparent in the late fall and winter. In the bathymetric maps in the Appendix, spatially varying patterns in the secondary channel are likewise seen. For example, in December through January,

a gradient of apparent deposition can be seen moving along channel to the secondary channel, where the sediment may have been deposited. The secondary channel was seen to experience changes consistent with deposition and infilling after the spring freshet (see Figure 4-9). By August, the secondary channel appeared to have been scoured once more. It is important to note that this region is quite complex, with the presence of sedimentary furrow bedforms during neap tide conditions previously documented in the northern portion of the secondary channel, highlighting its spatial heterogeneity (Dellapenna et al., 1999).

Though not analyzed as part of this study, it is important to mention the shoal region associated with an inactive oyster reef is situated between the main and secondary channels. Found to be influenced by both physical and biological processes, the seabed in this shoal sub-environment follows a typical pattern of laminations in the fall and winter and bioturbation in the spring and summer (Schaffner et al., 2001; Dellapenna et al., 2003; Kniskern and Kuehl, 2003; Dickhudt et al., 2009; and Rodriguez-Calderon and Kuehl, 2013). This particular region of the seabed was found by others to have sandier sediment than either the main or secondary channel as well as a higher elevation, forming a concave morphology between the two channels.

4.6.4 Possible Role of storms

The highest average bed elevations recorded in this study for the secondary channel region occurred in June 2009, soon after several large storms moved through the York River estuary. For several days in June, wind gusts blew at or greater than 30 mph ($> 13 \text{ m s}^{-1}$) and riverine discharge reached over $200 \text{ m}^3 \text{ s}^{-1}$, the largest of all discharge events throughout the year-long set of surveys. This stormy period may have contributed to the significant changes in observed seabed elevation, when the secondary channel became relatively filled with sediment, possibly because of erosion from neighboring shallows and/or transport of sediment from the

upper York. The upper York River Estuary had previously been documented as being susceptible to occasional large seabed mixing events, which can include extreme tides, extratropical storms, nor'easters, as well as flooding events (Dellapenna et al., 2003).

4.7 Historical Bathymetry

Though the seven high-resolution bathymetric surveys completed in 2008 and 2009 provided insight to the seasonal variation of the morphology of Clay Bank, a deeper historic understanding of the historic nature of the system would be beneficial. Digitized echosounder data collected by the National Ocean Service in 1947 was located, which surveyed the Clay Bank and Aberdeen Creek Region of the York River (NOS Survey H07189). The original sounding data were corrected for actual sound velocity. In order to compare modern surveys to the historic digital echosounder data, the 1947 collected bathymetry points were interpolated using a linear kriging method (Figure 4-13). Though the resolution of the historic bathymetry is considerably coarser than the surveys completed for this study (Figure 4-14), the comparison shows that the slumps found within the main channel and used for the postage stamp analysis have been present for more than 50 years. This provides a greater confidence in our selection of ground control points in the region, providing a historic reference that the features have been persistent for decades. Unfortunately, the spacing of the 1947 sounding was too great for a more quantitative analysis, especially with regards to the secondary channel.

4.8 Conclusions

Seven high-resolution bathymetric surveys were conducted between September 2008 and August 2009 in the Clay Bank region of the York River Estuary. This environment, which is composed of mostly fine-grained cohesive sediment, is dynamic in nature and experiences event

to seasonal-scale cycles in erosion and deposition as energy and circulation patterns change in response to storms, spring-neap tidal oscillations, and fluctuating fresh water discharge.

Overall, the data presented here suggest that significant seasonal net deposition, averaging 0.19 ± 0.07 m, occurred over the secondary channel subregion of Clay Bank in 2009 in response to the spring freshet and associated secondary turbidity maximum. This result is consistent with the timing and cause of depositional patterns inferred in this region by other investigators using different methods. Nonetheless, this is the first time that seasonal net deposition has been directly documented in the York River Estuary by changes in bed elevation rather than inferred indirectly by changes in bed properties. Although significant net deposition was broadly observed across the secondary channel region in this study, results from the main channel did not provide a regional signal of net change that exceeded the uncertainty bounds.

Examination of small subsections of bathymetric surveys at locations near control points provided additional insights into patterns of deposition in both the main and secondary channel subregions in association with the likely presence of the STM. Across-channel transects in both subregions showed that surface elevations in depressions between bathymetric promontories increased during spring, while the elevations of the promontories themselves remained relatively constant. This pattern was likewise consistent with the migration of mobile pools of mud downstream toward the Clay Bank region in response to the spring freshet.

Cohesive estuarine environments are among the most challenging of all for quantitatively mapping seasonal bathymetric changes. Given the relatively subtle bathymetric changes, continual time variation in water elevation, and relatively low number of prominent bed features to use as control points, uncertainties in individual bathymetric point measurements may be large. In this project we were fortunate to have high quality VECOS tide gauge data continually

available immediately adjacent to our study region. The times when the vessel-based Real-time Kinematic (RTK)-GPS was operating reliably indicated that use of the VECOS water level data rather than RTK-GPS added only ~ 1 to 3 cm of uncertainty to individual depth observations.

Difficulties associated with translating a consistent, RTK-GPS-based vertical datum to our small vessel from one survey to the next led us to utilize a dozen identifiable bathymetric promontories as control points that were assumed not to change in elevation between cruises. Based on the standard deviation of control point shifts from cruise-to-cruise, the confidence intervals on individual point measurements of bathymetric change in the main and secondary channel regions were then estimated to be ± 0.46 m and ± 0.24 m, respectively. Averaging across many bathymetric soundings was then used to reduce uncertainties in estimates of regional values of mean depth. This approach improved uncertainty estimates for average depths across the main and secondary channel regions for individual cruises to ± 0.22 m and ± 0.09 m.

Though a more detailed understanding is needed to fully constrain the dynamic changes occurring in cohesive, estuarine seabeds such as that of the York River, this study nonetheless demonstrates the types of spatial and morphologic changes that can be identified using high-resolution interferometric bathymetry. Overall, this study helped to provide a high-resolution analysis of seabed evolution within the York River Estuary on a seasonal scale. Further studies are needed to elucidate the changes associated with events that occur on even shorter time scales and to reduce uncertainties in depth estimates associated with individual bathymetric soundings.

References

- Burchard, H., Bolding, K., & Villarreal, M. R., 2004. Three-dimensional modelling of estuarine turbidity maxima in a tidal estuary. *Ocean Dynamics*, 54(2), 250-265.
- Byrnes, M. R., Baker, J. L., and Li, Feng, 2002. "Quantifying potential measurement errors associated with bathymetric change analysis," ERDC/CHL CHETN-IV-50, U.S. Army Engineer Research and Development Center, Vicksburg, MS.
- Carron, M.J., 1976. Geomorphic Processes of a Drowned River Valley: Lower York River Estuary, Virginia. , 115. M.S. thesis, Virginia Institute of Marine Science/School of Marine Science, The College of William and Mary, Virginia.
- Cartwright, G.M., C.T. Friedrichs, P.J. Dickhudt, T. Gass, and F.H. Farmer, 2009. Using the acoustic Doppler velocimeter (ADV) in the MUBED real-time observing system. OCEANS 2009, Institute of Electrical and Electronics Engineers, 1428-1436.
- Cartwright, G.M., C.T. Friedrichs, and L.P. Sanford, 2011. In situ characterization of estuarine suspended sediment in the presence of muddy flocs and pellets. In: P. Wang, J.D. Rosati, and T.M. Roberts (eds.), *Coastal Sediments 2011*, World Scientific, pp. 642-655.
- Cartwright, G.M., 2013. Application of acoustics and optics for the characterization of suspended particulate matter within an estuarine observing system. Ph.D. Dissertation, School of Marine Science, The College of William and Mary, Virginia Institute of Marine Science, Gloucester Point, Virginia.
- Coppens, A. B., 1981. Simple equations for the speed of sound in Neptunian waters *Journal of the Acoustical Society of America* 69(3), pg 862-863.
- Dalrymple, R. W., Zaitlin, B. A., & Boyd, R., 1992. Estuarine facies models; conceptual basis and stratigraphic implications. *Journal of Sedimentary Research*, 62(6), 1130-1146.
- Dellapenna, T.M., Kuehl, S.A., Schaffner, L.C., 1998. Sea-bed Mixing and Particle Residence Times in Biologically and Physically Dominated Estuarine Systems: a Comparison of Lower Chesapeake Bay and the York River Subestuary. *Estuarine Coastal and Shelf Science* 46, 777-795.
- Dellapenna, T., Kuehl, S., Pitts, L., 2001. Transient, longitudinal, sedimentary furrows in the York River subestuary, Chesapeake Bay: Furrow evolution and effects on seabed mixing and sediment transport. *Estuaries and Coasts* 24, 215-227.
- Dellapenna, T.M., Kuehl, S.A., Schaffner, L.C., 2003. Ephemeral deposition, seabed mixing and fine-scale strata formation in the York River estuary, Chesapeake Bay. *Estuarine Coastal and Shelf Science* 58, 621-643.
- Dickhudt, P. J., Friedrichs, C. T., Schaffner, L. C., & Sanford, L. P., 2009. Spatial and temporal variation in cohesive sediment erodibility in the York River estuary, eastern USA: A

- biologically influenced equilibrium modified by seasonal deposition. *Marine Geology*, 267(3), 128-140.
- Dickhudt, P. J., Friedrichs, C. T., & Sanford, L. P., 2011. Mud matrix solids fraction and bed erodibility in the York River estuary, USA, and other muddy environments. *Continental Shelf Research*, 31(10), S3-S13.
- Dyer, K.R., 1986. *Coastal and Estuarine Sediment Dynamics*. Wiley, Chichester; New York.
- Eisma, D., & Li, A., 1993. Changes in suspended-matter floc size during the tidal cycle in the Dollard estuary. *Netherlands Journal of Sea Research*, 31(2), 107-117.
- Fall, K.A., 2012. Relationships among fine sediment settling and suspension, bed erodibility, and particle type in the York River estuary Virginia. M.S. Thesis, M.S. thesis, Virginia Institute of Marine Science/School of Marine Science, The College of William and Mary, Virginia
- Friedrichs, C.T., G.M. Cartwright, and P.J. Dickhudt, 2008. Quantifying benthic exchange of fine sediment via continuous, non-invasive measurements of settling velocity and bed erodibility. *Oceanography*, 21(4): 168-172.
- Friedrichs, C. T., Wright, L. D., Hepworth, D. A., & Kim, S. C., 2000. Bottom-boundary-layer processes associated with fine sediment accumulation in coastal seas and bays. *Continental Shelf Research*, 20(7), 807-841.
- Friedrichs, C.T. 2009. York River physical oceanography and sediment transport. *Journal of Coastal Research*, SI 57: 17-22.
- Geyer, W., 1993. The importance of suppression of turbulence by stratification on the estuarine turbidity maximum. *Estuaries and Coasts* 16, 113-125.
- Geyer, W. R., Woodruff, J. D., & Traykovski, P., 2001. Sediment transport and trapping in the Hudson River estuary. *Estuaries*, 24(5), 670-679.
- Gillett, D. J., & Schaffner, L. C., 2009. Benthos of the York River. *Journal of Coastal Research*, 80-98.
- Gostnell, C., Yoos, J., and S. Brodet, 2006. NOAA Test and Evaluation of Interferometric Sonar Technology. *Proceedings of the 2006 Canadian Hydrographic Conference*.
- Guan, W. B., Kot, S. C., & Wolanski, E., 2005. 3-D fluid-mud dynamics in the Jiaojiang Estuary, China. *Estuarine, Coastal and Shelf Science*, 65(4), 747-762.
- Hicks, D.M., and Hume, T.M., 1997. "Determining sand volumes and bathymetric change on an ebb-tidal delta," *Journal of Coastal Research* 13(2), 407-416.
- Hinchey, E. K., 2002. Organism-sediment interactions: the role of seabed dynamics in structuring the mesohaline York River macrobenthic community. Ph.D. Dissertation,

School of Marine Science, The College of William and Mary, Virginia Institute of Marine Science, Gloucester Point, Virginia.

- Hobbs, C., 2009. York River Geology. *Journal of Coastal Research*, 10-16.
- Kim, S.C., Friedrichs, C.T., Maa, J.P.-Y., Wright, L.D., 2000. Estimating bottom stress in a tidal boundary layer from acoustic Doppler velocimeter data. *ASCE Journal of Hydraulic Engineering* 126, 399–406.
- Kniskern, T.A. and Kuehl, S.A., 2003. Spatial and temporal variability of seabed disturbance in the York River subestuary. *Estuarine Coastal and Shelf Science* 58, 37-55.
- Lin, J., Kuo, A., 2003. A model study of turbidity maxima in the York River estuary, Virginia. *Estuaries and Coasts* 26, 1269-1280.
- Lin, J., Kuo, A., 2001. Secondary turbidity maximum in a partially mixed microtidal estuary. *Estuaries and Coasts* 24, 707-720.
- McNinch, J. E., 2004. Geologic control in the nearshore: shore-oblique sandbars and shoreline erosional hotspots, Mid-Atlantic Bight, USA. *Marine Geology*, 211(1), 121-141.
- Nichols, M. N., & Biggs, R. B., 1985. Estuaries: in RA Davis, (Ed.), *Coastal Sedimentary Environments*, Springer-Verlag, pp. 77-186.
- Nichols, M.M., S.C. Kim, and C.M. Brouwer, 1991. Sediment characterization of the Chesapeake Bay and its tributaries, Virginian Province. *National estuarine inventory: supplement*. NOAA.
- Nation Ocean Service (NOS). 1947. Hydrographic Sheet 7181: Aberdeen Creek and Vicinity, York River, Virginia. U.S. Department of Commerce, Washington, D.C.
- Postma, H., 1967. *Sediment transport and sedimentation in the estuarine environment*. American Association for the Advancement of Science Publication, 83.
- Pritchard, D. W., 1967. What is an estuary: physical viewpoint. *Estuaries*, 83, 3-5.
- Reay, W. G., & Moore, K. A., 2009. Introduction to the Chesapeake Bay National Estuarine Research Reserve in Virginia. *Journal of Coastal Research*, 1-9.
- Rinehimer, J.P. 2008. *Sediment Transport and Erodibility in the York River Estuary: A Model Study*. MS Thesis, School of Marine Science, College of William and Mary, Gloucester Point, VA.
- Roberts, W.P. and Pierce, J.W., 1976. Deposition in upper Patuxent River Estuary, Maryland, 1968-1969. *Estuarine and Coastal Marine Science* 4, 267-280.
- Rodríguez-Calderón, C., & Kuehl, S. A., 2012. Spatial and temporal patterns in erosion and deposition in the York River, Chesapeake Bay, VA. *Estuarine, Coastal and Shelf Science*.

- Romine, H.M., 2004. Documenting the suspended and bottom sediment dynamics of a two estuarine turbidity maximum system using ^7Be and ^{234}Th . M.S. thesis, Virginia Institute of Marine Science/School of Marine Science, The College of William and Mary, Virginia.
- Schaffner, L.C., Dellapenna, T.M., Hinchey, E., Friedrichs, C.T., Neubauer, M.T., Smith, M.E., Kuehl, S.A., 2001. Physical Energy Regimes, Seabed Dynamics, and organism–sediment Interactions Along an Estuarine Gradient, in: Aller, J.Y., Woodin, S.A., R.C. Aller, R.C. (Eds.), *Organism–Sediment Interactions*. University of South Carolina Press, Columbia, pp. 159-179.
- Scully, M. E., & Friedrichs, C. T., 2003. The influence of asymmetries in overlying stratification on near-bed turbulence and sediment suspension in a partially mixed estuary. *Ocean Dynamics*, 53(3), 208-219.
- Umbach, M. J., 1976. "Hydrographic manual: Fourth edition," U.S. Department of Commerce, Rockville, MD, 400 pp.
- USGS, 2013. USGS Water Data for the Nation. <http://waterdata.usgs.gov/nwis> (as of July 2013).
- VECOS, 2012. Virginia Estuarine and Coastal Observing System. <http://www3.vims.edu/vecos/Default.aspx> (as of July 2013).
- Whitehouse, R., 2000. *Dynamics of Estuarine Muds: A Manual for Practical Applications*. T. Telford, London.
- Winterwerp, J. C., & Van Kesteren, W. G., 2004. *Introduction to the physics of cohesive sediment dynamics in the marine environment*. Elsevier, London.
- Woodruff, J. D., Geyer, W. R., Sommerfield, C. K., & Driscoll, N. W. (2001). Seasonal variation of sediment deposition in the Hudson River estuary. *Marine Geology*, 179(1), 105-119.
- Wright, L.D., Schaffner, L.C., Maa, Y.P.Y., 1997. Biological mediation of bottom boundary layer processes and sediment suspension in the lower Chesapeake Bay. *Marine Geology* 141, 27-50.

York River Estuary, Chesapeake Bay VA, USA

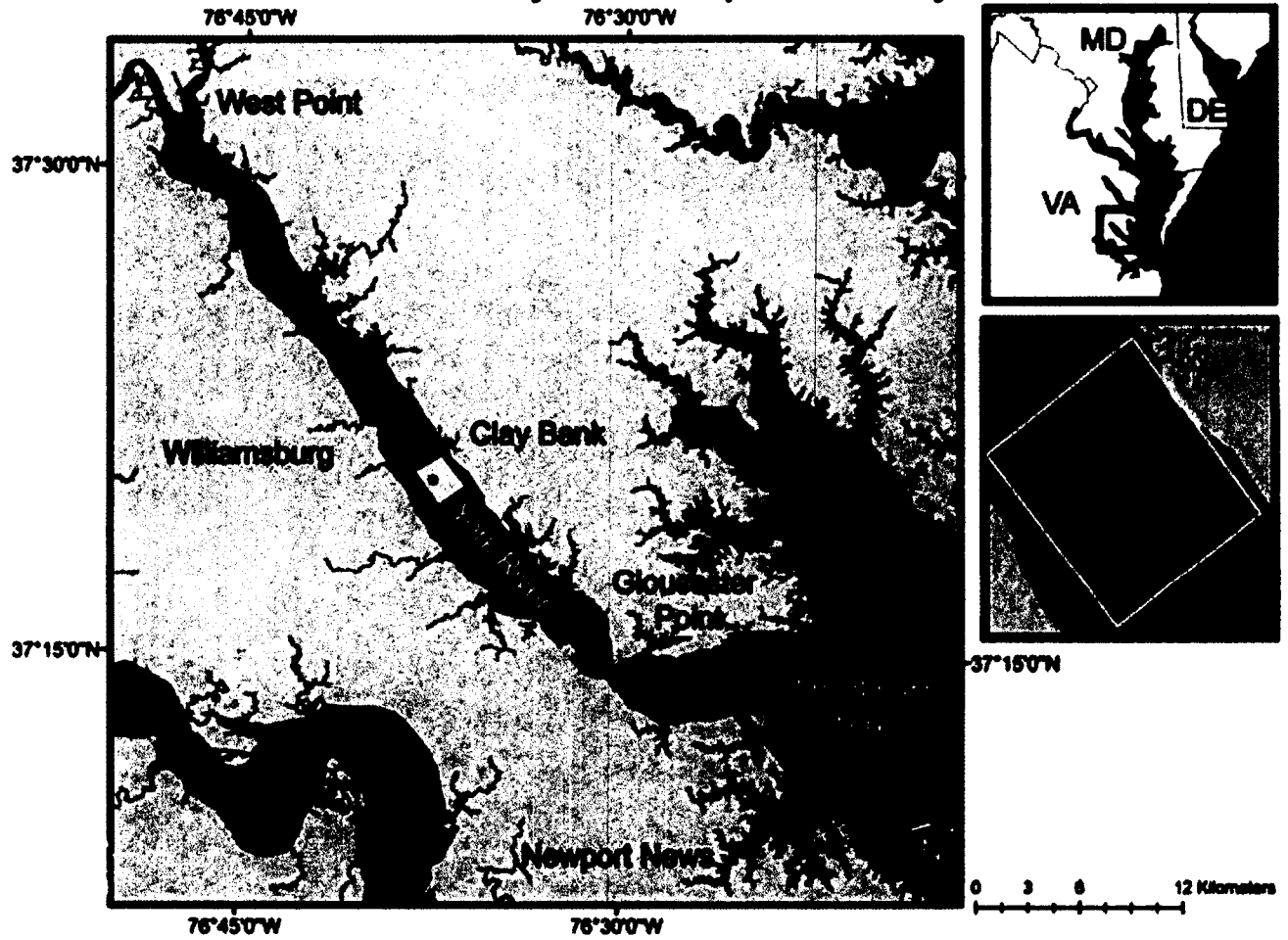
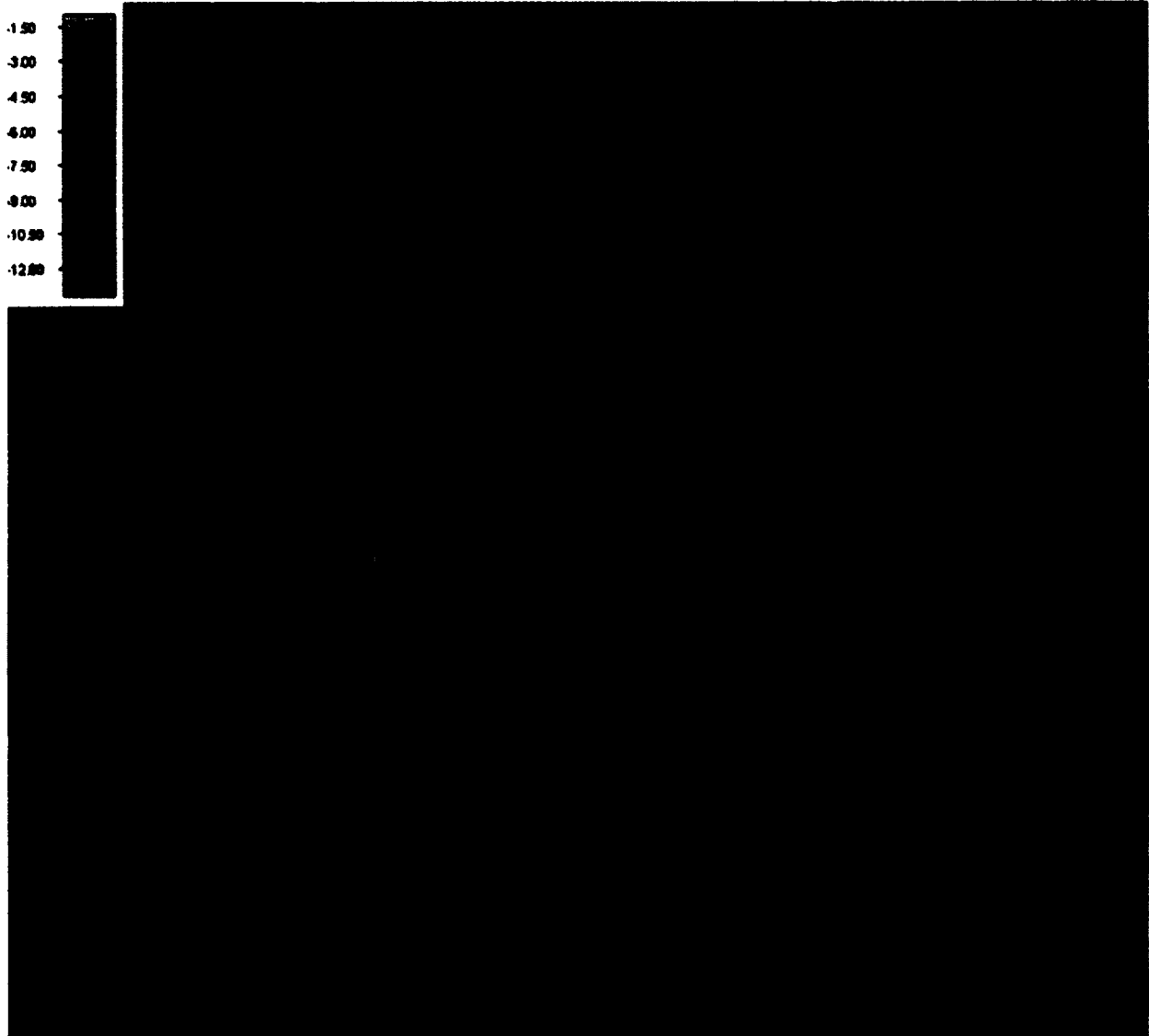


Figure 4-1. Map of the York River Estuary. Location of the Clay Bank high-resolution bathymetry surveys are indicated by the yellow box. The dot represents the VIMS Clay Bank Observing station and the red lines represent the survey lines repeated on each cruise.



0 800 m

Figure 4-2. Location of the VECOS monitoring station in relation to the 2008-2009 bathymetric surveys. The VIMS Clay Bank Piling and the MUDBED core locations are shown for data comparisons between studies.

Table 4-1. Cruise survey dates, day elapsed between sampling, and the tidal regime during the bathymetric surveys.

Bathymetric Survey Dates	Days between surveys	Tidal Regime
Septemeber 8 and 9, 2008		Neap tide one day before (9/7)
	100	
December 17, 2008		Neap tide two days later (12/19)
	28	
January 13, 2009		Spring tide three days earlier (1/10)
	23	
February 4, 2009		Neap tide two days earlier (2/2)
	106	
May 20, 2009		Neap tide three days earlier (5/17)
	36	
June 24, 2009		Spring tide two days earlier (6/22)
	58	
August 20, 2009		Full Spring tide

Table 4-2. Estimated mean speed of sound velocities for each survey based on the Coppen (1981) shallow depth equation as a function of temperature and salinity.

Survey	Speed of Sound Velocity (m/s)	Std. Dev
Sept. 8	1512	1.46
Sept. 9	1521	0.79
Dec	1463	1.47
Jan	1452	4.18
Feb	1438	3.52
May	1499	2.14
June	1515	1.84
Aug	1525	1.53

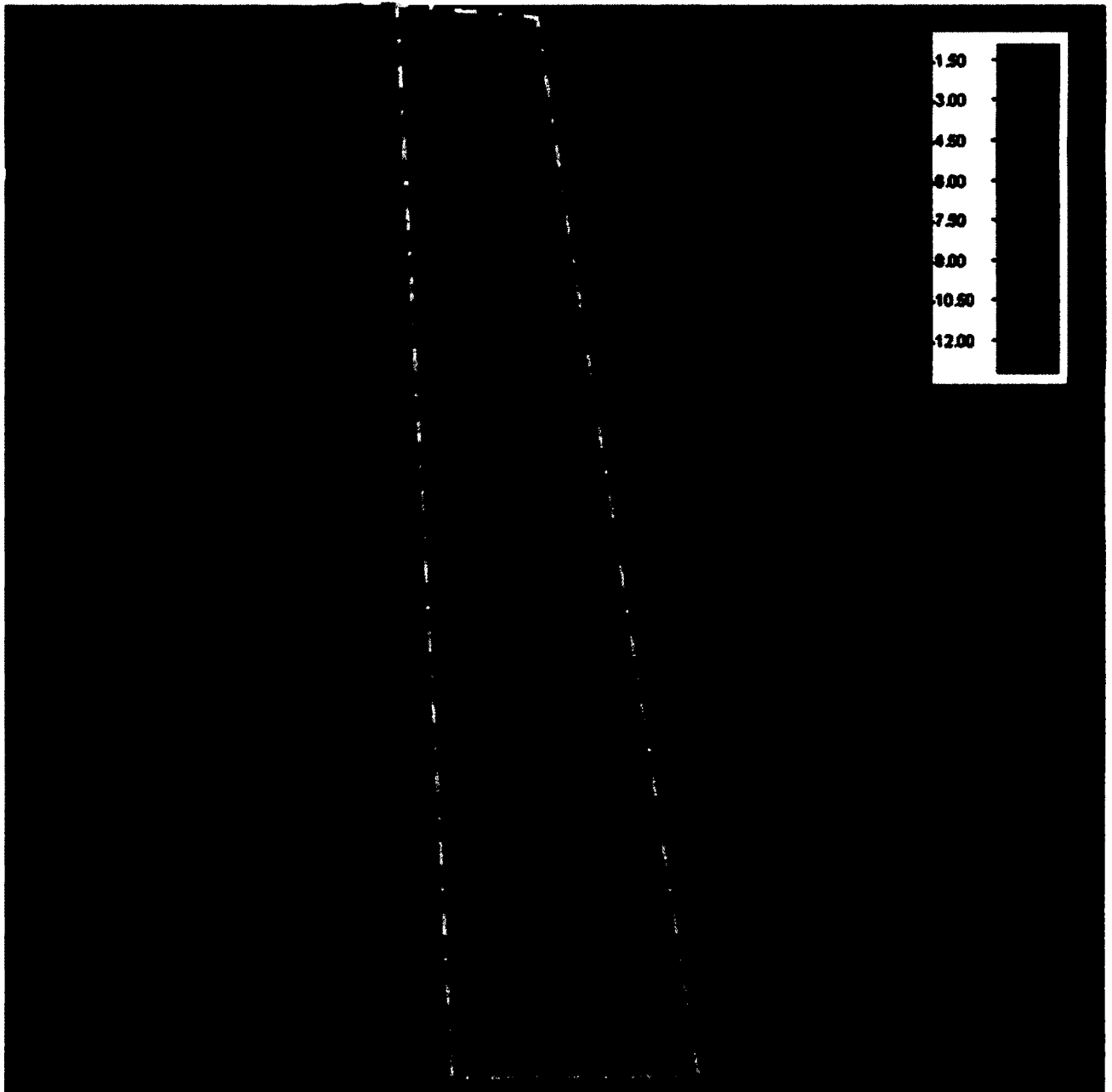


Figure 4-3 . A bathymetry plot generated from the interferometric system covers a 3.75km² section of the York River Estuary. This example is from the December 2008 cruise. For this study, the survey area was divided into three blocks based on bathymetry and the availability for quality ground control points. The main channel block is delineated by the purple dashed line and the secondary channel/shoal region is highlighted by the light-blue dashed line. Between the main channel and secondary channel no reliable ground control points could be found, and therefore the region in white is not further analyzed within this study.

Table 4-3. Seabed elevation for ground control points, along with calculated bathymetric change between surveys before the control points were used to shift the bathymetry. The December survey was used as the baseline bed elevation for this study. The overall average bathymetric change value between cruises was then used as the shift variable to align seabed elevations with the December survey.

Control Points			Depth							Bathymetric Change from December Survey					
Secondary Channel and Shoal															
x	y	Pt.	Sept	Dec	Jan	Feb	May	June	Aug	Sept-Dec Change	Dec-Jan Change	Dec-Feb Change	Dec-May	Dec-June	Dec-Aug
355888.3	4134371.7	1	2.94	3.05	3.29	2.8	3.12	3.42	3.09	0.11	-0.24	0.25	-0.07	-0.37	-0.04
356021.6	4134236.0	2	3.41	3.45	3.97	3.27	3.35	3.83	3.55	0.04	-0.52	0.18	0.1	-0.38	-0.1
355880.1	4134525.8	3	3.17	3.3	3.64	2.9	3.09	3.28	3.36	0.13	-0.34	0.4	0.21	0.02	-0.06
356329.1	4133957.3	4	2.71	2.75	3.04	2.46	2.72	2.8	2.79	0.04	-0.29	0.29	0.03	-0.05	-0.04
355883.5	4134404.3	5	3.09	3.12	3.56	2.96	3.19	3.66	3.41	0.03	-0.44	0.16	-0.07	-0.54	-0.29
356114.2	4134252.8	6	3.05	2.99	3.32	2.75	2.84	3.09	3.04	-0.06	-0.33	0.24	0.15	-0.1	-0.05
355891.3	4134368.4	7	2.99	3.09	3.38	2.85	3.16	3.58	3.31	0.1	-0.29	0.24	-0.07	-0.49	-0.22
Average										0.06	-0.35	0.25	0.04	-0.27	-0.11
Std. Dev.										0.06	0.10	0.08	0.12	0.23	0.10
Main Channel															
x	y	Pt.	Sept	Dec	Jan	Feb	May	June	Aug	Sept-Dec Change	Dec-Jan Change	Dec-Feb Change	Dec-May	Dec-June	Dec-Aug
356578.8	4135138.8	8	8.42	8.33	8.73	8.41	8.46	8.56	8.71	-0.09	-0.4	-0.08	-0.13	-0.23	-0.38
356470.3	4134812.0	9	4.52	4.61	5.05	4.28	4.68	4.64	4.27	0.09	-0.44	0.33	-0.07	-0.03	0.34
357499.1	4133899.9	10	6.71	6.54	6.72	6.42	6.38	6.99	6.95	-0.17	-0.18	0.12	0.16	-0.45	-0.41
357167.3	4133921.2	11	4.39	4.47	4.92	4.09	4.67	4.89	4.5	0.08	-0.45	0.38	-0.2	-0.42	-0.03
356692.7	4135062.4	12	7.87	7.79	8.09	6.96	7.61	7.47	7.54	-0.08	-0.3	0.83	0.18	0.32	0.25
Average										-0.03	-0.35	0.32	-0.01	-0.16	-0.05
Std. Dev.										0.11	0.11	0.34	0.17	0.32	0.35
Overall Average										0.02	-0.35	0.28	0.02	-0.23	-0.09
Standard Dev.										0.10	0.10	0.22	0.14	0.26	0.22

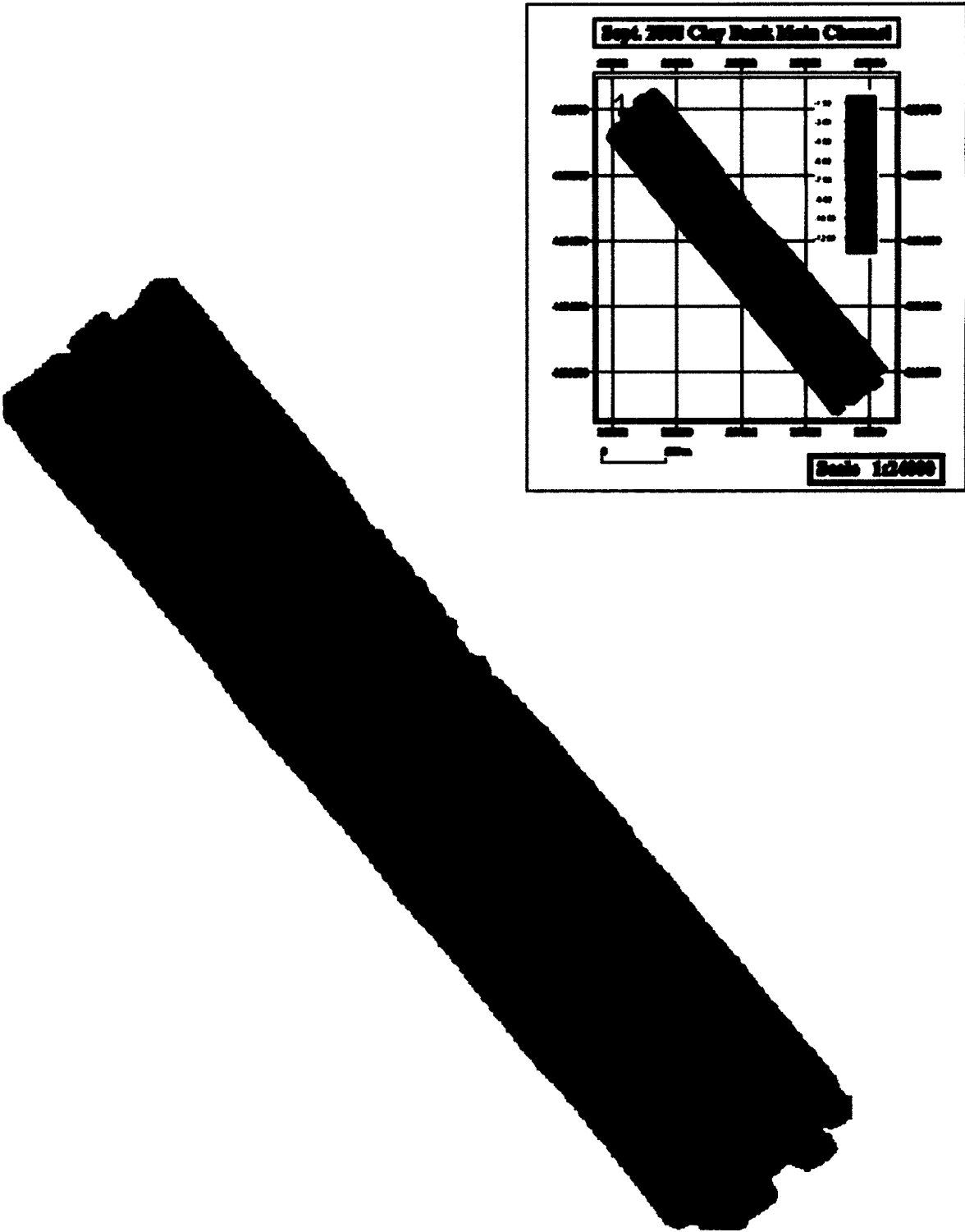


Figure 4-4. Location map of ground control points (red circles) selected in Section 1 of the study area. This region is consists of the main channel, southeast flank, and shoal.

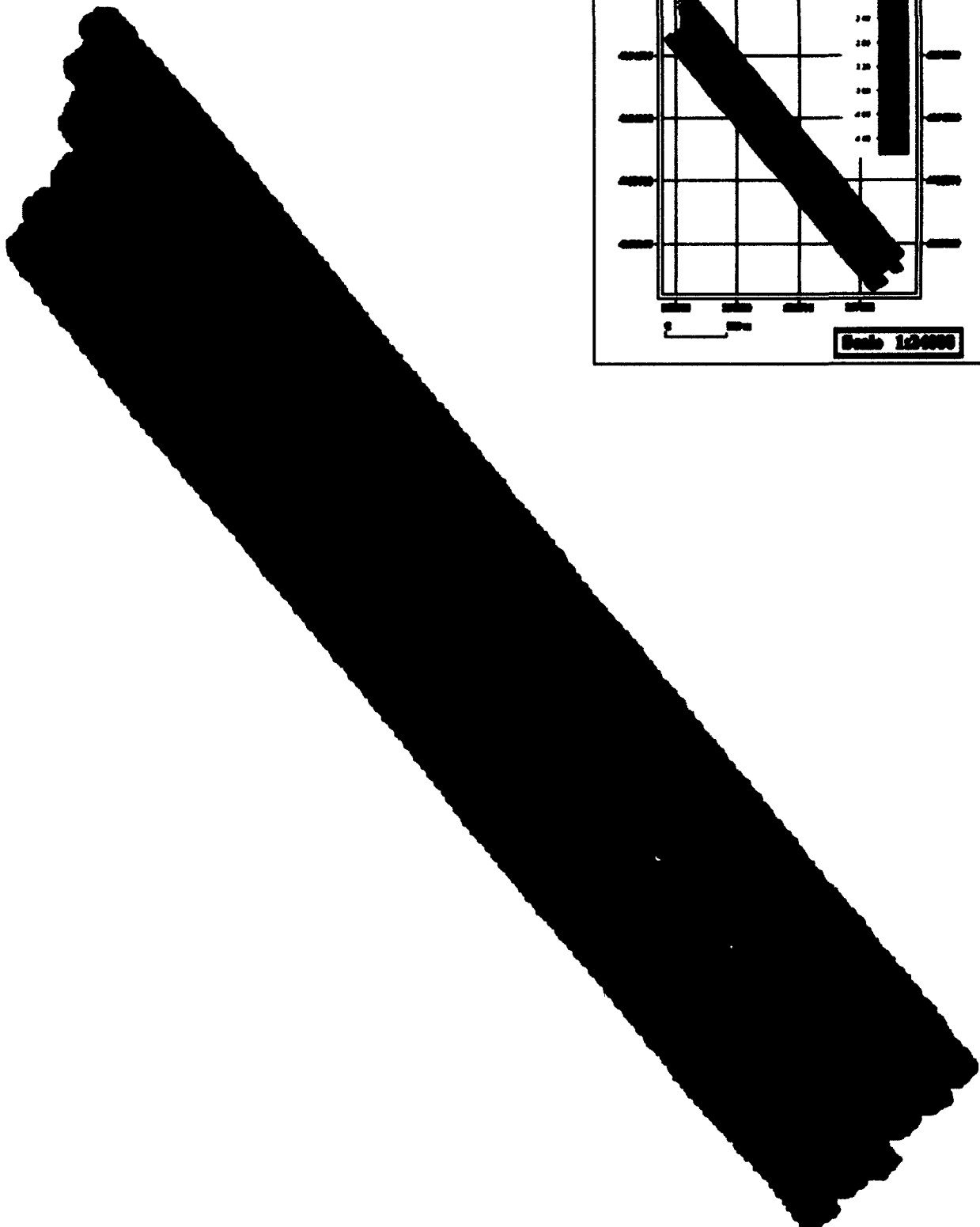


Figure 4-5. Location map of ground control points (red circles) selected in Section 3 of the study area. This region consists of the secondary channel and shoal.

Table 4-4. Potential errors and uncertainties associated with bathymetric surveying (Modified from Umbach, 1976 and Byrnes et al., 2002).

Horizontal Positioning	Vertical Positioning
<p>Station Control</p> <ul style="list-style-type: none"> • Incorrect geodetic datum • Use of unaadjusted or incorrect geodetic positions • Misidentification of control stations • Incorrectly plotted control • Loss of RTK signal • Base station movement (pier settling, human movement, etc.) 	<p>Tidal and water level observations</p> <ul style="list-style-type: none"> • Incorrect water depth measurements collected with YSI 6600 data sondes with the Clean Sweep Extended Deployment System • Data gaps between YSI data collection of 15-minute intervals • Undetected tide or water level anomalies caused by meteorological conditions • Improper correction for barometric pressure • Distance of survey for tidal gauge location • Vessel positioning shift throughout the survey
<p>Vessel Control</p> <ul style="list-style-type: none"> • Improper use of calibration or field check data • Undetected errors of jumps in distance • Electronic interferences with the position system • Use of improper operative frequencies • Failure to reduce electronic center of the ship to transducer location • Fluctuation of vessel speed throughout each survey 	<p>Transducer errors</p> <ul style="list-style-type: none"> • Incorrectly measurement of transducer to RTK-GPS, motion sensor, and data collection computer • Electronic interferences with the swath bathymetry transducers • Improper estimation of speed of sound variation profiles • Angle and depth errors • Additive external noise
	<p>Depth recorder errors</p> <ul style="list-style-type: none"> • Incorrect threshold receiving frequency • Incorrect calibration • Scaling errors • Improperly accounted heave
Errors effecting Horizontal and Vertical Positioning	
<ul style="list-style-type: none"> • Measurement method • Sea State • Meteorological Conditions • Water temperature and salinity • Transducer beam width • Bottom sediment type and surface irregularity • Vessel heave, pitch, and roll • Survey line overlap • Inter-instrument connectivity • Human error 	

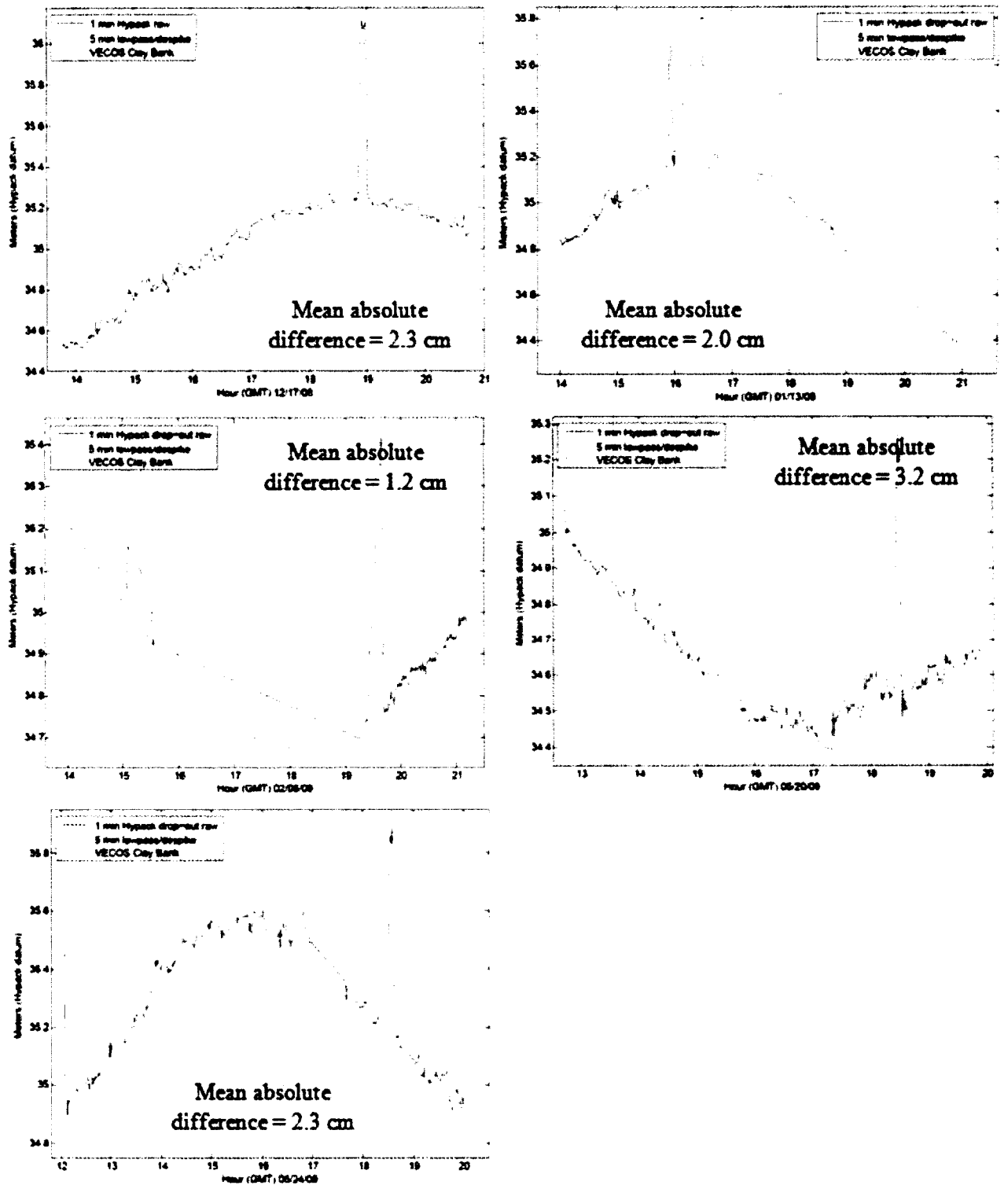


Figure 4-6. Comparison analysis to assess the consistency between the VECOS tide gauge data and water height elevation captured in real-time during the surveys with Hypack. The mean absolute difference between the VECOS and despiked/low-passed filtered data for the 5 surveys averaged 2.2 centimeters. Values for each month are found within their respective sub-plots. Note that the analysis for the February comparison was for only the last 1.5 hours of the cruise.

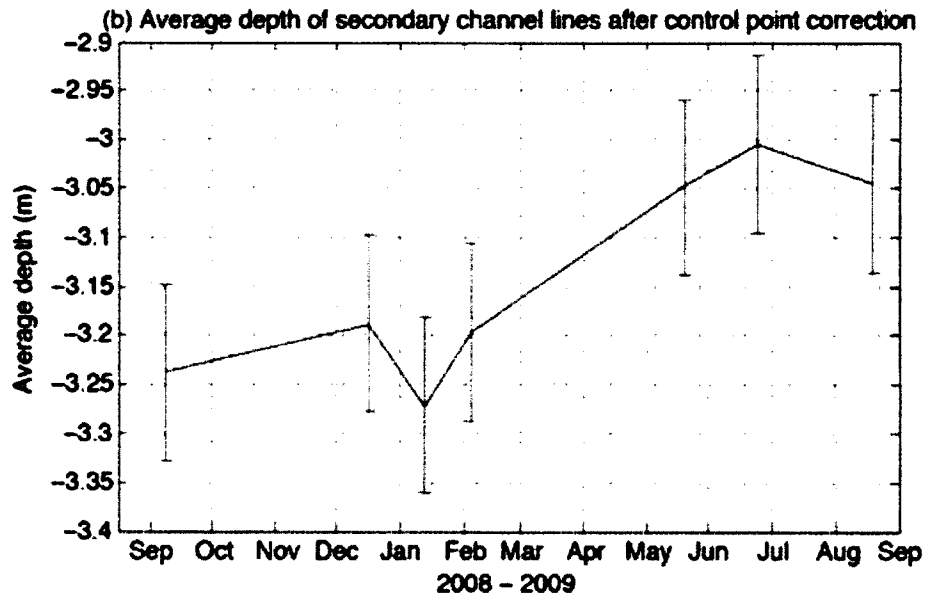
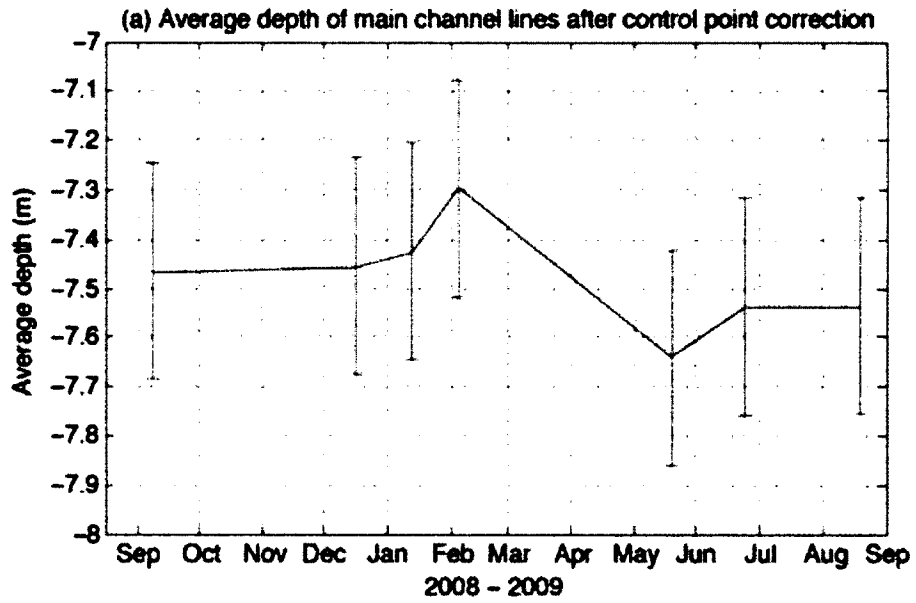
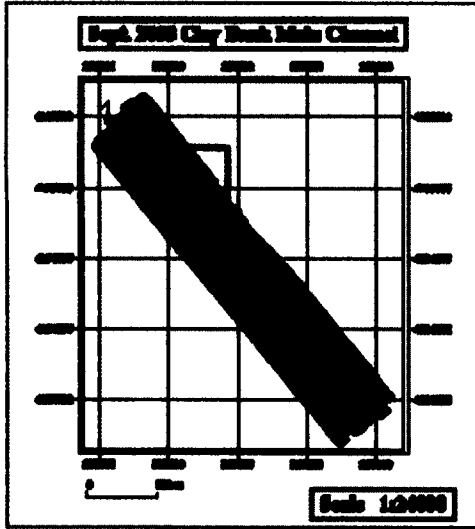
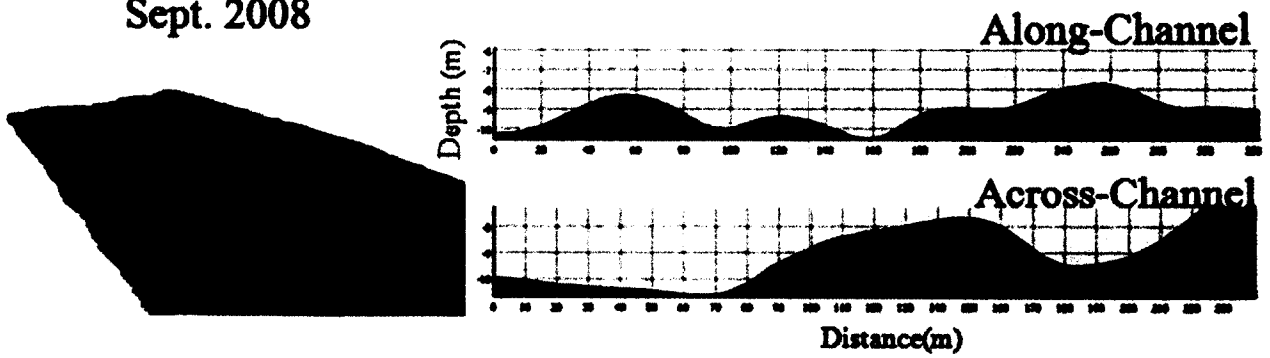


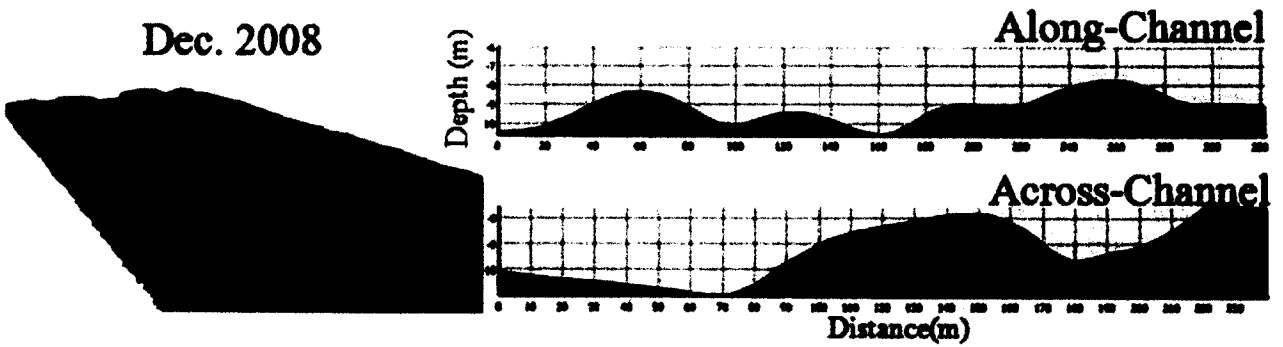
Figure 4-7. Time-series of mean seabed elevation of the (a) main channel and (b) secondary channel. Error bars indicate 95% confidence intervals.



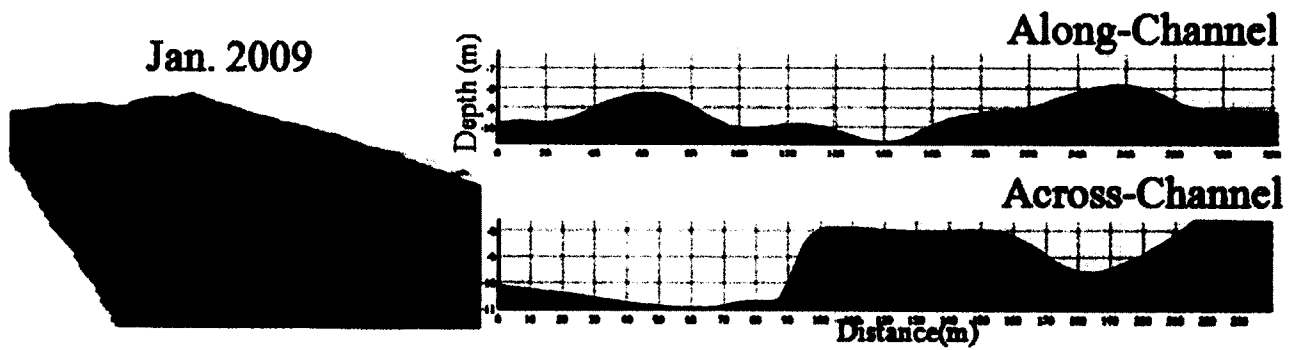
Sept. 2008



Dec. 2008



Jan. 2009



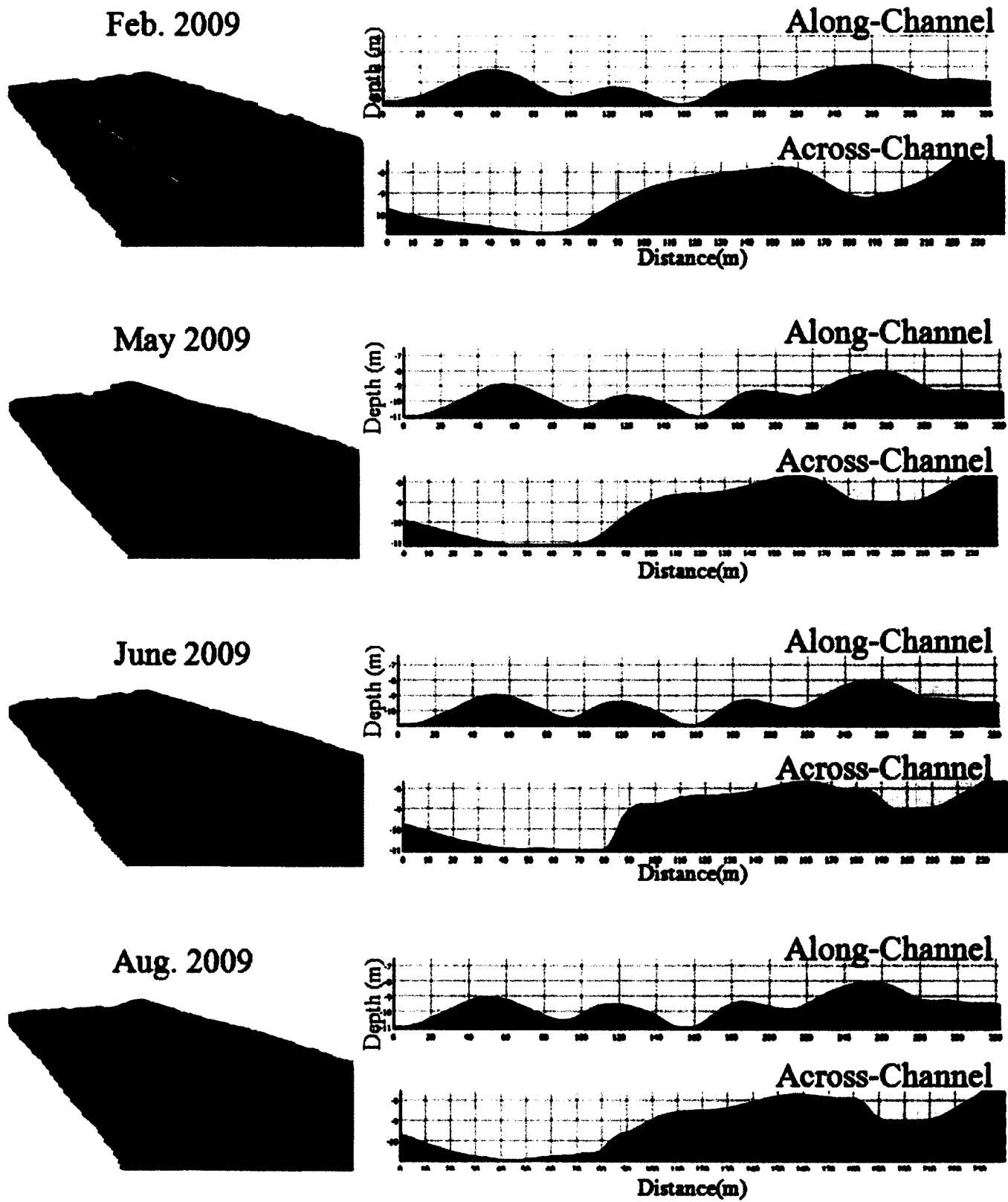
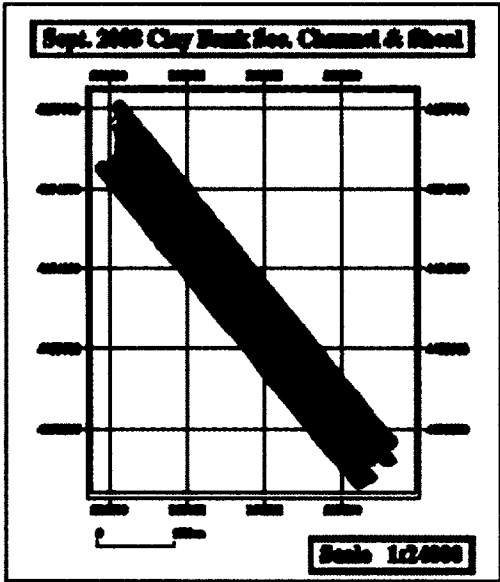
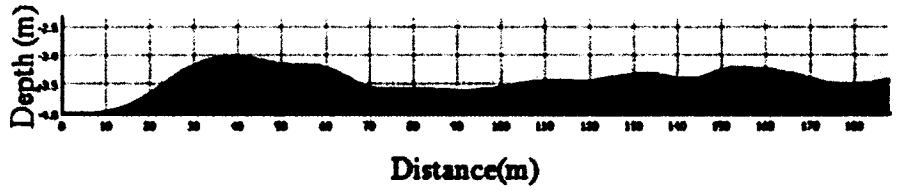


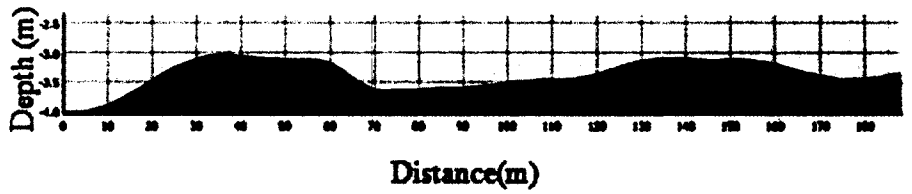
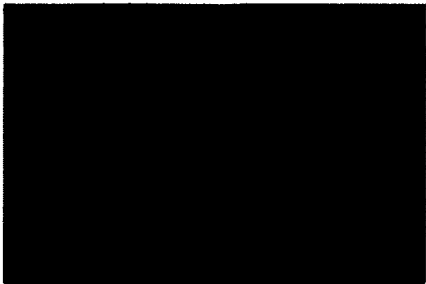
Figure 4-8. Time-series of transect analyses of the Clay Bank main channel sub-section.



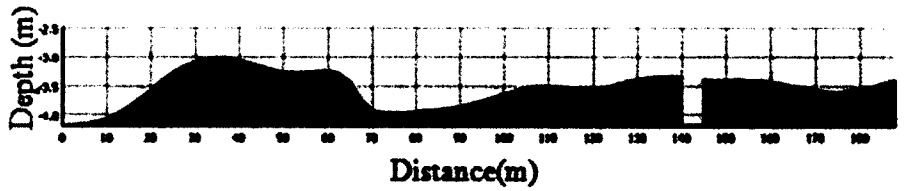
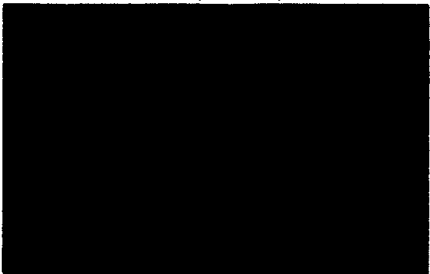
Sept. 2008



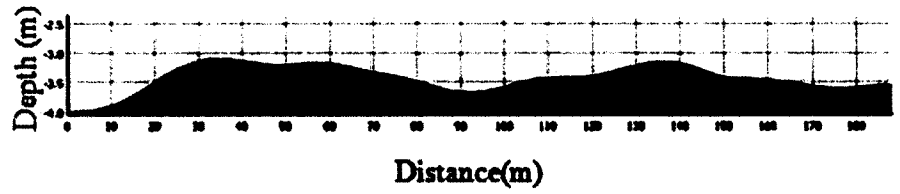
Dec. 2008



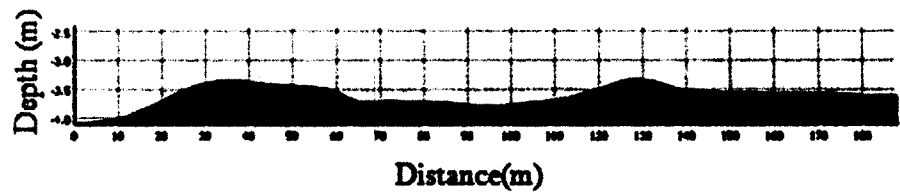
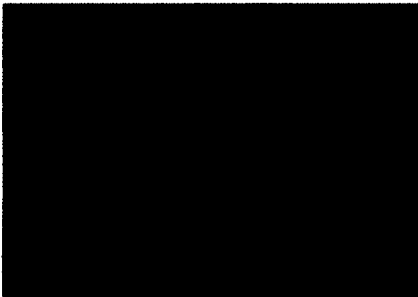
Jan. 2009



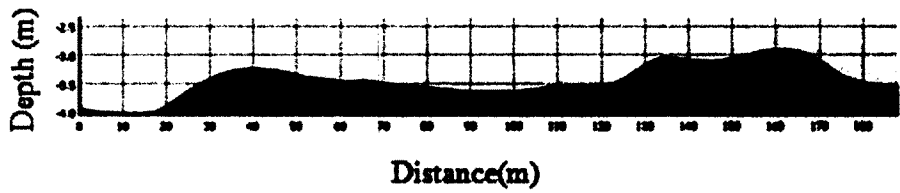
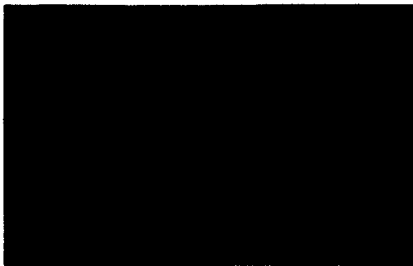
Feb. 2009



May 2009



June 2009



Aug. 2009

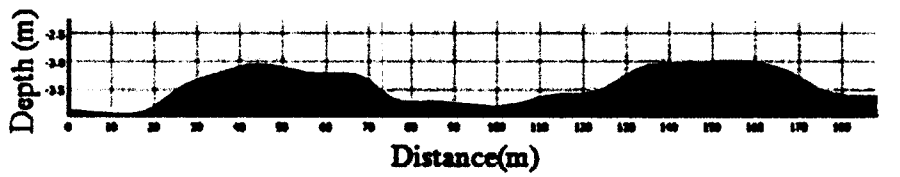
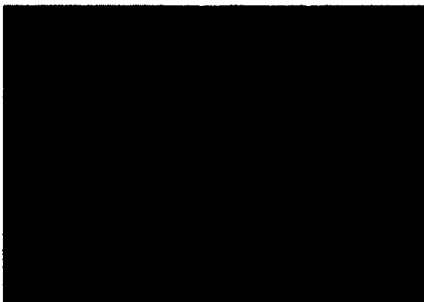


Figure 4-9. Time-series of transect analyses of the Clay Bank secondary channel sub-section.

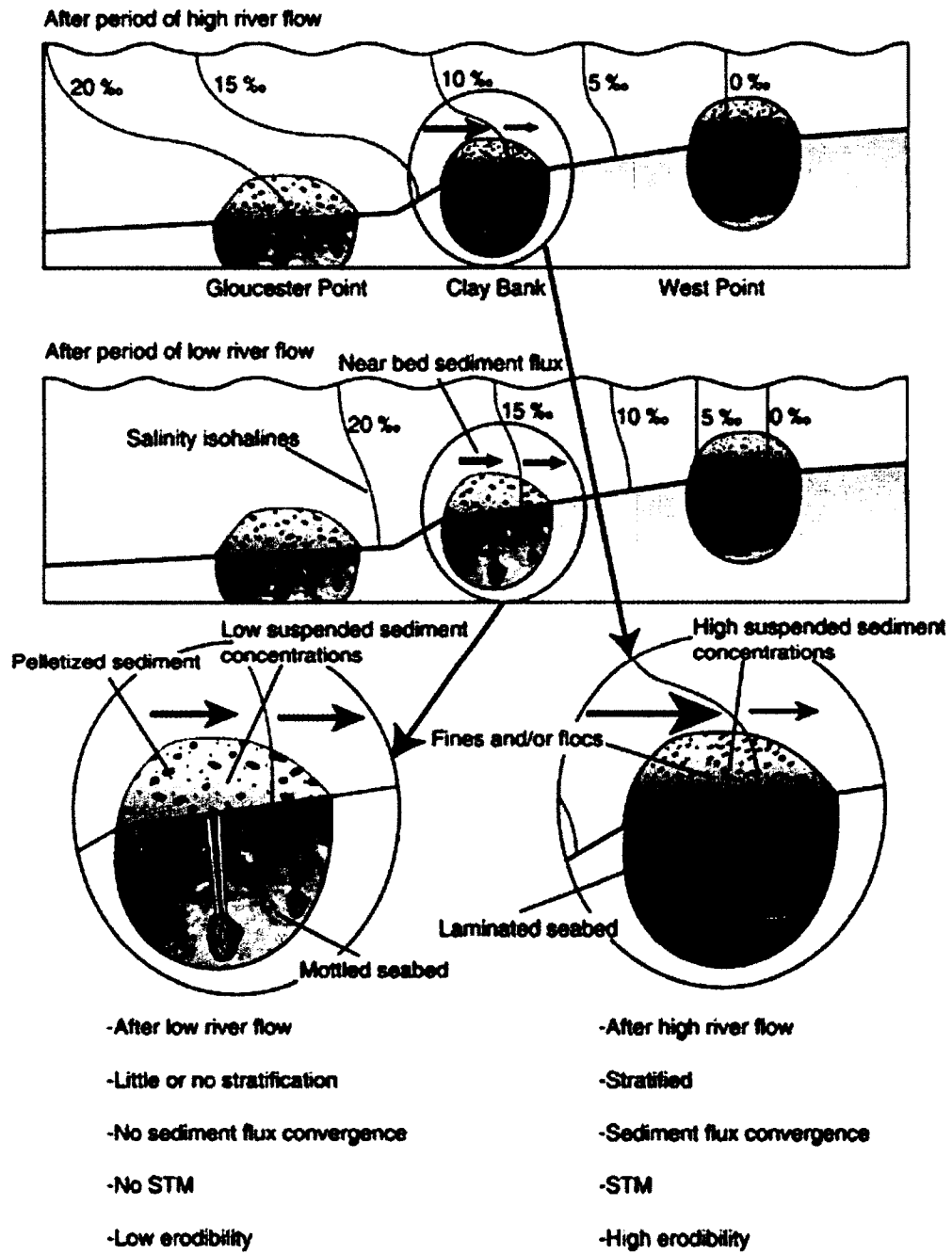


Figure 4-10. Dickhudt et al. (2009) conceptual diagram depicting sediment transport processes in the York River Estuary.

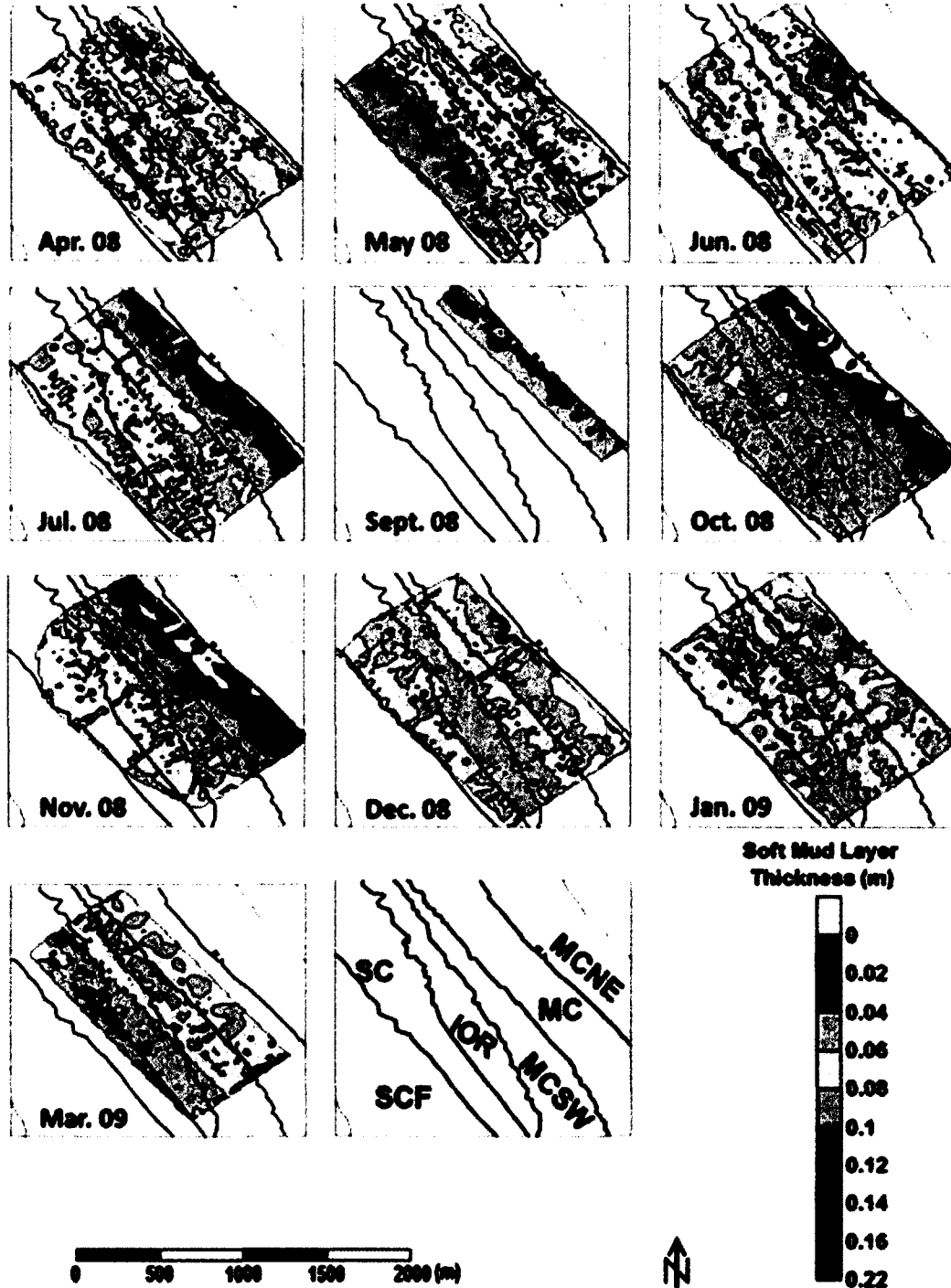


Figure 4-11. April 2008 through March 2009 soft mud layer thickness contour maps for Clay Bank captured using a dual-channel echosounder (from Rodriguez-Calderon and Kuehl, 2012). The last panel identifies the location of each of the channel sub-environments: main channel NE flank (MCNE), main channel (MC), main channel SW flank (MCSW), inactive oyster reef (IOR), secondary channel (SC), secondary channel flank (SCF).

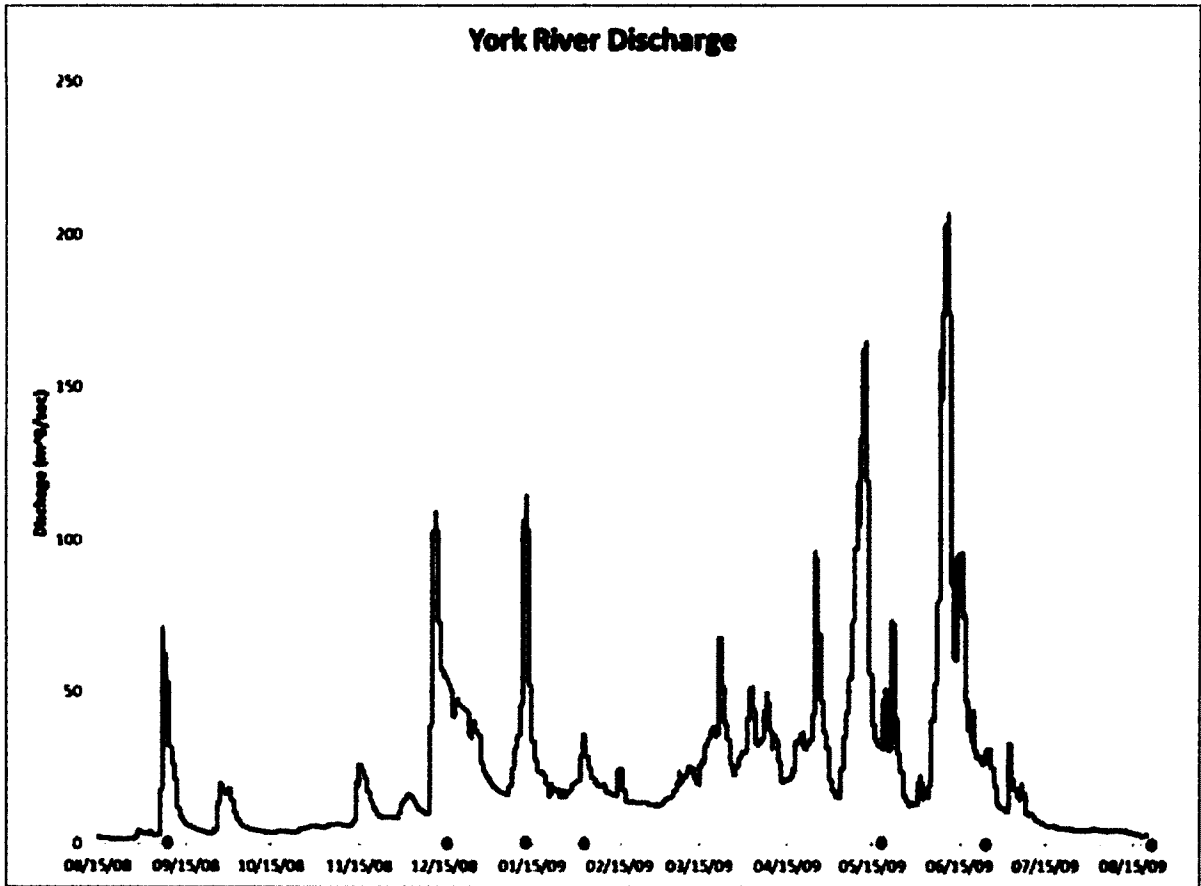


Figure 4-12. USGS riverine discharge data for the Mattaponi plus Pamunkey Rivers between September 2008 and August 2009 (USGS, 2009: <http://waterdata.usgs.gov/nwis>).

Bathymetric Map of Clay Bank ~ 1947

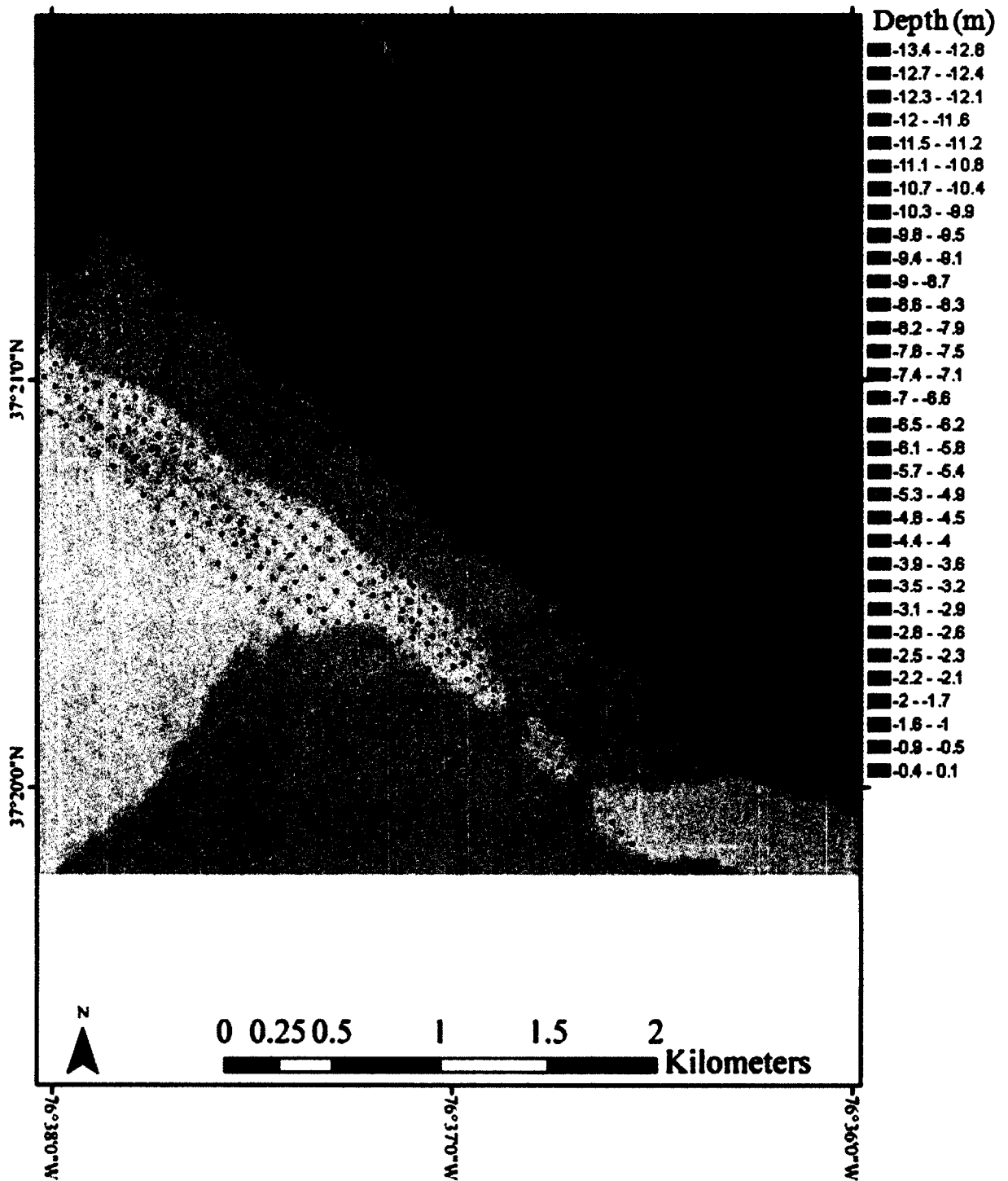


Figure 4-13. Bathymetric map of NOAA Digital Echo Sounder Data collected in 1947 (Survey H07181). Data was corrected for actual sound velocity and reprojected from NAD27 to NAD83, maintaining MLW as the vertical datum. Original sound positions are delineated by the circles. The bathymetric raster was interpolated using the kriging method. The slump mounds within the main channel, used for the postage stamp analysis, are highlighted by the red circle.

Bathymetric Map of Clay Bank ~ Dec. 2008

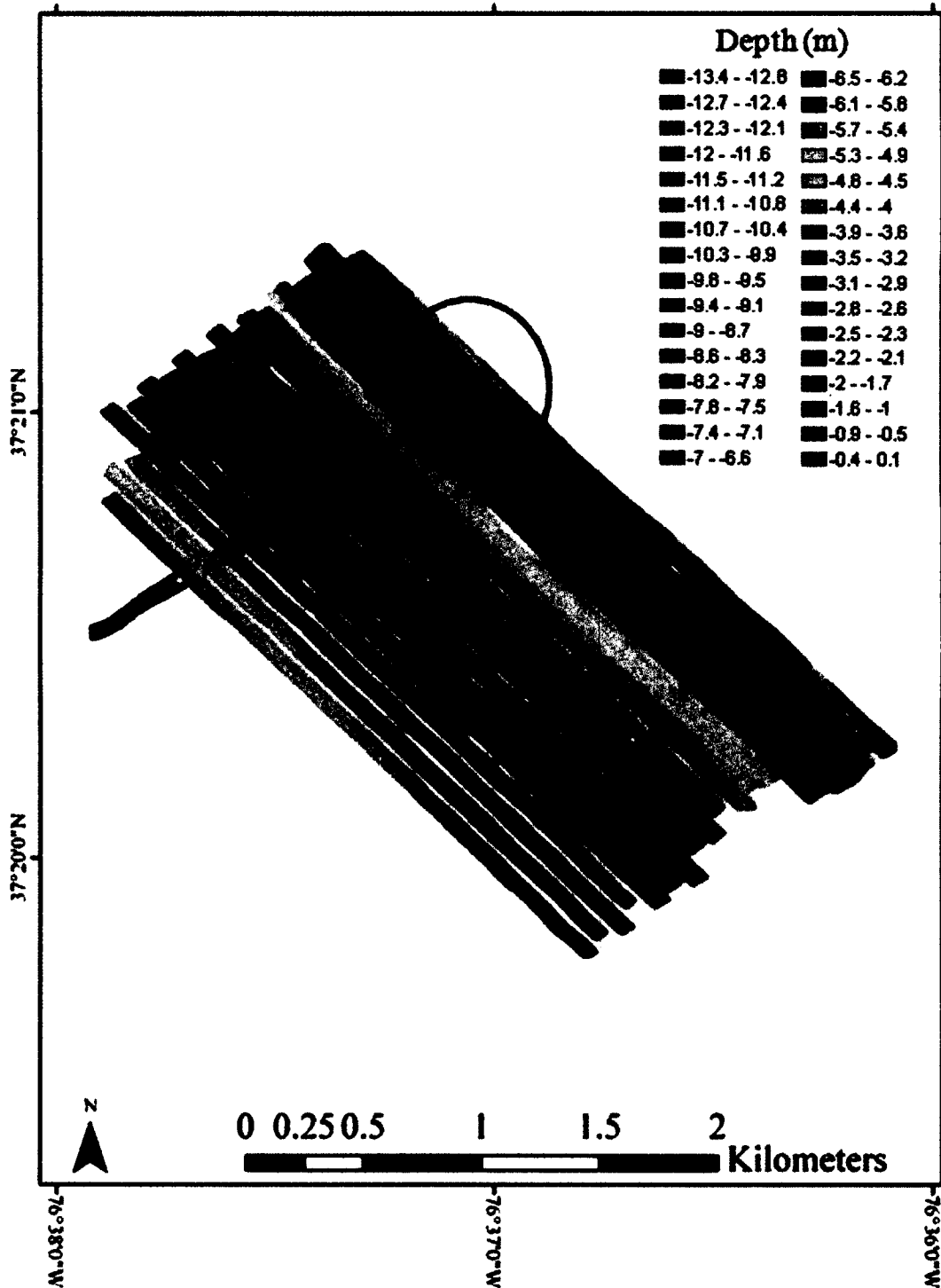
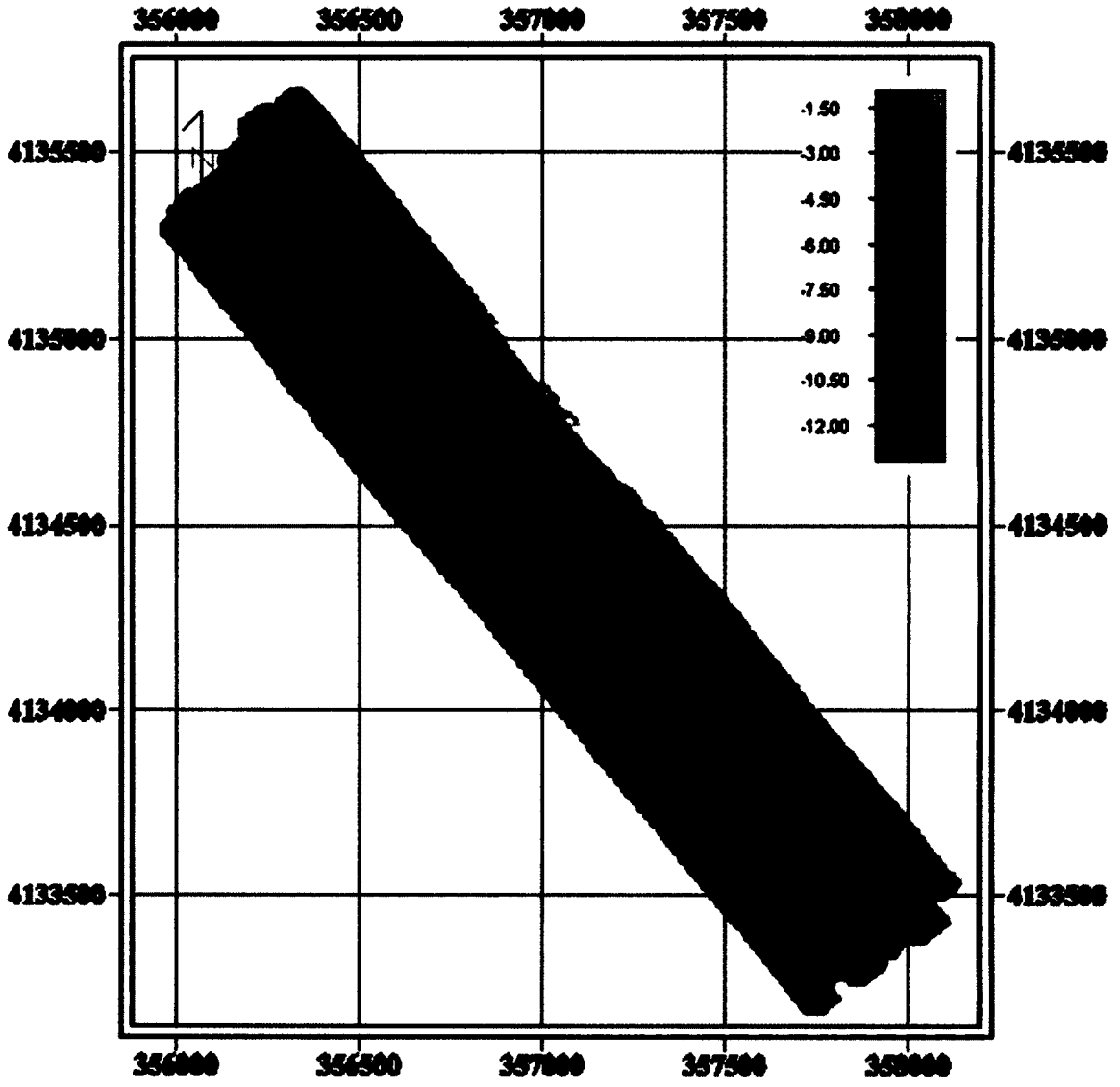


Figure 4-14. Bathymetric map of the Clay Bank region in December of 2008 used for comparison of the historic NOAA data. The slump mounds within the main channel, used for the postage stamp analysis, are highlighted by the red circle.

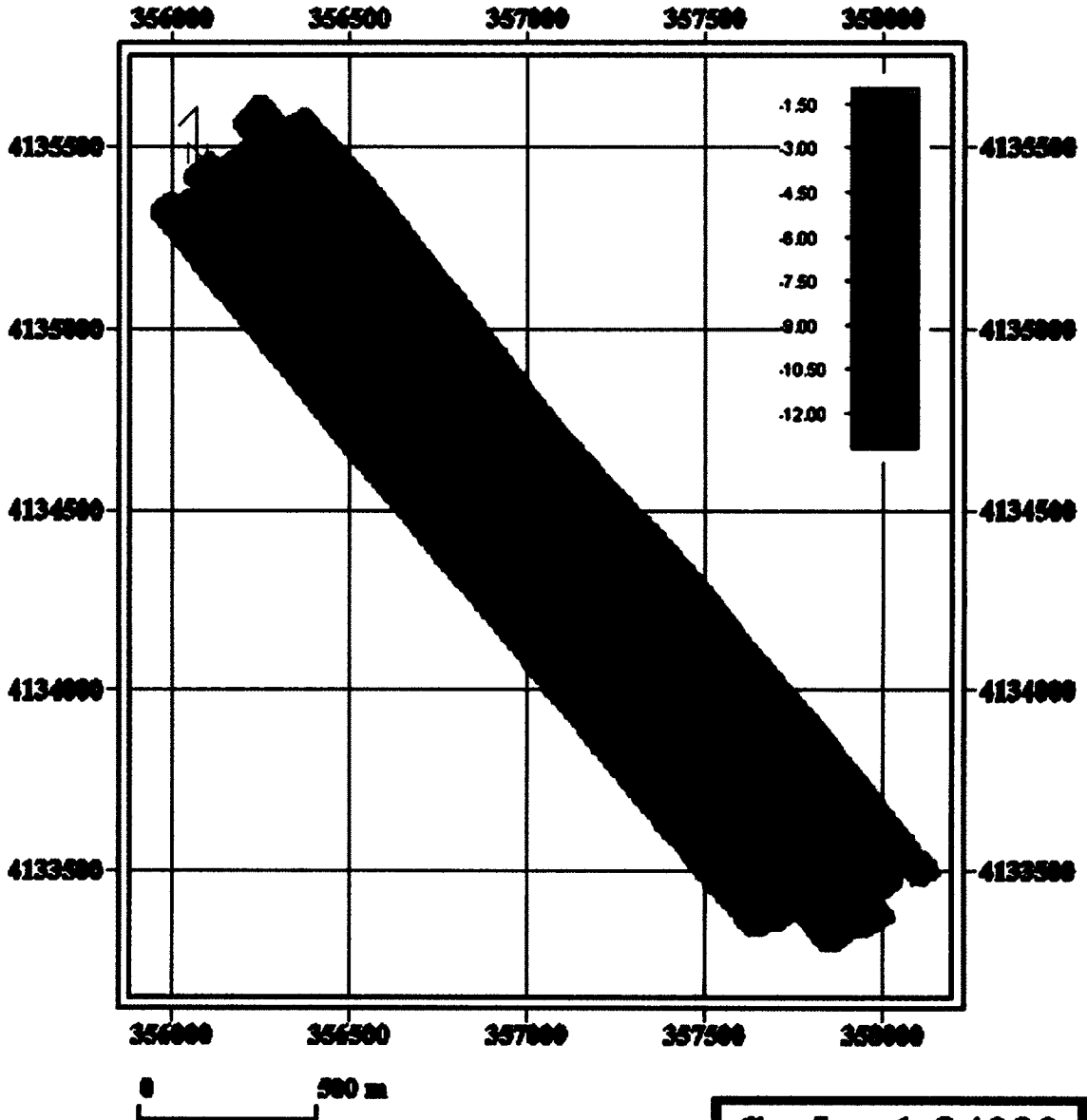
Appendix II: Monthly bathymetric maps for the Clay Bank main channel for seven months between 2008 and 2009, corrected for datum shift.

Sept. 2008 Clay Bank Main Channel

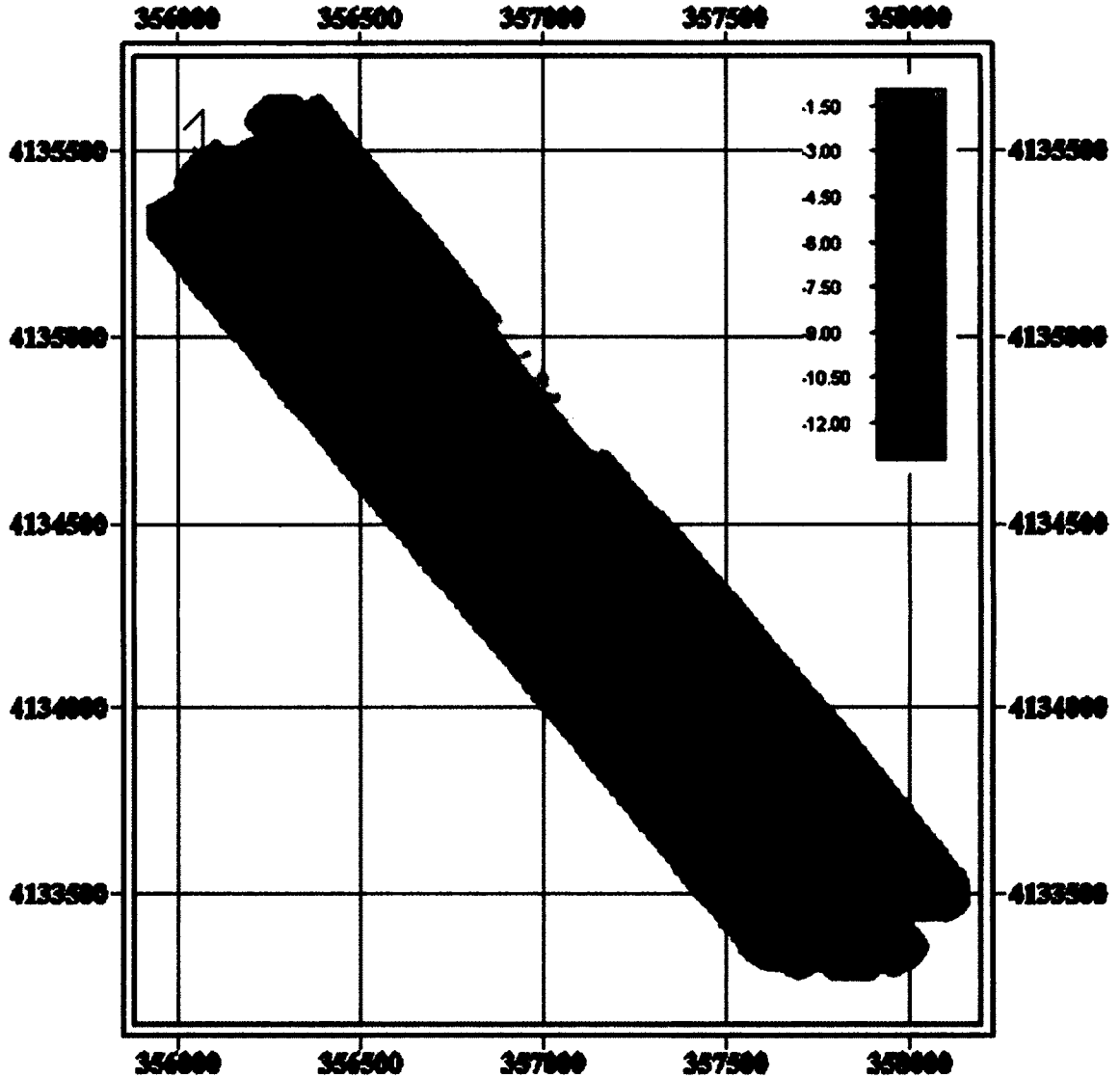


Scale 1:24000

Dec. 2008 Clay Bank Main Channel

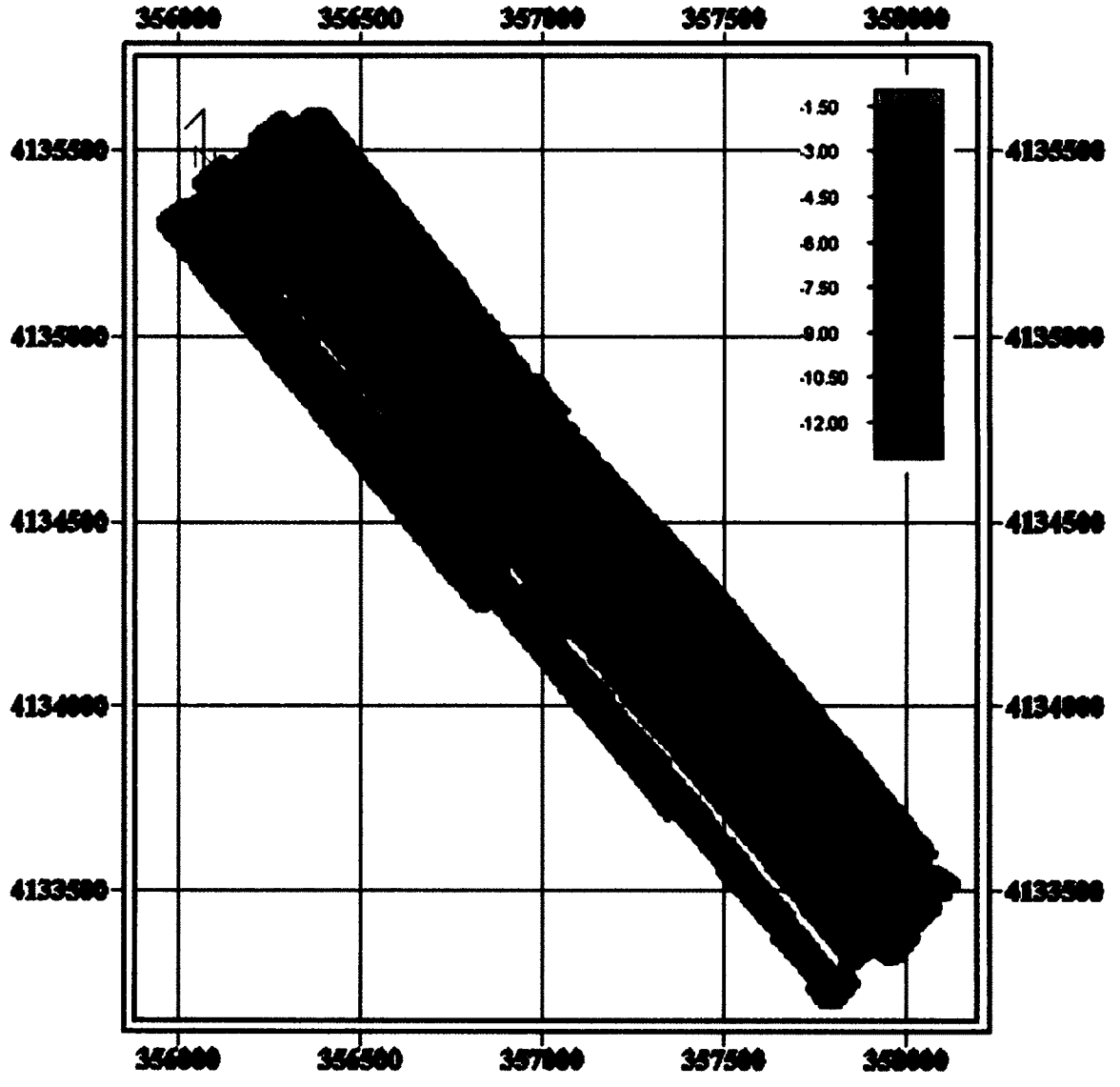


Jan. 2009 Clay Bank Main Channel



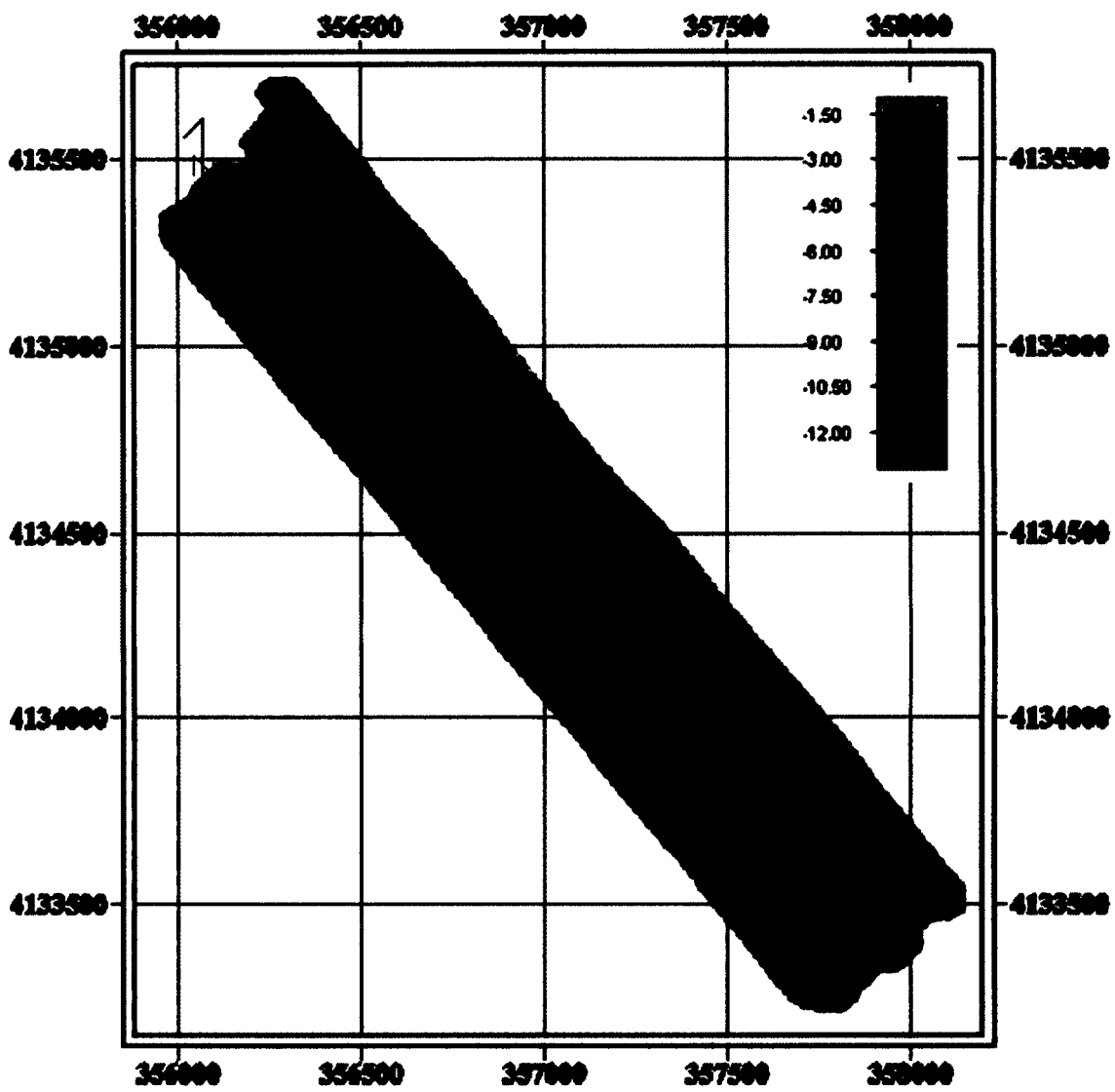
Scale 1:24000

Feb. 2009 Clay Bank Main Channel



Scale 1:24000

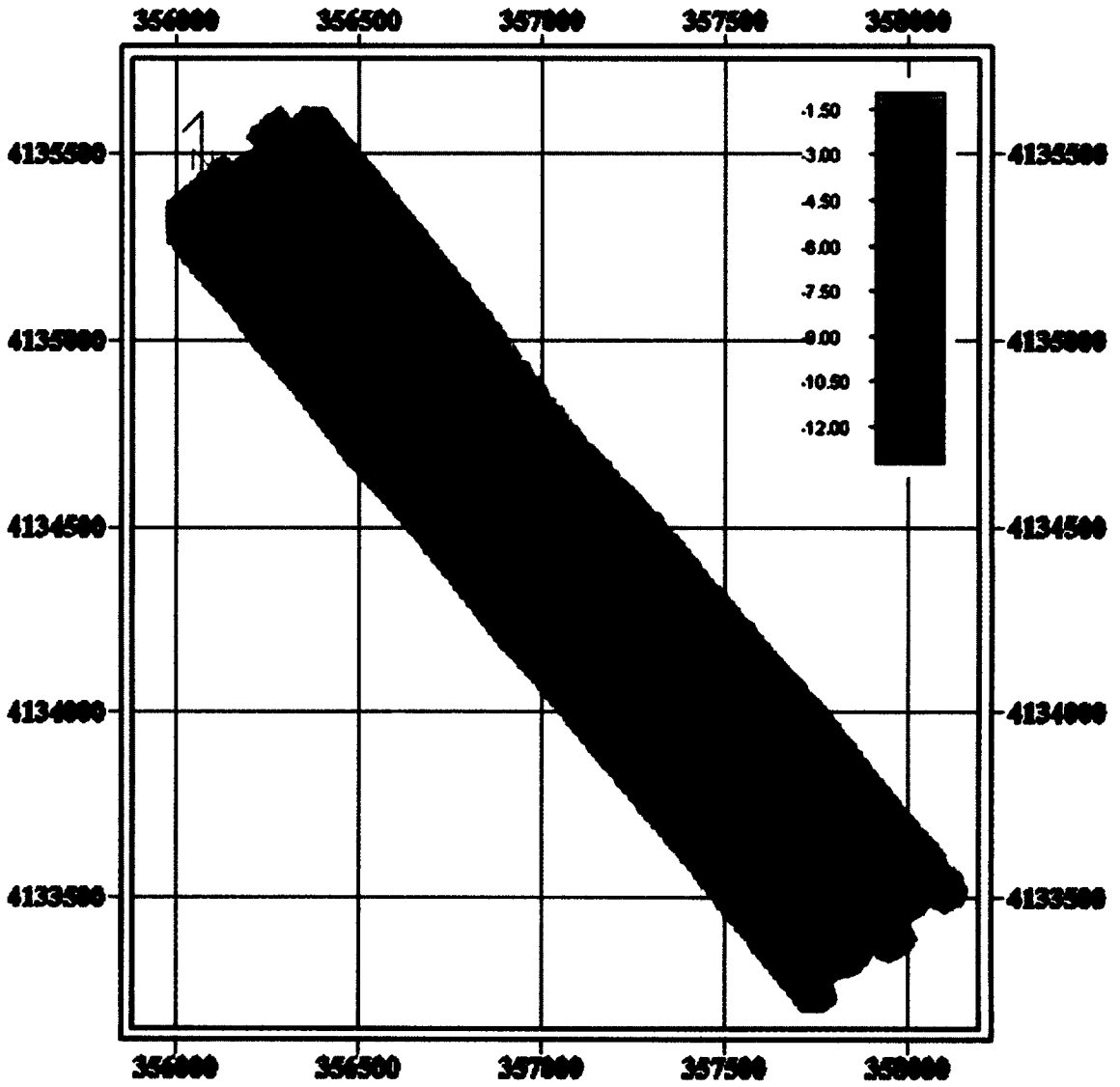
May 2009 Clay Bank Main Channel



0 500 m

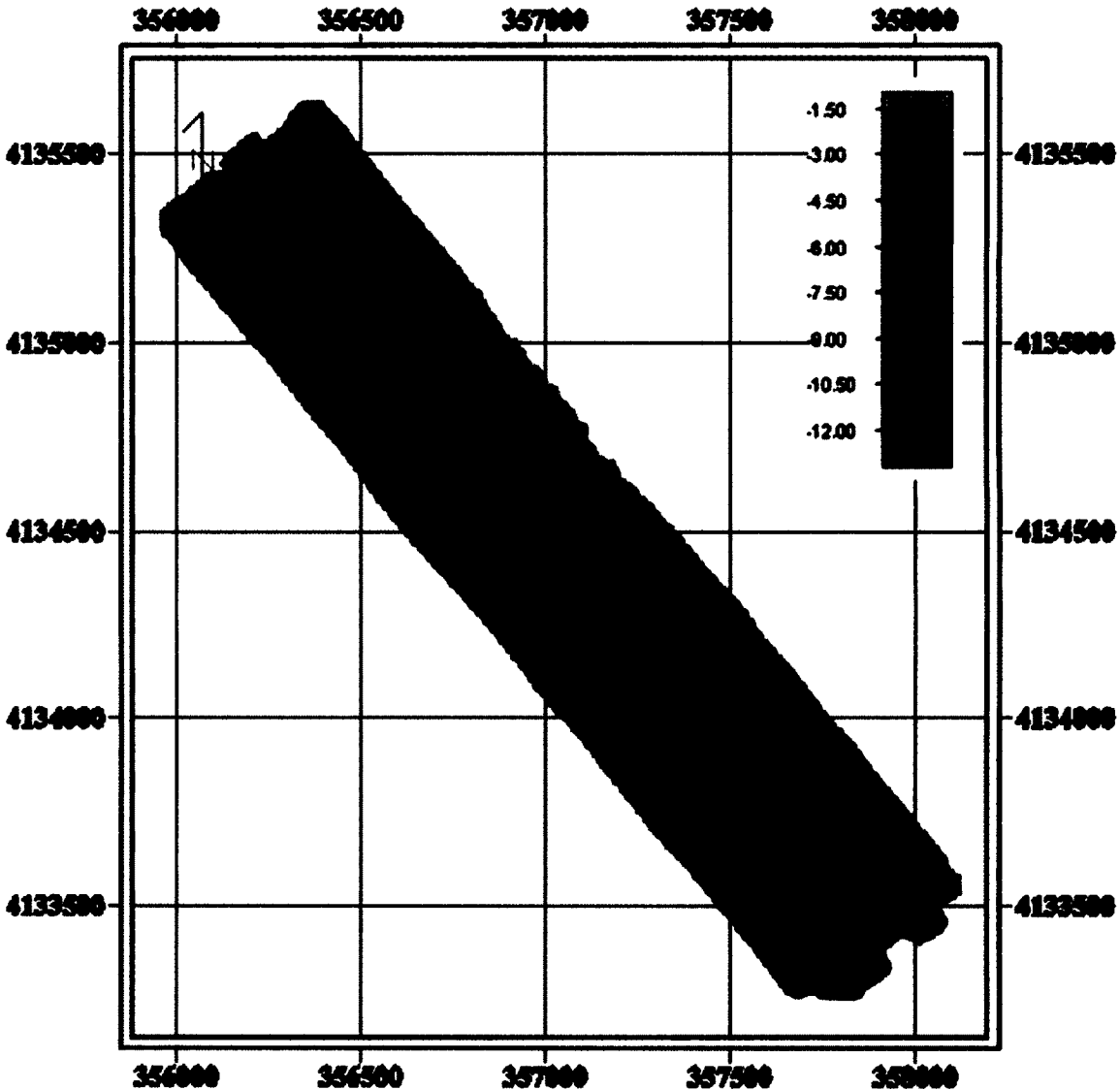
Scale 1:24000

June 2009 Clay Bank Main Channel



Scale 1:24000

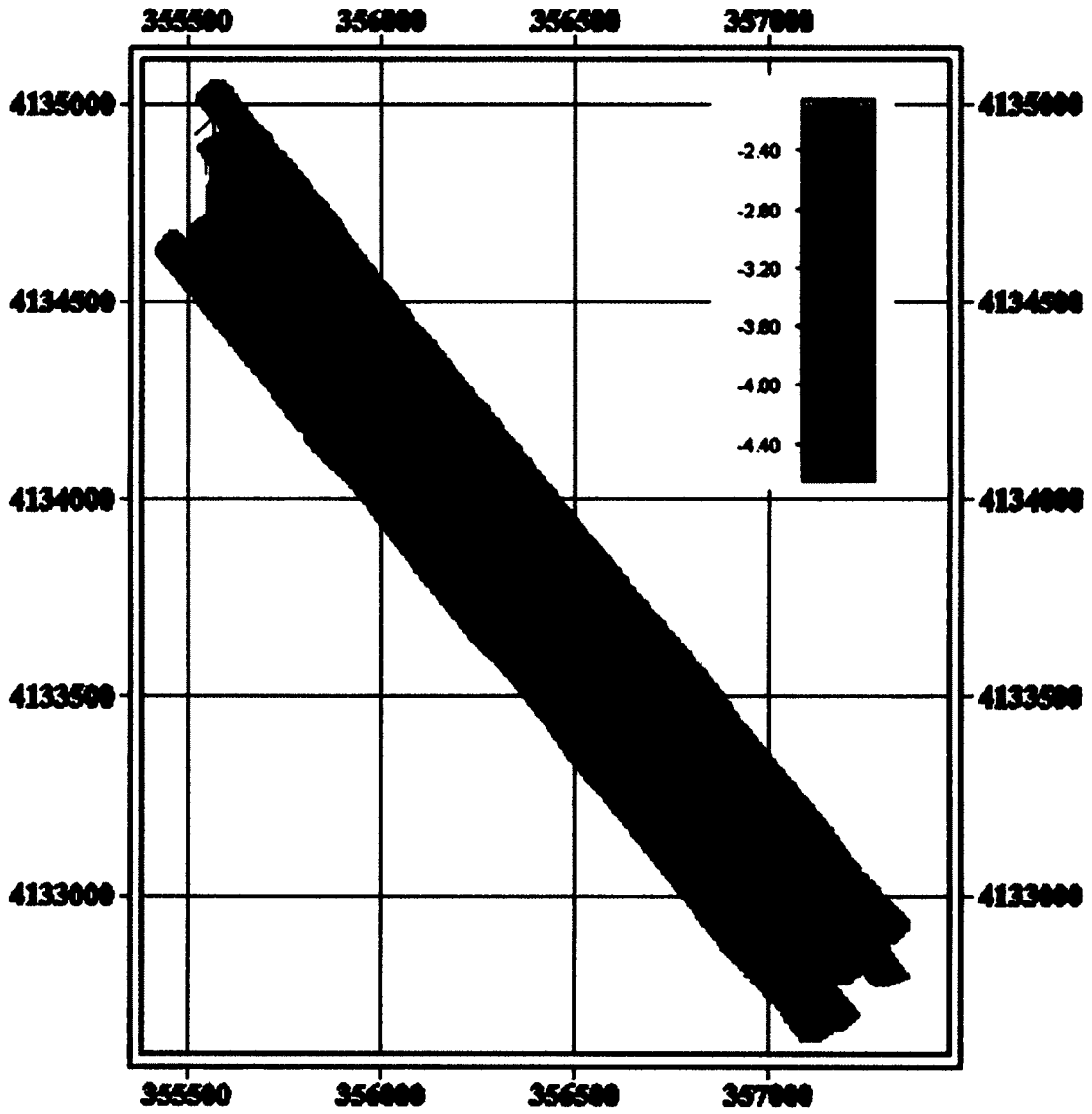
Aug. 2009 Clay Bank Main Channel



0 500 m

Scale 1:24000

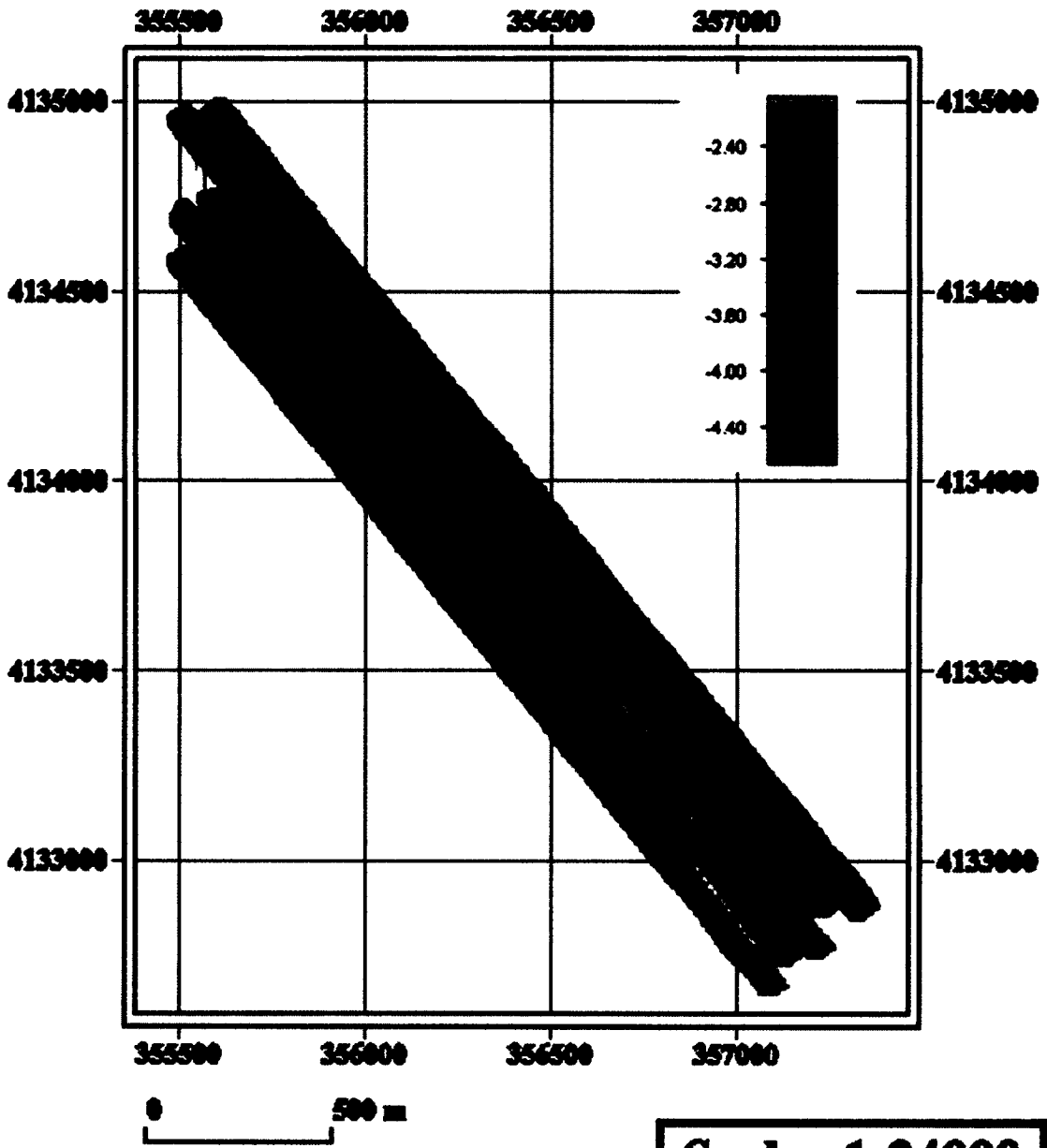
Sept. 2008 Clay Bank Sec. Channel & Shoal



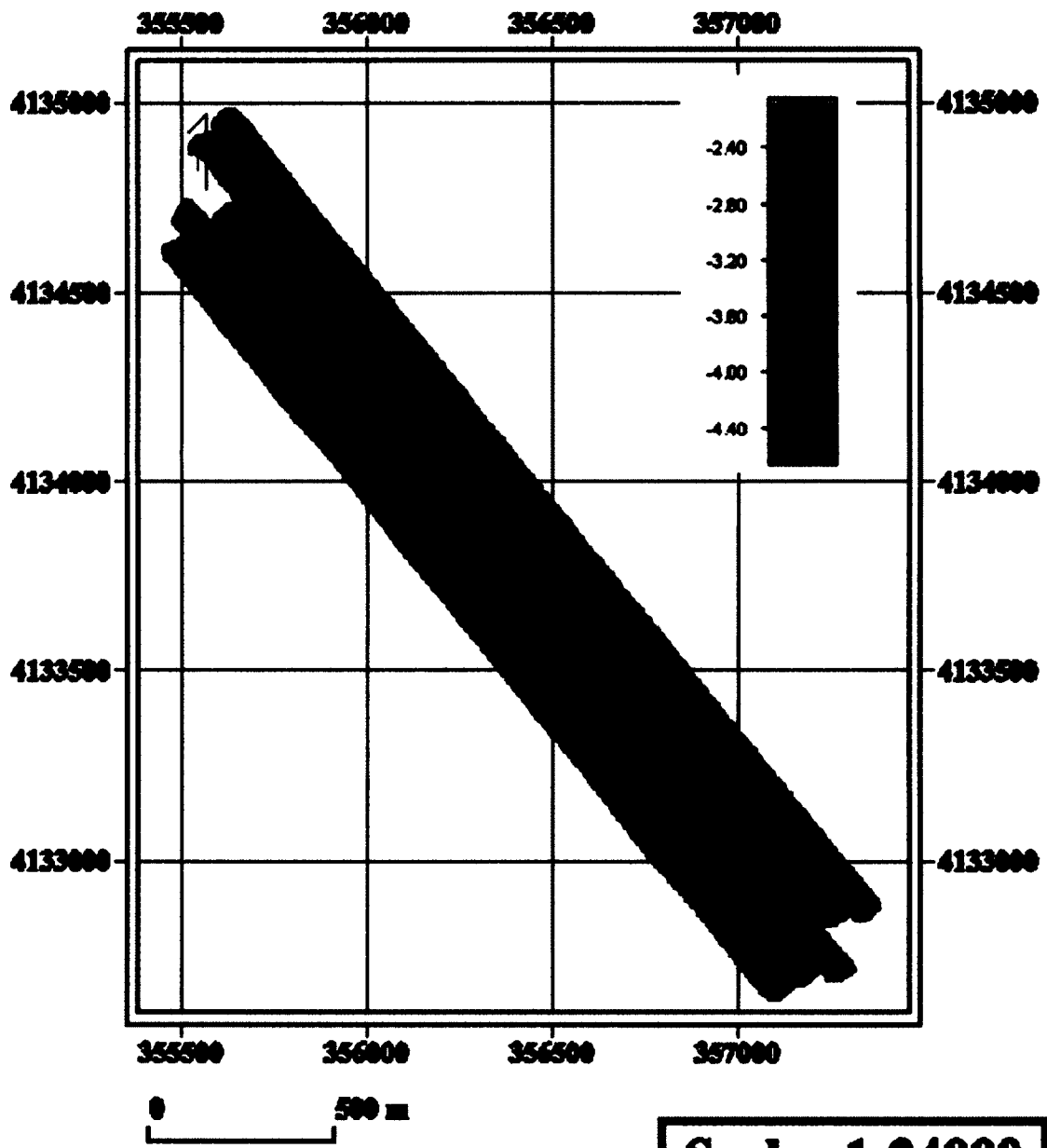
0 500 m

Scale 1:24000

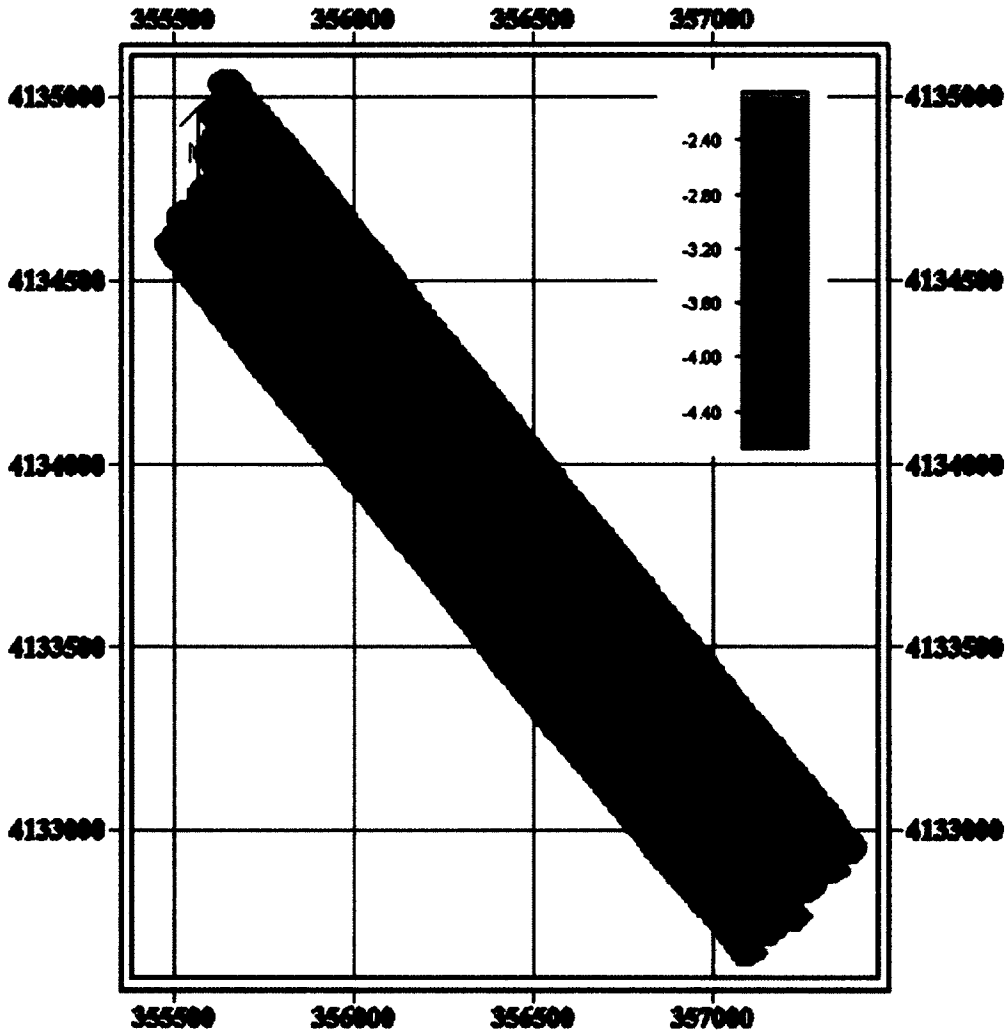
Dec. 2008 Clay Bank Sec. Channel & Shoal



Jan. 2009 Clay Bank Sec. Channel & Shoal

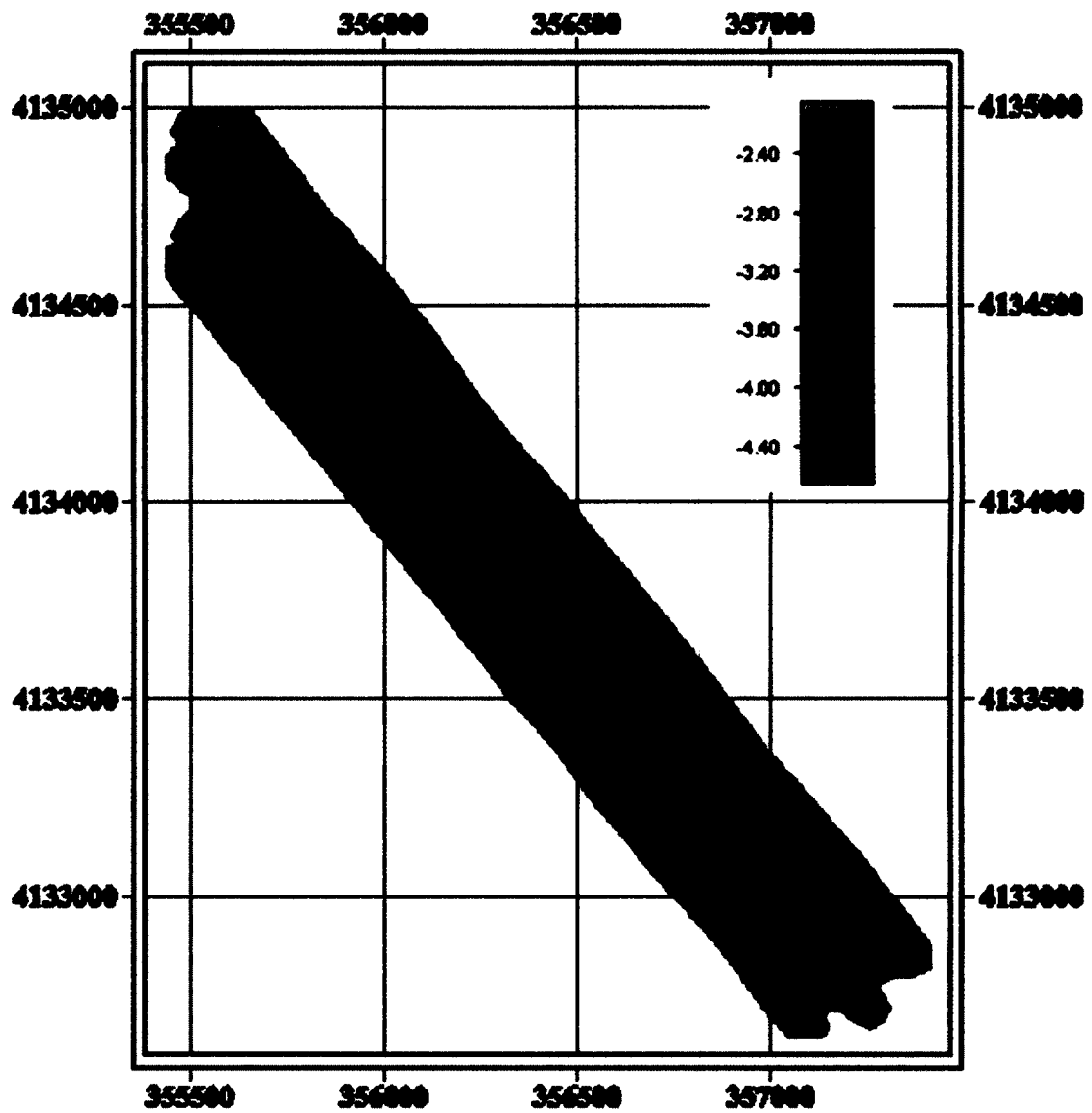


Feb. 2009 Clay Bank Sec. Channel & Shoal



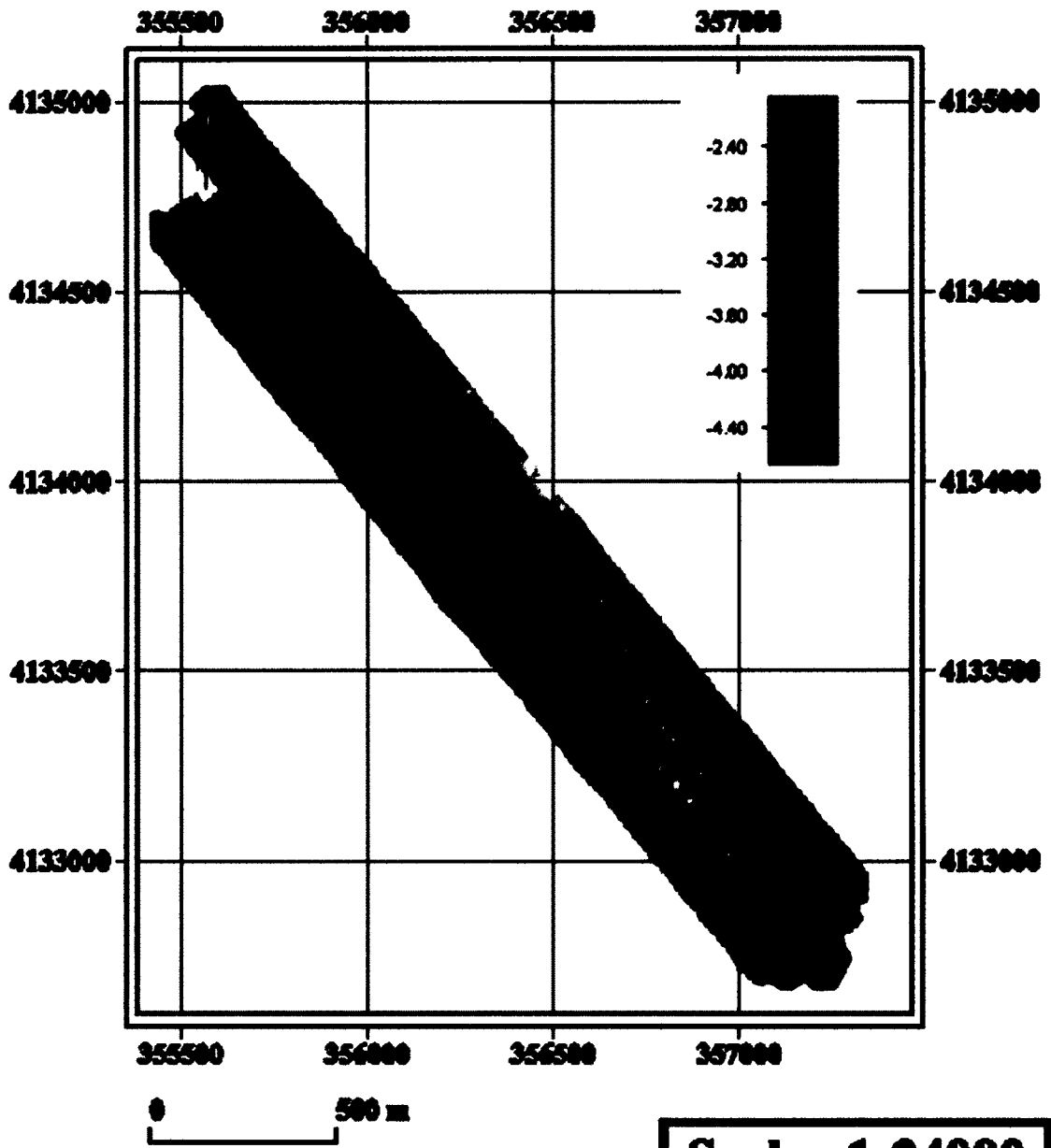
Scale 1:24000

May 2009 Clay Bank Sec. Channel & Shoal



Scale 1:24000

June 2009 Clay Bank Sec. Channel & Shoal



Aug. 2009 Clay Bank Sec. Channel & Shoal

